

**ROLLING CONTACT FATIGUE BEHAVIOR  
OF PEARLITIC RAIL STEELS**

**Vivek A. Dikshit**

**B.Tech., Indian Institute of Technology,  
Bombay, India, 1985**

**A dissertation submitted to the faculty of  
The Oregon Graduate Institute of Science and Technology  
in partial fulfillment of the requirements for  
the degree Doctor of Philosophy  
in  
Materials Science and Engineering**

**April 1992**

The dissertation "Rolling Contact Fatigue Behavior of Pearlitic Rail Steels" by Vivek A. Dikshit has been examined and approved by the following Examination Committee:

---

Paul Clayton, Thesis Advisor  
Professor

---

Roger K. Steele  
Association of American Railroads

---

David G. Atteridge  
Associate Professor

---

Lemmy L. Meekisho  
Assistant Professor

## ACKNOWLEDGEMENTS

First and foremost, I would like to express my gratitude to my thesis advisor Dr. Paul Clayton for all his help, co-operation and above all patience. Next I'd like to thank the rest of my thesis committee, Drs. Roger Steele, David Atteridge and Lemmy Meekisho for their help and advice in the correction of this manuscript.

The Burlington Northern Railroad, The Department of Transportation - Federal Railroad Authority and The Association of American Railroads deserve thanks for providing the funds and materials for this research, as also does Dr. Desmond Fegredo of CANMET for providing materials for testing.

I am extremely grateful for the invaluable support and input of "The Wear Group" - Dr. Devanathan Ramaswamy, Dr. Daniel Danks, Dr. Milton Scholl and Dale Christensen. I would also like to thank John Simmons, Dr. R. Parthasarathy, Dr. Sinjang Chen and Dr. Uppilli Sudarsan for their encouragement and support. Also, a big thanks to all the people at the Institute for making the last five years an enjoyable experience.

Jo Torgessen deserves an extra special thanks for her patience, understanding and support.

Finally, my eternal gratitude to my parents and my sister without whose emotional support and encouragement I would not have dreamt of doing graduate research.

ACKNOWLEDGMENTS  
DEDICATION  
TABLE OF CONTENTS  
LIST OF FIGURES  
LIST OF TABLES  
ABSTRACT

CHAPTER I INTRODUCTION

1.1 Background  
1.2 Objectives

1.3 Scope

1.4 Organization

1.5 Summary

**Dedicated to my parents, my sister and Jo**

CHAPTER II LITERATURE REVIEW

2.1 Introduction

2.2 Literature Review

2.3 Summary

2.4 Conclusions

2.5 References

2.6 Appendix

## TABLE OF CONTENTS

ACKNOWLEDGEMENTS .....	iii
DEDICATION .....	iv
TABLE OF CONTENTS .....	v
LIST OF TABLES .....	viii
LIST OF FIGURES .....	x
ABSTRACT .....	xiv
CHAPTER 1 : LITERATURE REVIEW .....	1
INTRODUCTION .....	1
RAILS .....	5
Rail Development .....	5
Failure of Rails .....	7
Wear .....	8
Plastic Deformation .....	8
CONTACT STRESSES .....	11
Hertzian Theory of Contact Stresses .....	11
Applications of the Hertzian Theory .....	17
Extensions of the Hertzian Theory .....	19
Material Response to Cyclic Stresses .....	22
ROLLING CONTACT FATIGUE LIFE .....	28
Effect of Contact Stress .....	28
Lubrication .....	30
Slide/Roll Ratio .....	37
Mechanical Properties and Microstructure .....	44
WHITE ETCHING LAYER AND RAIL GRINDING .....	47
CHAPTER 2 : EXPERIMENTAL TECHNIQUES .....	51
MATERIALS .....	51
Model Development .....	51
Model Validation .....	51
Sub-surface Deformation Studies .....	51
Crack Growth and White Etching Layer Studies .....	54
Tests to Study the Effect of Lubricant .....	55
Lubricants .....	55
SITE TRIAL .....	57
RCF TESTING .....	60
The Amsler Twin Disk Rolling/Sliding Testing Machine .....	60
The MTI Testing Machine .....	66

HEAT TREATMENTS .....	73
Model Development .....	73
MTI Rollers .....	77
RCF TEST ROLLERS .....	78
Amsler Rollers .....	78
MTI Rollers .....	82
RCF TESTS TO STUDY EFFECT OF LUBRICANT .....	83
SUB-SURFACE DEFORMATION TESTS .....	85
RCF TESTS FOR CRACK GROWTH STUDIES .....	88
RCF TESTS ON WHITE ETCHING LAYER SAMPLES .....	89
REPEATABILITY TESTING .....	90
SPECIMENS FOR METALLOGRAPHIC OBSERVATION .....	91
Failed RCF Test Rollers .....	91
Crack and White Etching Layer Study Samples from Rails in Service .....	92
PEARLITE INTERLAMELLAR SPACING MEASUREMENTS .....	94
INCLUSION COUNTS .....	96
HARDNESS MEASUREMENTS .....	98
CALCULATION OF MAXIMUM HERTZIAN CONTACT STRESS .....	99
 CHAPTER 3 : RESULTS .....	 100
MODEL DEVELOPMENT .....	100
Heat Treatments .....	100
RCF Tests on the Amsler Machine .....	104
Modification of the Model to Include Pearlite Interlamellar Spacing .....	113
Validation of the Model .....	119
CRACK AND WHITE ETCHING LAYER STUDIES .....	122
RCF Tests on White Etching Layer Samples .....	144
Correlation Between WEL and Cracks in Rails in Service .....	152
Study of Cracks in Amsler Test Samples .....	163
SUB-SURFACE DEFORMATION TESTING .....	191
RCF TESTS TO STUDY EFFECT OF LUBRICANT .....	195
 CHAPTER 4 : DISCUSSION .....	 198
Comparison of Failures .....	199
MODEL FOR RCF LIFE OF RAIL STEELS .....	205
Modification of Model to Include Coefficient of Friction .....	212
Effect of Bottom Roller Hardness on RCF Life .....	215
Validation of Model Using I Series Steels .....	223

Model Predictions for Bainitic Steels .....	225
CRACK AND WHITE ETCHING LAYER STUDIES .....	229
COMPARISON OF CRACKS IN AMSLER ROLLERS AND RAILS	234
SUB-SURFACE DEFORMATION .....	238
COMPARING RCF LIFE AND WEAR RATE MODELS .....	240
SUGGESTIONS FOR FUTURE WORK .....	247
CONCLUSIONS .....	250
REFERENCES .....	252
AUTHORS BIOGRAPHICAL NOTE .....	261

### LIST OF TABLES

Table I : Maximum shear stress as a function of $\mu$ [56] .....	21
Table II : Data from Literature .....	30
Table III : Range of maximum shear stress [20] .....	42
Table IV : Chemical compositions of rail steels .....	52
Table V : Chemical compositions of I series steels .....	53
Table VI : Summary of materials used .....	56
Table VII : Details of rail samples for crack and WEL studies .....	59
Table VIII : Summary of Amsler test series and parameters .....	65
Table IX : Ratios of ratios of rotational speeds .....	71
Table X : Summary of parameters for MTI tests .....	72
Table XI : Salt bath temperatures .....	76
Table XII : Summary of Amsler RCF tests for sub-surface deformation .....	86
Table XIII : Summary of MTI RCF tests for sub-surface deformation .....	87
Table XIV : Heat treated steel hardness and pearlite spacings .....	101
Table XV : Amsler RCF test results for model development .....	105
Table XV : Continued .....	106
Table XVI : Regression parameters for RCF data .....	110
Table XVII : Hardness and pearlite spacing of rail steels .....	114
Table XVIII : Regression parameters for hardness versus S .....	115
Table XIX : Properties of I series steels .....	119
Table XX : Maximum crack depth - high rails at MP 97.6 .....	125
Table XXI : Maximum crack depth - low rails at MP 97.6 .....	126
Table XXII : Maximum crack depth - high rails at MP 97.3 .....	127
Table XXIII : Maximum crack depth - low rails at MP 97.3 .....	127
Table XXIV : Crack densities - high rails at MP 97.6 .....	133
Table XXV : Crack densities - low rails at MP 97.6 .....	134
Table XXVI : Crack densities - high rails at MP 97.3 .....	135
Table XXVII : Crack densities - low rails at MP 97.3 .....	136
Table XXVIII : Microhardness values for WEL .....	147
Table XXIX : Crack and WEL data for rails .....	148
Table XXIX : Continued .....	149
Table XXX : Summary of crack development measurements .....	165
Table XXXI : RCF life for water and oil lubrication (i-m and iii-a series in Table VIII, p65) .....	196
Table XXXII : Relative RCF life .....	209
Table XXXIII : RCF life for water and oil lubrication (i-m and iii-a series in Table VIII, p65) .....	213
Table XXXIV : Regression data for RCF life versus hardness .....	217

Table XXXV : Regression parameters for RCF life versus $P_o$ for test series i-a and i-m (Table VIII, p65) . . . . .	221
Table XXXVI : RCF data for bainitic steels . . . . .	227
Table XXXVII : Parameters for relationship between wear rate and pearlite interlamellar spacing [97] . . . . .	241
Table XXXVIII : Regression data for "a" and "b" (Table XXXVII) . . . . .	242
Table XXXIX : Regression data for power relation between RCF life and pearlite interlamellar spacing . . . . .	243
Table XXXX : Regression data for $a_o$ and $b_o$ (Table XXXIX) . . . . .	244

## LIST OF FIGURES

Figure 1 : Lateral flow and "lip" in gauge corner of high rail [45] . . . . .	10
Figure 2 : General case of contacting bodies [38] . . . . .	13
Figure 3 : Contact between cylinders . . . . .	14
Figure 4 : Surface stresses in contacting bodies [15] . . . . .	15
Figure 5 : Stresses along centerline of contact [35] . . . . .	16
Figure 6 : "Counter-formal" wheel/rail contact [60] . . . . .	18
Figure 7 : Stress field around contacting body [10] . . . . .	19
Figure 8 : $\sigma_x$ due to normal and tangential loads [56] . . . . .	21
Figure 9 : Material response to cyclic stress [15] . . . . .	23
Figure 10 : Shakedown map [15] . . . . .	27
Figure 11 : Crack orientation [32] . . . . .	31
Figure 12 : Effect of slide/roll ratio on RCF life [31] . . . . .	39
Figure 13 : Plastic flow in the rail head [55] . . . . .	43
Figure 14 : Spalling in head hardened rail in BN track [79] . . . . .	58
Figure 15 : Amsler twin disk rolling/sliding testing machine . . . . .	60
Figure 16 : Amsler roller geometries . . . . .	62
Figure 17 : The MTI testing machine . . . . .	66
Figure 18 : Schematic of the MTI machine . . . . .	68
Figure 19 : MTI roller geometries . . . . .	70
Figure 20 : Bars from rails for heat treating . . . . .	73
Figure 21 : ITT curves for standard carbon steels [84] . . . . .	74
Figure 22 : ITT curves for chromium-molybdenum alloyed steels [85] . . . . .	75
Figure 23a : Hardness profiles for A, B and C rails . . . . .	79
Figure 23b : Rollers from A,B and C rails . . . . .	79
Figure 24a : Hardness profile for D rail . . . . .	80
Figure 24b : Rollers from D rail . . . . .	80
Figure 25 : Rollers from I series steels . . . . .	81
Figure 26 : MTI rollers from B steel . . . . .	82
Figure 27 : Schematic of friction trace from Amsler machine . . . . .	84
Figure 28 : Sectioning of failed RCF rollers . . . . .	91
Figure 29 : Sectioning of F and G rails . . . . .	93
Figure 30 : Hardness versus salt bath furnace temperature . . . . .	100
Figure 31 : Pearlitic microstructure from B1 . . . . .	102
Figure 32 : Pearlitic microstructure from B4 . . . . .	102
Figure 33 : Microstructure from C1 . . . . .	103
Figure 34 : Microstructure from C3 . . . . .	103
Figure 35 : RCF life versus $P_0$ for four as received rail steels . . . . .	107
Figure 36 : RCF life versus $P_0$ for B rail heat treated samples . . . . .	108

Figure 37 : RCF life versus $P_o$ for C rail heat treated samples .....	109
Figure 38 : N versus hardness .....	112
Figure 39 : C versus hardness .....	112
Figure 40 : Correlation of test results and model predictions .....	113
Figure 41 : Hardness versus pearlite interlamellar spacing .....	116
Figure 42 : Correlation of test results and model predictions .....	118
Figure 43 : Model predictions for I series steels .....	120
Figure 44 : RCF test results for I series steels .....	121
Figure 45 : Notation for crack and WEL studies .....	122
Figure 46 : Maximum crack depth versus MGT - High rails at MP 97.6 - Section #3 only .....	128
Figure 47 : Maximum crack depth versus MGT - High rails at MP 97.6 - Sections 2, 3 & 4 .....	128
Figure 48 : Maximum crack depth versus MGT - Low rails at MP 97.6 - Section #3 only .....	129
Figure 49 : Maximum crack depth versus MGT - Low rails at MP 97.6 - Sections 2, 3 & 4 .....	129
Figure 50 : Maximum crack depth versus MGT - High rails at MP 97.3 - Section #3 only .....	130
Figure 51 : Maximum crack depth versus MGT - High rails at MP 97.3 - Sections 2, 3 & 4 .....	130
Figure 52 : Maximum crack depth versus MGT - Low rails at MP 97.3 - Section #3 only .....	131
Figure 53 : Maximum crack depth versus MGT - Low rails at MP 97.3 - Sections 2, 3 & 4 .....	131
Figure 54 : Crack density data for MP 97.6 .....	137
Figure 55 : Crack density data for MP 97.3 .....	138
Figure 56 : Cracks in high rail at MP 97.6 after 6.7 MGT .....	139
Figure 57 : Cracks in high rail at MP 97.6 after 10.8 MGT .....	139
Figure 58 : Cracks in high rail at MP 97.6 after 16.1 MGT .....	140
Figure 59 : Cracks in high rail at MP 97.6 after 48.2 MGT .....	141
Figure 60 : Cracks in high rail at MP 97.6 after 48.2 MGT .....	141
Figure 61 : Cracks in high rail at MP 97.6 after 52.4 MGT .....	142
Figure 62 : Cracks in low rail after grinding at 53.5 MGT .....	143
Figure 63 : Naturally occurring WEL in rail .....	145
Figure 64 : Artificially induced WEL in rail sample .....	145
Figure 65 : Artificially induced WEL in Amsler test roller .....	146
Figure 66 : WEL in used Amsler roller .....	148
Figure 67 : Cracks in WEL on used Amsler roller .....	150
Figure 68 : Cracks in WEL on rail in service .....	150
Figure 69 : Spalling of WEL in used Amsler Roller .....	151
Figure 70 : Spalling of WEL in rail in service .....	151

Figure 71 : WEL in rail in service and associated cracks . . . . .	152
Figure 72 : Percentage surface area coverage by WEL - MP 97.6 . . . . .	155
Figure 73 : Percentage surface area coverage by WEL - MP 97.3 . . . . .	156
Figure 74 : Maximum and average WEL depth - MP 97.6 . . . . .	158
Figure 75 : Maximum and average WEL depth - MP 97.3 . . . . .	159
Figure 76 : WEL in low rail of MP 97.6, 1 MGT after grinding . . . . .	160
Figure 77 : Correlation between cracks and WEL - MP 97.6 . . . . .	161
Figure 78 : Correlation between cracks and WEL - MP 97.3 . . . . .	162
Figure 79 : Microhardness profile for 5000 cycle RCF test . . . . .	166
Figure 80 : Microhardness profile for 10000 cycle RCF test . . . . .	167
Figure 81 : Microhardness profile for 50000 cycle RCF test . . . . .	168
Figure 82 : Microhardness profile for 100000 cycle RCF test . . . . .	169
Figure 83 : Microhardness profile for 151000 cycle RCF test . . . . .	170
Figure 84 : Microhardness profile for 206000 cycle RCF test . . . . .	171
Figure 85 : Maximum hardness versus number of cycles . . . . .	172
Figure 86 : Depth of deformation - 5000 cycles . . . . .	173
Figure 87A : Maximum crack depth - 10000 cycles . . . . .	174
Figure 87B : Depth of deformation - 10000 cycles . . . . .	175
Figure 88A : Maximum crack depth - 50000 cycles . . . . .	176
Figure 88B : Depth of deformation - 50000 cycles . . . . .	177
Figure 89A : Maximum crack depth - 100000 cycles . . . . .	178
Figure 89B : Crack network depth - 100000 cycles . . . . .	179
Figure 89C : Depth of deformation - 100000 cycles . . . . .	180
Figure 90A : Maximum crack depth - 151000 cycles . . . . .	181
Figure 90B : Crack network depth - 151000 cycles . . . . .	182
Figure 90C : Depth of deformation - 151000 cycles . . . . .	183
Figure 91A : Maximum crack depth - 206000 cycles . . . . .	184
Figure 91B : Crack network depth - 206000 cycles . . . . .	185
Figure 91C : Depth of deformation - 206000 cycles . . . . .	186
Figure 92 : Maximum crack depth versus number of cycles . . . . .	187
Figure 93 : Length of longest crack versus number of cycles . . . . .	188
Figure 94 : Crack network depth versus number of cycles . . . . .	189
Figure 95 : Depth of deformed layers versus number of cycles . . . . .	190
Figure 96 : Sub-surface deformation in roller SSM04 . . . . .	192
Figure 97 : Microhardness profile of sample in Figure 96 . . . . .	193
Figure 98 : Trace of corrugations in roller SSM04 . . . . .	194
Figure 99 : RCF life plots for oil and water lubrication . . . . .	197
Figure 100 : Longitudinal section through head of spalled rail [79] . . . . .	200
Figure 101 : Spalling in Amsler test roller . . . . .	201
Figure 102 : Crack networks in Amsler test roller . . . . .	204
Figure 103 : Model predictions for RCF life of B & C series steels . . . . .	208

Figure 104 : Relative RCF life .....	210
Figure 105 : RCF life plots for oil and water lubrication .....	214
Figure 106 : RCF life versus hardness for $P_o = 1413 \text{ N/mm}^2$ .....	218
Figure 107 : RCF life versus hardness for $P_o = 1302 \text{ N/mm}^2$ .....	219
Figure 108 : RCF life versus hardness for $P_o = 1224 \text{ N/mm}^2$ .....	220
Figure 109 : RCF life versus $P_o$ for test series i-a and i-m (Table VIII, p65) .	222
Figure 110 : RCF data for bainitic steels with model predictions .....	228
Figure 111 : Type III wear rate and RCF life as functions of pearlite spacing	246

### ABSTRACT

Railroad rails can fail by a number of mechanisms including wear and surface initiated rolling contact fatigue (RCF). Higher strength and deformation-resistant rail steels have been successful in helping to alleviate wear, but have led to concerns about the relationship between material properties and RCF resistance.

A simple material model has been developed to predict the RCF life of eutectoid rail steels for water lubricated conditions using an Amsler twin-disc rolling/sliding testing machine. RCF life is found to be a function of the maximum Hertzian contact stress,  $P_0$ , the hardness,  $H$  and  $HP_0$ . This empirical relationship predicts that as  $P_0$  increases and/or  $H$  decreases, RCF life decreases. The model can be modified by replacing the hardness by the pearlite interlamellar spacing of the steel. The effect of different lubricants can be included by considering the coefficient of friction.

Validation studies showed that the model predictions agreed very well with experimental results when the steels used had properties similar to those used in formulating the model.

A laboratory analysis of head-hardened rails, removed from a heavy haul site at various stages of life, has enabled a study to be made of the incidence of RCF cracks and the role of the white etching layer (WEL) found on the rail

head. The cracks occurring down the center of the rail were shown to be associated with the WEL formed very early in the life of the rail. The extent of the WEL and the population of cracks decreased with increasing traffic. Some cracks penetrated beyond the WEL-pearlite interface and grew to a depth that was not always removed during normal maintenance grinding. The crack growth rates found in these rails were about 8.5 times lower than those found in Amsler test specimens.

This work also looked at developing a test procedure to generate subsurface contained plastic deformations. An attempt was made to relate an existing wear rate prediction model and the RCF life model to arrive at a relationship to predict the pearlite interlamellar spacing/hardness to minimize the wear rate and maximize the RCF life.

## **CHAPTER 1 : LITERATURE REVIEW**

### **INTRODUCTION**

Railroads have been one of the most important means of ground transportation of bulk goods and passengers for well over a century. Since the very beginning, there has been a steady increase in the loads, and total traffic, that the railroad tracks have had to carry, accompanied by increased train speeds [1-5]. As a result, the rails are frequently required to perform at levels much higher than their original designs called for, leading to excessive wear of the rail head and a consequent decrease in rail life. Each time these problems reached an unacceptable level the railroad industry countered by increasing the rail head cross section and/or increasing the strength of the rail steel to provide greater wear resistance [1,6,7]. While such measures have successfully countered the wear problem, there is a concern that rolling contact fatigue, another failure mechanism, might come into prominence [4,5,8,9].

Rolling contact fatigue (RCF) failures occur in engineering components that are in contact with each other under the influence of a cyclic load [10]. Common examples of components that suffer from RCF failures are gears and bearings, in addition to railroad rails. While a great amount of research has gone into the understanding of RCF in gears and bearings, and in trying to reduce the

incidence of such failures [11-14], this vast body of literature is of little use in application to rails. The reasons for this being that gears and bearings are made of significantly harder steels than are rails, and they are used with carefully selected lubricants [15], whereas in railroad operations the presence of a lubricant is often inadvertent and unintentional (except in lubricated curves).

Rolling contact fatigue defects in rails can be broadly divided into surface initiated and subsurface initiated defects [16]. Surface initiated RCF defects in rails include head checks [17], squats [18] and shallow surface spalling [19], whereas shells and transverse defects [20,21] belong to the category of subsurface initiated defects. While subsurface initiated defects can lead to catastrophic failure of the rail if left to progress unchecked [22,23], surface initiated defects are usually not fatal to the life of the rail. However, the relatively harmless surface initiated defects have been known to mask the more dangerous shell and transverse defects during ultrasonic testing of the rails in service [24,25]. Surface initiated RCF defects such as shallow surface spalling and squats often lead to increased levels of vibration [22] which are unacceptable. This necessitates the use of costly maintenance procedures like rail grinding.

The steady increase in the axle loads, and the total tonnages, combined with the higher strength rails that are in use currently, have led to questions about the relationship between train loads, rail properties and the incidence of (both

surface and subsurface initiated) RCF defects in rails [1,6-9].

Ideally, the best conditions for studying the relationship between operating parameters, and response of the system to such changes, are service conditions. Service scale trials are not only very expensive but also time consuming. The Facility for Accelerated Service Testing (FAST) at Pueblo, Colorado, is the only one of its kind in the United States where such service scale testing can be carried out [26]. Consequently, although a lot of excellent work is done at FAST, there is a need for laboratory scale tests to study and understand the effect of various parameters on the behavior of rails, and rail steels, under rolling contact conditions.

While laboratory scale testing is a good starting point in the understanding of the behavior of rails in service, it suffers from a major drawback. Test conditions in the laboratory are often idealized and usually deal with the different parameters in isolation. Hence, extrapolation of the results obtained in the laboratory to field conditions is an extremely difficult task. This is further complicated by factors such as the occurrence of the White Etching Layer (WEL) found on rails [18,27]. To date there are no means by which to simulate the conditions to test rail steels in the laboratory while accounting for the effect of such factors; mainly because there is little data from the field to relate the laboratory test results to.

Research into RCF of rails has progressed along two fronts. Some work has been done to study the generation of RCF defects in the laboratory using rolling/sliding testing machines and to determine the effect of different parameters on RCF behavior [17,20,28-33]. On the other hand, some work has been done to model the process of RCF, and RCF defect growth, using the finite element method and other numerical analysis tools [15,20,34-38]. However, there has been no systematic project to study the relationship between the microstructural, or mechanical, properties of rail steels and RCF behavior.

The main aim of this project was to correlate the microstructural (specifically the pearlite interlamellar spacings) and the mechanical properties (specifically the hardness) of the steel, the contact stresses, and the RCF life of rail steels. Additional goals of this work can be summarized as follows:

- \* To study the evolution of cracks in rails in service and their relation to the White Etching Layer, and correlate this to laboratory test results.
- \* To include the effect of coefficient of friction in RCF life predictions.
- \* To combine the RCF life prediction model and existing wear rate prediction model and predict the steel hardness/pearlite interlamellar spacing to optimize RCF life and wear rate.

## RAILS

### Rail Development

The world's first self-propelled rail vehicle, built by R. Trevithick in 1804, ran on cast iron tram rails [39]. These rails were able to carry the 25 ton weight of the vehicle for only a few days before they failed as a result of their inherently low strengths. While the wrought iron steels were stronger than their predecessors, the cast iron rails, they were still not strong enough to hold up to the increasing traffic and loads. Hence, in 1862, when the Bessemer process made steel cheaply available, the railway industry switched over to the stronger and more wear resistant material for making rails [6,40]. Since then the configuration of rails has remained substantially constant, except for increases in the cross sections of the rail head. On the other hand, the metallurgy of the rail steels has undergone an almost continuous evolution [1,6]. The introduction of basic oxygen technology in the mid 1900's vastly improved the quality of steels and succeeded in greatly reducing hydrogen, thus significantly lowering the incidence of shatter cracks [24]. Further, the cleanliness of the steels was improved to such an extent that the effect of oxide inclusions was drastically reduced [41].

For the past 4 - 5 decades plain, medium and high carbon steels have been almost universally used in rail manufacture. These hypo-eutectoid steels

often have a fully pearlitic microstructure. The compositions and properties of these steels are dictated by various international standards [6,9,22,42].

In the railroad industry, as in any other industry, most changes are introduced to maintain profitable operation. Hence, since the earliest days of commercial railroads, the traffic and axle loads of the railroad cars have been steadily increasing [1-5]. As a result, rails have had to perform at loads greatly exceeding the levels that they were originally designed for. This has led to excessive wear of the rails and the industry has countered by increasing the strength of rail steel [1,6,7]. For the pearlitic steels in current use this increase in strength has been brought about by refining the interlamellar spacing of the pearlitic structure [1,6,22].

The most common methods for decreasing the pearlite interlamellar spacing are heat treatment of the rail [22,43] and the addition of alloying elements to the steel [44,46]. Head hardened rails belong to the first category [22]. The alloyed chromium-molybdenum and chromium-vanadium steels belong to the category of alloyed steels [45].

The gauge corner of the high rail in curves is the area which is most severely affected by wear. Due to the higher cost of manufacturing the higher strength (premium) rails, by heat treatment or alloying, these rail steels are presently used mainly in curved track sections.

### Failure of Rails

Deterioration and failure of railroad rails can take place by one or more of the following important failure mechanisms :

- \* *Abrasive and/or mechanical wear by microfracture (in shallow curves) [47-49].*
- \* *Gross plastic deformation of the rail head due to the wheel load, causing lateral spreading of the rail head (in curves <600m) [3,50].*
- \* *Cracks generated in the rail surface and subsurface due to rolling contact fatigue and or plastic deformation resulting in either flaking off of material from the surface or in the extreme, fracture of the rail (in tangent track and lubricated curves) [17-21].*

Deterioration of the rail occurs simultaneously by all three mechanisms [3]. The contribution of each mechanism will vary depending upon the position of the rail in track and other factors. Thus, the above can be thought of as competing mechanisms. For example, rails with moderately high wear rates show lower rates of rolling contact fatigue defect occurrence [2]. On the other hand, there is also an interdependence between the different mechanisms [2,3]. The plastic deformation occurring in the surface layers leads to the initiation of fatigue cracks [2,17,50,51]. The incidence of each of the above problems depends upon numerous factors like the loading conditions, the amount and direction of

tangential tractions, material properties and lubrication. The location of the rail in the track and the position on the rail can also have a significant effect on the occurrence of the various failure modes.

### Wear

Wear of rails can be divided into two categories. The first type of wear occurs in tangent track or shallow curves, with no acceleration or braking of the trains [47-49]. In this case the wear rates (vertical rail head wear) are fairly low and do not pose a critical problem. This type of wear has been referred to as "fatigue wear" by Kalousek *et al* [51].

The second type occurs on the gauge face of high rails of sharp curves [51]. In this situation there is substantial sliding due to curve negotiation and hence the wear rates are very high. Wear rates in such instances are reduced by using grease lubricators and rails having greater deformation resistance [51].

### Plastic Deformation

Due to the high loads imposed on the rails, the material in the rail head flows plastically and this alleviates the stresses by making the rail profile more conformal with the wheel profile [53]. This leads to the formation of a "lip" on the gauge face of the high rails, Figure 1 [45]. Cracks can initiate on the under

side of the lip and in the presence of internal inhomogeneities can lead to "horizontal fissures" [54]. This kind of plastic deformation occurs as a consequence of the high normal loads.

Another kind of deformation occurs on the rail running surface resulting from the shearing stresses generated by the normal and tangential loads [2,15,17,39,50,51]. Such plastic deformation occurs with each cycle of stress and is cumulative in nature [15,39]. As a result, the surface layers undergo plastic shearing along the longitudinal direction and can lead to crack initiation [2,17,50,51]. A complicated pattern of surface flow was detected by Sugino *et al* [55] but cracks were found to initiate only when the plastic flow was in the longitudinal direction.

Rolling contact fatigue cracks are thus closely related to the plastic deformation occurring in the surface layers. Before studying the mechanism and effect of plastic deformation on rolling contact fatigue, it is necessary to understand the stresses that are generated within the contacting bodies.

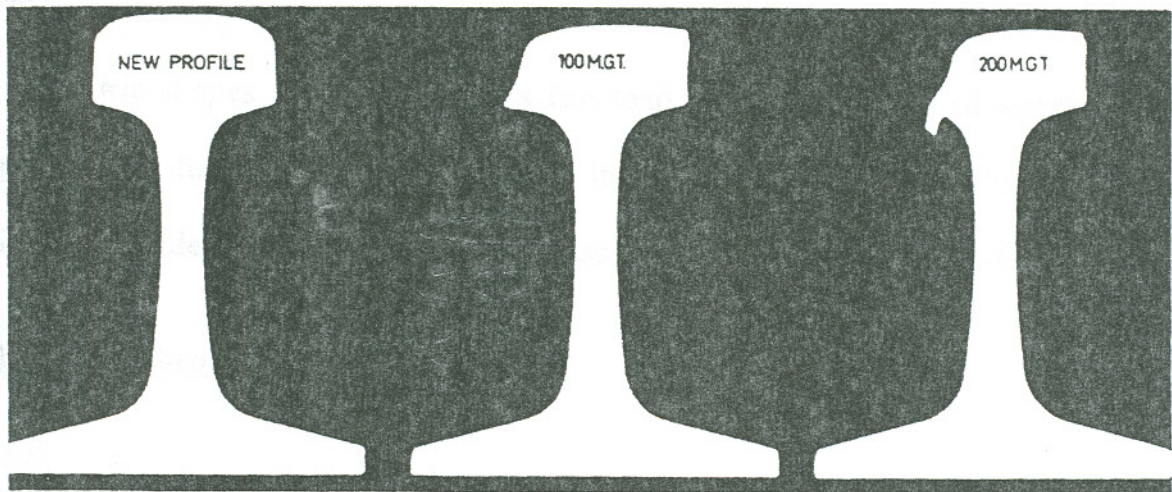


Figure 1 : Lateral flow and "lip" in gauge corner of high rail [45]

## CONTACT STRESSES

The stresses generated in the contacting bodies are by far the most important factors controlling RCF behavior [34,56-58]. Calculation and analysis of the stress fields generated by a load in rolling contacts are extremely complex. The application of even a simple distributed static, normal load in the simplest of geometric shapes in ideal materials can lead to a whole array of stresses. The problem is further complicated by the introduction of tangential loads, dynamic loads, non-ideal materials, residual stresses and complex shapes [56-58].

### Hertzian Theory of Contact Stresses

The first reliable, mathematical solution to the problem of finding stresses in contacting bodies was given by H. Hertz in 1881 [58,59]. The assumptions that form the basis of the simplifications used by Hertz are [58,59]:

- \* *The contacting bodies are homogeneous, isotropic and linear elastic,*
- \* *The contacting surfaces are frictionless,*
- \* *The dimensions of the contact patch are small compared to the principal radii of curvature of the undeformed bodies,*
- \* *The undeformed contacting surfaces are continuous and can be represented by second degree polynomials, and*

- \* The contact is "counter-conformal" or "non-conformal", i.e., point or line contact.

For the general case of a sphere loaded against an elastic half space, the contact patch and force distributions are as shown in Figure 2 [38]. As a specific case of the contact problem, consider the contact between two cylinders running against each other with their axes parallel, Figure 3. For this case, the contact patch is effectively a long narrow rectangle with the half width of contact [along the X-axis], "b" given by [56]:

$$b = \left[ \frac{2P \Delta}{2a \pi} \right]^{\frac{1}{2}} \quad (1)$$

where P is the contact load, 2a is the contact width of the cylinders [along the Y-axis] and,

$$\Delta = \frac{1}{\frac{1}{2} \left[ \frac{1}{R_1} + \frac{1}{R_2} \right]} \left[ \frac{1-\mu_1^2}{E_1} - \frac{1-\mu_2^2}{E_2} \right] \quad (2)$$

All the other stresses, namely  $\sigma_x$ ,  $\sigma_y$  and  $\sigma_z$ ; the principal stresses,  $\sigma_1$ ,  $\sigma_2$  and  $\sigma_3$ ; the maximum shearing stress,  $\tau_{\max}$ ; and the maximum octahedral shearing stress,  $\tau_{\max\text{-oct}}$ , can be expressed as functions of  $P_0$ . Also, the distance  $Z_{\max}$ , below the surface at which the maximum shear stress occurs can be found once  $P_0$  is

known. Typical plots of some of the important stresses are shown in Figure 4 [15] and Figure 5 [35].

In Figure 4, the magnitudes of the surface stresses are plotted as functions of the distance along the X-axis. The magnitudes of the stresses along the centerline of the contact patch are plotted as functions of the depth in Figure 5. We find that the maximum shear stresses occur at a depth of  $0.78b$  under the center of the patch and the magnitude at this point is  $0.3P_0$ .

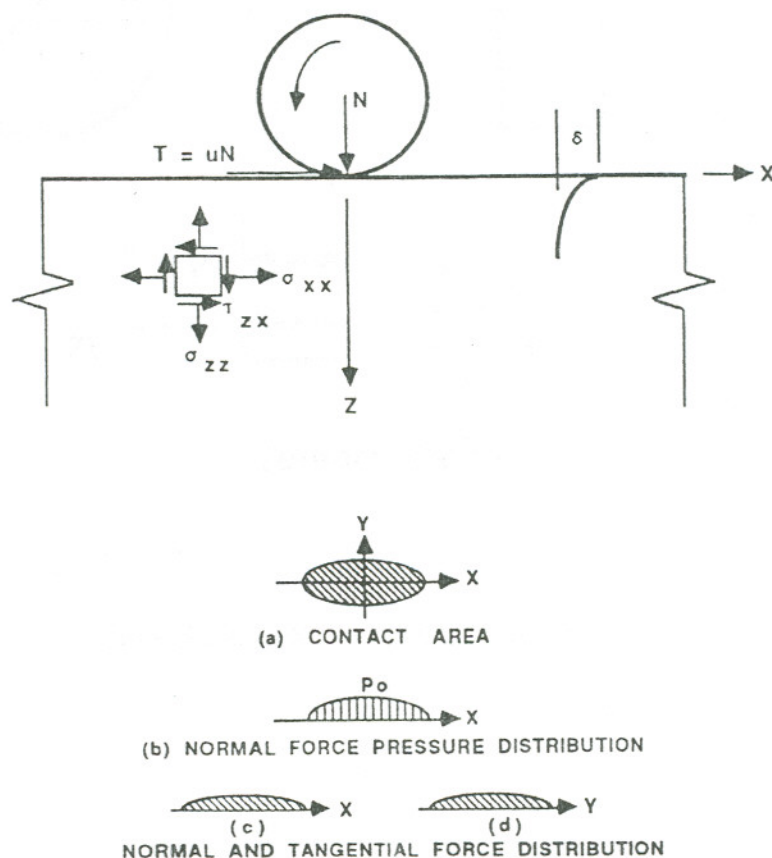


Figure 2 : General case of contacting bodies [38]

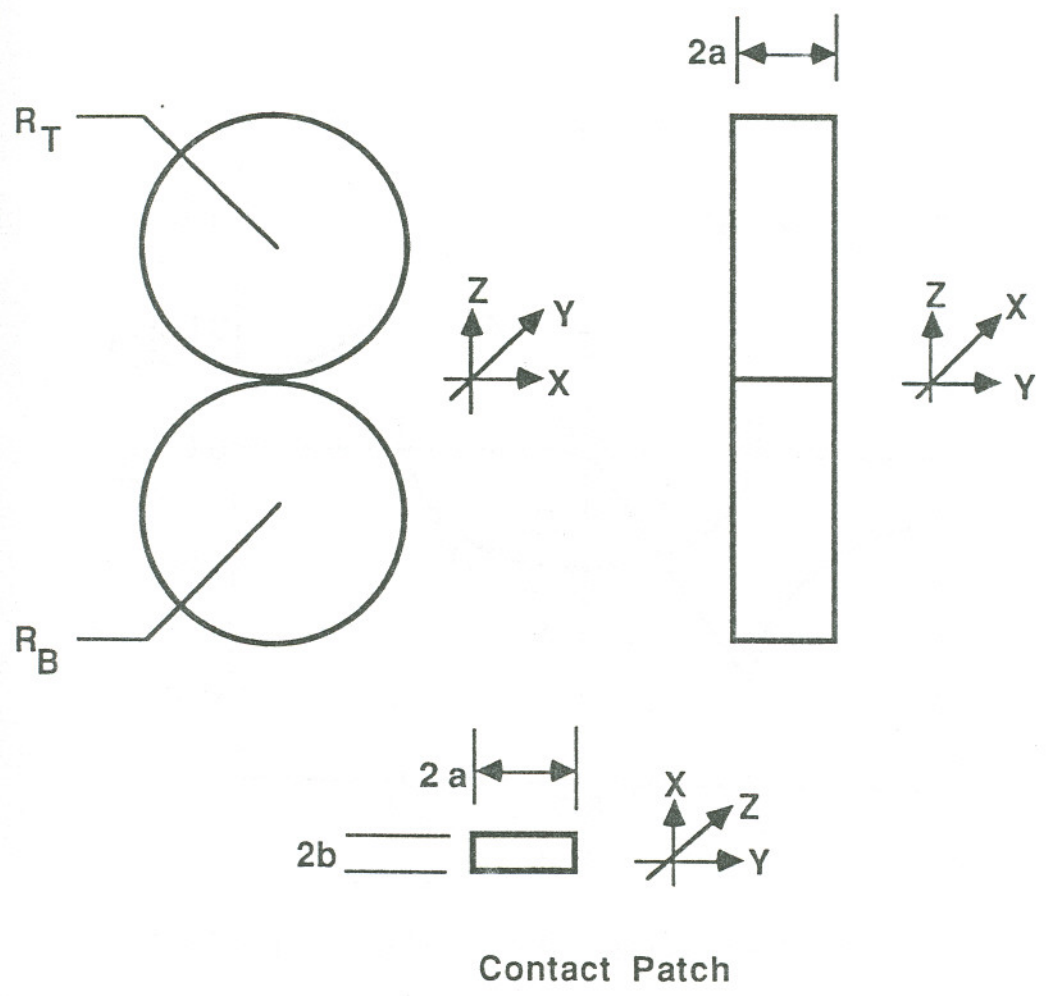
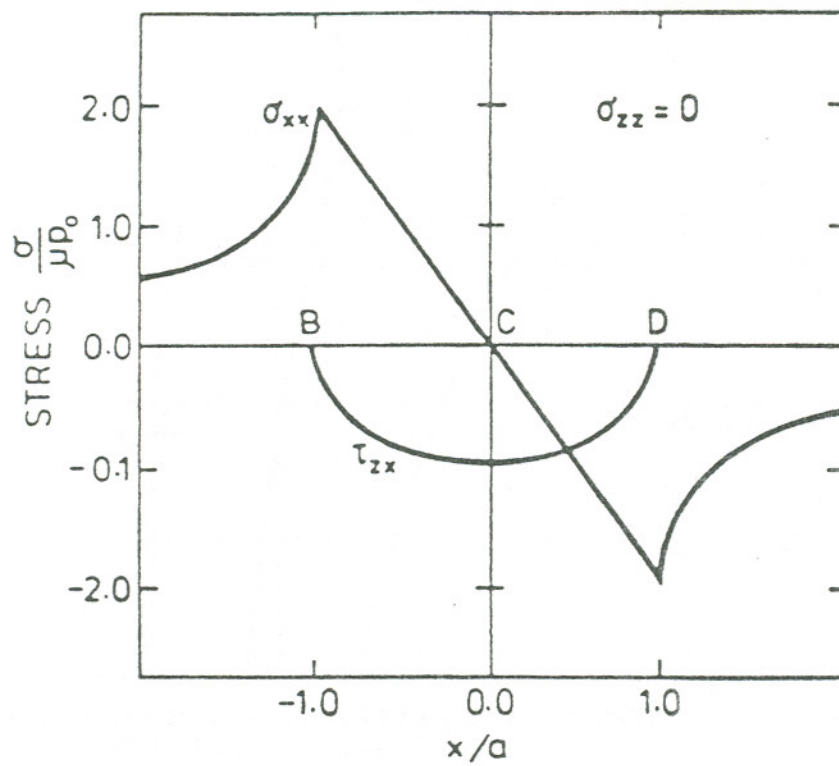
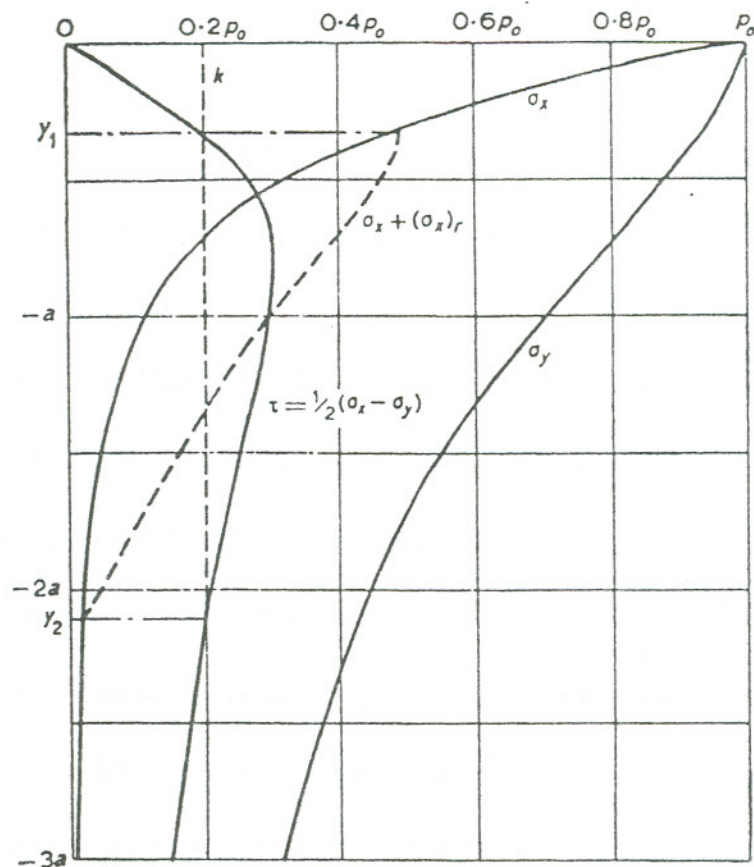


Figure 3 : Contact between cylinders



("a" corresponds to "b" in Equation 1, p12)

Figure 4 : Surface stresses in contacting bodies [15]



Note that  $\tau$  may be limited to a maximum value  $k$  by the addition of residual stresses  $(\sigma_x)_r$  in the layer  $y_2 < y < y_1$ .

("a" corresponds to "b" in Equation 1, p12)

Figure 5 : Stresses along centerline of contact [35]

### Applications of the Hertzian Theory

Although Hertz's solution is for a highly simplified and idealistic case, it can be used as a first approximation in the determination of the stresses existing in real wheel/rail contacts.

According to Paul [60], for the case of a new wheel running on a new rail, the only combination providing the requisite "counter-formal" contact, the wheel and rail can be modeled as two cylinders running against each other with their axes crossed, Figure 6 [60]. For such a combination of profiles, assuming a static load, it has been shown by Andrews [61] that the dimensions of the contact patch predicted by the Hertzian theory for wheel/rail contacts matches closely with measured contact patch dimensions. Andrews measured the dimensions of the contact patch by taking imprints of the wheel/rail contacts at different contact loads.

Since the calculation of contact patch size is the first step in the computation of contact stresses, a close match between measured and calculated values of the contact patch dimensions should imply that the calculated values of the contact stresses will closely correspond to the actual values. Calculations by Johns *et al* [62] show that for an axle load of 30 tons, the maximum Hertzian contact stress is  $1500 \text{ N/mm}^2$  for a new wheel/rail profile combination and  $830 \text{ N/mm}^2$  for a worn wheel/rail profile combination.

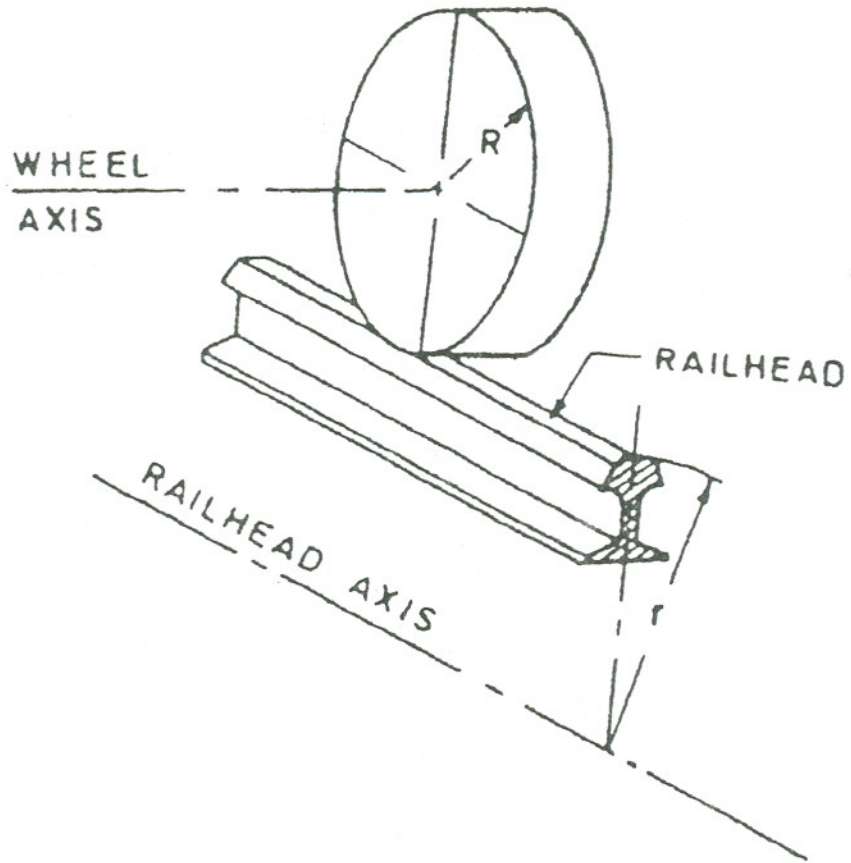


Figure 6 : "Counter-formal" wheel/rail contact [60]

### Extensions of the Hertzian Theory

A lot of work has been done to extend the Hertzian theory to more realistic situations, by taking into account the effects of friction, tangential loads between the bodies and dynamic loading. The step from static loading to dynamic loading can be taken by simply assuming that a system of stresses exists in the space around the contacting bodies and that each point in the bodies passes through this stress field, Figure 7 [10].

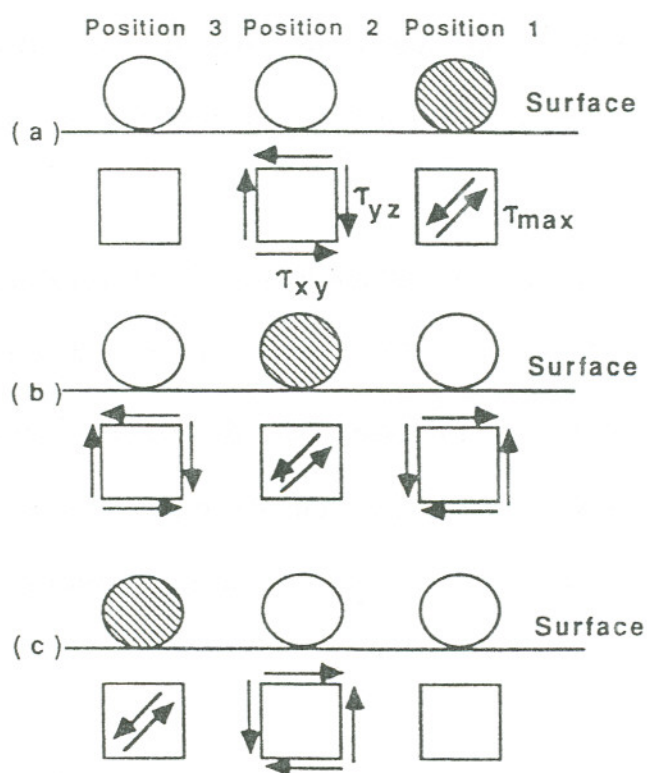


Figure 7 : Stress field around contacting body [10]

Smith and Liu [56] superimposed the effect of tangential loads and friction between the surfaces on the stresses generated by pure normal loads in frictionless bodies. According to Mindlin [63], this can be done provided:

$$q_0 = \mu \times P_0 \quad (3)$$

i.e., if the maximum stress due to the tangential load is proportional to the maximum Hertzian contact stress and the constant of proportionality is the coefficient of friction, " $\mu$ ". It was found that the stresses resulting from the combination of the normal and tangential loads could still be expressed as functions of  $P_0$ .

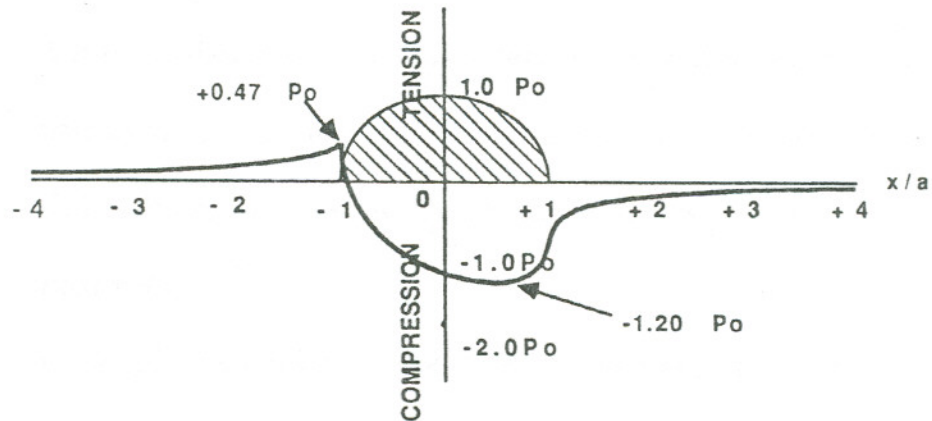
Figure 8 shows the result of combining the contributions from the normal and tangential loads to  $\sigma_x$  for a coefficient of friction of 0.25 [56].

In addition to increasing the magnitude of the contact stresses, tangential loads also change the depth at which the maxima of these stresses occur. As an example consider the following results from the work by Smith and Liu [56]:

Table I : Maximum shear stresses as function of  $\mu$  [56]

	$\tau_{\max}$	$\tau_{\max\text{-oct}}$	Depth
$\mu = 0$	$0.30P_o$	$0.27P_o$	$0.78b$
$\mu = 0.25$	$0.43P_o$	$0.37P_o$	$0.30b$

where,  $\mu$  is the coefficient of friction, taken to be an indication of the tangential traction,  $P_o$  is the maximum Hertzian contact stress and  $b$  is the half width of the contact patch.



Range of values of  $\sigma_x^*$  at a point O (fixed)  
as load moves past point

**Figure 8 :  $\sigma_x$  due to normal and tangential loads [56]**

It has been found that as the tangential traction increases, the maximum stresses move closer to the surface. Beyond  $T/N = 0.3$ , the shear stress maxima occur at the surface.

### Material Response to Cyclic Stresses

The preceding section provided some background about the stresses generated within contacting bodies. This gives us the basis by which the response of materials to cyclic loading can be studied. On repetitive cyclic loading the materials can respond in one of the following ways [15]:

- (i) *Perfectly elastic* : If the maximum stress during the cycle does not exceed the yield stress, the material will be perfectly elastic, Figure 9a.
- (ii) *Elastic shakedown* : The elastic limit of the material is exceeded in the first cycle, but as a result of changes in the material due to plastic deformation, the steady cyclic state lies within the elastic limit, Figure 9b.
- (iii) *Cyclic plasticity (plastic shakedown)* : The steady cyclic state consists of a closed plastic stress-strain loop with no net accumulation of unidirectional plastic strain, Figure 9c.

(iv) *Incremental collapse (ratchetting) : The steady state consists of an open cycle of plastic stress and strain such that an increment of unidirectional plastic strain is accumulated with each cycle of stress, Figure 9d.*

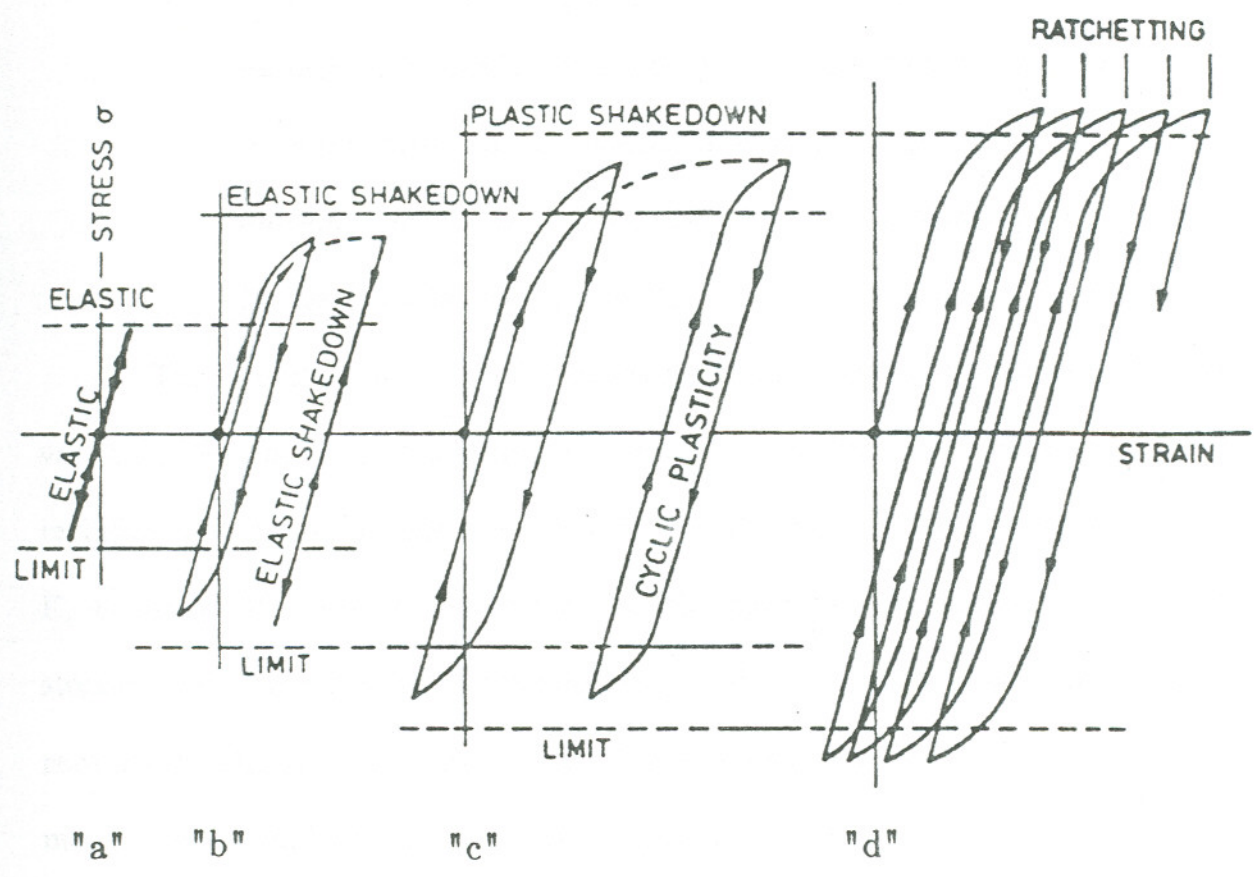


Figure 9 : Material response to cyclic stresses [15]

Shakedown can occur as a result of one or more of the following three mechanisms [15]:

- (a) *Plastic deformation during the early cycles of the load gives rise to residual stresses which protect the material against additional plastic deformation during subsequent cycles.*
- (b) *Strain hardening of the material.*
- (c) *Plastic deformation of the material during the early cycles makes the surfaces more conformal, which, for a constant load, reduces the intensity of the resulting stresses. For an elastic-perfectly-plastic material under plane strain conditions, only residual stresses can influence shakedown [15,34,35].*

The evolution of residual stresses in rolling contacts has been studied by various researchers. Johnson and co-workers [15,34,35] used numerical analysis techniques to show that for loads not greatly exceeding the factor  $P_o/K_e$ , (where  $K_e$  is the yield stress in shear) the material reaches a steady state of residual stresses within the first 4 - 5 loading cycles. Similar results were obtained more recently by Bhargava *et al* [36]. Using finite element modelling they were able to model the residual stresses within the contacting bodies. While the qualitative trends are identical to those obtained in earlier work, there are discrepancies with respect to the actual values of the residual stresses.

Along with residual stresses, most of the modelling work has also dealt with the prediction of plastic strains in the contacting bodies. The numerical analysis techniques used by Johnson *et al* [15,34,35] yielded estimates of the accumulated shear strains that were in excellent agreement with experimental measurements made by Hamilton [64] and Crook [65] for pure rolling tests. However, when tangential tractions were considered, these models greatly underestimated the shear strains.

The finite element approach of Bhargava *et al* [36], while qualitatively agreeing with the results of previous work by Johnson *et al* [15,34,35], predicts plastic strains 5 times greater than the latter. However, even these values are much smaller than those measured experimentally.

Using the concept of distributed dislocations Bower [38] was able to show that the inaccuracies in the predictions of the earlier models lie in the fact that they all considered perfectly plastic materials and neglected the effect of strain hardening. Considering a non-linear kinematic hardening model, Bower successfully predicted the ratchetting rates (rate of accumulation of plastic strain) for copper and pearlitic rail steel. Subsequent experiments, where the samples were subjected to a complex non-proportional cycle of tension and torsion, support the predictions of Bower's model [15].

Based on the various responses of the material to cyclic loading and the material properties, Johnson has formulated a "shakedown" map, Figure 10 [15]. Using this map it is possible to predict how a material is ideally supposed to behave under given loading conditions.

Most of the work and the results described above, relate to highly simplified cases of contact, for example, cylinder on plane or ball on plane. While some work has used rails and wheels in modelling, such a task requires making numerous simplifications. While these types of models provide invaluable insight into the behavior of materials they are still a long way from being useful in predicting the response of materials in practical situations. Meanwhile, research has also progressed along another front. Since field trials to test the model predictions would be prohibitively expensive, a lot of work has gone into the development of laboratory tests that are capable of validating the predictions of the models.

Laboratory tests have a big advantage over field trials as there is a lot more control over the test parameters in the laboratory than in the field. Hence it is easy to isolate and study the effect of individual variables such as contact stresses, lubricant, slide/roll ratio, mechanical properties and microstructural parameters.

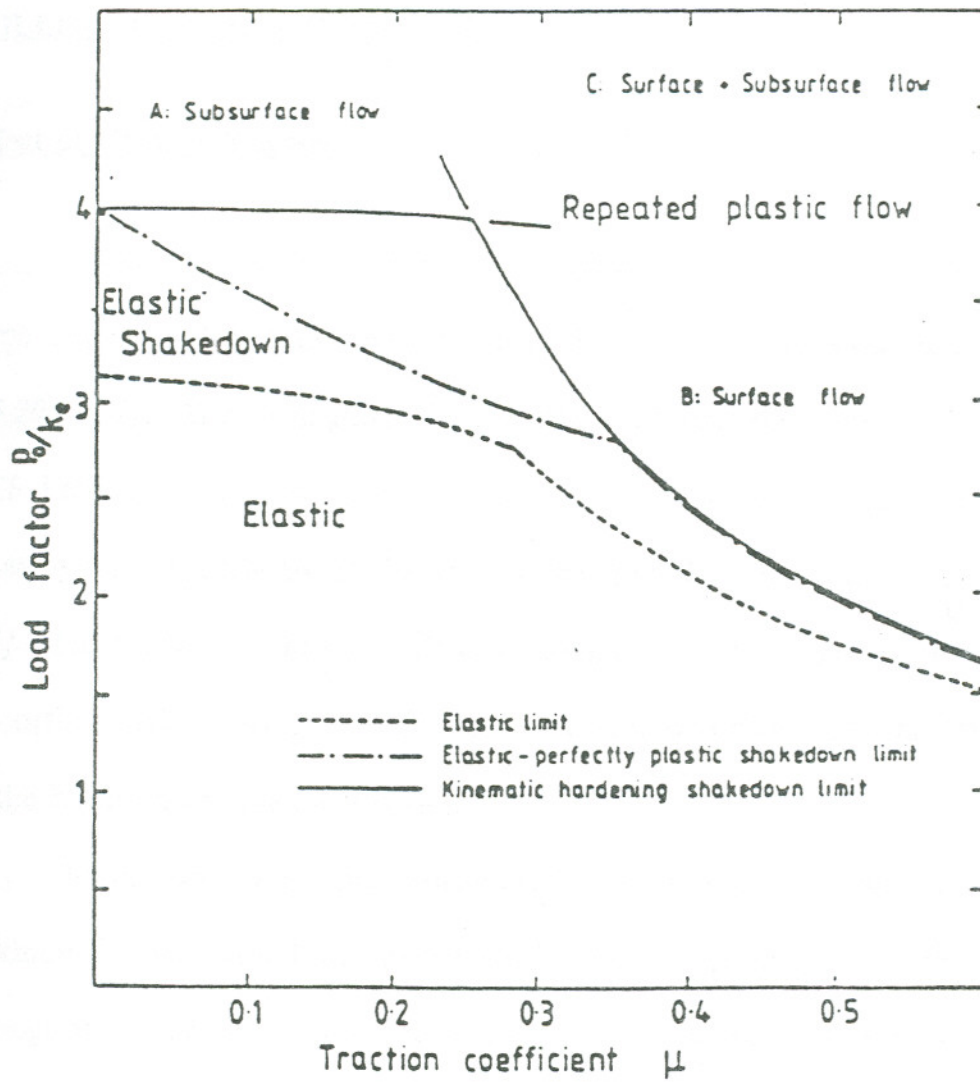


Figure 10 : Shakedown map [15]

## ROLLING CONTACT FATIGUE LIFE

### Effect of Contact Stresses

Of the various stress components generated within contacting bodies, only some are considered as being of critical importance in determining RCF life [15,20,56,57]. The orthogonal shear stress has been commonly used in modelling RCF behavior. This is so because the variation in the range of stresses is the greatest for the orthogonal shear stress compared to any other stress component [15]. The maximum shearing stress, although initially of a greater magnitude than the orthogonal shearing stress, is usually attenuated after the first few cycles due to the build up of residual stresses.

Smith and Liu [56] considered that the stress component with the maximum range would determine RCF life. Since they did not consider the orthogonal shear stress, they found that, in the absence of tangential traction, the maximum range is due to the maximum shearing stress, and, in the presence of tangential traction ( $\mu = 1/3$ ), the maximum range is due to the octahedral shearing stress. It has been suggested by McKelvey and Moyer [57] that  $P_o$  is the stress governing RCF life.

For most laboratory tests, the data is reported as a function of  $P_o$ , since

irrespective of which stress is of critical importance, they can all be expressed as linear functions of  $P_o$ . Also,  $P_o$  is the easiest to calculate.

Numerous attempts have been made to correlate RCF life to  $P_o$  [17,31]. Many different criteria, such as the number of cycles to crack initiation, appearance of the first loss of surface material as a "spall" or "pit", or the accumulation of a predetermined level of surface distress have been used to define RCF life. Until recently, it had been extremely difficult to determine the initiation of cracks in roller samples without destructive testing of the samples. Garnham and Beynon [67] have recently reported that they have been able to detect the initiation of cracks in samples during testing using a scanning, high resolution differential eddy current device. Unfortunately, no results are available. Irrespective of the criterion used, RCF life is proportional to  $P_o^{-B}$ . Table II shows the results, for rail steels, obtained in the past by researchers using either the twin disc type or the "nut cracker" type rolling/sliding machines. The results in this table pertain to, at most three, steels.

The data in Table II indicate a strong dependence of RCF life on the type of lubricant used and the slide/roll ratio.

**Table II : Data from literature**

Authors [Ref. #]	$P_o$ (N/mm <sup>2</sup> )	Lubricant	Slide Roll Ratio (%)	B*
Ollerton <i>et al</i> [29]	620-1650	Water	0.0	1.0
Masumoto <i>et al</i> [17]	1100-2250	Turbine Oil	20.0	5.0
Akaoka <i>et al</i> [30]	500-1600	Mineral Oil	11.0	1.5
Clayton <i>et al</i> [31]	250-1500	Water	0.3	1.8
			5.0	4.2
			10.0	4.2

$$* \text{RCF Life} = A(P_o)^{-B}$$

### **Lubrication**

In practical engineering situations, elements that are in contact under rolling/sliding conditions are almost always run in the presence of lubricants. In many cases, like gears and ball bearings, the lubricants are carefully selected and they provide a condition of elastohydrodynamic lubrication. However, in rails, except for grease lubrication on sharp curves, [53] the presence of water (from rain) is unintentional and unavoidable. Such grease or water as is present on the rails can provide at most a condition of partial lubrication.

RCF testing in the laboratory has always been carried out under lubricated conditions because it has been found to be impossible to propagate surface initiated RCF defects in the absence of a lubricant. Way [32] was the first to recognize that a fluid lubricant was necessary for RCF failures to occur. He suggested that rolling contact fatigue in the presence of a lubricant occurred by mechanical pressurization of the crack tip by the lubricant.

Consider the presence of a very small crack extending along the plane B-A, Figure 11 [32], If B-A is oriented such that the normal stress at A is less than that at B, penetration of the lubricant into the crack would cause a high tensile stress at A. Consider that the distributed oil pressure is  $p_2$  at the point B in Figure 11. The entrance of the lubricant into the crack would raise the pressure on the walls of the crack from a value less than  $p_2$  to  $p_2$ .

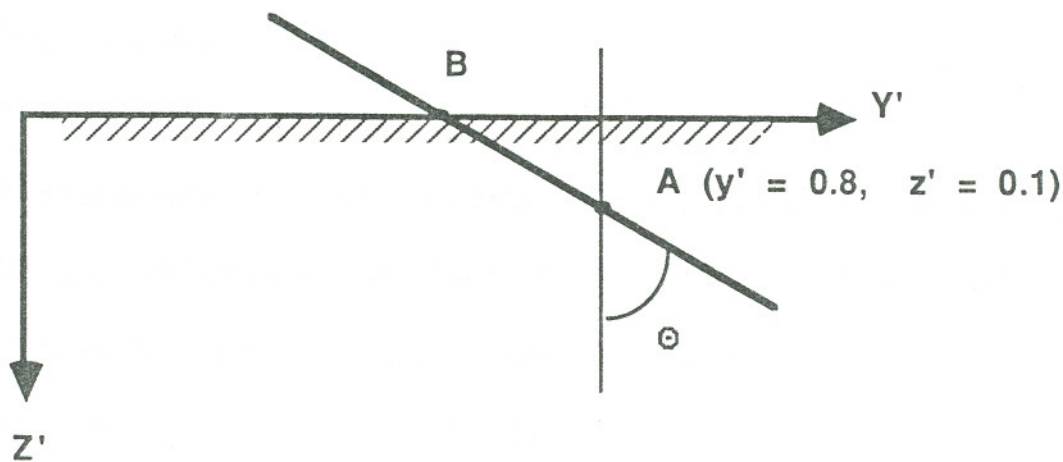


Figure 11 : Crack orientation [32]

The stress system resulting from these added forces on the walls of the crack would give a concentrated tensile stress at the end of the crack. This implies that the crack needs to be oriented such that the "mouth" of the crack enters the contact zone before the tip; otherwise, the lubricant would be forced out of the crack.

The general conclusions drawn by Way on the basis of his work are as follows [32]:

- \* *Presence of a lubricant is necessary for pitting [surface initiated RCF defects],*
- \* *The lubricant should be of a viscosity low enough to permit penetration of fine cracks,*
- \* *Even in the presence of a lubricant, cracks will grow only if they have a certain initial direction,*
- \* *The rougher the surface finish and the softer the initial substrate, the greater the chance of pitting,*
- \* *Pits originate from cracks that start at the surface.*

Since Way's experiments in 1935, numerous other researchers have done work to study the effect of lubricants and lubrication [29-31,39,68,69]. It has been found that rolling contact tests run without a lubricant give rise to much higher RCF lives than those run using a lubricant for the same load.

A typical example of this is provided by the results obtained by Ollerton and Morey [29]:

No Lubrication      at  $P_o = 220$  ksi :    Life > 32.1 M cycles

Oil Lubrication      at  $P_o = 236$  ksi :    Life = 1.51 M cycles

Water Lubrication    at  $P_o = 225$  ksi :    Life = 0.4 M cycles

In another test, a specimen was run dry for 40.4 M cycles at 284 ksi without any signs of failure. On the introduction of a lubricant, the specimen failed after just 300,000 additional cycles.

The above test shows that running under dry conditions modifies the surface to facilitate pitting upon the addition of a lubricant. Way explained that dry rolling, due to the localized deformation at, and under, the surface, gives rise to micro-fine cracks. In the absence of a lubricant, these cracks fail to propagate and remain as micro-fine cracks. Dawson [70] also found such cracks in the surface layers of both rollers. He called them embryonic cracks and found that they were typically  $1 \mu\text{m}$  long and contained within the surface layers. On adding a lubricant, the embryonic cracks in the test roller (the driven or slower moving roller) propagated while the ones in the standard (driving or faster moving) roller stayed the same. Although Ollerton and Morey's [29] results agree with Way's

conclusions, they report that there is no conclusive evidence that the cracks start from the surface and they found some cracks that had no apparent link to the surface. Burr's work [71] also points towards the same fact. Way, while not disputing that the cracks may indeed be totally sub-surface, doubts if such cracks could play any role in pitting.

That cracks can propagate only if they are inclined in a particular direction is shown by the work of Dawson [70], among others. In one experiment carried out by Dawson a sample was run with a lubricant until fine cracks developed. When the direction of rolling was reversed it was found that the cracks did not propagate.

The effect of lubricant viscosity can be seen in the work of Clayton and Hill [31]. They found that RCF life using glycerol lubrication was higher than when using other more viscous lubricants. This is so because the higher the viscosity of the lubricant, the more difficult it is for the lubricant to penetrate the fine cracks.

The mechanism of crack tip pressurization by fluid entrapment is not the only possibility in the propagation of surface breaking cracks in rolling contacts. Bower [38] considered two more mechanisms in addition to fluid entrapment; lubrication of the crack faces, and the hydraulic mechanism where the fluid is forced into the crack. He developed a theoretical model whereby the mode I and

mode II stress intensity factors, ( $\Delta K_I$  and  $\Delta K_{II}$  respectively) can be calculated for each of the three cases. For the case of crack face lubrication, only  $\Delta K_{II}$  was sufficiently high. The model also predicted the influence of the direction of loading. However, it has been found to be close to impossible to propagate cracks under mode II conditions in the presence of compressive stresses as are found in rolling contacts [72]; hence this mode of propagation has been discounted.

For the hydraulic mechanism Bower found that, although  $\Delta K_{II}$  was sufficiently high, its value was not sensitive to the direction of loading. Since experiments [70] have shown that crack propagation is sensitive to the direction of loading, this mechanism can also be discounted.

For the last mechanism, fluid entrapment, Bower found that the stress intensity factors were high enough to aid crack propagation and they were sensitive to the loading direction. From this Bower concluded that the mechanism of fluid entrapment was the only one that gave results consistent with experiments. However, the model predicts a complicated non-proportional cycle of mode I and mode II stress intensities at the crack tip, so it is difficult to predict the direction and rate of growth of the crack.

The possibility that the lubricant influences crack initiation as well as propagation, has also been investigated [31]. It has been suggested that the role

of the lubricant is to reduce wear of the surface to a level below which the embryonic cracks are allowed to stay and grow. Clayton and Hill [31] examined the effect of wear rate reduction, but showed that this alone would not result in RCF. Solid lubricants reduced wear to almost zero but did not result in fatigue cracks.

Recent results from Allery [73] suggest that the influence of lubricant viscosity on RCF life could be linked to crack initiation as well as crack propagation. In experiments started under dry conditions, with lubricant added later, lubricant viscosity had no effect on RCF life.

The laboratory experience that the presence of a fluid is required to develop RCF cracks has some support from field observations. In some track adhesion experiments in Japan [74] rails were maintained in a wet condition by a water spray. Severe problems with surface initiated RCF were encountered. When the rails were allowed to return to their natural state, not only did new RCF defects not form, but existing defects ceased propagating. RCF. Solid lubricants reduced wear to almost zero but did not result in fatigue cracks.

Recent results from Allery [73] suggest that the influence of lubricant viscosity on RCF life could be linked to crack initiation as well as crack propagation. In experiments started under dry conditions, with lubricant added later, lubricant viscosity had no effect on RCF life.

The laboratory experience that the presence of a fluid is required to develop RCF cracks has some support from field observations. In some track adhesion experiments in Japan [74] rails were maintained in a wet condition by a water spray. Severe problems with surface initiated RCF were encountered. When the rails were allowed to return to their natural state, not only did new RCF defects not form, but, existing defects ceased propagating.

### Slide/Roll Ratio

The slide/roll ratio is defined as the amount of sliding per unit distance rolled between bodies rolling against each other. The value of the slide/roll ratio depends upon the diameters of the bodies and their speeds of rotation. For the case of rolling/sliding testing machines, where the samples are run with their axes parallel, the slide/roll ratio,  $\gamma$ , is given by :

$$\gamma = \frac{2[R D_b - D_t]}{[R D_b + D_t]} \quad (4)$$

where,  $D_b$  and  $D_t$  are the bottom and top roller diameters respectively and  $R$  is the ratio of rolling speeds (in rpm) of the two rollers given by :

$$R = \frac{\text{Speed of bottom body}}{\text{Speed of top body}} \quad (5)$$

Laboratory experiments to study the effect of slide/roll ratio on RCF life have been carried out by a number of investigators. Clayton and Hill [31], testing cylindrical samples made of a 0.5% C rail steel, found that the highest RCF life was obtained under conditions of pure rolling, i.e. 0% slide/roll ratio, Figure 12 [31]. As the slide/roll ratio was increased, there was a complex dependence of RCF life on slide/roll ratio up to a value of about 5%. Beyond this the RCF life was essentially independent of the slide/roll ratio. The authors attributed the complicated effect of the slide/roll ratio on RCF life to the interactive effect of the slide/roll ratio with traction and surface roughness.

Using a twin disc machine and turbine oil as a lubricant, Ichinose *et al* [28] tested cylindrical samples made from rail steels having different microstructures. They found that the RCF life decreases when the slide/roll ratio is increased from 10% to 25% to 45%. For wheel/rail contact, the slide/roll ratio described previously can be considered as resulting from what has been termed the "longitudinal-tangential pressure distribution" by Martin and Hay [20]. According to the authors, this effect is mainly due to the fact that the axle and wheels of a railroad car act as one piece and the wheel on the high rail must travel a greater

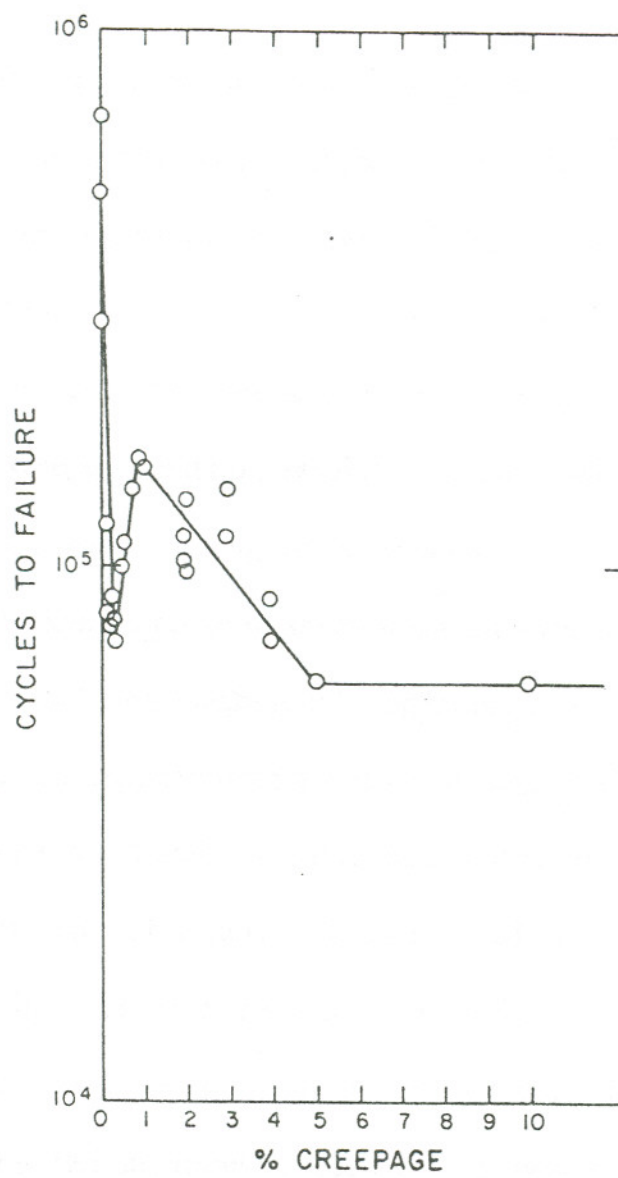


Figure 12 : Effect of slide/roll ratio on RCF life [31]

distance than the one on the low rail. In track the rail which is on the outside of a curve is elevated (banked) with respect to the inner rail to make curve negotiation easier. Hence the outer rail is designated the "high" rail and the inner rail is the "low" rail.

A second kind of tangential pressure distribution, termed the "transverse tangential pressure distribution", results from the back and forth motion of the wheels along the rails. Using finite element analysis, Martin and Hay [20] calculated the maximum range of shear stress for various combinations of normal, transverse tangential, and longitudinal tangential pressure distributions, Table III. They found that the application of a transverse tangential load directed away from the centerline of the rail and a longitudinal slip directed opposite to the direction of motion, combined with a normal load, resulted in the greatest range of shear stress. If the tangential forces were directed in the opposite directions, the range of shear stresses was the least. The authors proposed that these cases represent the high and low rail situations respectively. Laboratory tests carried out on a twin disc machine using SAE 30 oil as a lubricant resulted in the formation of a shell under the first set of conditions after 1.2 M cycles while the second set of conditions did not lead to failure even after 2.5 M cycles.

Martin and Hay's work [20] dealt with the second maxima of the shear stress range that occurs in the sub-surface, and they assumed that the maximum

shear stress range is a measure of the RCF life of the rail.

Sugino *et al* [55] reported plastic flow in the running surface of rails in service that appeared to be rotating around an axis perpendicular to the running surface, Figure 13 [55]. The authors tried to explain this phenomenon as follows. Consider that the rail surface receives from the wheels a small tangential force at right angles to the traffic direction, towards the gauge side, in addition to a positive tangential force acting in the direction opposite to the traffic direction on the gauge side and a negative tangential force acting in the same direction as the traffic direction on the field side. While the explanation seems to describe their observations, there is no proof of the existence of the negative tangential force on the field side.

**Table III : Range of maximum shear stress [20]**

LOAD <sup>a</sup>			Range of Shear Stress (ksi)
Normal <sup>b</sup>	Transverse	Longitudinal	
+1	+0.1	+0.1	62.3
+1	+0.1	0	61.4
+1	+0.1	-0.1	62.8
+1	0	+0.1	58.5
+1	0	0	57.5
+1	0	-0.1	58.7
+1	-0.1	+0.1	56.1
+1	-0.1	0	55.2
+1	-0.1	-0.1	55.0

a Positive value indications

Type of load	Direction
Normal	Downward
Transverse	Toward the gage corner
Longitudinal	Same as rolling direction

b 19,000 lb wheel load assumed, no yielding occurs and transverse and longitudinal loads are multiples of normal load.

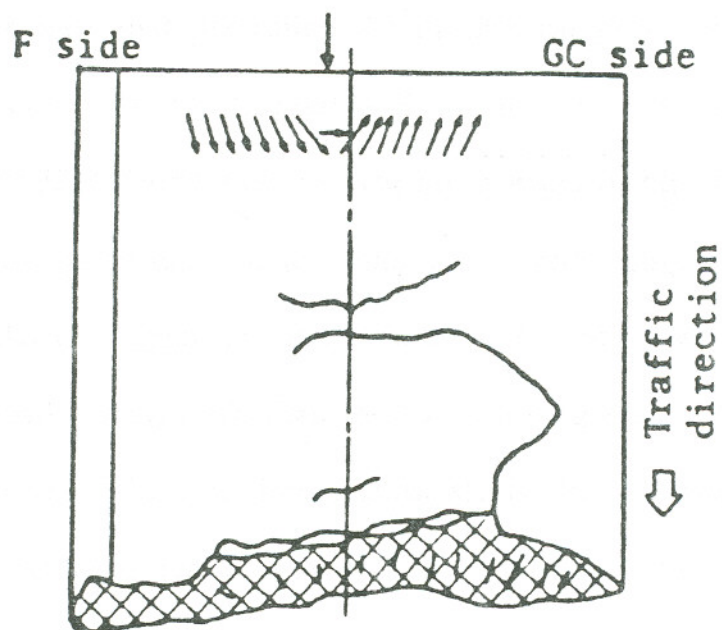
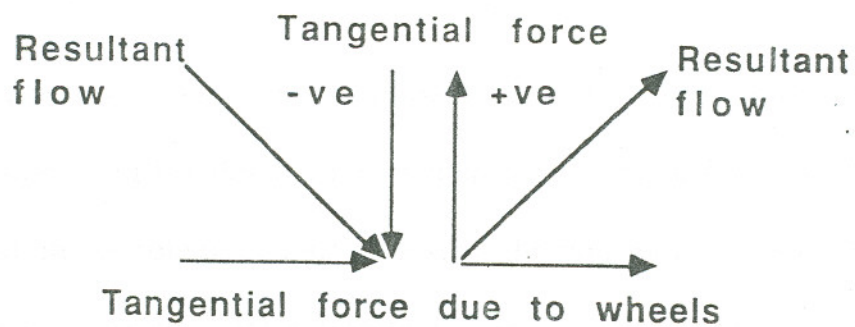


Figure 13 : Plastic flow in the rail head [55]

### Mechanical Properties and Microstructure

To date, not much work has been done to directly study the effect of either mechanical properties or microstructure on the performance of rail steels under conditions of rolling contact. Most of the conventional rail steels in use at present are of a pearlitic microstructure. For pearlitic steels, one of the most important parameters that determine the mechanical properties is the pearlitic interlamellar spacing [44,75]. In relating RCF life to microstructural parameters, Masumoto *et al* [22] found that in laboratory experiments, steels with a fine pearlite structure performed better than those with tempered martensite or bainite. Similarly, Sugino *et al* [76] showed that steel with a pearlitic microstructure had a longer life than steel with a tempered martensitic structure of comparable tensile strength. For pearlitic steels, they concluded that RCF life increases with increasing tensile strength. Recent results from Devanathan [77] show that certain kinds of bainitic structures can perform at least as well as pearlitic structures of comparable hardness values.

Decreasing the pearlitic interlamellar spacing of the steel results in a higher hardness and higher tensile strength [2,22,44,45,76,78]. As previously mentioned, (p6) the most common methods used to improve the tensile strength of the steel, or refine the pearlitic interlamellar spacings in rail steels, are heat treating the rail or adding alloying elements to the steel [22,43-46]. In the case of

heat treatment of the rail, the lower diffusion rates of carbon at lower isothermal transformation temperatures result in a refinement of the pearlitic microstructure. The addition of alloying elements like Cr, V and Mo retard the diffusion of carbon and hence give rise to finer pearlitic interlamellar spacings.

Besides the hardness and tensile strength of the material, the only other mechanical properties that have a significant effect on the RCF life of rail steels are fatigue resistance in conventional fatigue tests and resistance to deformation. Some of the previously reported work [17,45] shows that the higher the tensile strength of the steel, the higher is its resistance to fatigue crack initiation and propagation. However, there is no quantitative relationship between the fatigue resistance in conventional testing and RCF.

Ollerton and Morey [29] tried to use the results of a reverse torsion fatigue test to predict the lifetime to failure under rolling contact conditions. They found that the ranking of the steels under rolling contact conditions and reversed torsion conditions were the same. Ichinose *et al* [28], testing rollers made of various rail steels under oil lubricated conditions, found that cracks propagate into the substrate only up to the depth of the deformed/work-hardened layer. Similar results are reported by Kalousek and Bethune [51]. Hence, if the strength of the material is high enough to resist the deformation taking place in the surface layers, it should have a higher RCF life.

Results from Qiu [19] show that the steel with the highest tensile strength and hardness had the best performance in RCF, wear and conventional fatigue tests. Also, in the steel with the highest tensile strength, the maximum depth of cracks was smallest compared to steels of lower tensile strengths.

### WHITE ETCHING LAYER AND RAIL GRINDING

Increasing axle loads and tonnages have led to the use of more wear resistant and higher strength steels. Such premium rails have found widespread use in curves on heavy haul lines. These rails were expected to perform well in service; however, in some cases [79] they have had to be replaced prematurely due to problems with rolling contact fatigue defects. In one instance, the head hardened low rails of 2° and 3° curves of unit coal train lines have had to be removed from track after only 200 million gross tons (MGT) of traffic compared to an expected life of >800 MGT. The cause was deep spalling from the center of the rail running surface. Laboratory tests [19] have shown that the head hardened rail is superior in all respects to both a conventional standard carbon and a premium alloyed rail steel, and no obvious metallurgical reason could be found for the premature failure of the rail.

The current practice of grinding the rail head to prevent corrugations also serves to curtail surface-initiated rolling contact fatigue damage [33]. Using a model developed to determine the economical timing for rail grinding and renewal, Roney *et al* [80] suggested grinding at intervals of 4 months for standard carbon rails and 8 months for heat treated standard carbon rails to remove all

visible signs of surface damage. They predict that this would lead to substantial improvement in the life of the rail along with considerable savings in maintenance and replacement costs.

According to Worth *et al* [27], grinding the rail at a stage where fatigue damage is visibly evident is of little value. They argue that once fatigue cracks have propagated from the shallow damaged layers into the underlying material, it is almost impossible for any reasonable depth of grinding to remove all the cracks. The cracks that remain after grinding continue to propagate at the same rate as before and can lead to spalling.

The paper by Worth *et al* [27] refers to spalling on the gauge corner of head hardened rails in the high rails of curves laid on concrete ties. On the basis of studies of rails removed from the track because of excessive spalling, they have suggested the following measures to improve rail life : (1) use of more conformal rail head profiles to reduce contact stresses and the formation of the white etching layer, (2) use of "superclean" steels to reduce the number of sites for cracks to propagate from the white etching layer into the pearlite matrix, (3) frequent, shallow (0.125 - 0.175 mm) grinding of rails.

They suggested that one of the most important factors contributing to initiation of RCF cracks is the white etching layer of about 900 HV hardness (as

compared to a base metal hardness of 350 HV) found on the rail running surface. Such white etching layers have also been reported by Clayton and Allery [18]. They found that a majority of the rails in service showed the presence of a white etching layer, to varying depths and extent, with a hardness up to 1000 HV. Although the white etching layer was associated with some surface cracks, the authors discounted the white etching layer as a cause of surface initiated "squat" defects in British track. However, in light of the work by Worth *et al* [27], the role of the white etching layer in surface initiated rolling contact fatigue failures warrants further study.

Similar white etching layers have been found to be produced by various machining processes [81,82]. In a review of the literature, Griffiths [82] points out that, while the hardness and appearance of the various white etching layers are similar, they could have different structures and be formed by different mechanisms. White etching layers of hardness in the range of 800 - 1300 HV could be formed by high temperatures, surface reactions, plastic deformation or some combination of these effects.

Newcomb and Stobbs [83] characterized the white etching layer on a BS 11 rail (as per Table I) using transmission electron microscopy and showed it to

be of a fully martensitic structure. They concluded that at an anticipated slip of 1%, austenitization of the rail head is extremely unlikely. An alternative explanation was proposed in which the white etching layer was considered to be ferrite containing dislocations supersaturated by carbon transfer from the carbides during the high frequency pulsed shear fatigue of the rail surface.

## **CHAPTER 2 : EXPERIMENTAL TECHNIQUES**

### **MATERIALS**

#### **Model Development**

Four commercial steels were used to develop a model relating the hardness/pearlite interlamellar spacing, maximum Hertzian contact stress and RCF life. These steels were received in the form of 4 foot lengths of unused rails. The chemical composition of these rails is given in Table IV.

#### **Model Validation**

Five specially prepared heats, I1 - I5, Table V, containing varying amounts and kinds of inclusions, were supplied by D. Fegredo of CANMET, in the form of 6"x6"x2" blocks in the as-rolled condition. These steels were also used in the studies carried out to validate the model.

#### **Sub-surface Deformation Studies**

Sub-surface deformation tests were carried out on an Amsler twin-disc machine and a MTI testing machine. For Amsler tests, the test rollers were made

**Table IV : Chemical compositions of rail steels**

Rail (OGI #)	Hardness Rc (HK)	Chemical Composition (Wt. %)							S $\pm \sigma_N$ (Å)	Incl. Vol. Fract.(%)
		C	Cr	Mo	Mn	Si	S	P		
A (X21)	28.0 (249)	.72	<.01	<.01	.85	.10	.032	.027	2848 $\pm$ 185	0.392 $\pm$ 0.108
B (X95)	29.5 (301)	.73	.17	<.01	.93	.28	.029	.008	2432 $\pm$ 141	0.204 $\pm$ 0.025
C (X87)	31.4 (304)	.67	.52	.16	.57	.35	.010	.007	2433 $\pm$ 226	0.146 $\pm$ 0.063
D (X84)	37.6 (327)	.74	.42	<.001	.92	.54	.004	.016	1809 $\pm$ 103	0.040 $\pm$ 0.021

**Table V : Chemical compositions of I series steels**

	Hardness	Chemical Composition* (Wt.%)					Comments
	Rc (HK)	C	Mn	Si	S	P	
I1	39.6 (380)	.68	.83	.35	.025	.011	"Dirty" Steel
I2	35.7 (355)	.70	.82	.32	.004	.010	Small oxides
I3	41.3 (420)	.69	.81	.40	.004	.009	Large Silicates
I4	38.1 (384)	.74	.74	.26	.006	.008	"Clean" Steel
I5	38.4 (381)	.76	.75	.27	.030	.009	----

\* Manufacturer's Analysis

from rail steel "B" (Table IV, p52). Test rollers for the MTI machine were made from three different materials.

Initially test rollers were made from a 1045 steel. The 1045 steel was in the form of a cylinder with a hard chromium coating (about 1 mm thick). For ease of machining, the cylinder was annealed (as described later) to soften the hard surface coating, resulting in a hardness of 18 HRc (185 HK); hence this material is referred to as the 1045 as-annealed. Since, for later tests, it was necessary to have the standard roller of a significantly higher hardness than the test roller, the 1045 as-annealed steel rollers were subjected to another heat treatment cycle.

This produced rollers of hardness about 51 HRc (520 HK). These rollers are designated as 1045 annealed + hardened. Test rollers made from rail steel "B" (Table IV, p52) were also used in MTI tests.

### Crack Growth and White Etching Layer Studies

For white phase and crack growth studies of rails in service, rail samples (F01 - F20) were received from a site trial carried out for Burlington Northern Railroad (BN). These rail samples were taken from both ends of a curve at mile posts (MP) 97.3 and 97.6.

Additional rail samples (G01 - G04) were taken from another curve in BN track with a prior history of surface initiated RCF. Samples were taken from both the high and low rails, just prior to and just after grinding, to supplement the data from the previously mentioned curve.

Laboratory tests to study crack growth rates and the effect of the white etching layer (WEL) were carried out on rail steel "B" (Table IV, p52). These tests were carried out on the Amsler testing machine.

### Tests to Study the Effect of Lubricant

At the start of the program, Amsler tests were carried out using two different lubricants; oil and water. The reason for these tests was to determine which of the two lubricants would be most suitable for use in subsequent tests. Since oil lubrication gave much higher RCF lives than water lubrication, it was decided to use water as the lubricant for the later tests.

These preliminary tests, using two different lubricants, have been used to study the effect of lubricant on RCF life. Rail steel "A" (Table IV, p52) was used in these series' of tests. Unlike the remaining tests in which the bottom (standard) roller was made from rail steel "B", the bottom roller for these tests was made from rail steel "A".

### Lubricants

All tests on the Amsler machine were run using water lubrication, except for one series of the preliminary tests and the sub-surface deformation tests. For the preliminary tests, one series was run using a light mineral oil having no additives. For sub-surface deformation tests a solid moly-disulfide lubricant and SAE40 motor oil were used.

The sub-surface deformation tests run on the MTI machine used the solid moly-disulfide lubricant and a SAE40 motor oil. A summary of the steels used for the different tests is given in Table VI.

**Table VI : Summary of materials used**

	Material	HK	Used For
A	Standard carbon rail steel	249	* Model development * Effect of lubricant
B	Standard carbon intermediate strength rail steel	301	* Model development * WEL RCF tests * Subsurface deformation * Crack growth rates
C	Chromium-molybdenum rail steel	304	* Model development
D	Silicon-chromium rail steel	327	* Model development
E	1045 steel	---	* Subsurface deformation
F	Head-hardened Nippon Kokan Koshua rail	---	* Crack and WEL studies in rails in service
G	Head-hardened Nippon Kokan Koshua steel	---	* Crack and WEL studies in rails in service
I	Steels with varying inclusion types and contents	---	* Model validation

### SITE TRIAL

To date there has been very little published work dealing with the behavior of cracks and WEL in rails in service. To gather data on the growth of cracks and the influence of the WEL, a site trial was carried out for Burlington Northern Railroad (BN).

The site trial was conducted in a newly rerailed three degree curve on wood ties in BN track at MP 97, Grand Island, Nebraska. In keeping with the emerging BN rail grinding policy at the time, all rails were ground immediately after being laid. The traffic on this line is 100 ton capacity car unit coal trains with an annual tonnage of about 110 MGT. The previous rails used at this location had experienced severe problems with surface initiated RCF on the running track of the rail head, Figure 14 [79].

Samples, typically 18" long, from both ends of the curve (MP 97.3 and MP 97.6), from both the high and the low rails, were taken from the track at 6.7, 10.8, 16.1, 48.2, 52.4 (just prior to grinding) and 53.5 MGT (just after grinding). The first sample involved removing 15 feet of rail and replacing it with a welded-in plug rail. The second sample was taken by removing the plug rail plus

two further feet of the original rail and replacing it with a longer plug rail. In this way, only a single replacement weld was required and all the samples were from the same rail.

Rail samples were also taken from another curve (at MP 54) to supplement the data from the curve at MP 97. All samples were amply protected against rusting and surface damage during transit to the laboratory. Details of all these rails are given in Table VII.

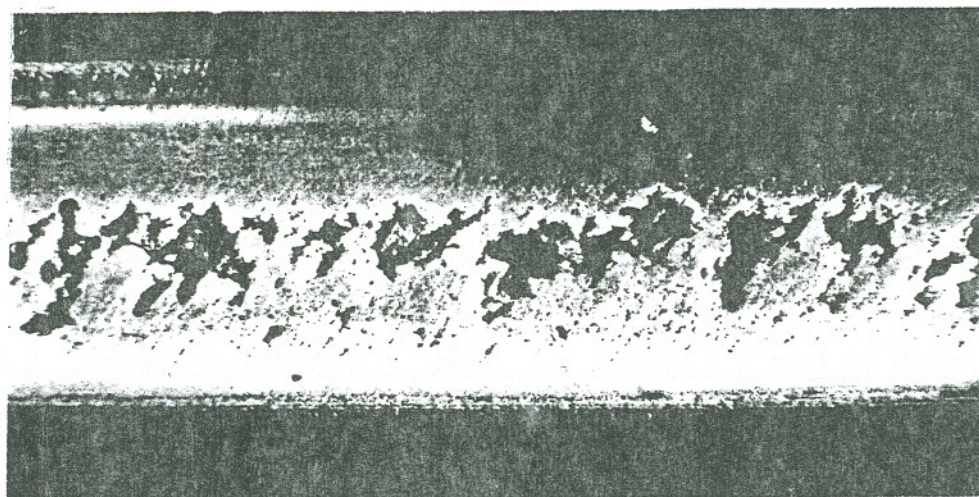


**Figure 14 : Spalling in head hardened rail in BN track [79]**

**Table VII : Details of rail samples for crack and WEL studies**

Rail	OGI Rail #	End #	High/Low	Date Removed	Total MGT	Comments
F01	X42	MP 97.6	Low	9/12/86	6.7	
F02	X43	MP 97.6	High	9/12/86	6.7	
F03	X40	MP 97.6	Low	9/26/86	10.8	
F04	X41	MP 97.6	High	9/26/86	10.8	
F05	X45	MP 97.6	Low	10/15/86	16.1	
F06	X44	MP 97.6	High	10/15/86	16.1	
F07	X46	MP 97.3	Low	10/24/86	23.1	
F08	X47	MP 97.3	High	10/24/86	23.1	
F09	X48	MP 97.6	Low	1/13/87	48.2	
F10	X50	MP 97.6	High	1/13/87	48.2	
F11	X49	MP 97.3	Low	1/13/87	48.2	
F12	X51	MP 97.3	High	1/13/87	48.2	
F13	X54	MP 97.6	Low	2/9/87	52.4	Pre-grinding
F14	X55	MP 97.6	High	2/9/87	52.4	Pre-grinding
F15	X52	MP 97.3	Low	2/9/87	52.4	Pre-grinding
F16	X53	MP 97.3	High	2/9/87	52.4	Pre-grinding
F17	X58	MP 97.6	Low	2/12/87	53.5	Post-grinding
F18	X59	MP 97.6	High	2/12/87	53.5	Post-grinding
F19	X56	MP 97.3	low	2/12/87	53.5	Post-grinding
F20	X57	MP 97.3	High	2/12/87	53.5	Post-grinding
G01	X36					Unground
G02	X37					Unground
G03	X38					Ground
G04	X39					Ground

## RCF TESTING

### The Amsler Twin Disk Rolling/Sliding Testing Machine

Most of the initial RCF testing was carried out on the Amsler Twin Disk Rolling/Sliding testing machine, Figure 15.

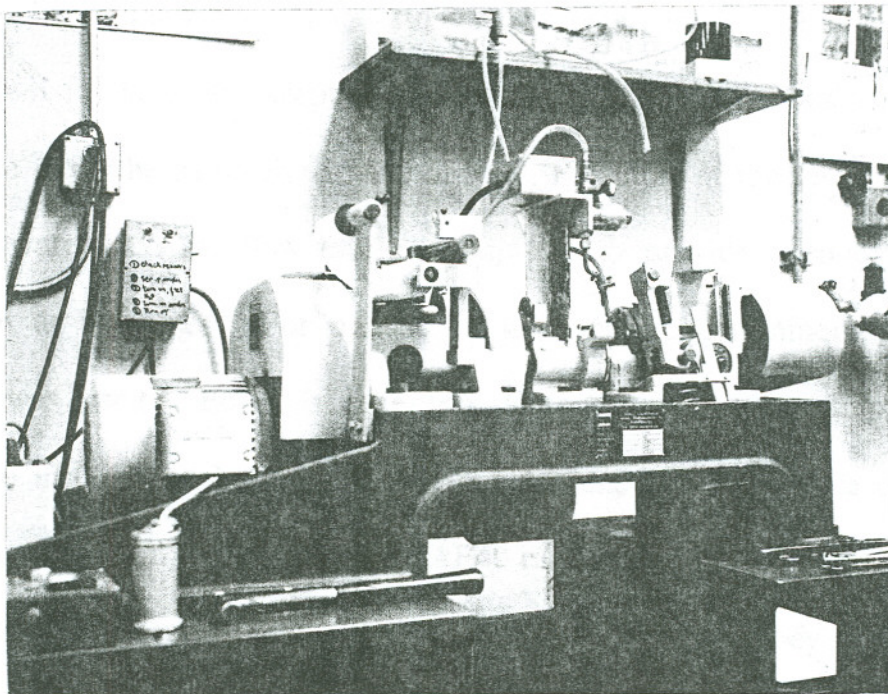


Figure 15 : Amsler Twin Disk Rolling/Sliding Testing Machine

The sample rollers are mounted on two parallel rotating shafts, and the load is applied by means of a compressed spring that provides a range of 0 - 2000N. The bottom shaft is driven by a motor and the upper shaft is driven by gearing to the bottom shaft. This results in the bottom shaft rotating 1.104 times faster than the upper shaft. In all the tests, the upper roller was made of the material being tested because, in RCF tests, the failures occur in the driven or slower moving roller [70]. The bottom rollers were made from the as-received "B" rail steel for all tests except for one series of tests where the bottom rollers were made from the as-received "A" rail steel. For most of the tests, the lubricant used was water and the flow rate was adjusted to provide a condition of over lubrication at all times. For one series of tests, a light mineral oil with no additives was used. For this case too, a condition of over lubrication was maintained throughout the test. In the tests to generate sub-surface deformation, a moly-disulfide solid lubricant and a SAE40 motor oil were used.

For all the tests, except the sub-surface deformation study tests, 35.00 mm diameter top rollers and 35.04 mm diameter bottom rollers were used. The truncated cone on flat geometry, shown in Figure 16, was used for the top roller to provide high enough contact stresses while at the same time providing sufficient support for the material in the running track. The running track on the top roller was 4 mm and the width of the bottom roller was 10 mm. These roller

dimensions along with the difference in speeds of rotation of the shafts ( $\omega_B = 1.104 \times \omega_T$  or  $R = 1.104$ ) provided a slide/roll ratio of 10% as calculated from Equation 4 (p37).

In these tests, it was desired to keep the slide/roll ratio constant throughout the duration of the test. However, as the test progresses, there is some change in the roller dimensions as a result of wear and/or plastic deformation and this leads to variations in the slide/roll ratio. Clayton and Hill [31] have shown that minor variations in the slide/roll ratio in the range of 5 - 10% do not significantly affect RCF life, hence the value of 10% was selected.

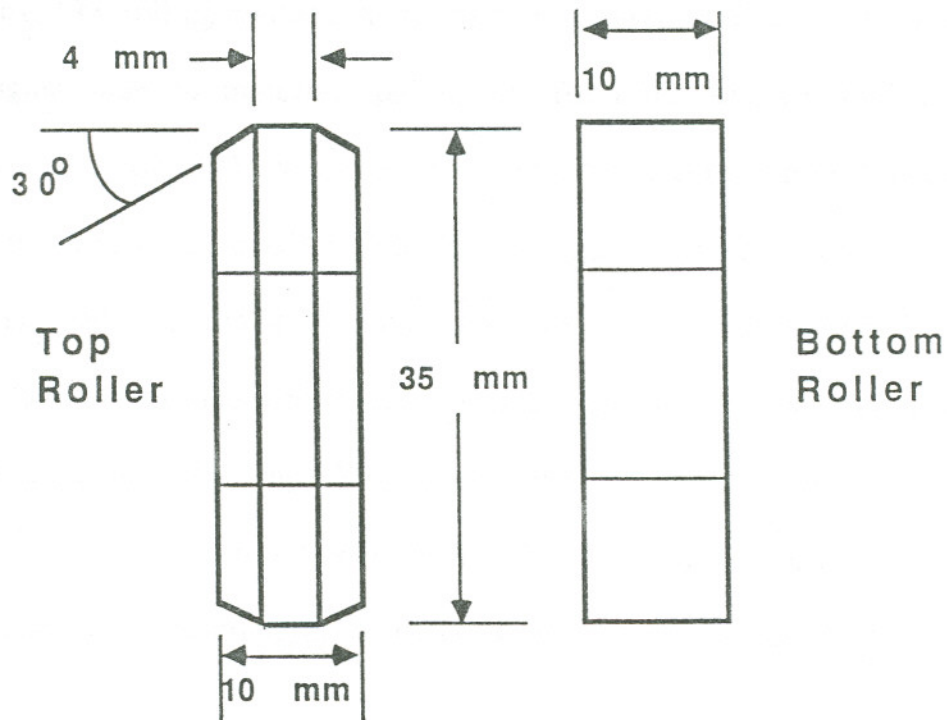


Figure 16 : Amsler roller geometries

For one of the sub-surface deformation study tests, the top roller was 35.00 mm in diameter with a running track width of 10 mm whereas the bottom roller was of the standard dimensions. In another test, the top roller was of the standard dimensions, whereas the bottom roller had a diameter of 31.70 mm to provide a slide/roll ratio of 0%.

A counter on the bottom shaft kept track of the number of revolutions during the test. A chart recorder, connected to a torque dynamometer, provided a continuous record of the torque from which the coefficient of friction was calculated. An accelerometer mounted on the machine was used to measure the vibration caused by rolling contact. As the test progressed, and the roller surfaces became rougher, due to material spalling off from the surface, the level of vibration increased. When the vibration level exceeded a certain preset value, the accelerometer activated a cut-off switch that shut off the machine and the water supply and released a methanol rinse onto the rollers to prevent rusting. Thus the criterion of failure was one which was not solely crack initiation but included crack propagation and spalling. With experience it was possible to set the accelerometer to a near constant level for all the tests. While the accelerometer enabled the tests to run unattended and was extensively relied upon to determine

RCF life, it was not the only means used to detect failure. When spalls appeared on the roller, the noise level increased audibly and this was taken as an indication of failure and the test was stopped.

In order to complete testing within a reasonable time span, a fatigue limit of 1.4 M cycles was chosen. Samples that did not exhibit any external signs of surface damage at 1.4 M cycles were assumed to be "run outs".

A summary of the parameters used for the various test series' is given in Table VIII.

**Table VIII : Summary of Amsler test series and parameters**

Test Series	#	Steel
Model Development	i-a	A
	i-b	B
	i-c	B1
	i-d	B2
	i-e	B3
	i-f	B4
	i-g	C
	i-h	C1
	i-i	C2
	i-j	C3
	i-k	C4
	i-l	D
	i-m	A
Model Validation	ii-a	I1
	ii-b	I2
	ii-c	I3
	ii-d	I4
	ii-e	I5
Effect of Lubricant	i-m	A
	iii-a	A
Subsurface Deformation	iv-a	B
	iv-b	B
Crack Growth Rate Studies	v	B
WEL Studies	vi	B

$D_T = 35.00$  mm

$D_B = 35.04$  mm except iv, where  $D_B = 31.70$  mm for some tests

Top roller running track = 4 mm, except iv, where it was 10 mm for one test

Lubricant was water except iii-a where a light mineral oil was used, iv-a where a SAE40 motor oil was used and iv-b where a solid moly-disulphide lubricant was used

Slide/roll ratio was 10%, except for iv where it was 0% for some tests

Contact load range was 0 - 2000 N

### The MTI Testing Machine

In the MTI testing machine, Figure 17, the test rollers are mounted on two parallel horizontal shafts that are geared together. Power input is through the lower shaft and the upper shaft is driven from it by a set of phasing gears.

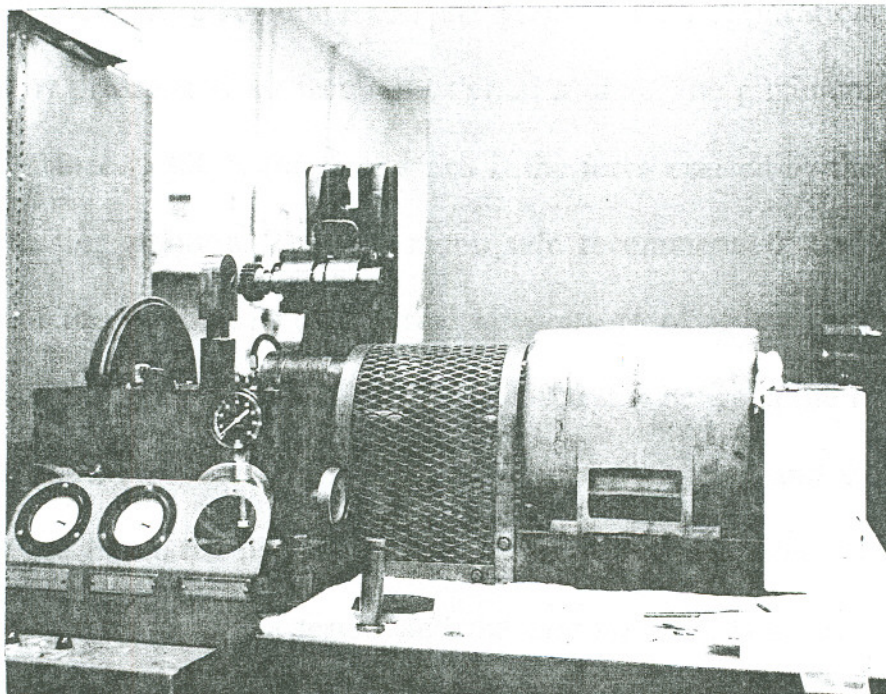


**Figure 17 : The MTI Testing Machine**

The upper shaft is mounted in a frame which is hinged at one end to the base that holds the lower shaft. This results in a "nutcracker" type of mechanism, Figure 18. The upper frame can be pivoted up for installation and inspection of the test rollers.

The load is applied to the free end of the upper frame through a lever arrangement which is actuated by a pneumatic cylinder. The rollers are located midway between the pivot point and the point of load application. The load is controlled by pressurized air from an external source. The minimum load without a counterbalance is 300 N (66 lbs), which is the force exerted by the upper frame in the operating position. The maximum, safe recommended load for extended operation of the machine is an external air pressure of 59 psi on the pneumatic cylinder that results in a load of 363636 N (80000 lbs) between the rollers.

The bottom shaft is driven at 1800 rpm by a motor and the top shaft is rotated by gearing to the bottom shaft. In all the tests carried out, the top roller is made of the material being tested and the bottom shaft is made of a standard reference material. The machine is provided with nine different sets of phasing gears that give a variety of differential rotational speeds, Table IX. The slide/roll ratio between the rollers can thus be varied from -142 to 0 to 142%, by varying the roller diameters and the gear set used to drive the upper shaft.

The bearings on the shafts and the gears are lubricated by flooding them with a SAE40 motor oil at about 50°F. For oil lubricated tests, the same oil used to lubricate the gears and bearings was used to lubricate the rollers by directing a jet of oil at the point of contact of the rollers.

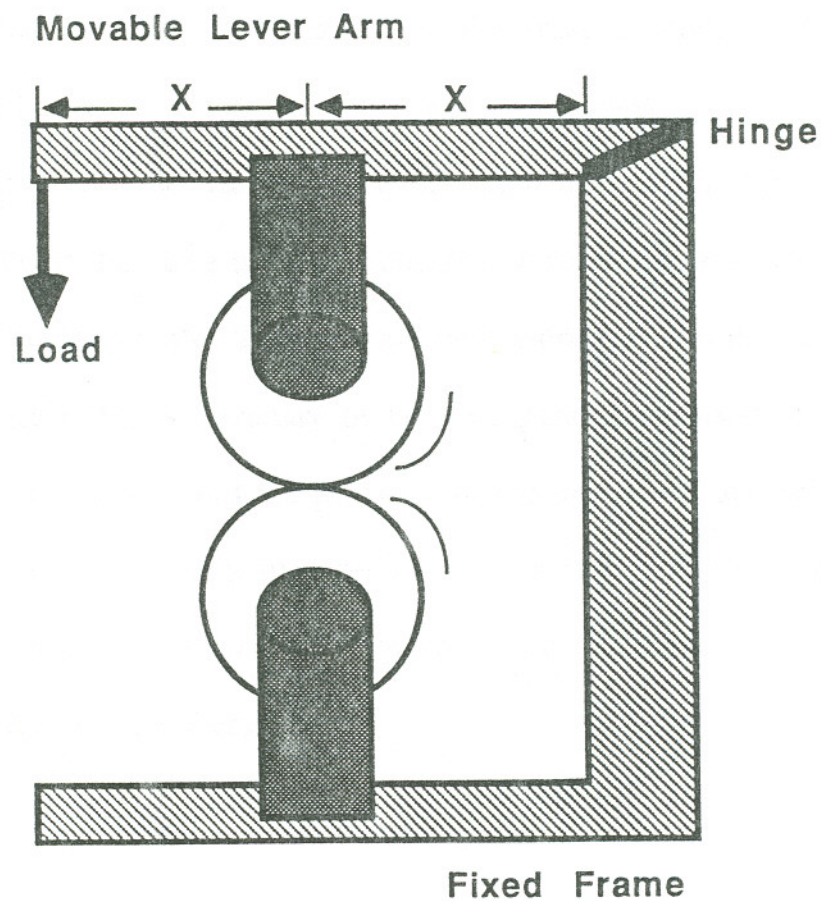
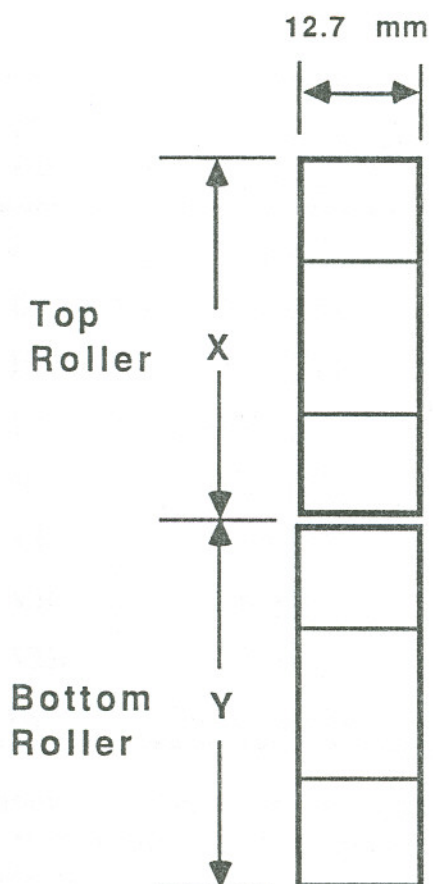


Figure 18 : Schematic of the MTI machine

The oil is collected in the tank enclosing the entire machine assembly and is recirculated after being passed through an oil/water separator and a series of filters. For tests using the solid moly-disulfide, the test was stopped periodically (55000 cycles - 0.5 hours) and the lubricant was applied by means of a syringe.

A mechanical counter is provided on the bottom shaft to count the number of revolutions during the test. For sub-surface deformation studies, the rollers were run for a fixed number of cycles and the test was stopped.

The diameters of the rollers were selected to provide the required slide/roll ratio while at the same time maintaining the requisite 76.2 mm (3") gap between the centers of the shafts. The running track width for both the rollers was 12.7 mm (0.5"), Figure 19. A summary of the test parameters used is given in Table X. Cut-off pressure switches are provided in the pneumatic and oil lines to shut off the machine in the event of a preselected pressure drop in either line. This prevents the gears from crushing together and overheating in case of excessive deformation of the rollers.



	1	2
X (mm)	76.2	61.0
Y (mm)	76.2	91.4

Figure 19 : MTI roller geometries

**Table IX : Ratios of rotational speeds**

Gear Pair	Pairing		X*	N**	R***
	Bottom	Top			
I	1Y85 [27]	1Y90 [32]	27	05	1.185
II	1Y86 [24]	1Y87 [36]	24	12	1.500
III	1Y91 [28]	1Y88 [31]	28	03	1.107
IV	1Y89 [29]	201-C-38 [30]	29	01	1.035
V	1Y92 [20]	1Y93 [40]	20	20	2.000
VI	1Y95 [22]	1Y94 [38]	22	16	1.727
VII	S.S. [12]	1Y227 [58]	12	46	4.833
VIII	L.S. [16]	1Y226 [56]	16	40	3.500
IX	201-C-38 [30]	201-C-38 [30]	30	00	1.000

The above combinations (i.e. top Gear > Bottom Gear) have been selected in order to provide rotational speed ratios greater than or equal to unity. Numbers in brackets, correspond to # of teeth on the gear.

\* : X = # of teeth on the bottom (smaller) gear

\*\* : N = Difference in # of teeth (Top - Bottom)

\*\*\* : R =  $1 + (N/X)$  : Used in Slide/roll ratio calculations

**Table X : Summary of parameters for MTI tests**

Test Series	#	Steel	D <sub>T</sub> mm (")	D <sub>B</sub> mm (")
Subsurface Deformation	vii-a	1045AA*	76.2 (3.0)	76.2 (3.0)
	vii-b	1045AA	76.2 (3.0)	76.2 (3.0)
	vii-c	1045AA	76.2 (3.0)	76.2 (3.0)
	vii-d	1045AA	61.0 (2.4)	91.4 (3.6)
	vii-e	B	61.0 (2.4)	91.4 (3.6)

\* 1045AA is the 1045 steel used in the as-annealed condition

D<sub>T</sub> = Top roller diameter

D<sub>B</sub> = Bottom roller diameter

Slide/roll ratio = 0%

Top and bottom roller running track widths = 12.7 mm (0.5")

Bottom rollers made from 1045 annealed + hardened steel except vii-a where they are made from 1045AA steel

Lubricant used was SAE40 motor oil for all except vii-b where solid molydisulphide lubricant was used

Contact load range is 0 -30 psi of inlet air pressure

## HEAT TREATMENTS

### Model Development

Cylindrical bars were machined from the heads of the B and C rails as shown in Figure 20. The bars were austenitized at 1500°F (816°C) for 1 hour

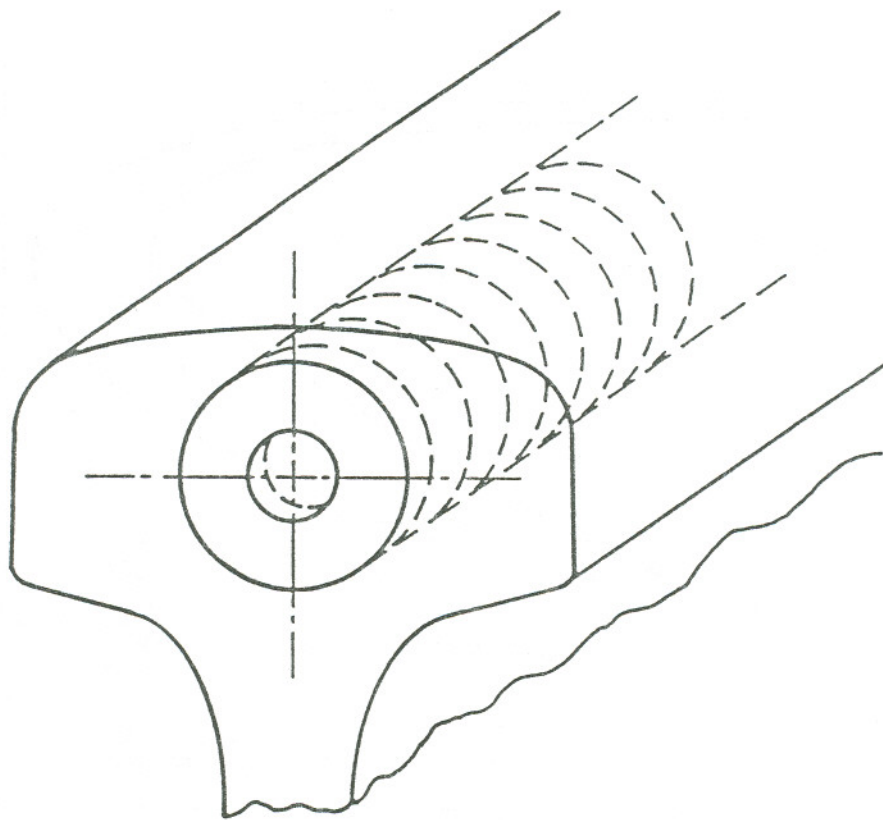


Figure 20 : Bars from rails for heat treating

and quenched to one of several isothermal transformation temperatures in a salt bath, Table XI. The temperatures given in Table XI are the measured temperatures of the salt bath. After holding at this temperature to allow full transformation, as determined from standard ITT curves (Figures 21 & 22), [84,85], the bars were quenched to room temperature in cold water.

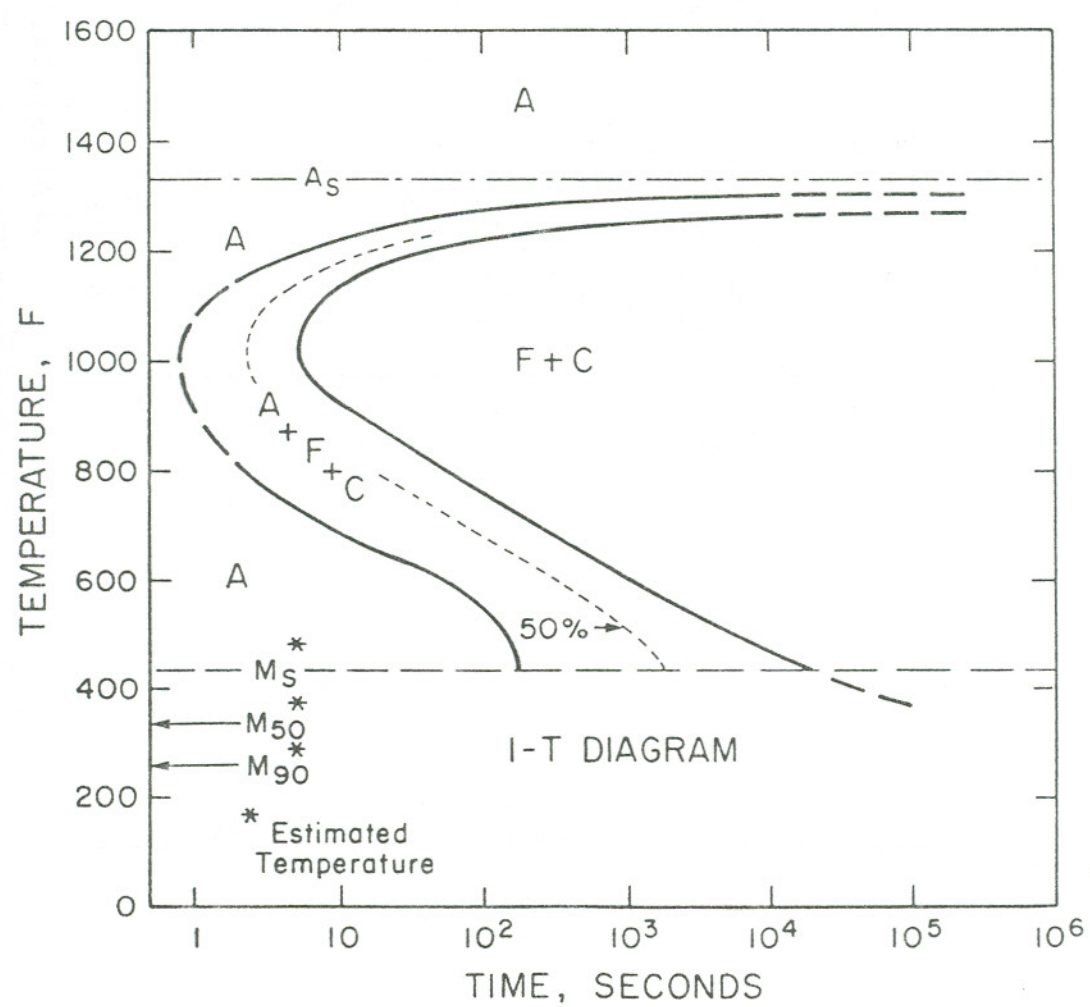


Figure 21 : ITT curves for standard carbon steels [84]

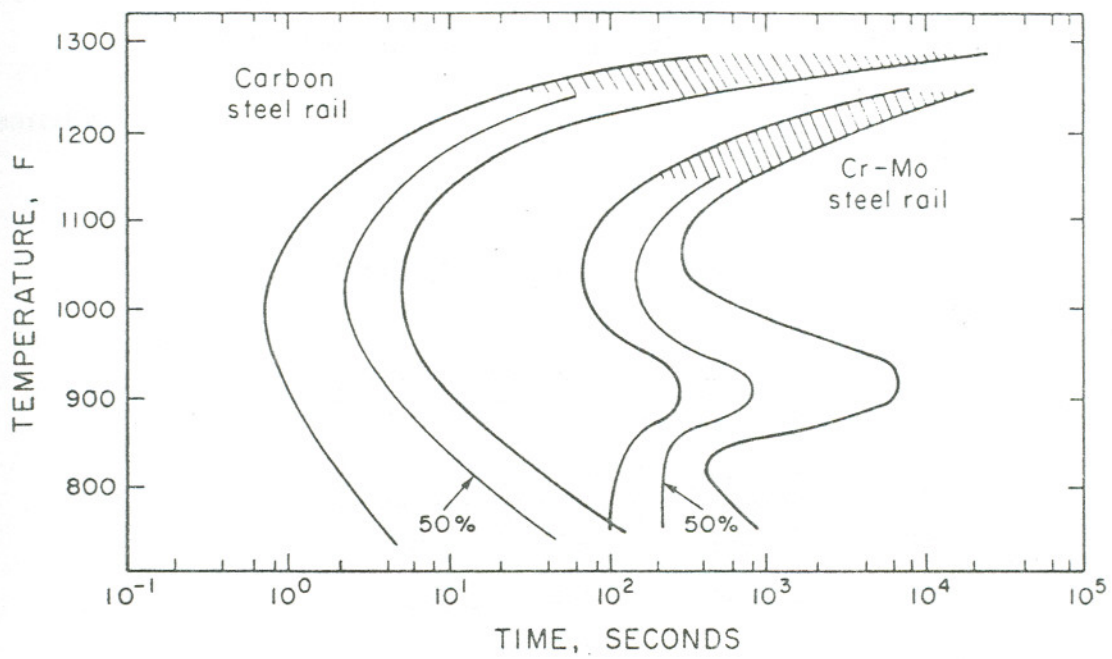


Figure 22 : ITT curves for chromium molybdenum alloyed steel [85]

These heat treatments provided a series of samples having different pearlite interlamellar spacings and hardness values. The heat treating temperatures for the two materials are given in Table XI.

Upper rollers for the Amsler RCF test were machined from these heat treated bars.

**Table XI : Salt bath temperatures**

Series	T*	
	(°F)	(°C)
B1	388	(198)
B2	985	(529)
B3	1150	(621)
B4	1200	(649)
C1	690	(366)
C2	990	(532)
C3	1100	(593)
C4	1250	(677)

\* Temperature of salt bath

### MTI Rollers

The 1045 steel used in the MTI tests was in the form of a 114.3 mm (4.5") diameter cylinder having a hard chromium coating (about 1 mm thick). For ease of machining, the as-received 1045 cylinder had to be heat treated to get rid of the hard surface layer. The heat treatment consisted of holding the steel at 1200°F (689°C) for 8 hours and then furnace cooling it to room temperature. Hence the MTI machine test rollers machined from this material are referred to as being from the 1045 as annealed steel.

For later tests, it was desired that the reference roller have a significantly higher hardness than that of the test roller. Hence rollers were machined from the same as annealed 1045 steel that was used in the preliminary tests, leaving sufficient tolerances for dimensional changes during heat treatment. The rollers were then individually heated at 1000°F (538°C) for 2 hours and then quenched to room temperature in cold water, resulting in an average hardness of 50 HRc. The heat treated rollers were then machined to final dimensions.

## RCF TEST ROLLERS

### Amsler Rollers

Amsler test rollers were machined from the different steels in such a manner that the hardness along the running track was uniform. For the A, B and C rail steels (Table IV, p52) the hardness from the running surface on the rail head towards the web of the rails was fairly constant (Figure 23a), hence, RCF rollers were machined from the "vertical" orientation as shown in Figure 23b. For the D rail, (Table IV, p52) the hardness varied significantly from the head to the web (Figure 24a), hence, RCF rollers were machined from the "horizontal" orientation as shown in Figure 24b. The difference in roller orientation (with respect to the rail head) has no effect on RCF life [19].

RCF rollers from the heat treated rail steels were taken as shown in Figure 20, p68.

For the I series steels, (Table V, p53) RCF rollers were taken from the blocks so as to maximize the number of rollers (Figure 25).

For all but one series of tests, the bottom rollers were machined from the as-received B steel; the exception being the "i-m" series of tests, (Table VIII, p65) where the bottom rollers were made from the A steel.

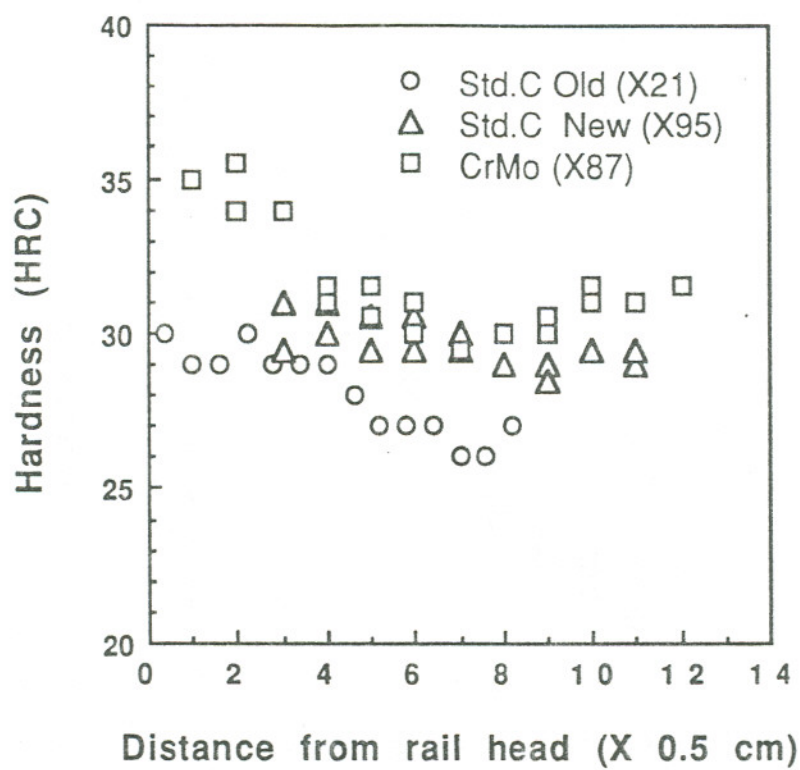


Figure 23a : Hardness profiles for A, B and C rails

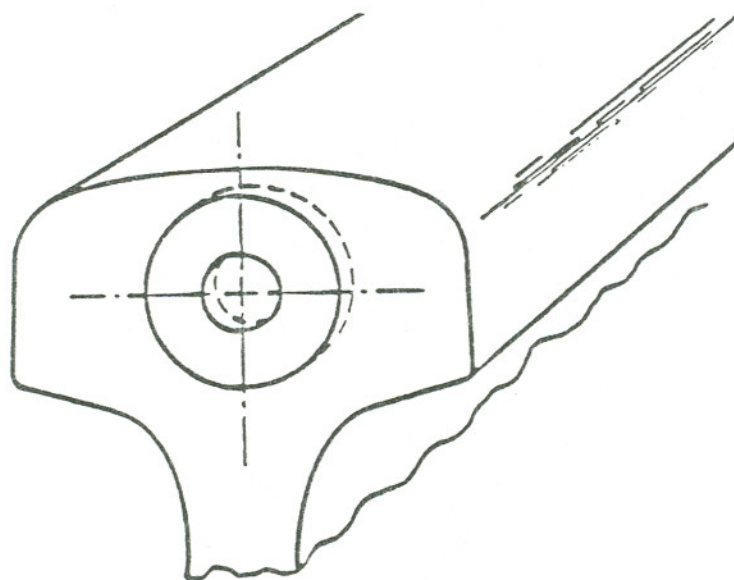


Figure 23b : Rollers from A, B and C rails

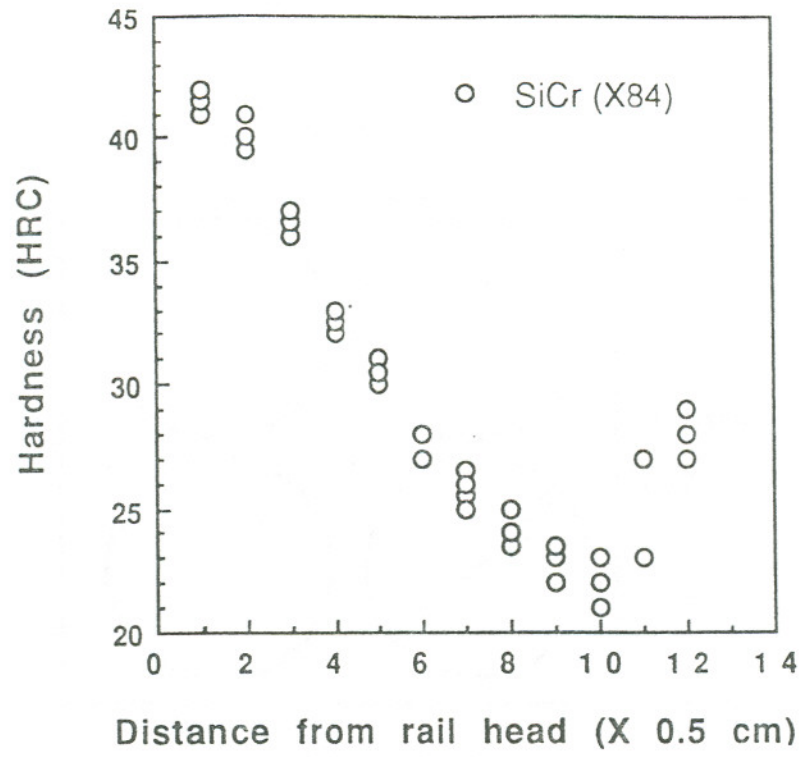


Figure 24a : Hardness profile for D rail

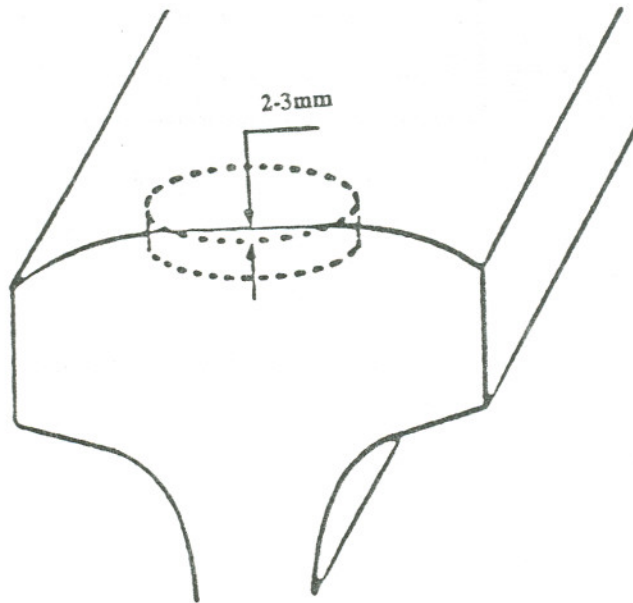
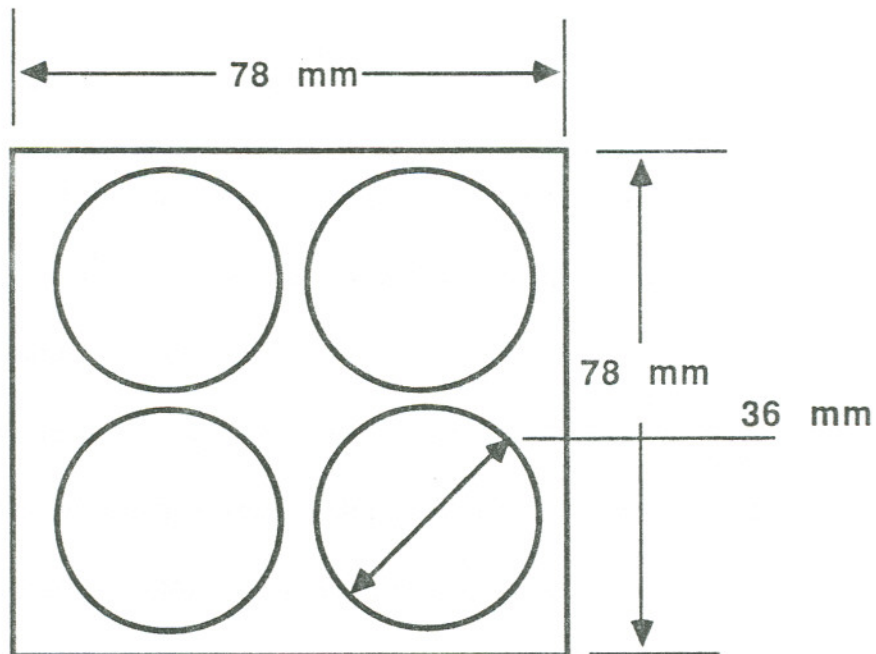
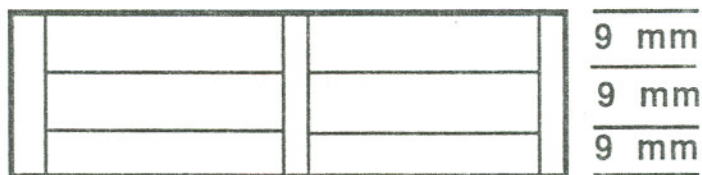


Figure 24b : Rollers from D rail



PLAN VIEW



SIDE VIEW

Figure 25 : Rollers from I series steels

### MTI Rollers

Initially, both the test and bottom rollers for the MTI test were machined from the 1045 as annealed steel bars. For later tests, the reference rollers were made from the same 1045 steel, but used in the annealed + hardened condition.

For MTI tests on rail steel "B", series "vii-2", (Table VIII, p65), rollers were machined from the as-received steel, from the orientation shown in Figure 26. This orientation was chosen to maximize the diameter of the rollers that could be machined from the rail head, while at the same time providing a reasonably constant hardness along the running track.

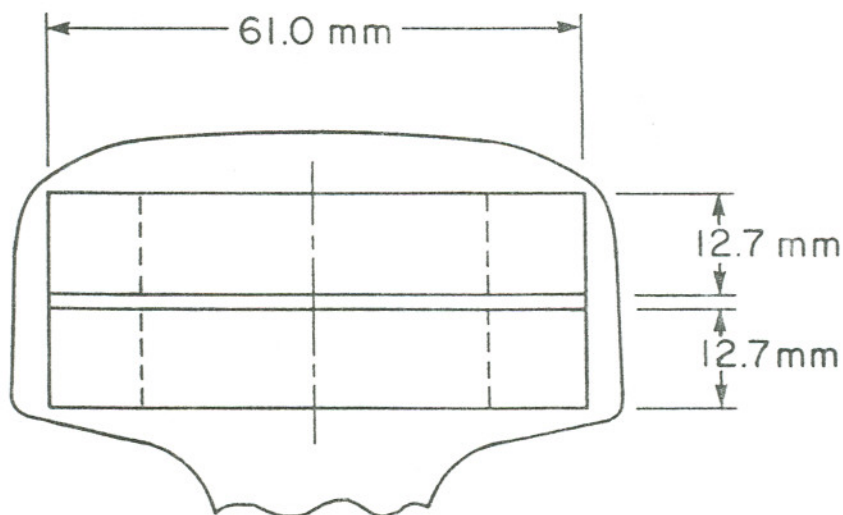
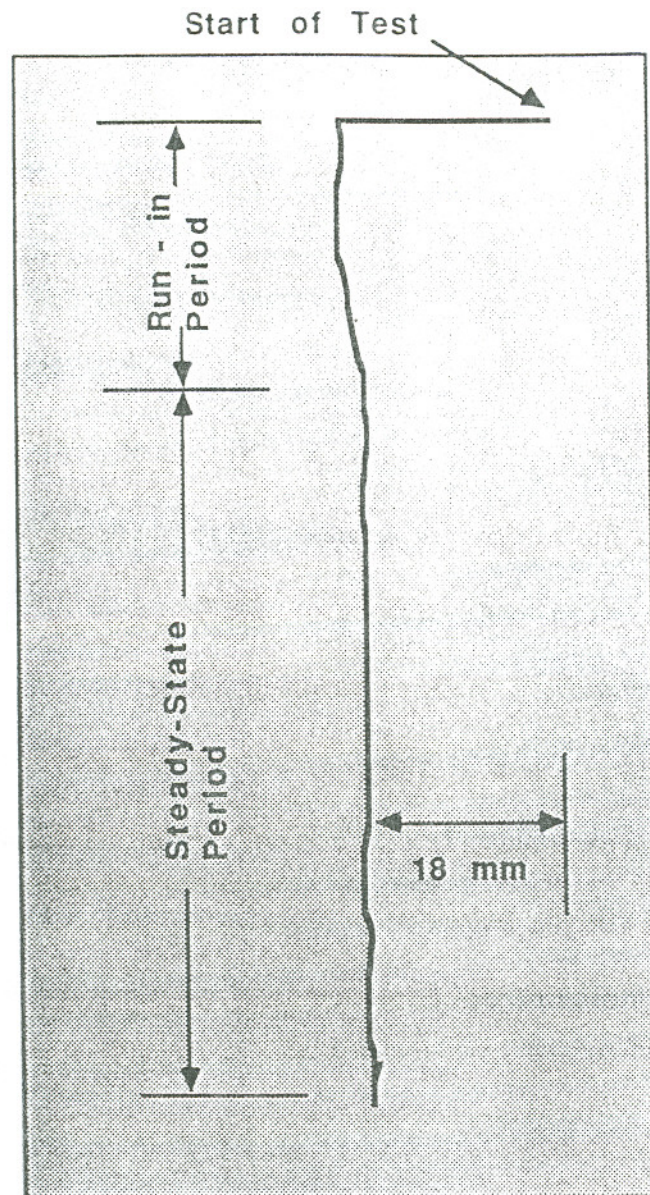


Figure 26 : MTI rollers from B steel

### RCF TESTS TO STUDY EFFECT OF LUBRICANT

Two different lubricants, water and a light mineral oil, were used in the preliminary tests to determine the lubricant for subsequent tests. Series' of RCF tests were run with each lubricant using the test conditions given in Table VIII, p65. The chart recorder on the Amsler machine is connected to a torque dynamometer and gives a continuous record of the torque. A schematic of the plot from the chart recorder is shown in Figure 27. After an initial period of higher friction, the value stabilizes to what can be termed the "steady state" value. On the graph, 40 mm corresponds to a coefficient of friction of 0.5. By measuring the height of the graph in the steady state region, the coefficient of friction can be calculated.



$$\mu = (0.5/43\text{mm}) * 18\text{mm} = 0.21$$

Figure 27 : Schematic of friction trace from Amsler machine

### SUB-SURFACE DEFORMATION TESTS

Previous research has succeeded in generating wholly sub-surface contained deformations in rolling contact tests [31,64,65]. Clayton and Hill [31] found that using a solid lubricant in free rolling tests (the test roller is driven only by the friction between the rollers) reduced the coefficient of friction to values well below 0.02, and under these conditions, they were able to get wholly sub-surface contained deformation in the test roller. Numerous tests were run on the Amsler and the MTI machines using a SAE40 motor oil or a solid moly-disulfide lubricant (series iv, Table VIII, p65); each providing a coefficient of friction lower than 0.05. The parameters were varied slightly from test to test to try and generate wholly sub-surface contained deformation in the test roller, Tables XII and XIII.

Table XII : Summary of Amsler RCF tests for sub-surface deformation

Test #	Test Roller	Bottom Roller	Width	$P_o$ (N/mm <sup>2</sup> )	Lubricant	Cycles
SSA01	35mm Steel B	35mm Steel B	10mm	895	MoS <sub>2</sub>	100000
SSA02	35mm Steel B	31.7mm Steel B	4mm	1450	MoS <sub>2</sub>	500000
SSA03	35mm Steel B	31.7mm Steel B	4mm	1450	MoS <sub>2</sub>	1000000
SSA04	35mm Steel B	31.7mm Steel B	4mm	1450	SAE40	1398000
SSA05	35mm Steel B	31.7mm Steel B	4mm	1450	MoS <sub>2</sub>	1535000
SSA06	35mm Steel A	31.7mm Steel B	4mm	1450	SAE40	3800000
SSA07	35mm Steel A	31.7mm Steel B	4mm	1450	SAE40	25000

Slide/roll ratio = 0% for all tests except SSA07 where the test was run under free rolling conditions

**Table XIII : Summary of MTI RCF tests for sub-surface deformation**

Test #	Test Roller	Bottom Roller	Load *	Cycles	Comments
SSM01	3.0" 1045AA	3.0" 1045AA	15psi	1000000	Surface deformation
SSM02	3.0" 1045AA	3.0" 1045AA	20psi	9000	Excess heating of samples
SSM03	3.0" 1045AA	3.0" 1045AA	20psi	64800	Corrugations
SSM04	3.0" 1045AA	3.0" 1045AA	30psi	9700	SUBSURFACE DEFORMATION Also corrugations
SSM05	3.0" 1045AA	3.0" 1045AA+H	30psi	141000	Excessive plastic deformation
SSM06	3.0" 1045AA	3.0" 1045AA+H	18psi	219800	Surface deformation
SSM07A	3.0" 1045AA	3.0" 1045AA+H	14psi	3200	Rollers scuffed - wrong gears
SSM07B	3.0" 1045AA	3.0" 1045AA+H	14psi	523800	WEL due to scuffing
SSM08	2.4" Steel B	3.6" 1045AA+H	10psi	1000000	Surface deformation
SSM09	2.4" Steel B	3.6" 1045AA+H	10psi	5000	Excessive vibration
SSM10	2.4" Steel B	3.6" 1045AA+H	10psi	800000	Pitting in bottom roller
SSM11	2.4" Steel B	3.6" 1045AA+H	10psi	5000	Micro-cracks in surface

\* Load represents inlet air pressure

### RCF TESTS FOR CRACK GROWTH STUDIES

To study the development of cracks in laboratory samples, a series of six RCF tests (series v in Table VIII, p65) were run on the Amsler machine using the as received "B" rail steel (Table IV, p52)

Instead of letting the tests run until failure, for this series, the tests were run for a specific number of cycles and stopped. The six tests were run for 5000, 10000, 50000, 100000, 151000 and 206000 cycles. The maximum Hertzian contact pressure was  $1302 \text{ N/mm}^2$  and the slide/roll ratio was 10%. A condition of over lubrication was maintained during the tests using water.

Transverse and longitudinal specimens from the test rollers were prepared for metallographic observation. Metallographic specimens were used in the unetched condition to measure the maximum crack depth and in the etched condition for measurement of the depth of deformation. Microhardness traverses were made on the longitudinal specimens.

### RCF TESTS ON WHITE ETCHING LAYER SAMPLES

The behavior of the white etching layer (WEL) occurring in rails in service was studied using rail samples from a field trial. However, it was impossible to get RCF test rollers from these rails so as to retain the WEL on at least a part of the roller surface.

Using an electro-spark deposition unit, WEL was generated on RCF test rollers from rail B (Table IV, p52). For the first test the WEL was generated at only certain locations along the roller running track and for the second test the whole running track was covered by overlapping layers of WEL. These tests are designated the vi series (Table VIII, p65).

To check the similarity of the WEL occurring in service and the WEL generated using the electro-spark deposition technique, WEL was first deposited on a section from rail B. Samples were taken from this section for metallographic studies and the WEL hardness was measured.

### REPEATABILITY TESTING

To check the reproducibility of the rolling/sliding testing machines used, tests were repeated under identical conditions. For the Amsler machine repeat tests were carried out on rail steel B rollers at  $1302 \text{ N/mm}^2$  and  $1413 \text{ N/mm}^2$ .

Six tests were run at  $1302 \text{ N/mm}^2$  using water lubrication and keeping all the test conditions the same. The only difference was the total width of the test rollers used. For three of the tests the total width of the test roller was 9 mm, for one test it was 8 mm and for the remaining three it was 10 mm. Test rollers of different widths were used to see if there would be any influence of the width on RCF life. This had to be checked since the number of rollers from the "I" series steels (Table V, p53) could be maximized by using 9 mm width rollers (Figure 25, p76).

Of the three tests carried out at  $1413 \text{ N/mm}^2$ , two used test rollers with a total width of 10 mm while the third used a test roller with a total width of 9 mm.

## SPECIMENS FOR METALLOGRAPHIC OBSERVATION

### Failed RCF Test Rollers

The failed Amsler and MTI machine test rollers were sectioned to obtain transverse and longitudinal specimens as shown in Figure 28. The specimens were nickel plated to provide good edge retention during the grinding and polishing operations.

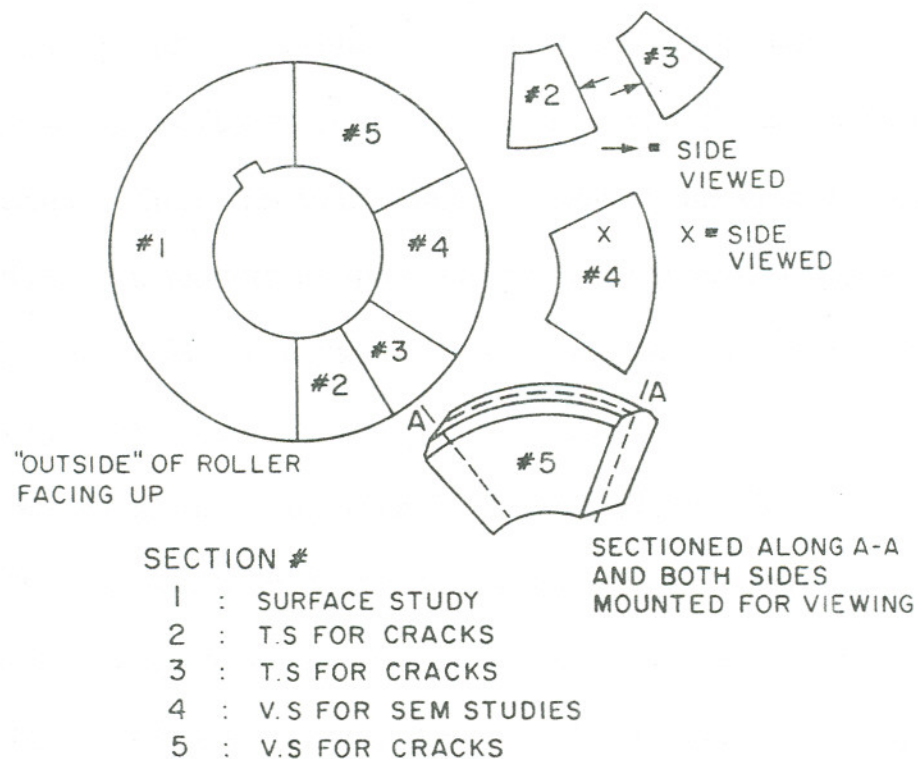


Figure 28 : Sectioning of failed RCF rollers

The nickel plated specimens were then mounted, ground and polished to a 0.25  $\mu\text{m}$  surface finish using standard specimen preparation techniques. The specimens in the as-polished condition were used for inclusion counts and crack studies. The same specimens after etching in a 2% nital solution were used for pearlite interlamellar spacing measurements and studies of the deformed layers in the rollers.

#### Crack and White Phase Study Samples from Rails in Service

Initially, the dye penetrant technique was used to highlight the areas on the rail that had surface cracks present, to determine the location from which to take specimens. Since, this method failed to show up any surface cracks specimens were taken from random locations on the rail. On metallographic observation, these specimens showed numerous cracks to be present. Hence, for later rail samples, specimens were taken at random locations.

Specimens were taken from the F and G (Table VI, p56) rails as shown in Figure 29. Care was taken to minimize heating of the samples during sectioning by using a low enough cutting speed and a copious supply of coolant.

Each specimen was marked prior to being plated so that its orientation with respect to the position in track was known. All transverse specimens were mounted so that they were viewed from the west side of the curve, i.e., in the

micrographs the direction of loaded travel is into the plane of the paper. The specimens, about 100 in number, were nickel plated, mounted, ground and polished to a  $0.25 \mu\text{m}$  surface finish.

Transverse specimens numbered 2, 3 & 4 (in Figure 29) were examined in the unetched condition and used to determine crack depths and densities. The same specimens etched in a 2% nital solution were used to study the white etching layer (WEL) and its relation to the cracks. These specimens were chosen to characterize RCF cracks and the WEL since they represented the location where the service problem occurred (p53 and Figure 14, p54).

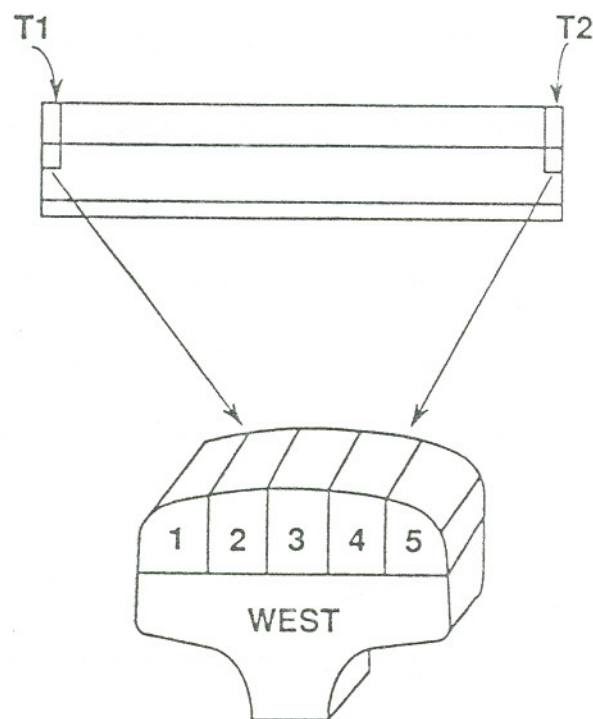


Figure 29 : Sectioning of F and G rails

### PEARLITE INTERLAMELLAR SPACING MEASUREMENTS

The circular intercept method described by Vander Voort and Roosz [86] was used to make measurements of the pearlite interlamellar spacings. The fineness of the pearlitic structure in the steels necessitated the use of a scanning electron microscope (SEM) for resolution of the lamellae. In the SEM used, the magnification displayed on the screen is not always the actual magnification of the image. Hence it was necessary to calibrate the magnification before making pearlite lamellae counts. For magnification calibrations, microhardness indentations, known distances apart, were made on the specimen. Measuring the distance between these indentations on the SEM screen at the working magnification, the actual magnification can be calculated.

A test circle of 100 mm diameter (314 mm circumference) was placed on the SEM screen and the intersections of the carbide lamellae with the test circle were counted. The spacing values reported are an average of at least 19 separate fields. To eliminate operator bias in field selection, the specimen was moved in a predetermined pattern.

The working magnification was selected so as to provide the maximum number of test circle/carbide lamellae intersections, while at the same time

ensuring that the orientation of the lamellae within the test circle was substantially constant.

The average of the intercept counts,  $n$ , was used to calculate the true mean pearlite interlamellar spacing,  $S$ , using the following relationship :

$$S (\mu\text{m}) = \frac{(\pi \times D)}{2 \times M \times n} \quad (6)$$

where,  $D$  is the diameter of the test circle (in mm) and  $M$  is the actual magnification of the SEM image.

The confidence intervals of the measurements were calculated using the method given in ASTM E-112-85 [87].

## INCLUSION COUNTS

Samples for inclusion counts were observed in the unetched condition. Care was taken during sample preparation to ensure that the inclusions were retained in the matrix and not pulled out due to excessive pressure. The volume fraction of inclusions was measured according to the method given in ASTM E-542-83 [88]. This method is based on the principle that a two dimensional area fraction can be used to provide a good estimate of the volume fraction of the microconstituent phase.

Measurements were made on an optical microscope at a magnification of 400x, by projecting the image onto a ground glass screen. A 20x20 grid with a line spacing of 2.54 mm (0.1") was superimposed on this image and the number of intersections of the grid points with the inclusions was counted. The inclusion volume fractions reported are averages of at least 20 separate fields. To avoid operator bias in field selection, the sample was moved in a predetermined manner.

The average of the counts of the fields,  $n_i$  can be used to calculate the volume fraction of inclusions,  $V_F$ , as given by the following relationship :

$$V_F (\%) = \frac{n_I}{M} \times 100 \quad (7)$$

where  $M$  is the magnification of the image on the ground glass screen.

The 95% confidence intervals, CI, of the counts were calculated using :

$$CI = 2 \times \sigma_n \times n^{-0.5} \quad (8)$$

where,  $\sigma_N$  is the standard deviation of the counts and  $n$  is the number of fields counted.

### HARDNESS MEASUREMENTS

Rockwell C hardness measurements were made on samples that were ground to a uniform surface finish. The measurements were made using a diamond indenter and a load of 150 kg.

The microhardness measurements reported are Knoop hardness values made using a 500 gm load, unless otherwise mentioned. These measurements were made on the samples prepared for metallographic observation.

### CALCULATION OF MAXIMUM HERTZIAN CONTACT STRESS

The maximum Hertzian contact stress is a function of the applied load, dimensions and material properties of the bodies. For two rollers in contact with each other with their rolling axes parallel, the maximum Hertzian contact stress,  $P_o$ , is given by Equations 1 and 2, p13 [56].

Using  $\nu_1 = \nu_2 = 0.3$  and substituting for  $\Delta$  in Equation 1 we get :

$$P_o = 0.418 \left[ \frac{PE (R_1 + R_2)}{2a (R_1 R_2)} \right]^{\frac{1}{2}} \quad (9)$$

where  $2a$  is the contact width as shown in Figure 3, p14.

## CHAPTER 3 : RESULTS

### MODEL DEVELOPMENT

#### Heat Treatments

Rail steels B and C (Table IV, p52) were each subjected to four different isothermal heat treatments (Table XI, p76). These heat treatments gave a range of samples having varying hardness and pearlite interlamellar spacings, Table XIV. Figure 30 shows a plot of the hardness versus the temperature of the salt bath furnace.

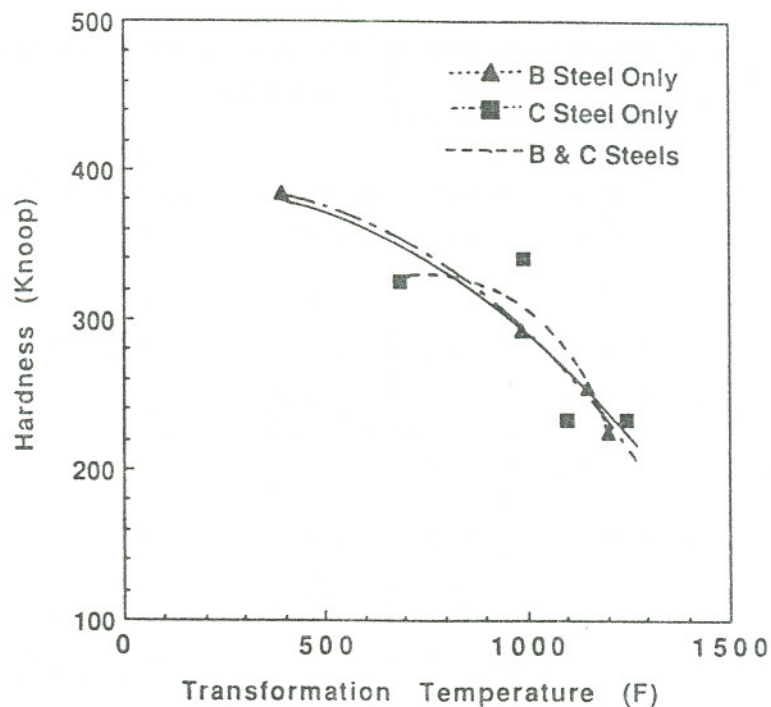


Figure 30: Hardness versus salt bath furnace temperature

Figures 31 and 32 show the range of pearlitic microstructures obtained by the heat treatments. Figures 33 and 34 show the microstructures of the samples obtained by heat treating rail steel C at 690°F (366°C) and 1100°F (593°C). The microstructure in Figure 33 is not a fully pearlitic one but rather a transitional one between pearlitic and bainitic. Due to the absence of lamellae in the microstructure, it was not possible to measure the pearlite interlamellar spacing. Figure 34 shows a significant amount of spheroidization of the carbides hence a representative pearlite interlamellar spacing could not be determined.

**Table XIV : Heat treated steel hardness and pearlite spacings**

Series	IT Temperature		Hardness		S $\text{\AA} \pm \sigma_N$
	(°F)	(°C)	Rc	HK	
B1	388	(198)	36.6	385.3	$876 \pm 70$
B2	985	(529)	30.0	292.9	$1754 \pm 105$
B3	1150	(621)	24.5	253.6	$2617 \pm 178$
B4	1200	(649)	18.1	225.6	$3434 \pm 326$
C1	690	(366)	33.9	325.0	--- $\pm$ ---
C2	990	(532)	37.0	340.4	$1433 \pm 90$
C3	1100	(593)	20.2	234.0	--- $\pm$ ---
C4	1250	(677)	15.4	233.8	$3038 \pm 167$

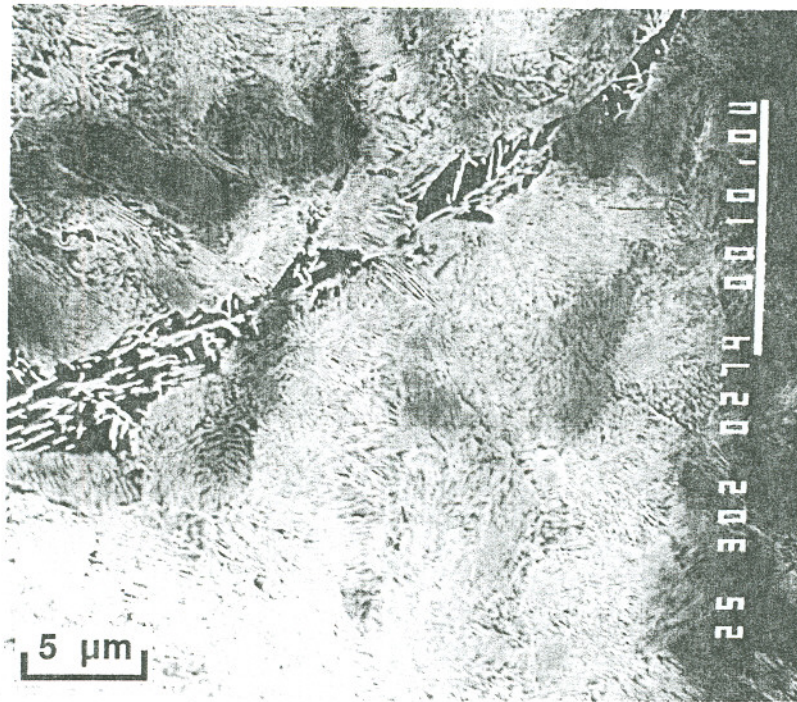


Figure 31 : Pearlitic microstructure from B1

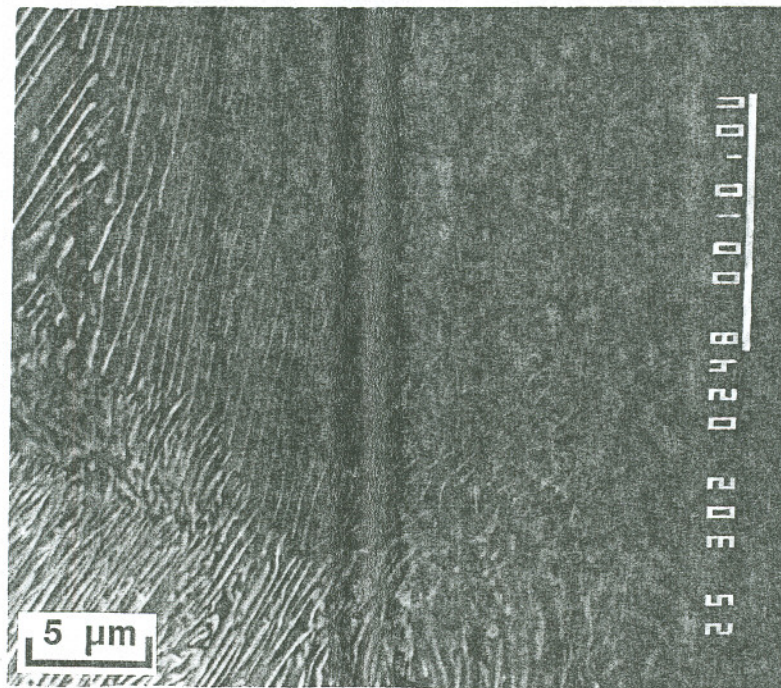


Figure 32 : Pearlitic microstructure from B4

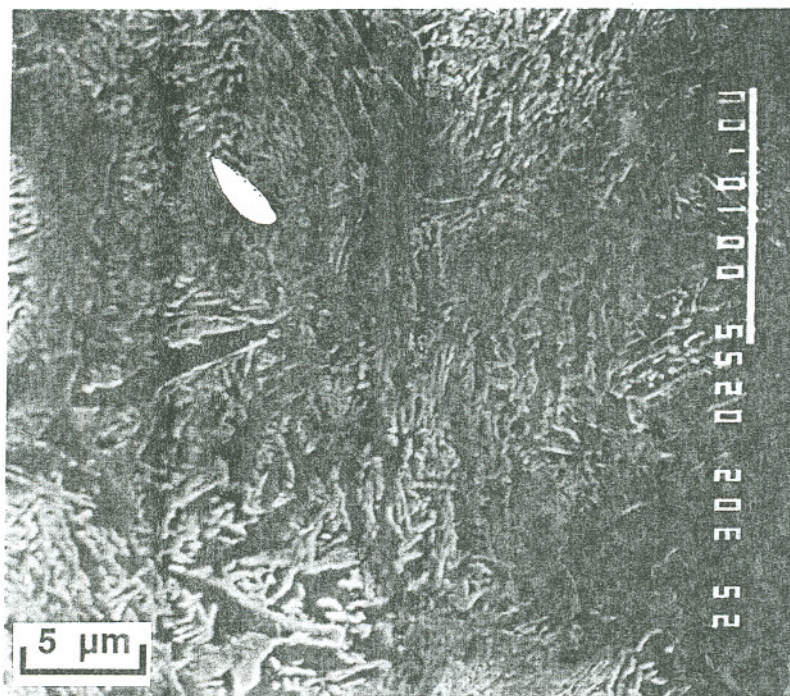


Figure 33 : Microstructure from C1

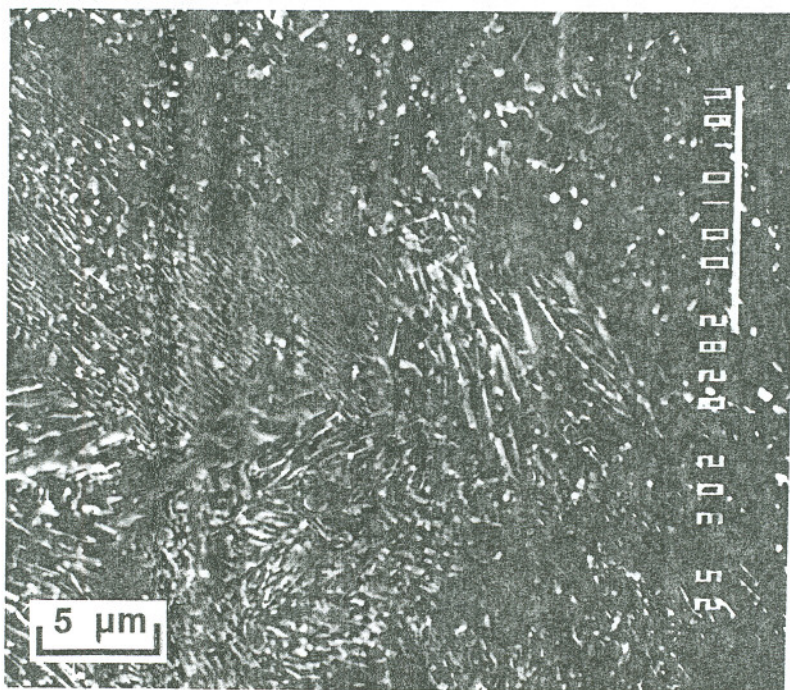


Figure 34 : Microstructure from C3

### RCF Tests on the Amsler Machine

Rail steels A, B, C and D (Table IV, p52) in the as-received condition and rail steel B and C in the heat treated condition (Table XI, p76) were used to develop a model relating the hardness/pearlite interlamellar spacing, maximum Hertzian contact stress and the RCF life. The results of the RCF tests carried out on the Amsler twin disk rolling/sliding testing machine for model development are summarized in Table XV. Figures 35, 36 and 37 show plots of the RCF life versus the maximum Hertzian contact stress for the four as-received steels, the A rail heat treatments and the B rail heat treatments respectively. In Table XV and in Figures 35 to 37, the RCF life is expressed in multiples of 100000 cycles.

The data for each of the steels can be described equally well by a power function of the type :

$$L = A (P_o)^{-B} \quad (10)$$

or by a linear relationship of the type :

$$L = N (P_o) + C \quad (11)$$

where  $L$  is the RCF life,  $P_o$  is the maximum Hertzian contact stress and  $A$ ,  $B$ ,  $N$  and  $C$  are constants.

Regression analysis of the data was carried out for both the power function and the linear function. The regression parameters are given in Table XVI.

**Table XV : Amsler RCF test results for model development**

(RCF Life is Expressed in Multiples of 100,000 Cycles)

$P_o$ N/mm <sup>2</sup>	Load N	A (249HK)	A* (249HK)	B (301HK)	C (304HK)	D (327HK)
1413	2000	1.52	1.10	1.17 1.65 1.96	0.42	4.22
1378	1900	1.64	---	---	2.44	---
1358	1850	---	---	3.33	---	5.67
1340	---	---	---	---	2.23	---
1302	1700	---	2.31	2.75 2.75 2.94 2.95 2.98 3.20	3.43	5.75
1244	1550	---	---	---	3.91	---
1223	1500	---	---	---	---	8.97
1182	1400	2.31 3.07 3.09	3.07	---	---	---
1161	1350	---	---	7.53	---	---
1139	1250	4.27	---	---	---	---
1094	1200	3.97 5.64	3.53	4.97	---	---
1047	1100	6.04	---	---	---	---
1024	1050	4.08	---	---	---	---
0998	1000	---	5.64	6.48	---	---
RO* (N)	---	0950	---	---	1400	---

RO\*: Run-out at approximately 1.42M cycles

HK: Knoop hardness @ 500gm load

A\*: Bottom roller made from B rail

A: Bottom roller made from A rail

Table XV : Continued

		Maximum Hertzian Contact Stress - Po (N/mm <sup>2</sup> ) (Applied Contact Load - N)									
	HK	1413 (2000)	1358 (1850)	1302 (1700)	1224 (1500)	1160 (1350)	1094 (1200)	0998 (1000)	0947 (0900)	0893 (0800)	RO* Load (N)
C4	233.8	0.481**	0.939	1.025	1.084	1.676	----	3.252	----	3.562	----
B4	225.6	0.790	0.903	1.721	1.634	1.454	4.191	3.629	----	3.885	----
C3	234.0	1.362	1.379	1.441	----	----	4.769	4.571	6.499	6.518	----
B3	253.6	1.101	1.527	1.822	----	----	4.289	----	7.219	----	----
B2	292.9	2.078	2.515	6.500	6.776	6.892	8.452	14.067	----	----	900
C1	325.0	2.943	2.044	5.959	----	7.480	8.054	13.200	13.465	----	----
B1	385.3	3.268	----	8.306	11.599	----	----	----	----	----	----
C2	340.0	3.070	6.652	8.583	----	13.877	----	----	----	----	1300

- \* RO: Run-out (Approx 1.42M cycles)
- \*\* RCF Life is X 100,000 Cycles
- HK: Knoop Hardness @ 500gm Load

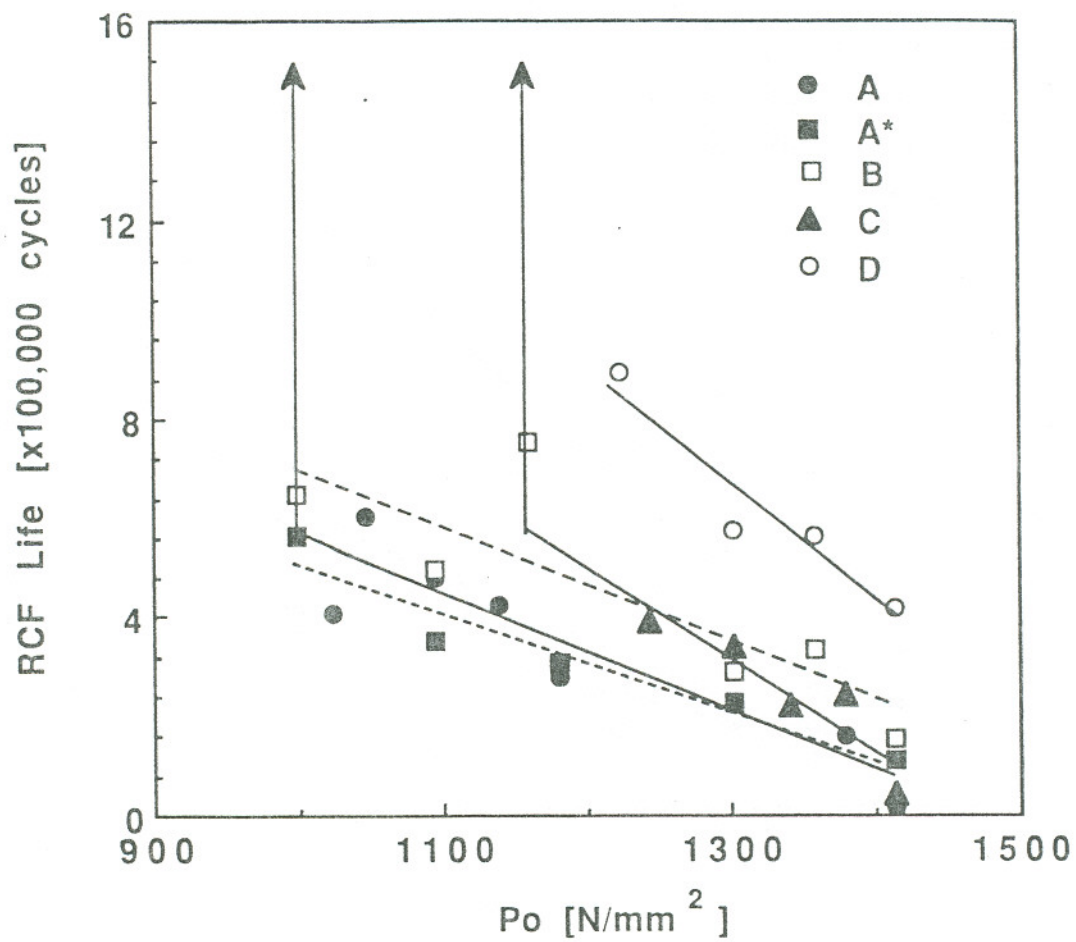


Figure 35 : RCF life versus  $P_o$  for four as received rail steels

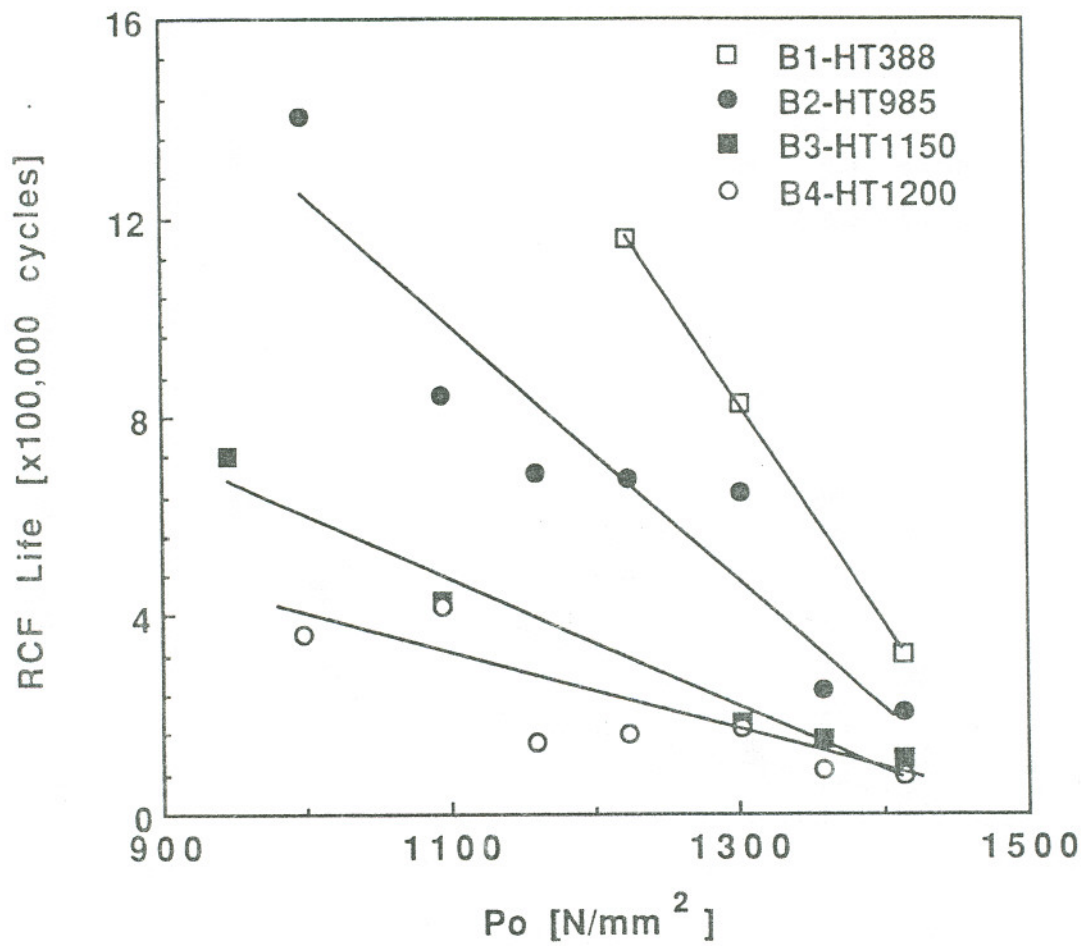


Figure 36 : RCF life versus  $P_o$  for B rail heat treated samples

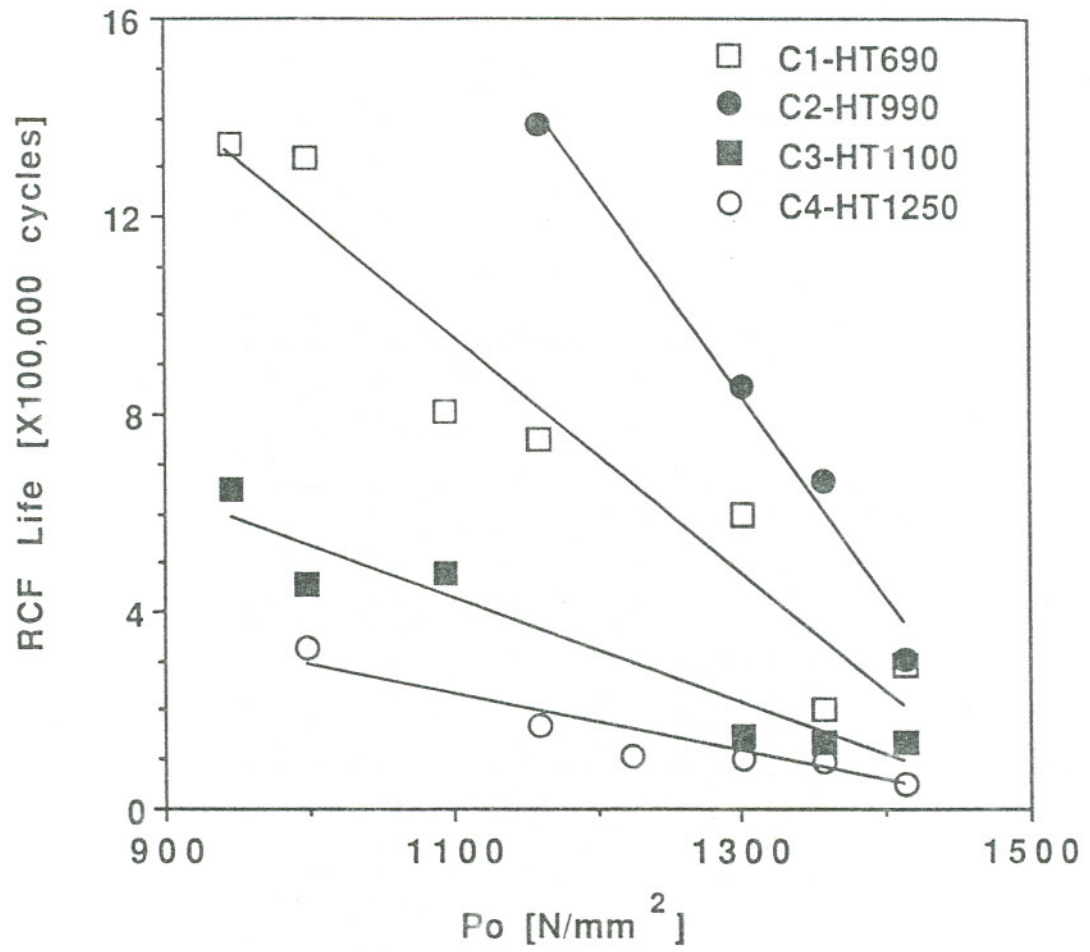


Figure 37 : RCF life versus  $P_o$  for C rail heat treated samples

Table XVI : Regression parameters for RCF data

LINEAR RELATION : $L = NP_0 + C$				
	HK	N	C	R <sup>2</sup>
A	249.0	-0.0112	16.75	-0.797
A*	249.0	-0.0099	14.92	-0.965
B	301.0	-0.0129	19.91	-0.879
B1	385.3	-0.0442	65.72	-0.999
B2	292.2	-0.0255	37.84	-0.941
B3	253.6	-0.0191	26.57	-0.940
B4	225.6	-0.0068	10.34	-0.881
C	303.6	-0.0188	27.53	-0.915
C1	325.0	-0.0249	36.96	-0.957
C2	340.4	-0.0348	52.95	-0.902
C3	234.0	-0.0108	16.20	-0.976
C4	233.8	-0.0070	10.20	-0.957
D	327.0	-0.0192	31.39	-0.898
POWER RELATION : $L = A(P_0)^B$				
	HK	B	log(A)	R <sup>2</sup>
A	249.0	-7.73	24.17	-0.768
A*	249.0	-4.25	13.49	-0.966
B	301.0	-4.23	13.62	-0.860
B1	385.3	-8.96	28.76	-0.983
B2	292.2	-5.02	16.30	-0.919
B3	253.6	-4.19	13.31	-0.993
B4	225.6	-3.68	11.58	-0.890
C	303.6	-14.48	45.55	-0.797
C1	325.0	-4.46	14.48	-0.929
C2	340.4	-6.12	22.17	-0.883
C3	234.0	-3.89	12.37	-0.975
C4	233.8	-4.31	13.39	-0.966
D	327.0	-4.08	13.48	-0.926

Since the degree of fit parameters for the power and the linear relationships are similar, the linear relationship, being the simpler of the two to handle, was used to develop the model.

In Table XVI, N and C are the slopes and y-intercepts of the plots according to the linear relationship. The values of N and C are plotted as functions of the hardness in Figures 38 and 39. Regression analysis shows that a linear function best fits these data and the relationships are :

$$N = -0.000205H + 0.039 \quad (12)$$

$$C = 0.31H - 60 \quad (13)$$

Substitution of the above relationships for N and C into Equation 11 (p98) yields :

$$L = 0.039P_o - 0.000205P_oH + 0.31H - 60 \quad (14)$$

To check how well the model fits the original RCF data, the hardness and maximum Hertzian contact stress for the various tests were substituted into the model and plotted against the actual test results, Figure 40.

The results of the repeatability tests are also shown in Figure 40. At 1302 N/mm<sup>2</sup>, the average life was 292800 - 16800 cycles for 6 tests and at 1413 N/mm<sup>2</sup> the average life was 159300 - 39800 cycles for 3 tests. Thus only a part of the scatter in the data in Figure 39 can be attributed to variability in the tests.

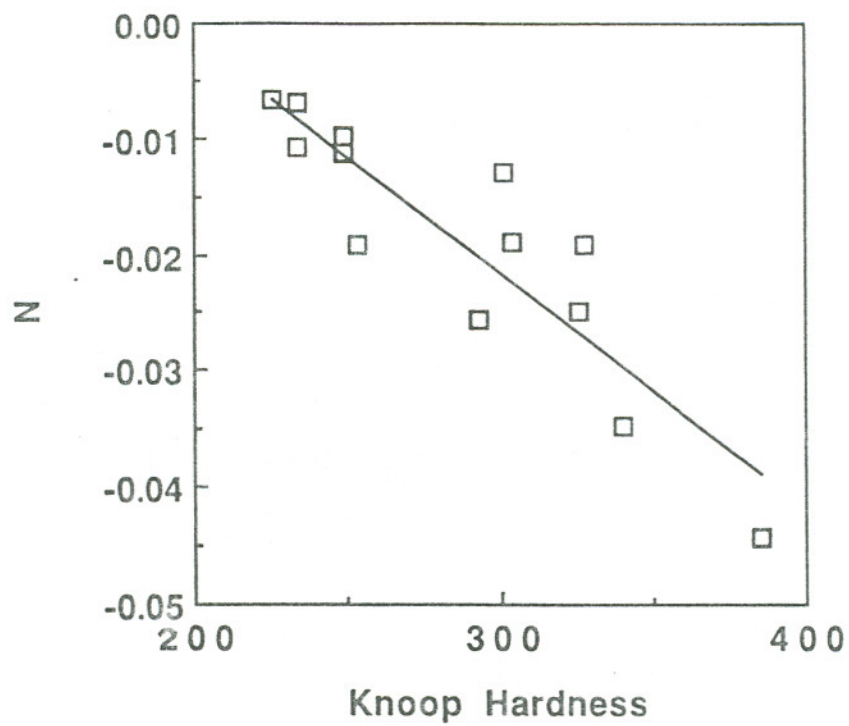


Figure 38 : N versus hardness

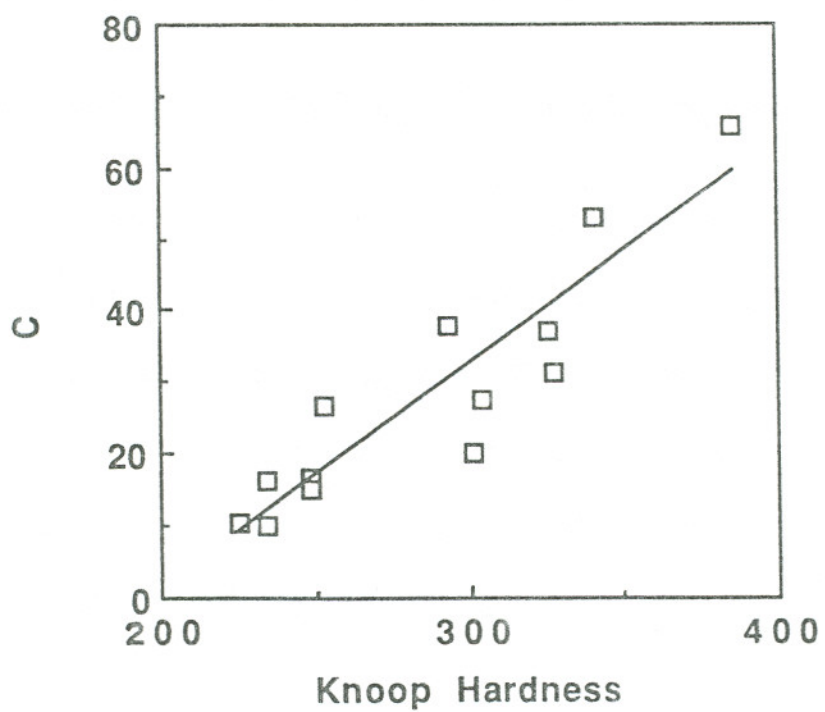


Figure 39 : C versus hardness

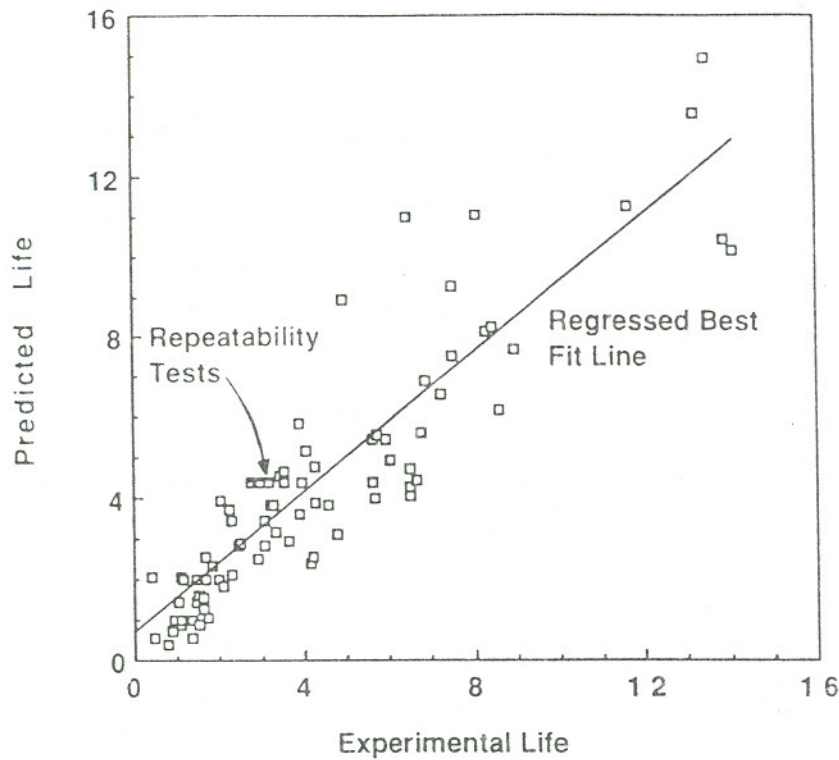


Figure 40 : Correlation of test results and model predictions

#### Modification of Model to Include Pearlite Interlamellar Spacing

Table XVII gives the hardness and the pearlite interlamellar spacing (S) for the four as-received rail steels and the two heat treated rail series. These data are plotted in Figure 41. Since rail steels B and C were of slightly different compositions their respective data were treated separately. Regression analysis of the data yielded the parameters given in Table XVIII. It is evident that the B and C rail steel data points can be treated as one group together with the A and D rail steels.

**Table XVII : Hardness and pearlite spacing of rail steels**

Series	Hardness		S $\text{\AA} \pm \sigma_N$
	Rc	HK	
A	28.0	249.0	2848 $\pm$ 185
B	29.5	301.0	2432 $\pm$ 141
B1	36.6	385.3	876 $\pm$ 70
B2	30.0	292.9	1754 $\pm$ 105
B3	24.5	253.6	2617 + 178
B4	18.1	225.6	3434 $\pm$ 326
C	31.4	303.6	2433 $\pm$ 226
C1	33.9	325.0	--- $\pm$ ---
C2	37.0	340.4	1433 + 90
C3	20.2	234.0	--- $\pm$ ---
C4	15.4	233.8	3038 $\pm$ 167
D	37.6	327.0	1808 $\pm$ 130

**Table XVIII : Regression parameters for hardness versus S**

LINEAR RELATION : $H = n(S) + c$			
Comments	n	c	R <sup>2</sup>
Only B Series Steels	-0.0594	423.70	-0.943
Only C Series Steels	-0.0635	438.62	-0.950
B & C Series Combined	-0.0603	427.81	-0.943
All Steels	-0.0617	431.13	-0.948
POWER FUNCTION : $H = m(S)^{-k}$			
Comments	k	log(m)	R <sup>2</sup>
Only B Series Steels	-0.363	3.658	-0.945
Only C Series Steels	-0.448	3.959	-0.899
B & C Series Combined	-0.377	3.709	-0.920
All Steels	-0.390	3.755	-0.920

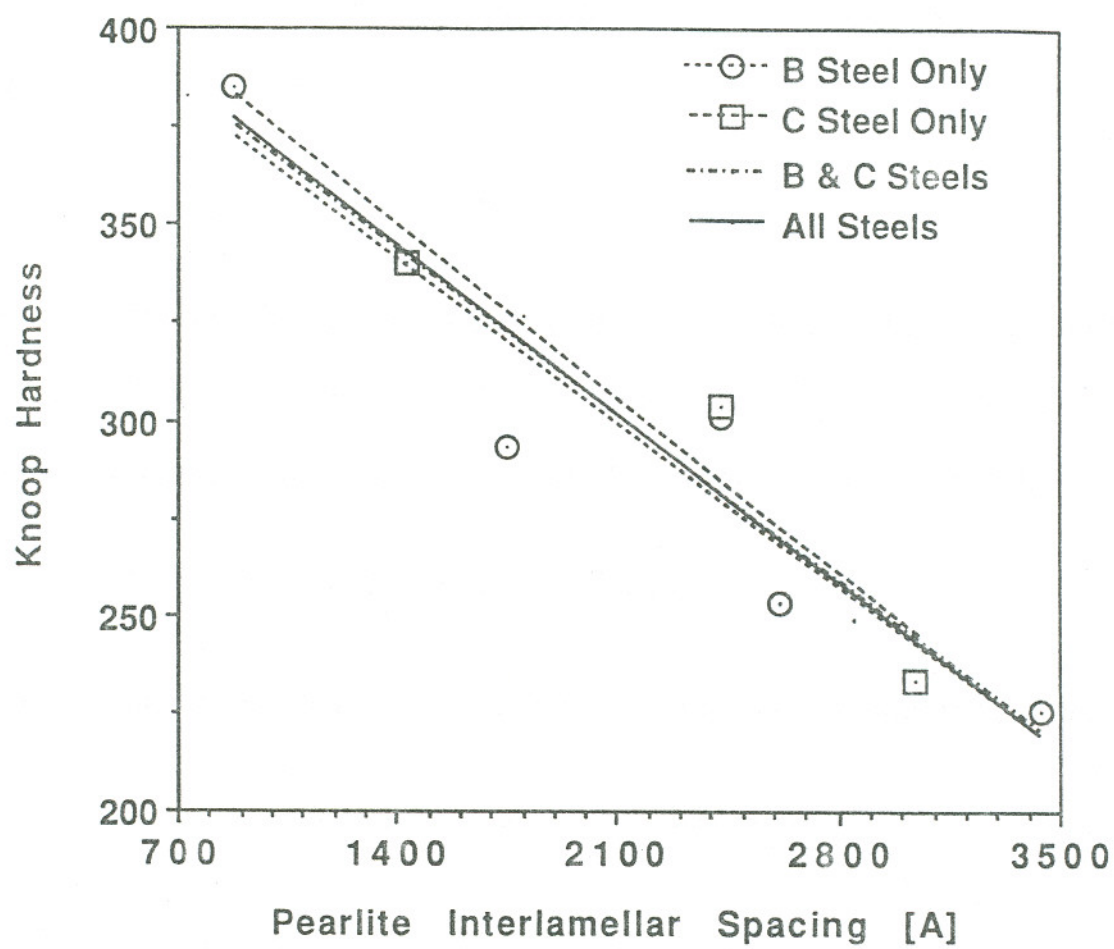


Figure 41 : Hardness versus pearlite interlamellar spacing

The relationship between the pearlite interlamellar spacing,  $S$ , and Knoop hardness,  $H$ , over a very wide range of hardness has been shown [89,90] to be a power relation of the form :

$$H \propto (S)^{-k} \quad (15)$$

However, comparing the regression parameters for the linear and the quadratic functions, we find that the  $R^2$  values for both are similar. Hence, for the sake of simplicity, the linear relationship was chosen. From Table XVIII we find that :

$$H = -0.0617(S) + 431.13 \quad (16)$$

The above equation can then be used to substitute  $S$  for  $H$  in Equation 5 to yield:

$$L = -0.049P_0 + 0.000012P_0S - 0.019S + 75 \quad (17)$$

To check how well this model fits the original RCF data, the pearlite interlamellar spacing and the maximum Hertzian contact stress for the various tests were substituted into the model and plotted against the actual test results, Figure 42.

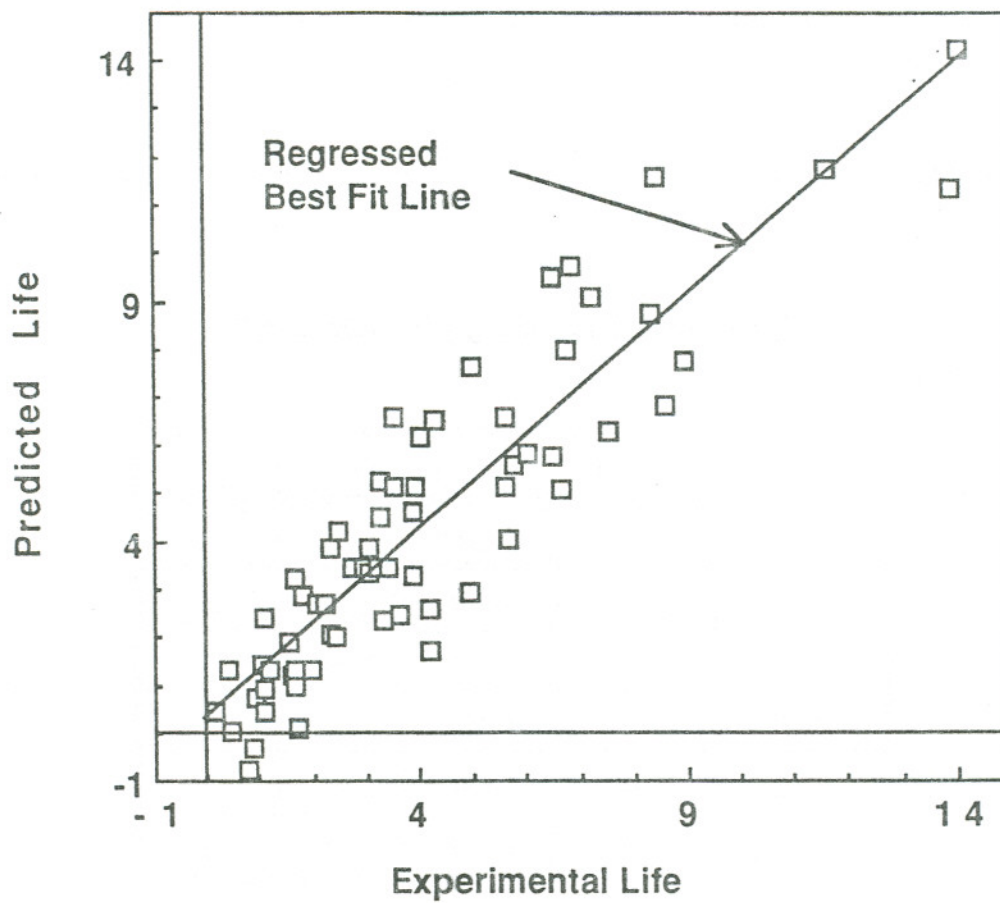


Figure 42 : Correlation of test results and model predictions

### Validation of the Model

Table XIX gives the hardness and inclusion counts of the five I series steels. Since these steels have chemistries and properties similar to the rail steels used to develop the model they were used to validate the model predictions.

**Table XIX : Properties of I series steels**

Steel	Hardness		Inclusion Volume Fraction (%)
	Rc	Knoop	
I1	39.6	379.6	0.315 ± 0.056
I2	35.7	355.4	0.129 ± 0.069
I3	41.3	420.1	0.154 ± 0.040
I4	39.6	383.7	0.054 ± 0.022
I5	38.4	381.4	0.229 ± 0.050

The model was used to generate RCF life plots using the hardness values of the I1 - 5 steels over a range of contact stresses, Figure 43. RCF test results for the same steels are given in Figure 44. Superimposing Figures 43 and 44 we find that the model predictions of RCF life I2 and I5 fit well with test results whereas for I1, I3 and I4 the predictions and test results do not agree well.

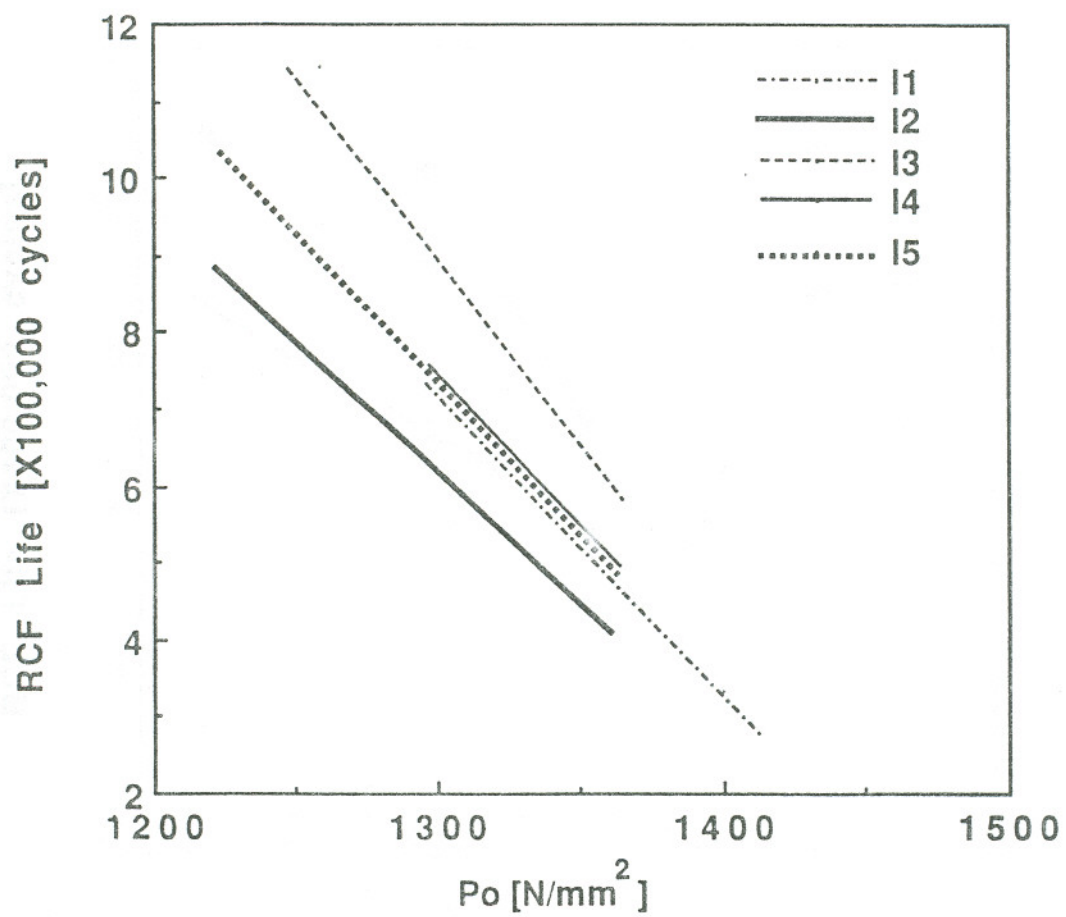


Figure 43 : Model predictions for I series steels

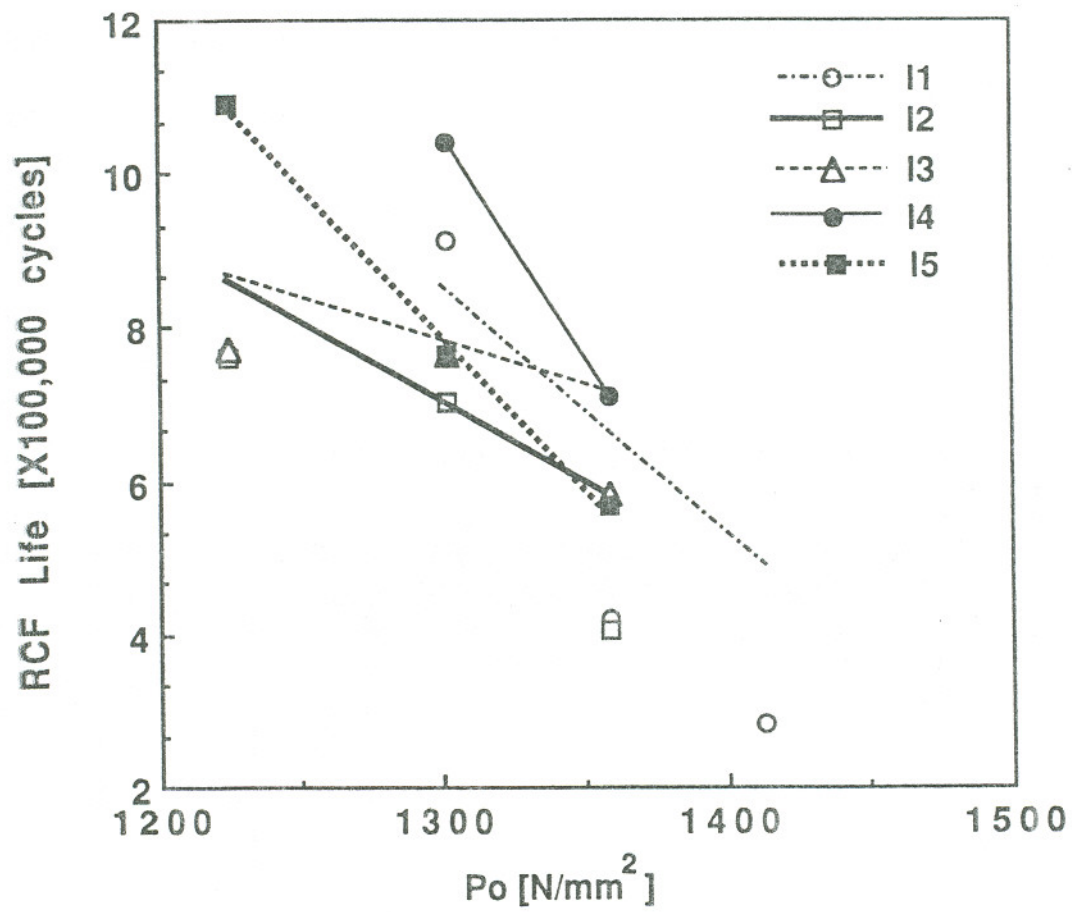


Figure 44 : RCF test results for I series steels

### CRACK AND WHITE ETCHING LAYER STUDIES

The primary purpose of this part of the investigation was to establish the behavior of surface cracks in terms of crack density, crack depth and the relation of the cracks to the white etching layer (WEL). A schematic definition of the various parameters is given in Figure 45.

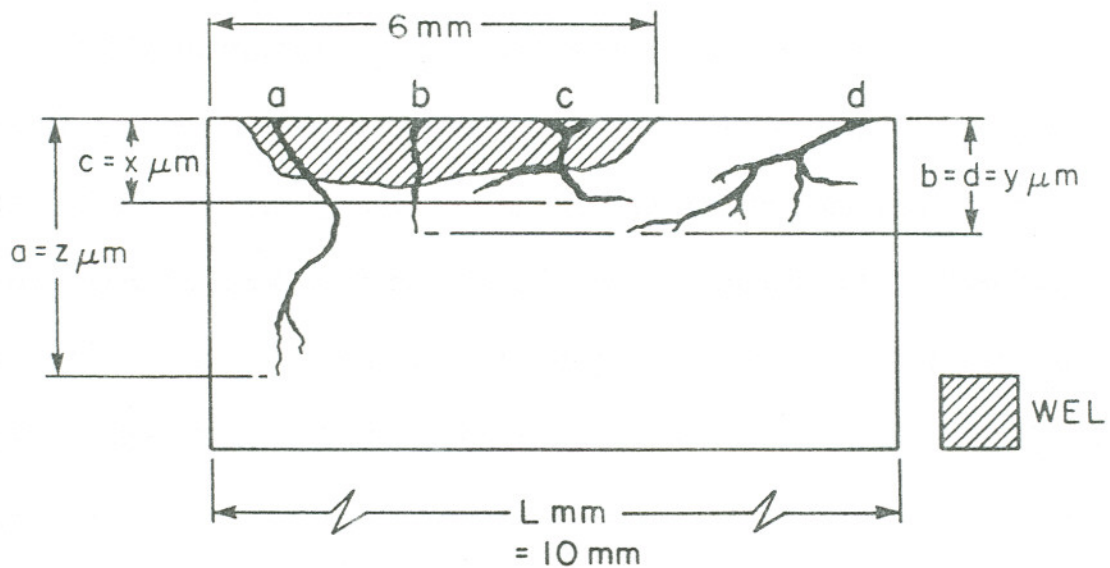


Figure 45 : Notation for crack and WEL studies

Crack depth is taken to be the perpendicular distance between the crack tip and the rail surface. Although crack "d" is longer, it has the same depth as crack "b". Further it is evident that crack "a" provides the maximum crack depth in this particular case. The crack density which is the number of cracks per unit length of the sample is thus  $4/10 \text{ mm} = 0.4 \text{ cracks per mm}$ . The percentage surface area coverage of the WEL is  $6\text{mm}/10\text{mm} = 60\%$ . Since three out of the four cracks in the sample are associated with the WEL, the correlation between the cracks and WEL is 75%.

While interpreting the data in this section an important aspect to bear in mind is the very nature of the data generated. As will be seen by comparing values of the different parameters for T1 and T2 (sections given in Figure 29, p93) samples from the same rail, there is a wide variation in the values depending on where the rail is sectioned. Examining just two locations for each rail provides, therefore, only a rough idea of the overall nature of the crack population. Further, it must be recalled that in examining the effect of gross tonnage on crack depth, we are not witnessing the development of a single set of cracks. Rather, the assumption has to be made that the samples from any given rail provide a good estimate of the total crack population at that gross tonnage level. This could lead to significant errors. Nonetheless, the results do produce

some general trends which can be considered to provide a reasonable qualitative picture of the behavior of the overall crack population and a guide to quantitative behavior.

Tables XX to XXIII provide a summary of the maximum crack depths observed in each transverse slice in terms of the #3 specimen only and for the #'s 2, 3 and 4 specimens combined (location of specimens is given in Figure 29, p93), for both high and low rails from the F series rails. These data are shown graphically in Figures 46 through 53 as functions of the cumulative MGT.

Cracks initiated very early on in the life of both the high and the low rails. Due to the scatter in the data, it is difficult to carry out a regression analysis to find the relationship between maximum crack depth and MGT. While one possible interpretation of the development of maximum crack depth is that it follows a parabolic growth rate it can equally well be argued that crack depth is linearly related to the MGT. Comparing data points on either side of the MGT at which grinding was done suggests that, in the high rails at least, 0.4 mm was removed along with all the cracks. However, in the low rails the apparent grinding depth was about 0.25 mm, with numerous cracks up to 0.25 mm being left in the rail.

**Table XX : Maximum crack depth - high rails at MP 97.6***(For locations of T1, T2, specimen #2, 3 and 4 refer Figure 29, p93)*

Rail #	MGT	#3 Section Only			#2, 3 & 4 Sections		
		T1	T2	Av.	T1	T2	Av.
F02	6.7	59	15	37	74	237	156
F04	10.8	59	89	74	799	89	444
F06	16.1	74	30	52	366	185	276
F10	48.2	319	189	254	708	354	531
F14	52.4	71	224	148	319	425	372
F18	53.5	--	0	0	--	0	0

**Table XXI : Maximum crack depth - low rails at MP 97.6***(For locations of T1, T2, specimen #2, 3 and 4 refer Figure 29, p93)*

Rail #	MGT	#3 Section Only			#2, 3 & 4 Sections		
		T1	T2	Av.	T1	T2	Av.
F01	6.7	37	44	41	118	148	133
F03	10.8	59	44	52	185	170	178
F05	16.1	481	148	315	481	148	315
F09	48.2	354	319	337	354	319	337
F13	52.4	47	519	283	271	519	359
F17	53.5	0	236	118	95	236	167

**Table XXII : Maximum crack depth - high rails at MP 97.3***(For locations of T1, T2, specimen #2, 3 and 4 refer Figure 29, p93)*

Rail #	MGT	#3 Section Only			#2, 3 & 4 Sections		
		T1	T2	Av.	T1	T2	Av.
F08	23.0	81	111	96	703	1317	1010
F12	48.2	566	661	614	1227	1121	1174
F16	52.4	153	95	124	814	684	749
F20	53.5	0	0	0	708	83	396

**Table XXIII : Maximum crack depth - low rails at MP 97.3***(For locations of T1, T2, specimen #2, 3 and 4 refer Figure 29, p93)*

Rail #	MGT	#3 Section Only			#2, 3 & 4 Sections		
		T1	T2	Av.	T1	T2	Av.
F07	23.0	170	229	200	200	229	215
F11	48.2	531	968	750	531	968	862
F15	52.4	755	968	862	755	968	862
F19	53.5	802	861	831	802	861	831

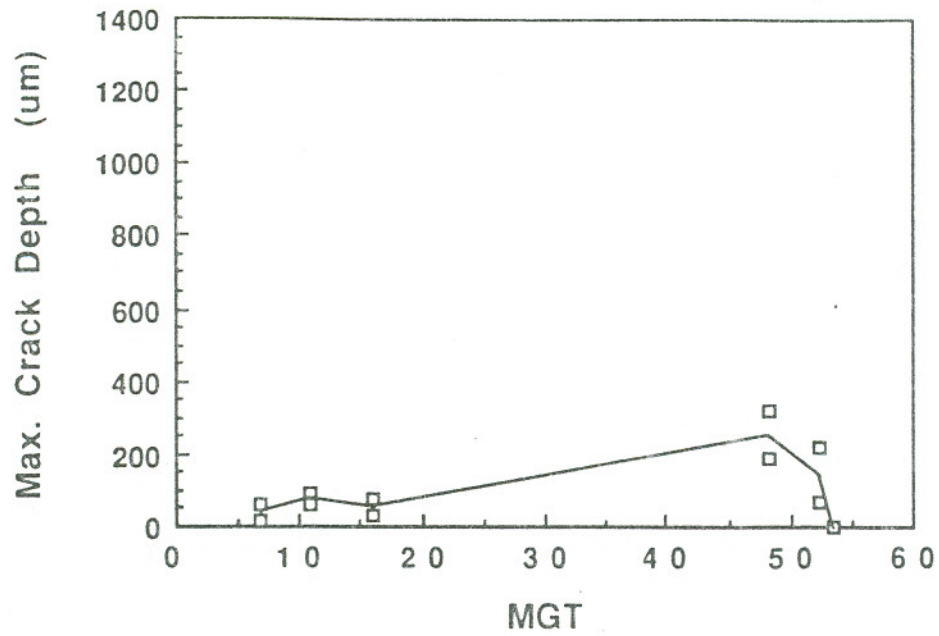


Figure 46 : Maximum crack depth versus MGT  
High rails at MP 97.6 - Section #3 only

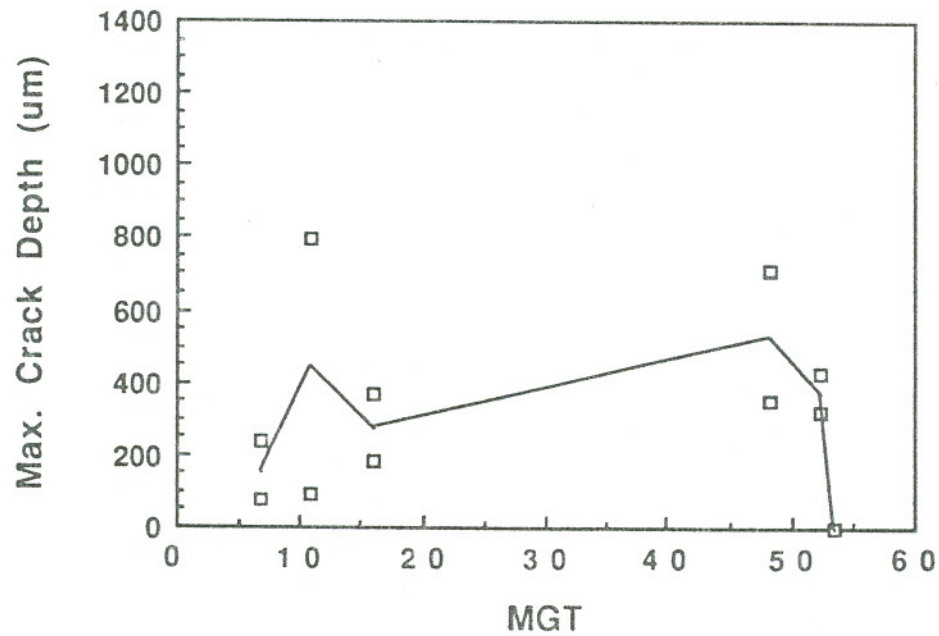


Figure 47 : Maximum crack depth versus MGT  
High rails at MP 97.6 - Sections 2, 3 & 4

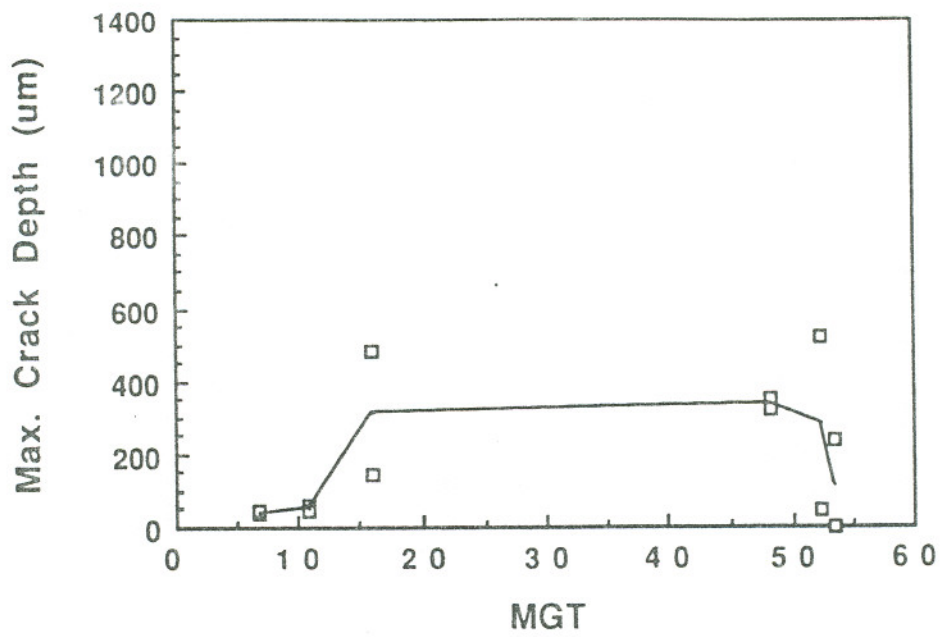


Figure 48 : Maximum crack depth versus MGT  
 Low rails at MP 97.6 - Section #3 only

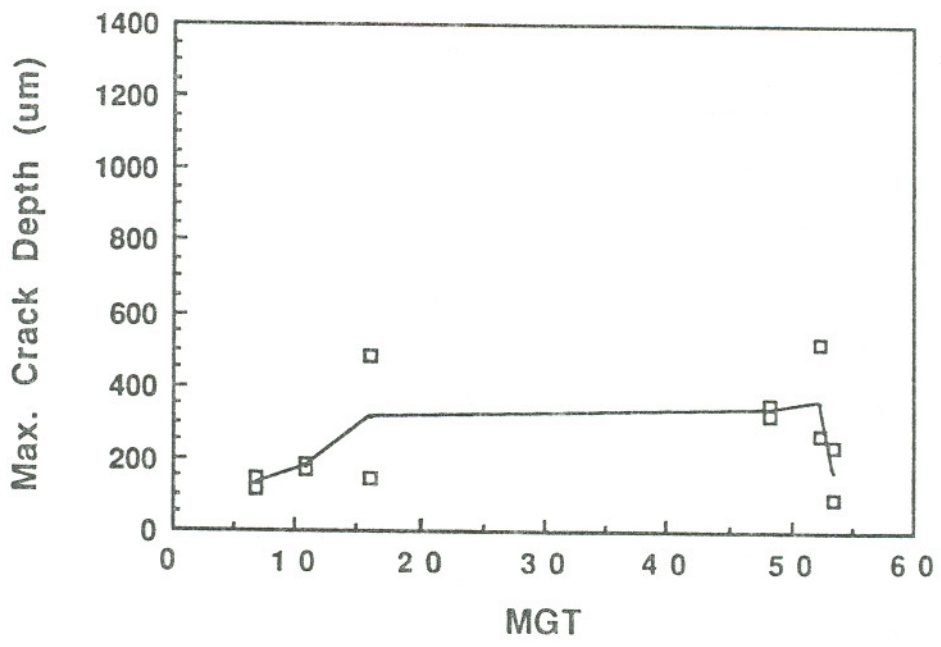


Figure 49 : Maximum crack depth versus MGT  
 Low rails at MP 97.6 - Sections 2, 3 & 4

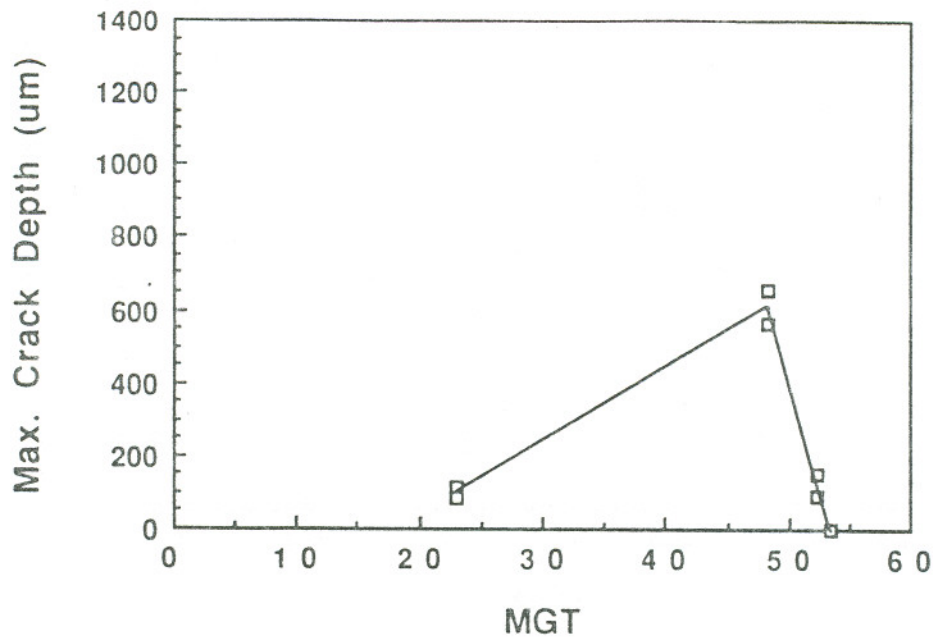


Figure 50 : Maximum crack depth versus MGT  
High rails at MP 97.3 - Section #3 only

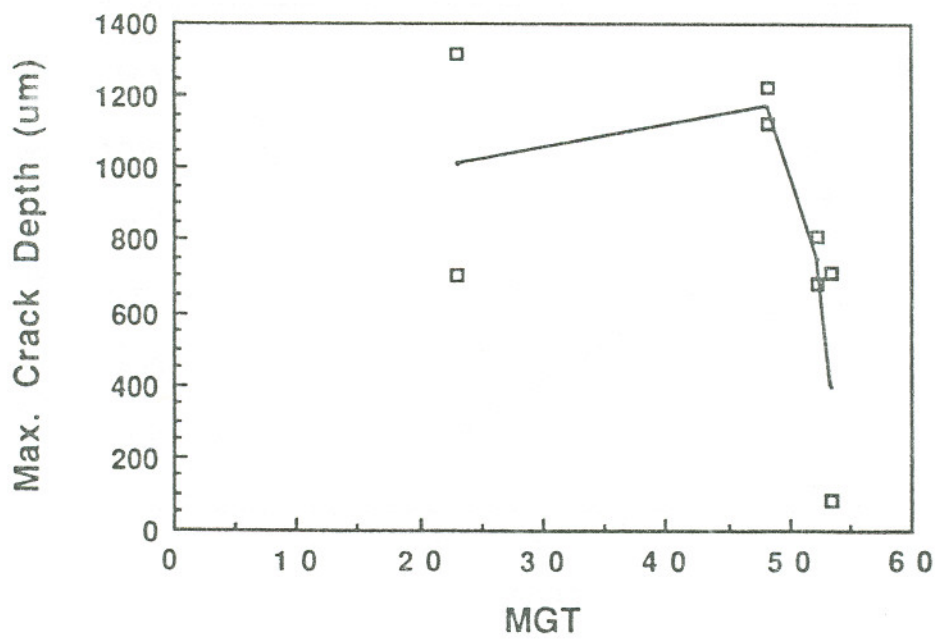


Figure 51 : Maximum crack depth versus MGT High rails at MP 97.3 - Sections 2, 3 & 4

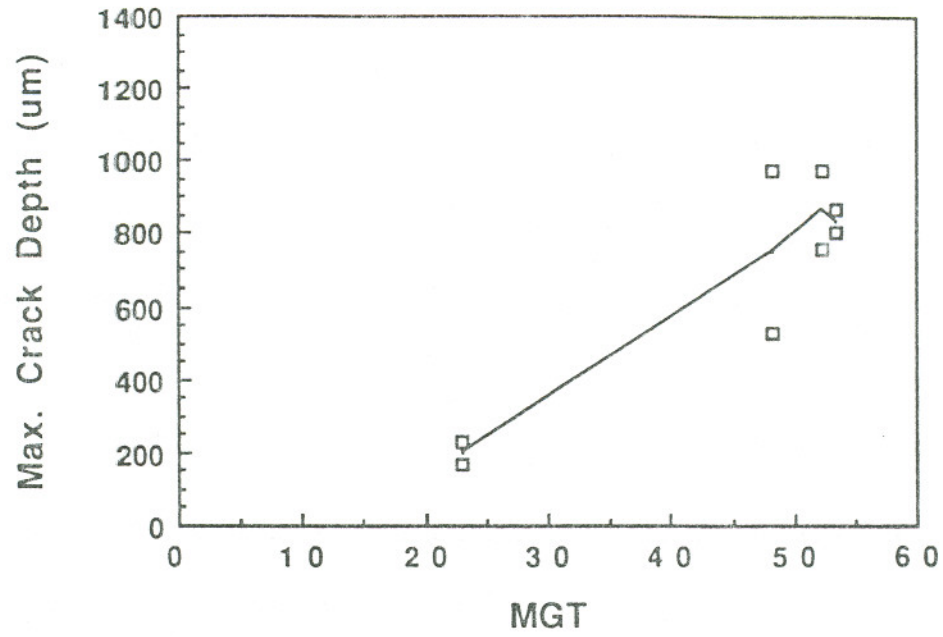


Figure 52 : Maximum crack depth versus MGT  
Low rails at MP 97.3 - Section #3 only

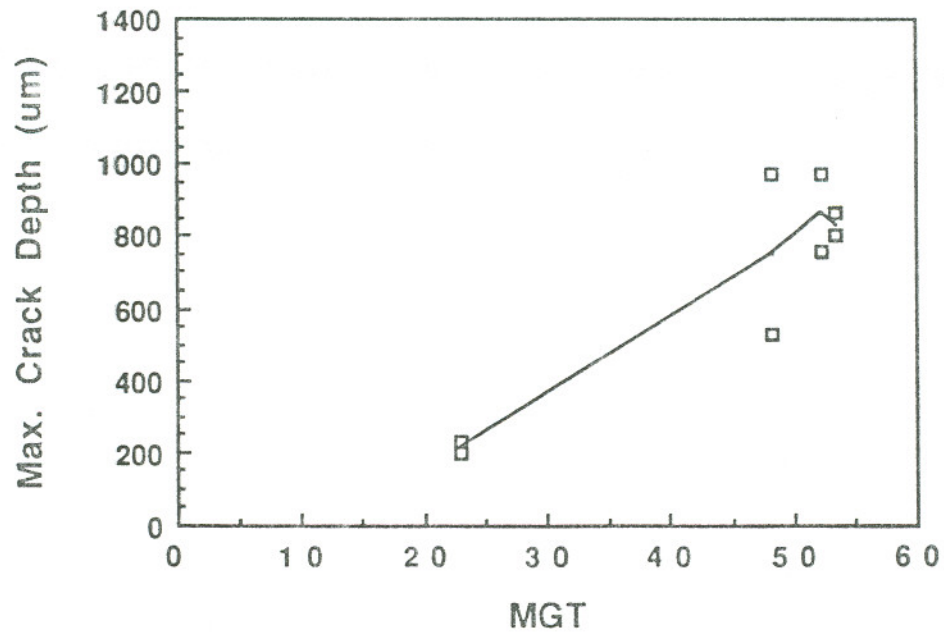


Figure 53 : Maximum crack depth versus MGT  
Low rails at MP 97.3 - Sections 2, 3 & 4

Tables XXIV through XXVII provide a summary of the total crack populations for each "T" slice (Figure 29, p93) and gives the crack densities for the various crack depth intervals. The crack density data as a function of the cumulative MGT are plotted in Figures 54 and 55. The number of short (0 -0.1 mm) cracks was at a maximum very early on in the life of both the high and the low rail and decreased steadily up to grinding, whereas the number of long cracks consistently increased. The total number of cracks decreased as the tonnage increased, suggesting that some of the initial short cracks continued to propagate and form long cracks but many of the original small cracks were lost through wear.

Typical rail microstructures showing the crack depth and density trends described above are shown in Figures 56 through 62.

**Table XXIV : Crack densities - high rails at MP 97.6**

Rail # X	Section # T	MGT	Number of Cracks						Length (mm)	Crack Density (#/mm)					
			A	B	C	D	E	F		A	B	C	D	E	F
43	1	6.7	20	7	3	0	0	0	35.5						
	2	6.7	6	8	3	2	0	0	32.0						
	1+2	6.7	26	15	6	2	0	0	67.5	0.385	0.222	0.090	0.030	0	0
41	1	10.8	2	8	6	4	2	2	49.1						
	2	10.8	2	1	3	0	0	0	25.0						
	1+2	10.8	4	9	9	4	2	2	74.1	0.054	0.122	0.122	0.054	0.027	0.027
44	1	16.1	10	15	3	6	2	0	43.5						
	2	16.1	1	8	5	6	0	0	47.7						
	1+2	16.1	11	23	8	12	2	0	91.2	0.121	0.251	0.088	0.132	0.022	0
50	1	48.2	6	5	8	3	1	1	39.0						
	2	48.2	6	3	5	4	2	0	50.0						
	1+2	48.2	12	8	13	7	3	1	89.0	0.135	0.090	0.146	0.079	0.034	0.011
55	1	52.4	1	6	9	6	1	0	46.7						
	2	52.4	1	1	1	7	1	0	41.7						
	1+2	52.4	2	7	10	13	2	0	88.4	0.023	0.079	0.113	0.147	0.023	0
59	1	53.5	--	--	--	--	--	--	--						
	2	53.5	0	0	0	0	0	0	43						
	1+2	53.5	0	0	0	0	0	0	43	0	0	0	0	0	0

Crack Lengths : A = 0-20  $\mu\text{m}$ ; B = 20-50  $\mu\text{m}$ ; C = 50-100  $\mu\text{m}$ ; D = 100-300  $\mu\text{m}$ ; E = 300 -700  $\mu\text{m}$ ; F = >700  $\mu\text{m}$

**Table XXV : Crack densities - low rails at MP 97.6**

Rail # X	Section # T	MGT	Number of Cracks						Length (mm)	Crack Density (#/mm)					
			A	B	C	D	E	F		A	B	C	D	E	F
42	1	6.7	7	23	4	3	0	0	34.0						
	2	6.7	2	23	8	1	0	0	36.5						
	1+2	6.7	9	46	12	4	0	0	70.5	0.128	0.653	0.170	0.057	0	0
40	1	10.8	3	16	13	5	0	0	39.0						
	2	10.8	9	41	11	4	0	0	39.0						
	1+2	10.8	12	57	24	9	0	0	78.0	0.154	0.731	0.308	0.115	0	0
45	1	16.1	41	23	7	6	1	0	39.8						
	2	16.1	9	23	12	6	0	0	45.0						
	1+2	16.1	50	46	19	12	1	0	84.8	0.590	0.543	0.224	0.142	0.012	0
48	1	48.2	0	5	12	7	1	0	42.5						
	2	48.2	1	3	2	6	1	0	36.0						
	1+2	48.2	1	8	14	13	2	0	78.5	0.013	0.102	0.178	0.166	0.025	0
54	1	52.4	2	6	1	5	0	0	43.8						
	2	52.4	3	9	12	18	6	0	47.7						
	1+2	52.4	5	15	13	23	6	0	91.5	0.055	0.164	0.142	0.251	0.066	0
58	1	53.5	0	0	1	0	0	0	43.8						
	2	53.5	0	0	0	1	0	0	41.0						
	1+2	53.5	0	0	1	1	0	0	84.8	0	0	0.012	0.012	0	0

Crack Lengths : A = 0-20  $\mu\text{m}$ ; B = 20-50  $\mu\text{m}$ ; C = 50-100  $\mu\text{m}$ ; D = 100-300  $\mu\text{m}$ ; E = 300 -700  $\mu\text{m}$ ; F = >700  $\mu\text{m}$

**Table XXVI : Crack densities - high rails at MP 97.3**

Rail # X	Section # T	MGT	Number of Cracks						Length (mm)	Crack Density (#/mm)					
			A	B	C	D	E	F		A	B	C	D	E	F
47	1	23.0	0	1	3	7	0	1	49.0						
	2	23.0	6	11	5	3	3	2	51.3						
	1+2	23.0	6	12	8	10	3	3	100.3	0.060	0.120	0.080	0.100	0.030	0.030
51	1	48.2	6	1	6	10	10	2	45.0						
	2	48.2	4	3	4	9	6	1	49.0						
	1+2	48.2	10	4	10	19	16	3	94.0	0.106	0.043	0.106	0.202	0.170	0.032
53	1	52.4	0	0	3	4	5	1	42.6						
	2	52.4	0	3	2	6	6	0	26.5						
	1+2	52.4	0	3	5	10	11	1	67.1	0	0.045	0.075	0.149	0.164	0.015
57	1	53.5	1	1	0	2	3	1	46.5						
	2	53.5	0	0	1	0	0	0	39.9						
	1+2	53.5	1	1	1	2	3	1	86.4	0.012	0.012	0.012	0.023	0.035	0.012

Crack Lengths : A = 0-20  $\mu\text{m}$ ; B = 20-50  $\mu\text{m}$ ; C = 50-100  $\mu\text{m}$ ; D = 100-300  $\mu\text{m}$ ; E = 300 -700  $\mu\text{m}$ ; F = >700  $\mu\text{m}$

Table XXVII : Crack densities - low rails at MP 97.3

Rail # X	Section # T	MGT	Number of Cracks						Length (mm)	Crack Density (#/mm)					
			A	B	C	D	E	F		A	B	C	D	E	F
46	1	23.0	16	22	8	5	0	0	49.9						
	2	23.0	17	19	13	6	0	0	51.0						
	1+2	23.0	33	41	21	11	0	0	100.9	0.330	0.410	0.210	0.110	0	0
49	1	48.2	9	8	3	3	1	0	51.0						
	2	48.2	3	1	3	5	2	0	40.5						
	1+2	48.2	12	9	6	8	3	0	91.5	0.131	0.099	0.066	0.087	0.033	0
52	1	52.4	5	2	2	4	3	1	45.2						
	2	52.4	5	5	4	6	2	2	47.4						
	1+2	52.4	10	7	6	10	5	3	92.6	0.108	0.076	0.065	0.108	0.054	0.033
56	1	53.5	3	0	1	2	2	1	41.1						
	2	53.5	0	0	1	3	3	1	44.0						
	1+2	53.5	3	0	2	5	5	2	85.1	0.035	0	0.024	0.059	0.059	0.024

Crack Lengths : A = 0-20  $\mu\text{m}$ ; B = 20-50  $\mu\text{m}$ ; C = 50-100  $\mu\text{m}$ ; D = 100-300  $\mu\text{m}$ ; E = 300 -700  $\mu\text{m}$ ; F = >700  $\mu\text{m}$

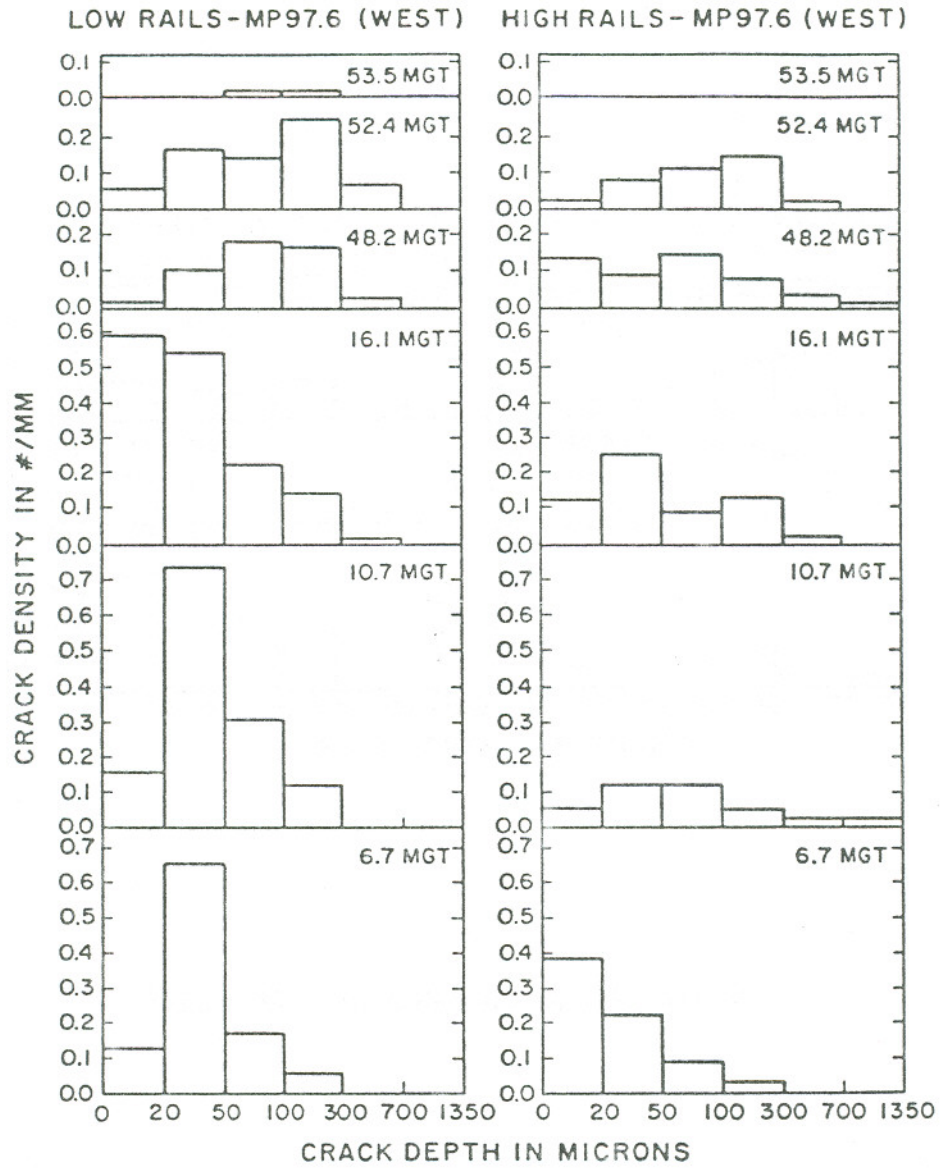


Figure 54 : Crack density data for MP 97.6

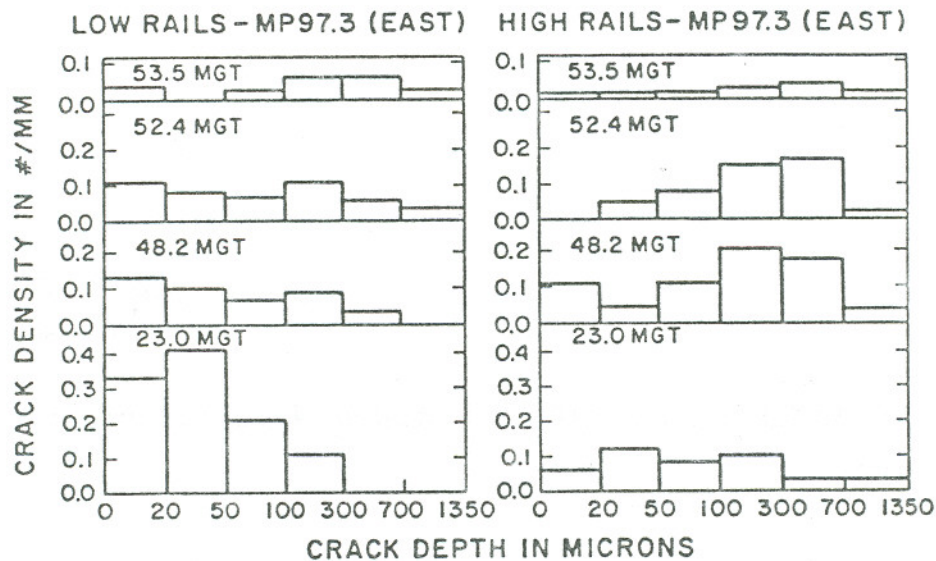


Figure 55 : Crack density data for MP 97.3

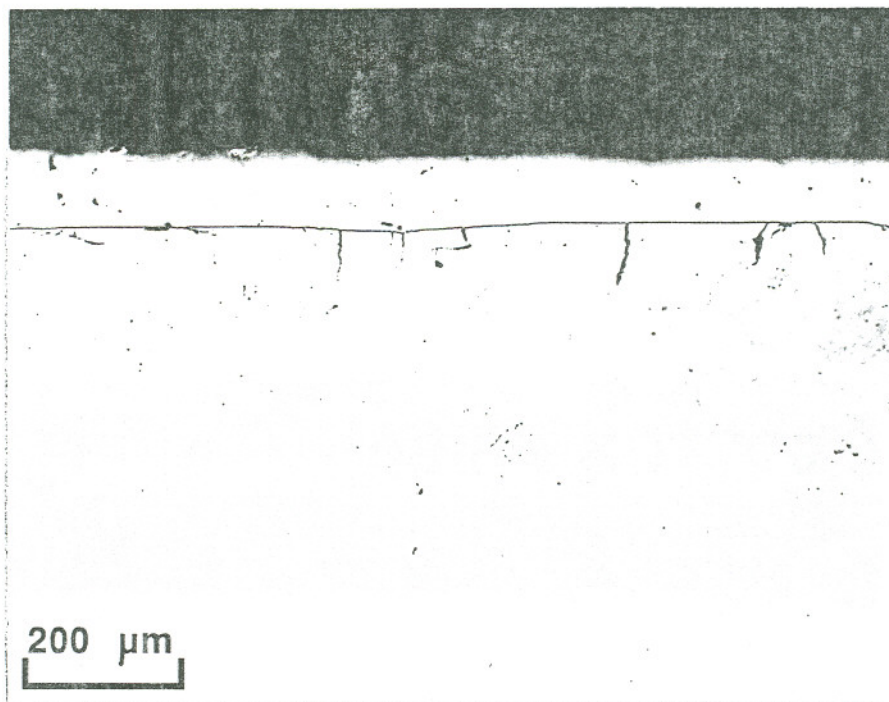


Figure 56 : Cracks in high rail at MP 97.6 after 6.7 MGT

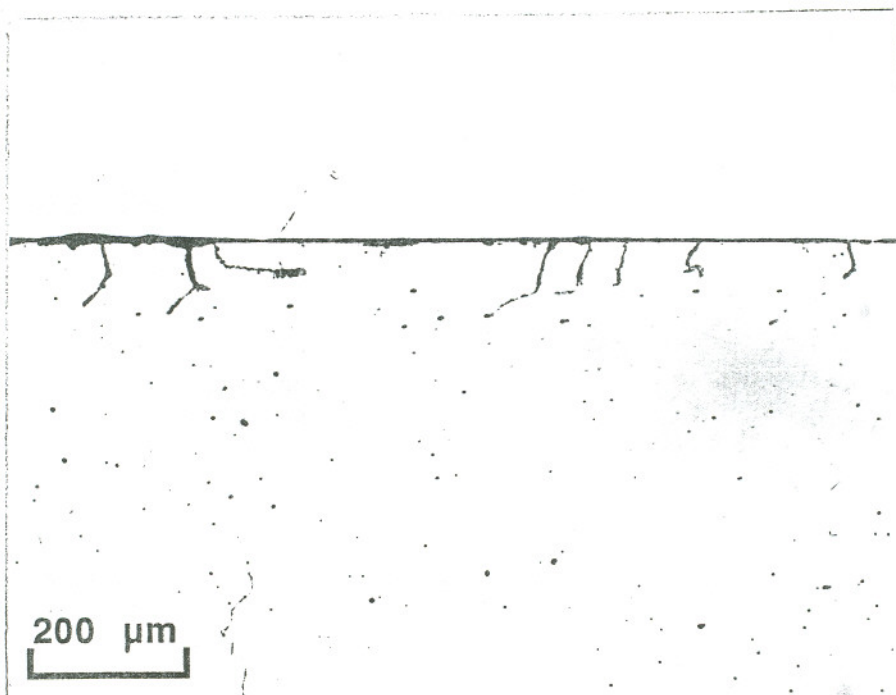


Figure 57 : Cracks in high rail at MP 97.6 after 10.8 MGT

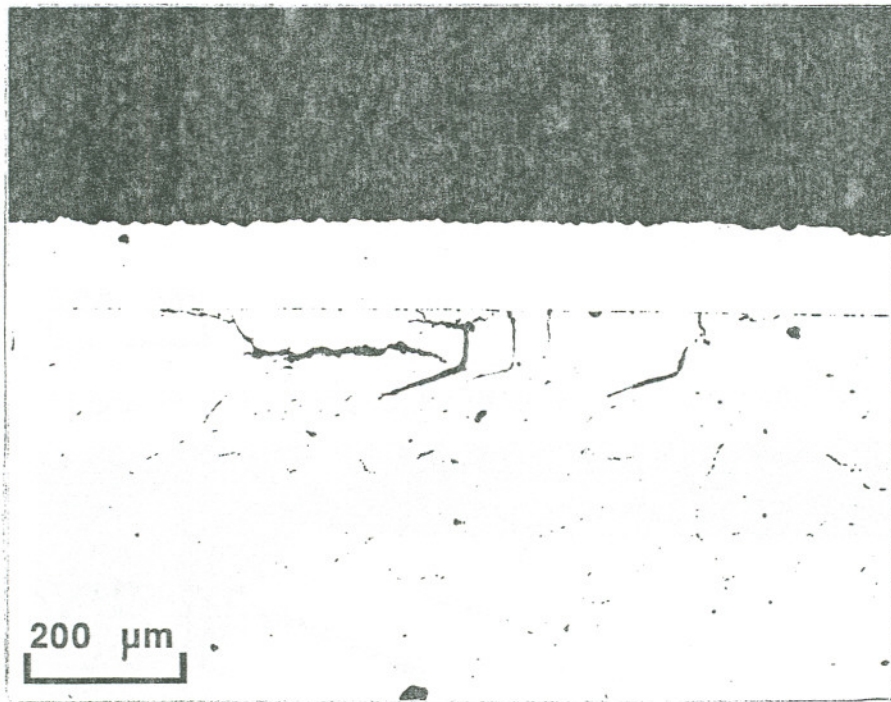


Figure 58 : Cracks in high rail at MP 97.6 after 16.1 MGT

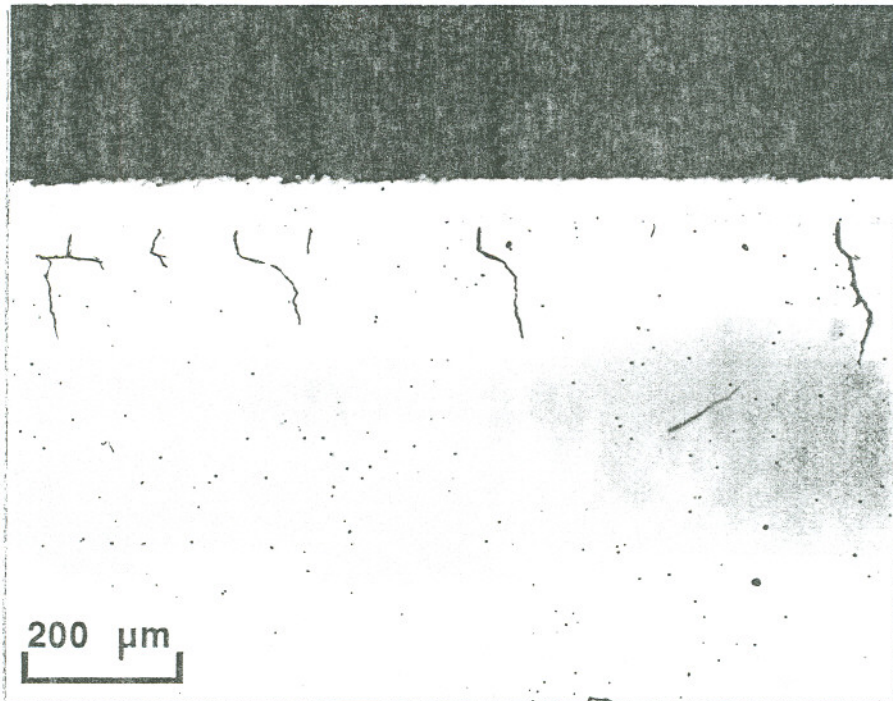


Figure 59 : Cracks in high rail at MP 97.6 after 48.2 MGT

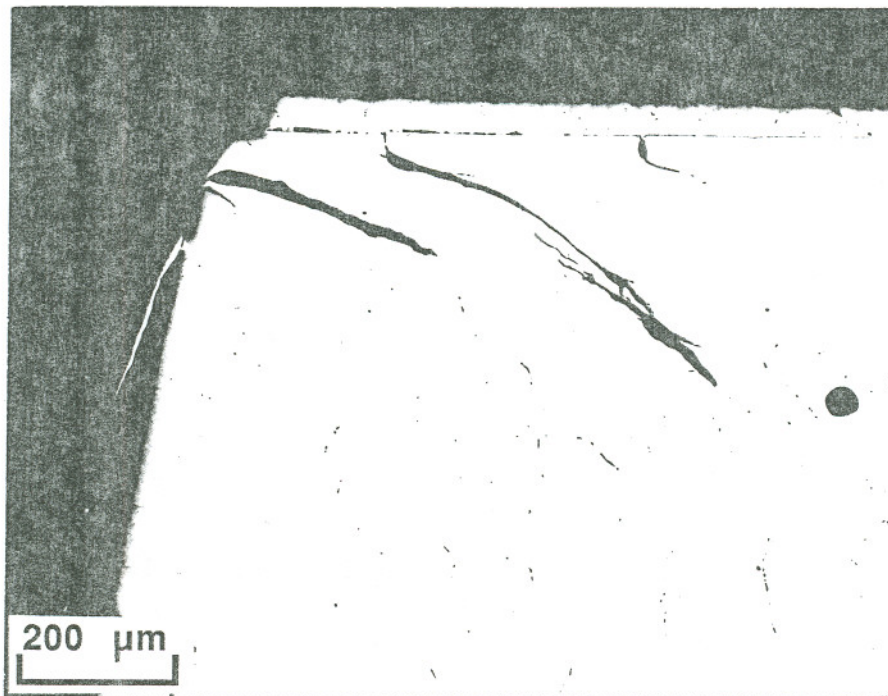


Figure 60 : Cracks in high rail at MP 97.6 after 48.2 MGT

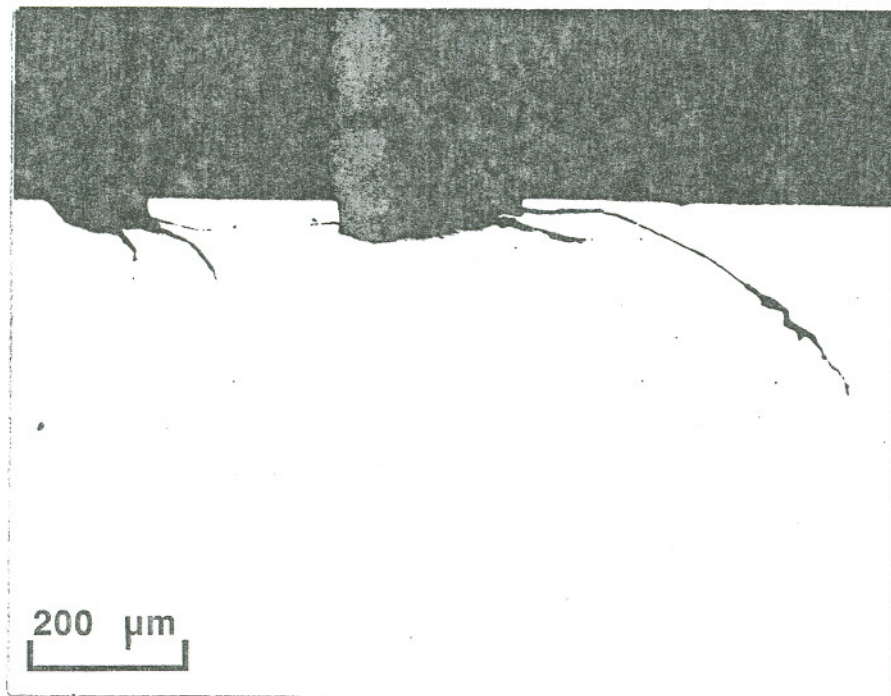


Figure 61 : Cracks in high rail at MP 97.6 after 52.4 MGT

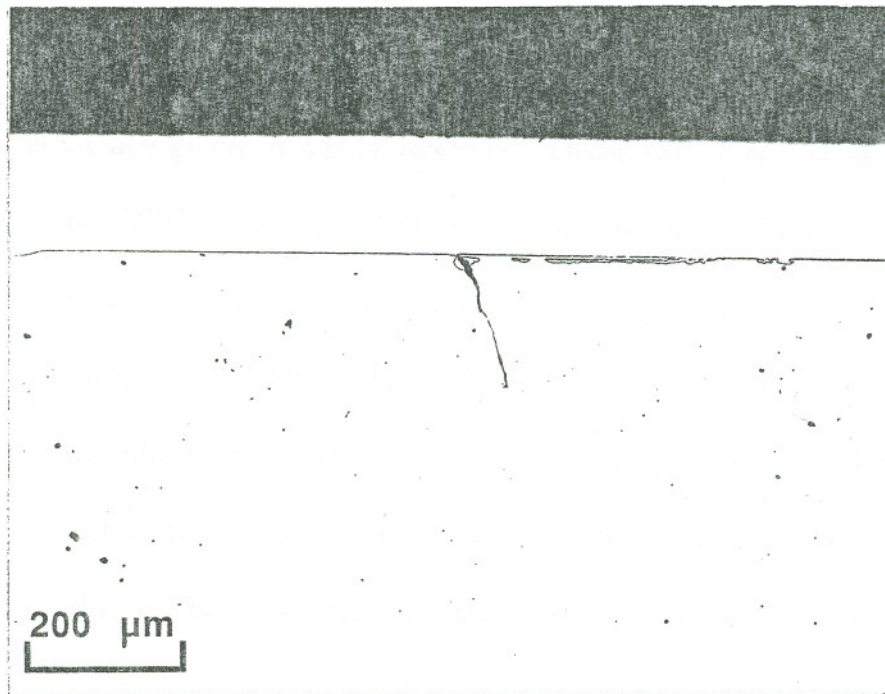


Figure 62 : Cracks in low rail after grinding at 53.5 MGT

### RCF Tests on White Etching Layer Samples

Figures 63 through 64 show representative examples of the White Etching Layer (WEL) found naturally occurring in rails and artificially induced on a rail sample and an Amsler roller respectively. The microhardness values of the WEL and base metal are given in Table XXVIII. These values are in agreement with the values for WEL hardness found in the literature [18,27]. All three microstructures show regions of discoloration within the WEL which appear to be regions that had transformed to WEL and then subsequently underwent tempering. Microhardness measurements made on the samples, Table XXVIII, also seem to reflect this. Further, the WEL generated on the rail sample and the Amsler roller did not have any cracks present in the layer after deposition.

The rollers on which WEL was generated using an electro-spark deposition method were subjected to RCF tests on the Amsler machine using water lubrication, a slide/roll ratio of 10% and a  $P_o$  value of 1302 N/mm<sup>2</sup>. The first sample on which WEL was produced at discrete locations resulted in the formation of a groove on the mating roller with a corresponding raised region on the test roller; there was no other apparent surface damage in the test roller. On sectioning the test roller through the area where the WEL had been generated, it was found that although cracked, all of the WEL had remained after 93,000 cycles while the material around it had been lost; most probably due to wear, Figure 66.

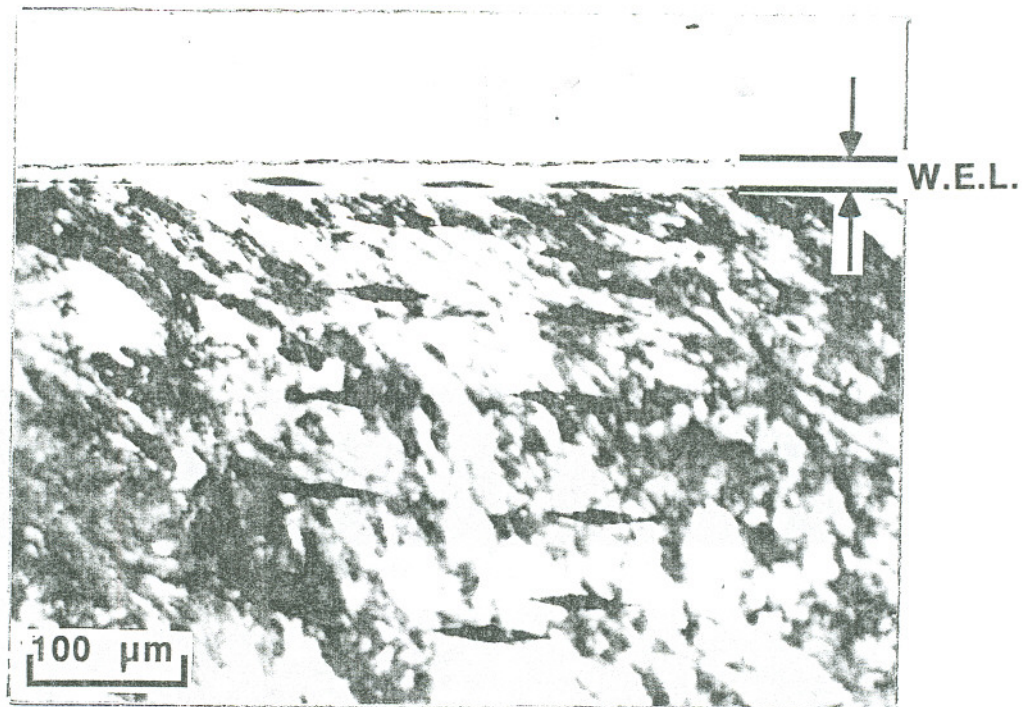


Figure 63 : Naturally occurring WEL in rail

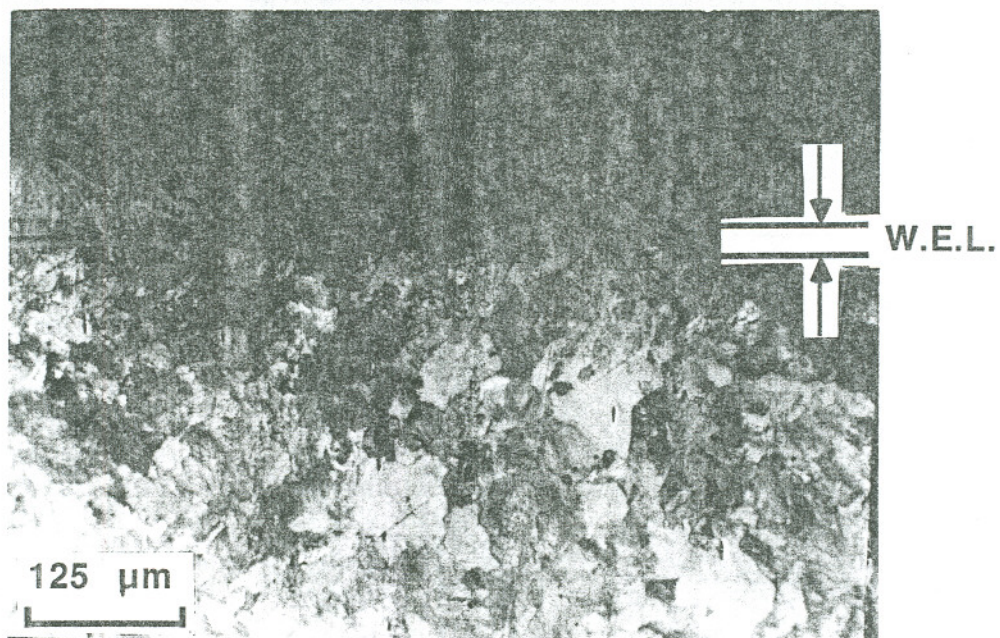


Figure 64 : Artificially induced WEL in rail steel sample

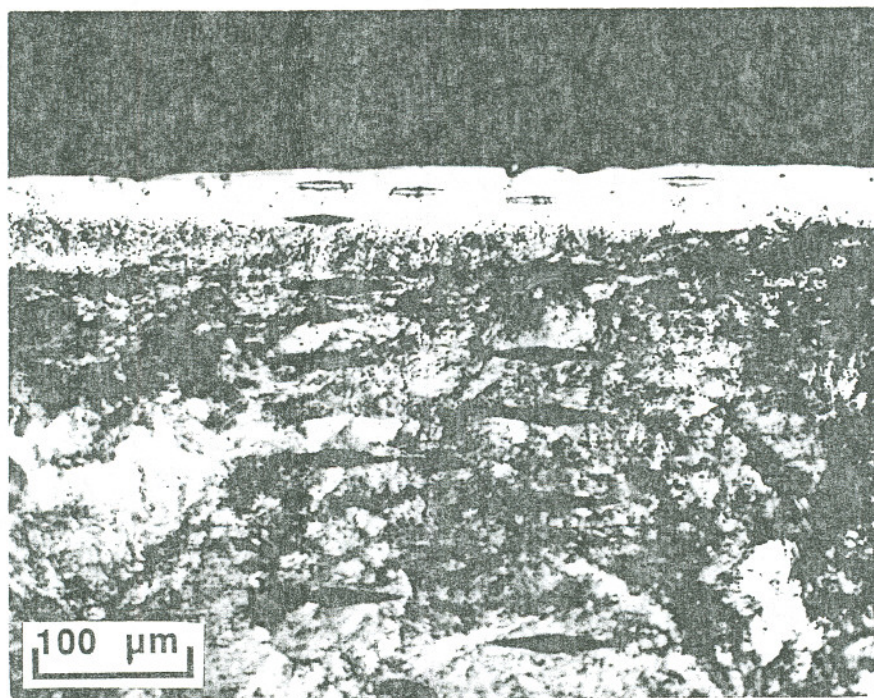


Figure 65 : Artificially induced WEL in Amsler test roller

**Table XXVIII : Microhardness values for WEL**

	Used Rail	Rail Steel	Amsler Roller
WEL Hardness	735	654	688
Matrix Hardness	381	294	294
Plots (Y axis = Hardness)			

\* All hardness measurements are Knoop hardness values at 50 gm load

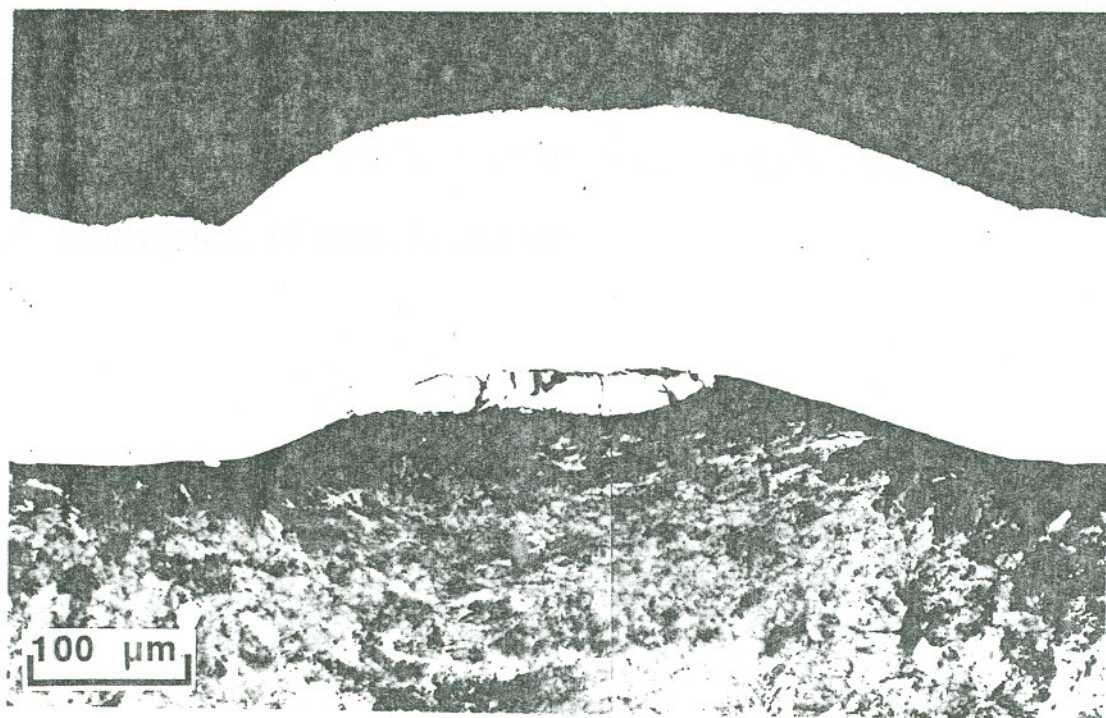


Figure 66 : WEL in used Amsler roller

For the next tests, the WEL was deposited on the test rollers in such a way that the entire running track was covered. To do this, it was necessary to make numerous passes over the surface with the electro-spark equipment. (This could explain the formation of the seemingly tempered regions). The samples were tested using the same parameters as before and the tests were run for 450,000 cycles, (a test roller without WEL failed after 280,000 cycles). The rollers

were then sectioned and studied using the optical microscope. The WEL showed the presence of cracks, Figure 67, that appear similar to the cracks found in the WEL in rails in service, Figure 68.

Figures 69 and 70 show the similarity in the spalled regions of the WEL in the Amsler roller and the rail in service.

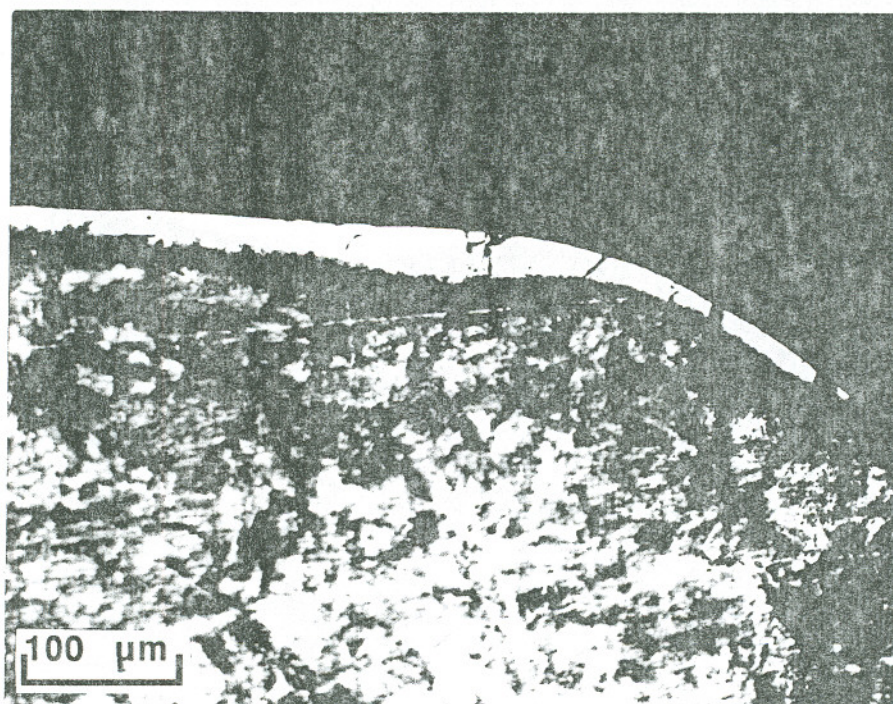


Figure 67 : Cracks in WEL on used Amsler roller

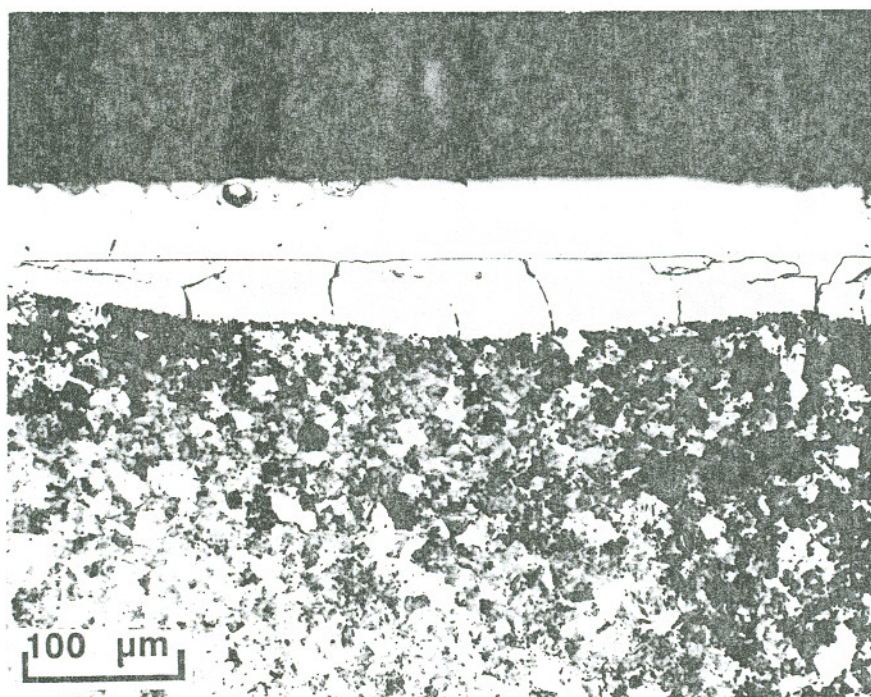


Figure 68 : Cracks in WEL on rail in service

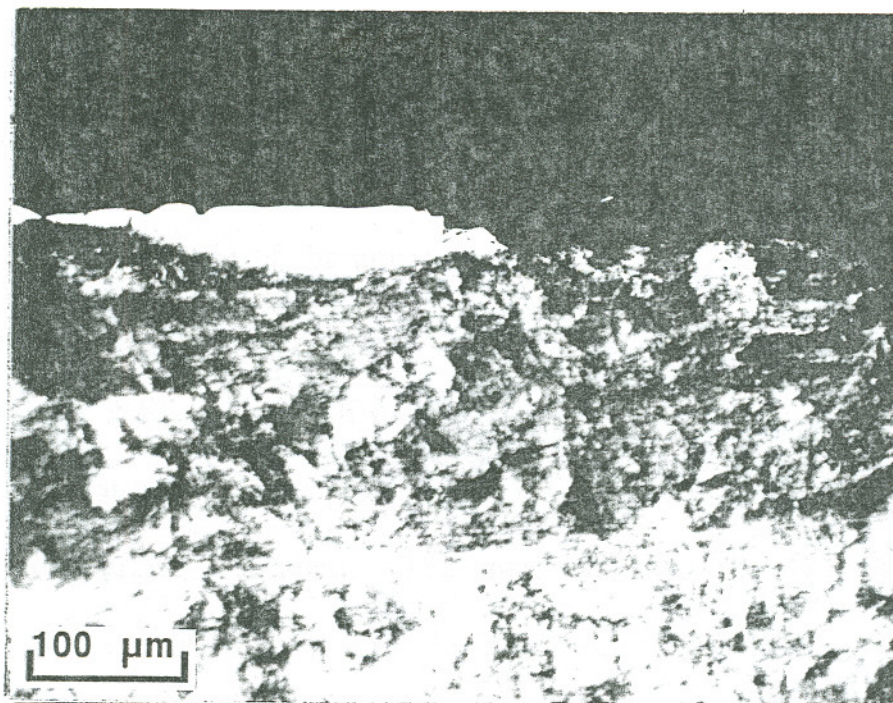


Figure 69 : Spalling of WEL in used Amsler roller

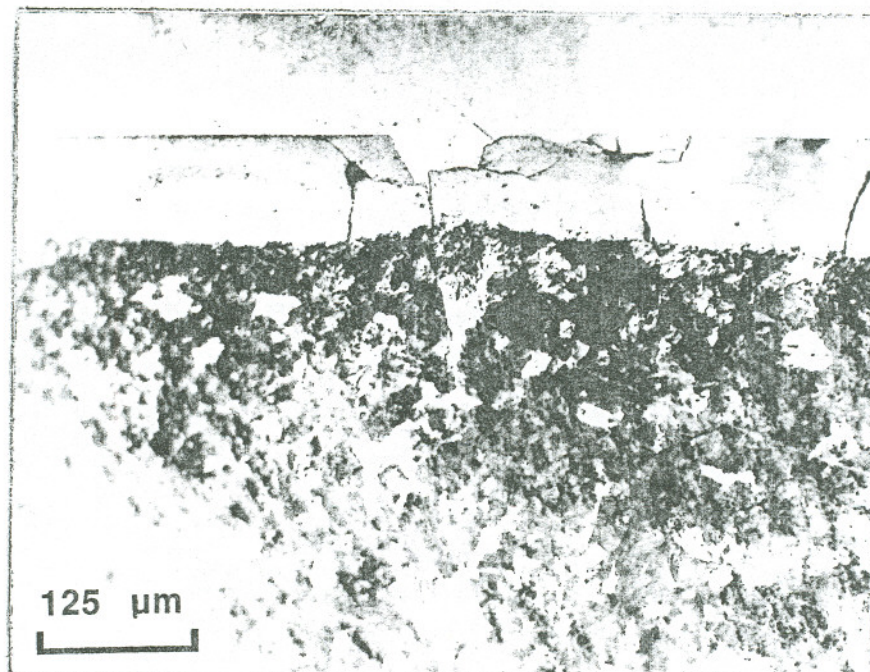


Figure 70 : Spalling of WEL in rail in service

### Correlation Between WEL and Cracks in Rails in Service

A typical example of the appearance of the WEL on the rail surface and the cracks associated with it is shown in Figure 71. To find the percentage area covered by the WEL, the length of the WEL on the surface of the transverse sections was measured and the percentages reported are with respect to the total length of the surface examined. The total number of cracks observed, the percentage surface area coverage by the WEL and the correlation between the cracks and the WEL is given in Table XXIX.

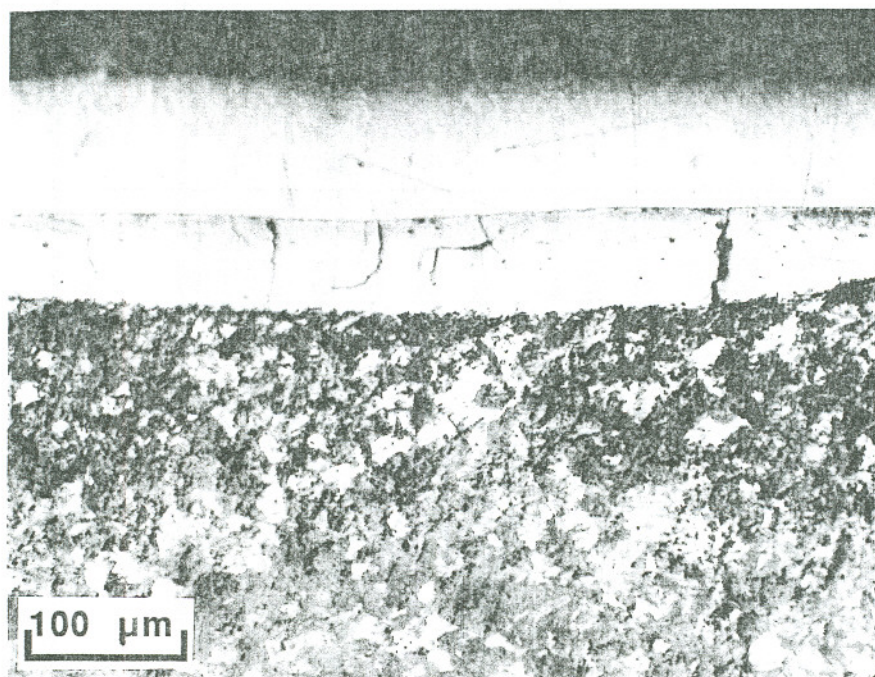


Figure 71 : WEL in rail in service and associated cracks

Table XXIX : Crack and WEL data for rails

	Rail #	MGT	% Cracks associated with WEL	% Length of WEL ( $\mu\text{m}$ )	Max. WEL Depth ( $\mu\text{m}$ )	Avg. WEL Depth ( $\mu\text{m}$ )
High Rails	F02	6.7	98	46	54	22
	F04	10.8	100	42	53	22
	F06	16.1	88	54	60	25
	F10	48.2	63	25	36	17
	F14	52.4	54	26	35	18
	---	Grinding	---	---	---	---
	F18	53.5	0	0	0	0
Low Rails	F01	6.7	73	58	48	21
	F03	10.8	87	66	57	27
	F05	16.1	88	58	36	16
	F09	48.2	43	34	32	15
	F13	52.4	76	41	33	13
	---	Grinding	---	---	---	---
	F17	53.5	100	85	8.2	4.3

Table XXIX : Continued

	Rail #	MGT	% Cracks associated with WEL	% Length of WEL ( $\mu\text{m}$ )	Max. WEL Depth ( $\mu\text{m}$ )	Avg. WEL Depth ( $\mu\text{m}$ )
High Rails	F08	23.0	74	35	61	
	F12	48.2	55	27	30	
	F16	52.4	39	10	32	
	---	Grinding	---	---	---	
	F20	53.5	40	16	6	
Low Rails	F07	23.0	54	31	14	
	F11	48.2	38	12	5	
	F15	52.4	28	26	21	
	---	Grinding	---	---	---	
	F19	53.5	93	87	22	

A significant percentage of the surface area was covered by the WEL at lower MGT values, Figures 72 and 73, but this decreased with increasing MGT up to grinding. After about 1 MGT following grinding, no WEL was observed on the high rails but about 85% of the surface area of the low rail was covered.

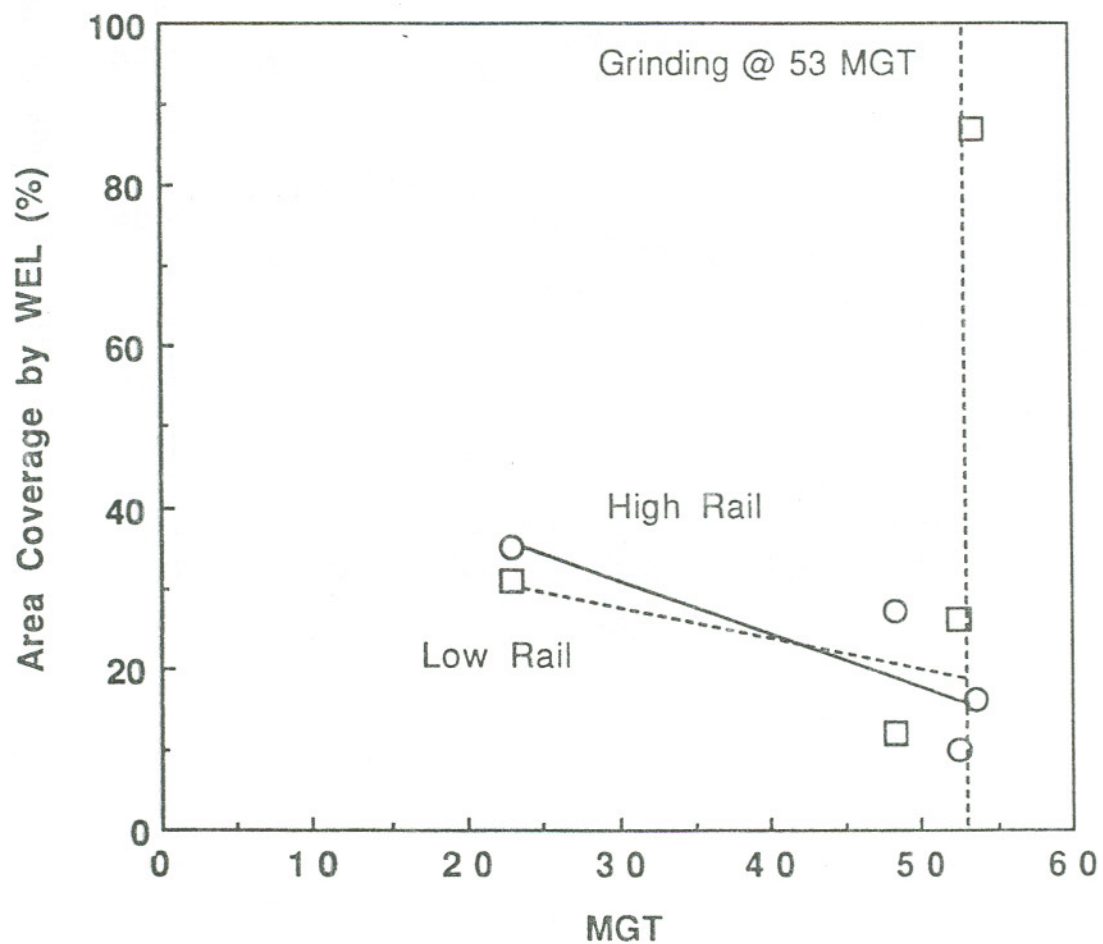


Figure 72 : Percentage surface area coverage by WEL - MP 97.6

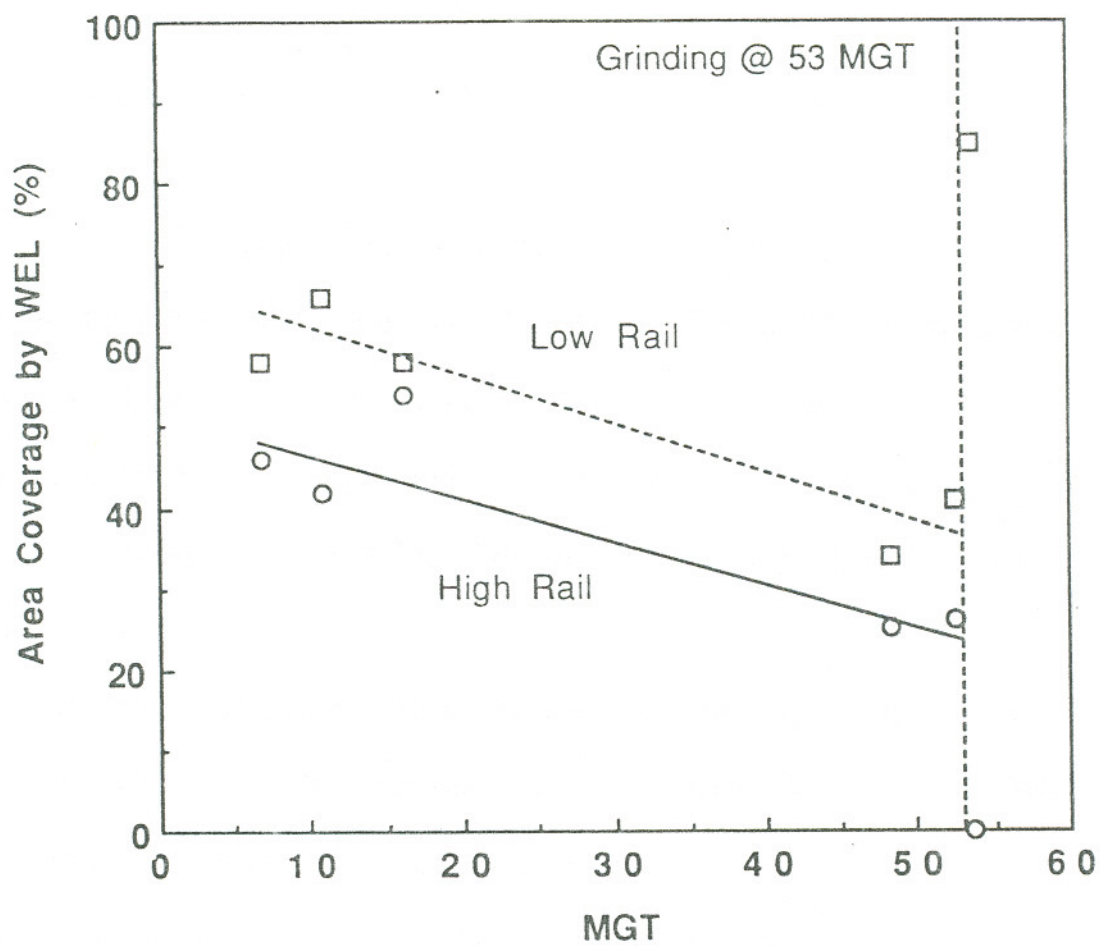


Figure 73 : Percentage surface area coverage by WEL - MP 97.3

Figures 74 and 75 show the variation of the maximum and average WEL depths observed in both high and low rails. After grinding, the maximum depth in the low rails was about 0.008 mm (Figure 76) and the average depth about 0.003 mm.

The percentage of cracks associated with the WEL for both rails is very high at the lowest MGT, Figures 77 and 78. The correlation then decreases steadily up to grinding. After grinding there is no possible correlation between cracks and WEL for the high rail but it is 100% for the low rail. This results from the formation of new WEL at the sites of the long cracks left behind after grinding.

A large number of cracks observed at the higher MGT levels were associated with surface features that could have been sites of spalled WEL. A representative micrograph of this situation is shown in Figure 70 (p145). This could explain why, at the higher MGT levels, the correlation between the number of cracks and the WEL is less than that at lower cumulative tonnage.

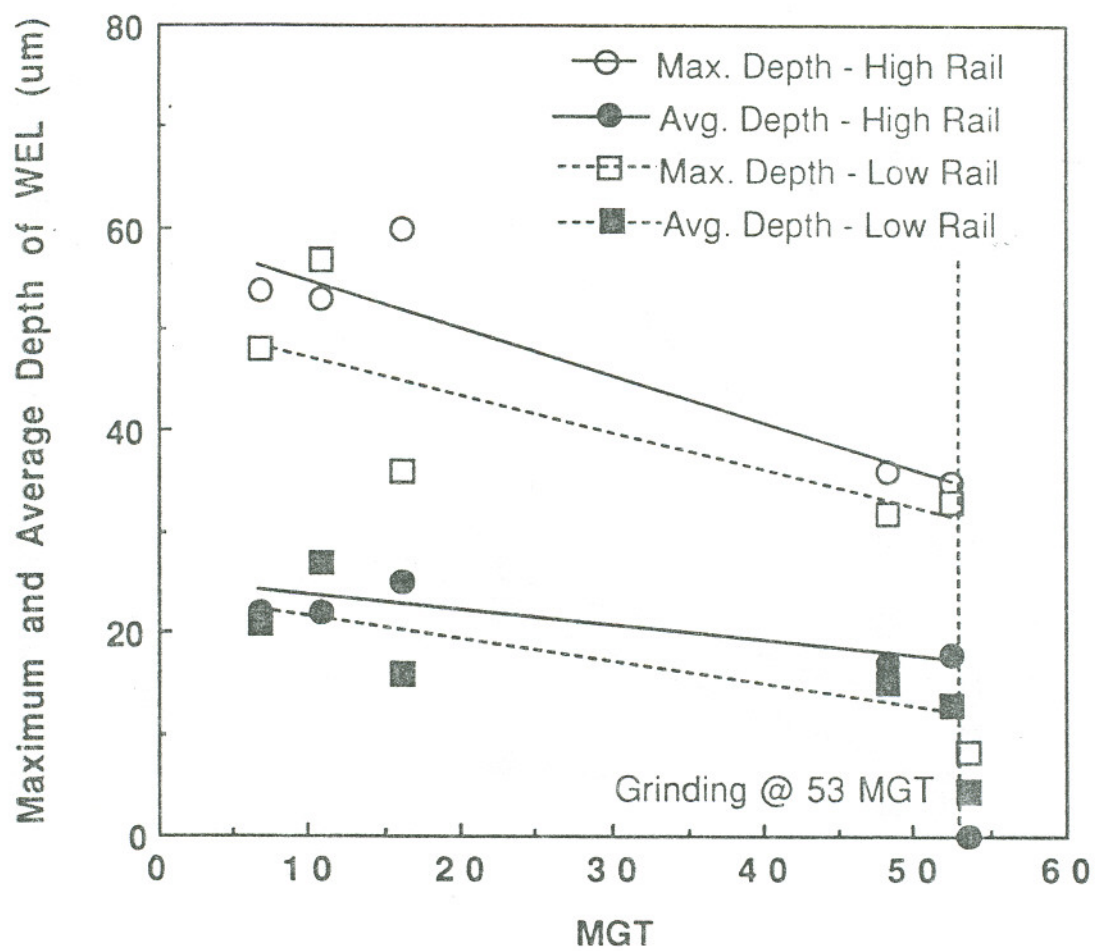


Figure 74 : Maximum and average WEL depth - MP 97.6

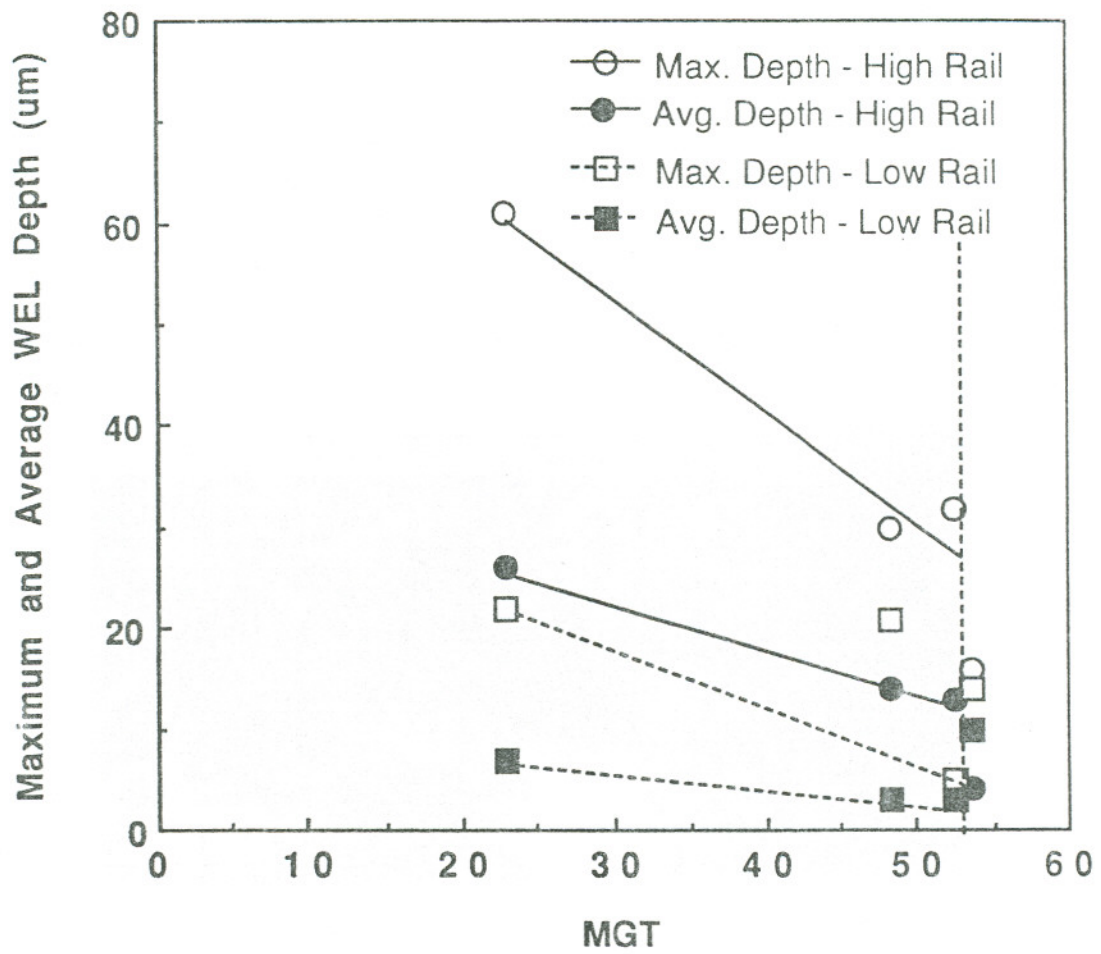


Figure 75 : Maximum and average WEL depth - MP 97.3

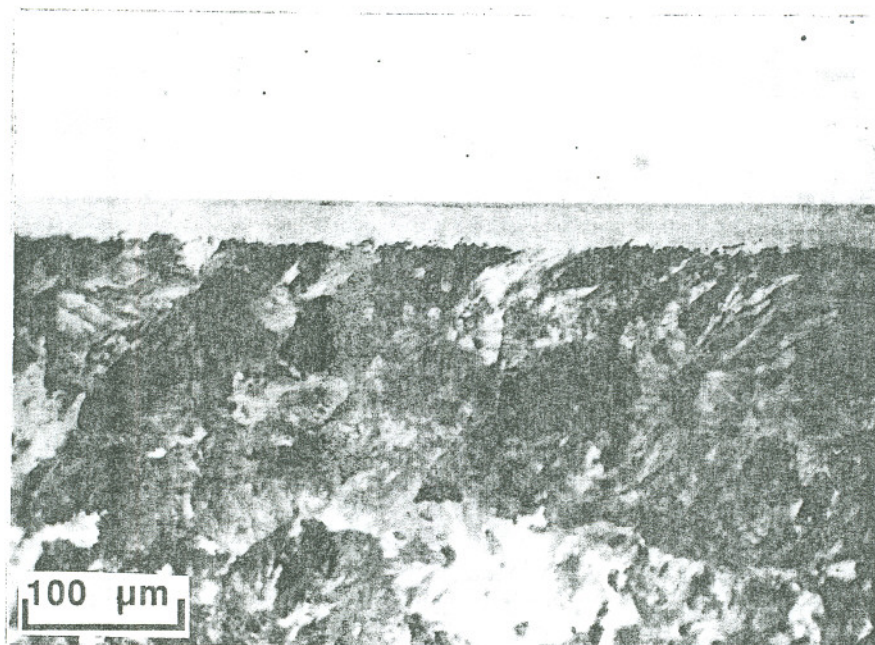


Figure 76 : WEL in low rail of MP 97.6 1 MGT after grinding

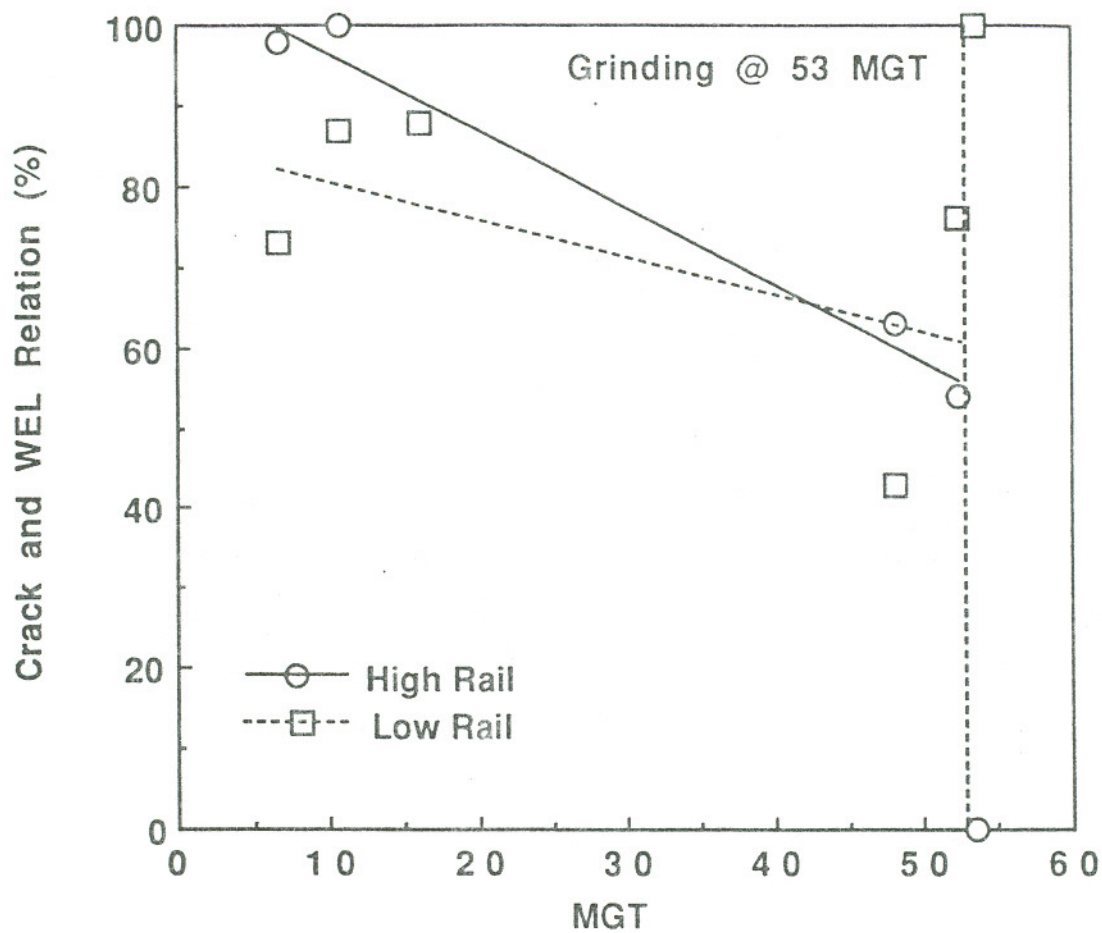


Figure 77 : Correlation between cracks and WEL - MP 97.6

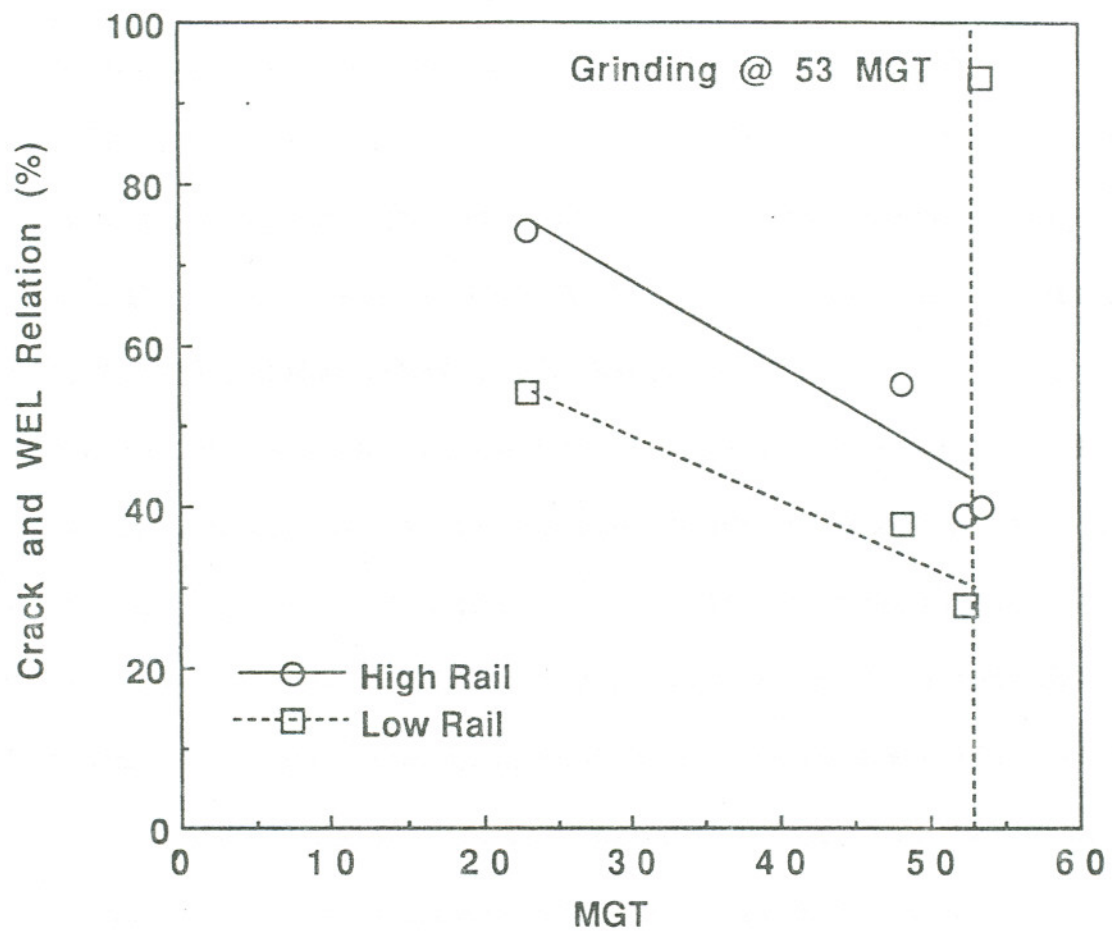


Figure 78 : Correlation between cracks and WEL - MP 97.3

### Study of Cracks in Amsler Test Samples

In the previous section, the progression of cracks in rails in service was studied. To study the development of cracks in the laboratory samples, a series of 6 rolling contact fatigue tests were run on the Amsler machine using the as-received B rail steel (series v, Table VIII, p65). The six tests were run for 5000, 10000, 50000, 100000, 151000 and 206000 cycles.

Figures 79 through 84 give the microhardness as a function of the depth for the 6 tests. In each of the microhardness profiles there is a region of low hardness immediately below the surface (Zone 1). This is followed by an increase in hardness until the maximum hardness is reached (Zone 2). Beyond this the hardness decreases again (Zone 3); in most cases, to below the hardness of the base material (Zone 4) and then increases again till it reaches the base material hardness. Figure 85 gives the maximum hardness in Zone 2 as a function of the number of cycles. One interpretation of the data is that the maximum hardness,  $H_{\max}$ , decreases as a power function of the number of cycles,  $N_{\text{total}}$ , given by:

$$H_{\max}(\text{HK}) = 386 \times (N_{\text{total}})^{-0.0202} \quad (18)$$

Although the trends described above are distinctly seen in the hardness profiles of the rollers from all six tests, it is not clear why these trends develop and there does not seem to be any correlation to the maximum crack depth, the depth of crack networks or the depth of deformation.

In Figures 86 to 91 (A) shows the deepest crack found in the longitudinal specimens (B) shows the depth of the crack networks found in the transverse specimens and (C) shows the deformed surface layers. A group of cracks is considered to form a network when the cracks are joined together. This is most clearly illustrated in Figure 91 where the crack network depth is shown along with the maximum crack depth. The depth of deformation is the maximum depth up to which the deformed layers are clearly visible at a magnification of 200x.

The maximum crack depth, length of longest crack, depth of crack networks and depth of deformed surface layers are given in Table XXX, and plotted as functions of the number of cycles in Figures 92, 93, 94 and 95 respectively.

Table XXX : Summary of crack development measurements

# of Cycles	Max. Crack Depth ( $\mu\text{m}$ )	Longest Crack Length ( $\mu\text{m}$ )	Depth of Crack Networks ( $\mu\text{m}$ )	Depth of Deformation ( $\mu\text{m}$ )
5000	0	0	-*-	10
10000	58	110	-*-	20
50000	180	350	-*-	25
100000	535	820	339	65
151000	494	860	319	99
206000	611	1000	309	116

-\*- No crack networks were observed

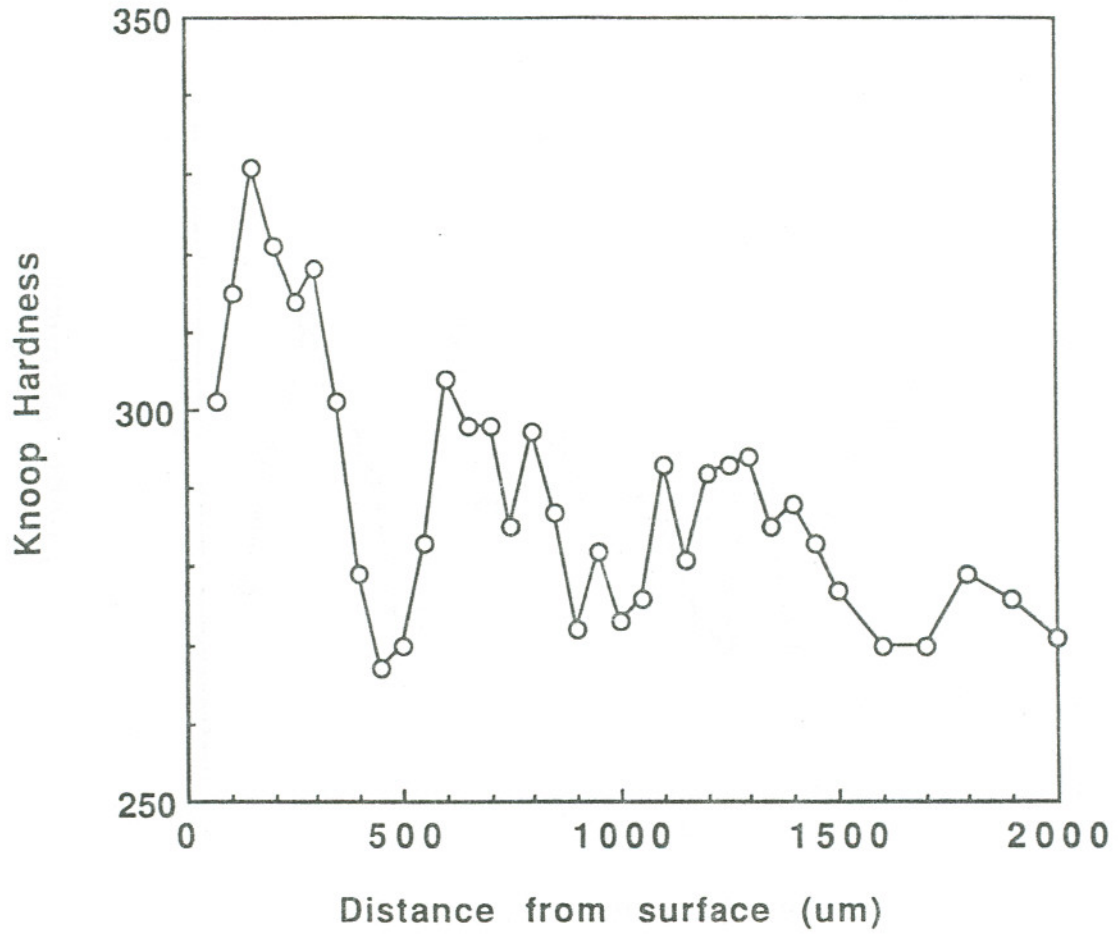


Figure 79 : Microhardness profile for 5000 cycle RCF test

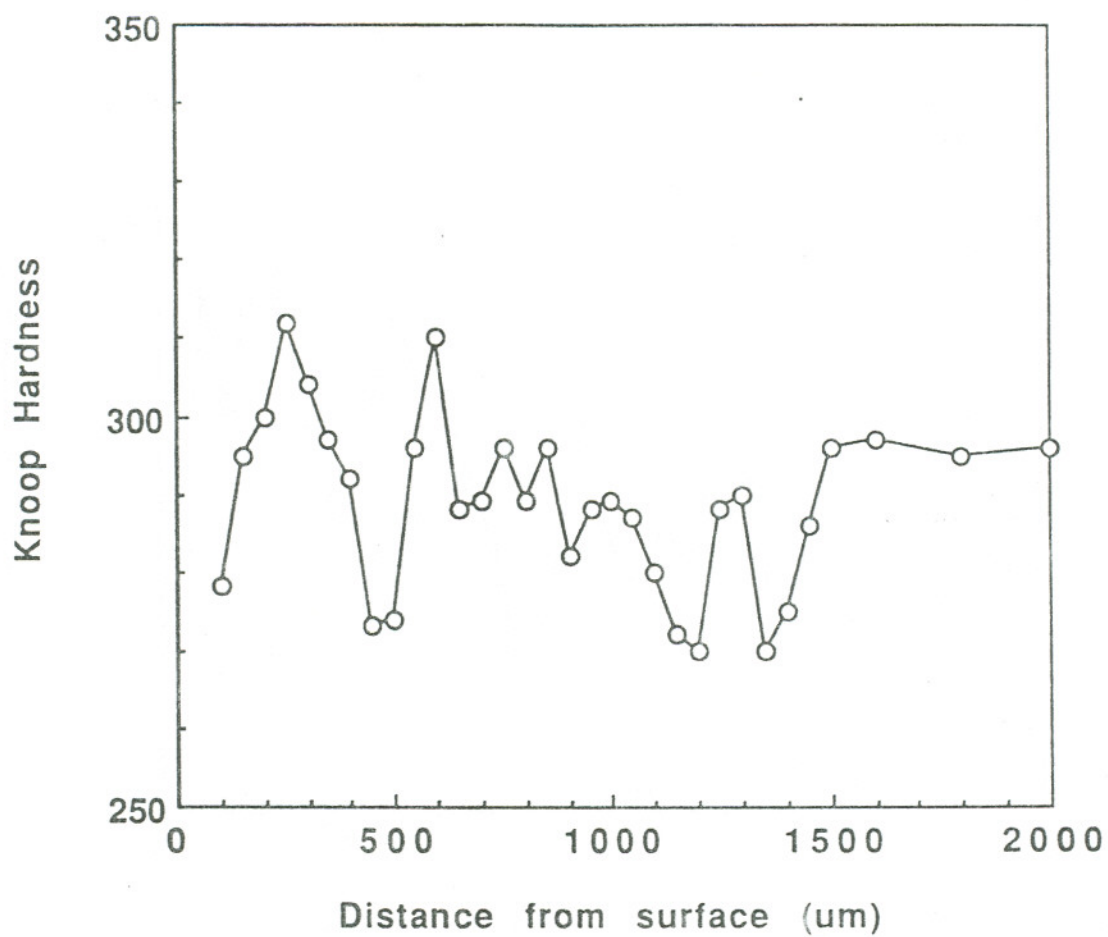


Figure 80 : Microhardness profile for 10000 cycle RCF test

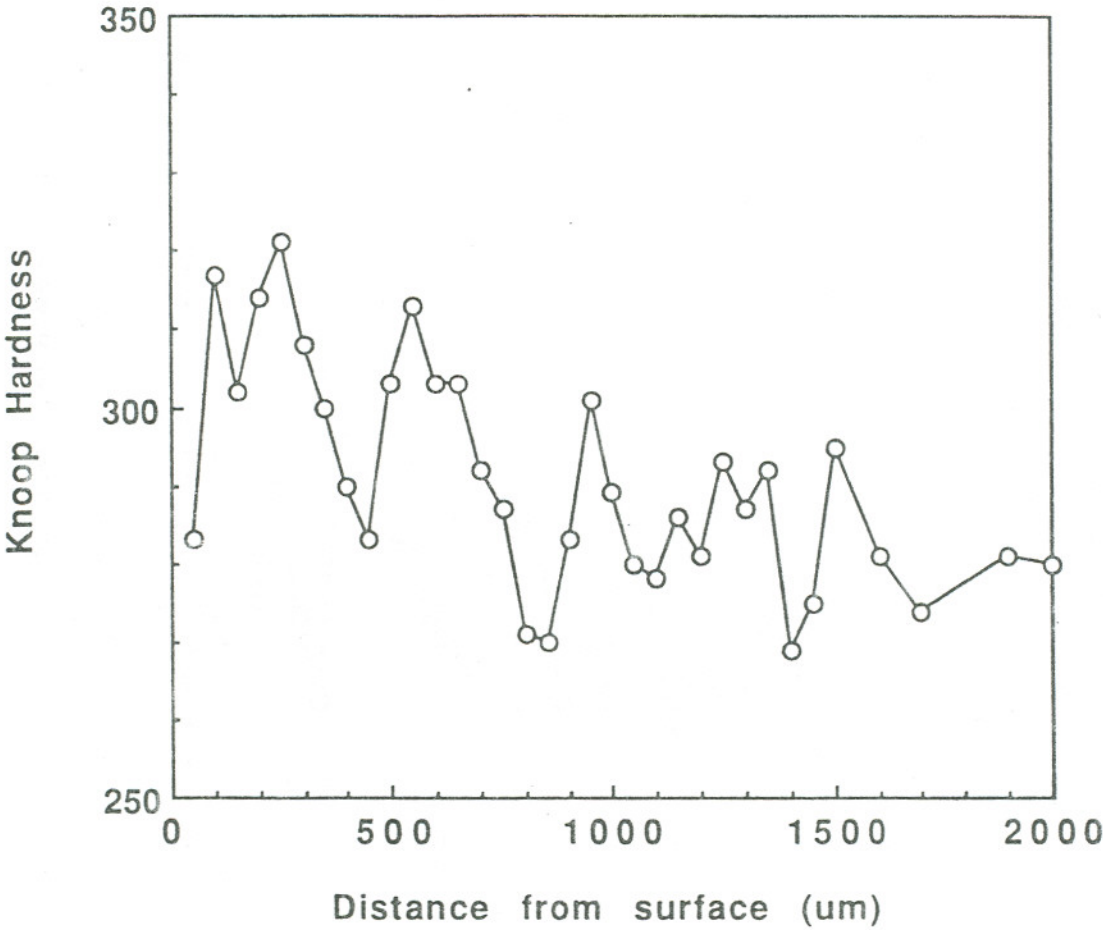


Figure 81 : Microhardness profile for 50000 cycle RCF test

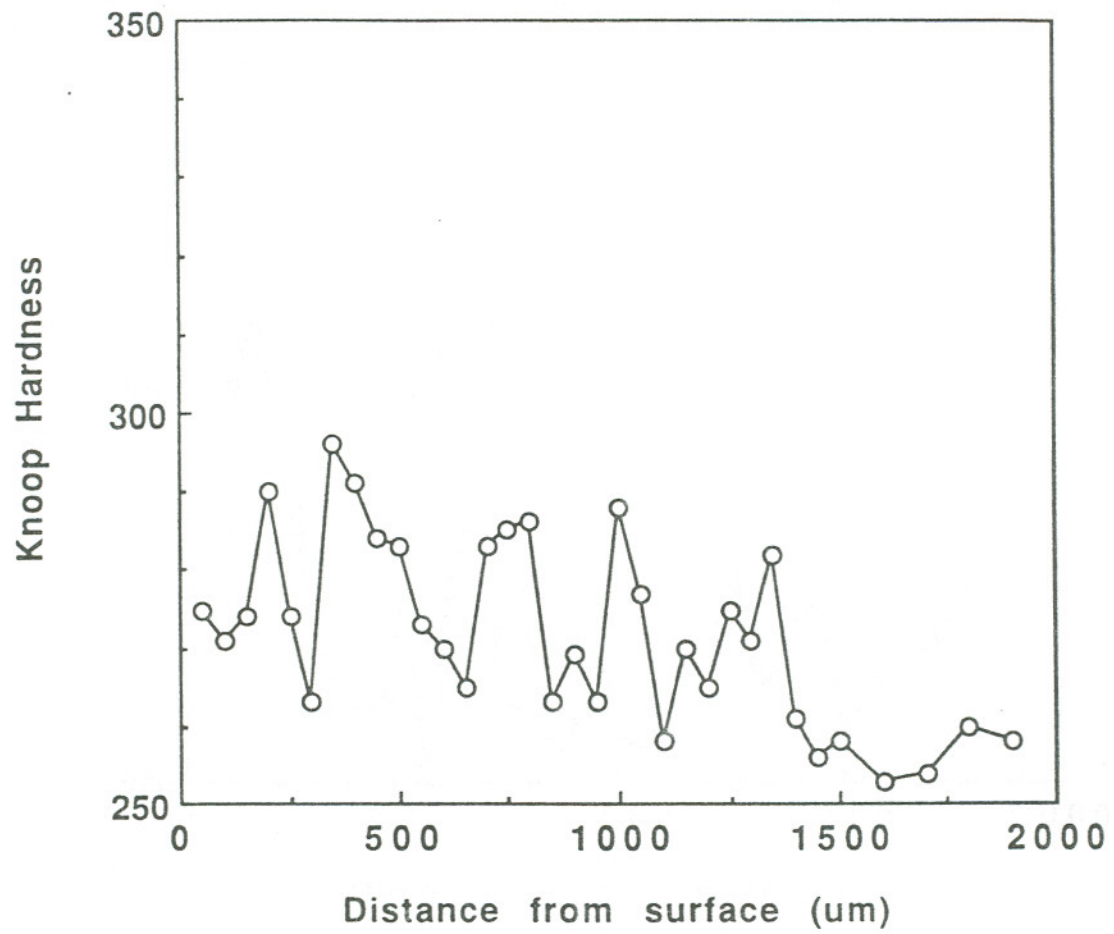


Figure 82 : Microhardness profile for 100000 cycle RCF test

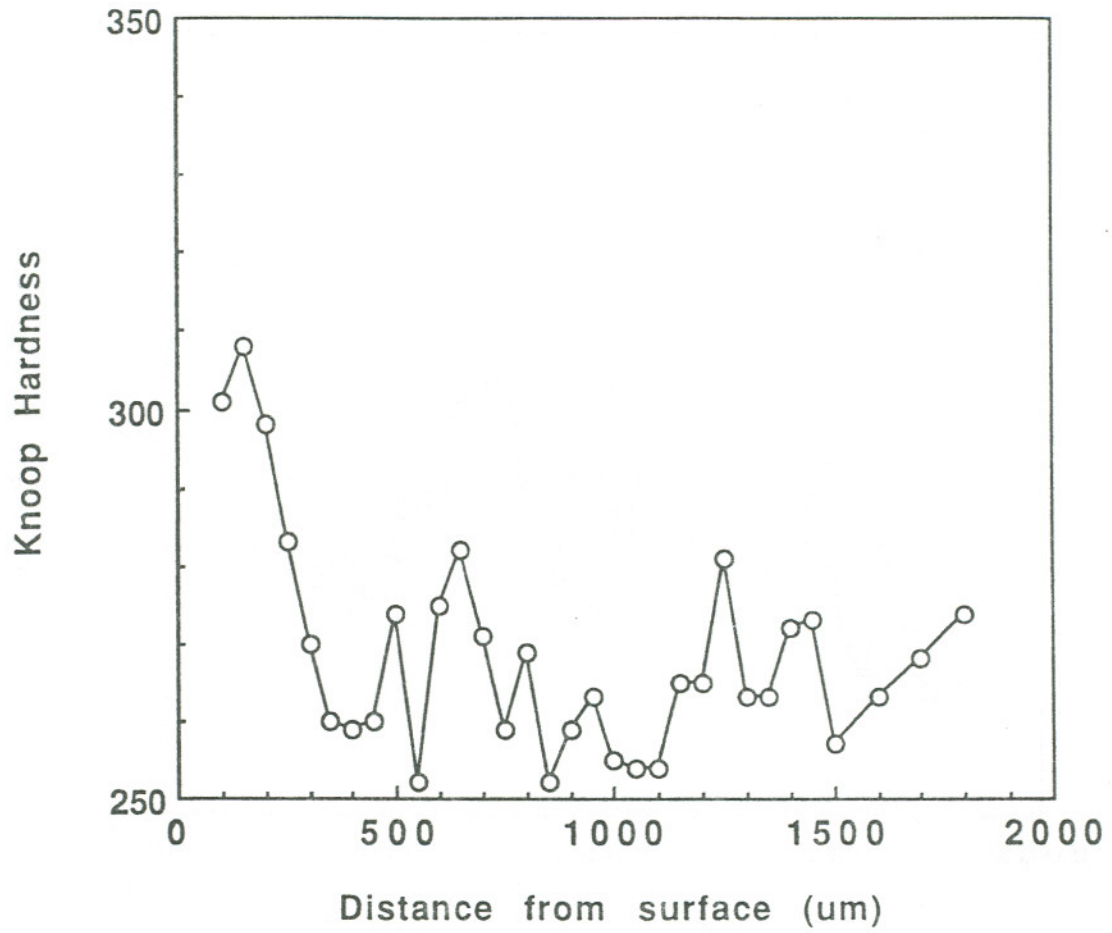


Figure 83 : Microhardness profile for 151000 cycle RCF test

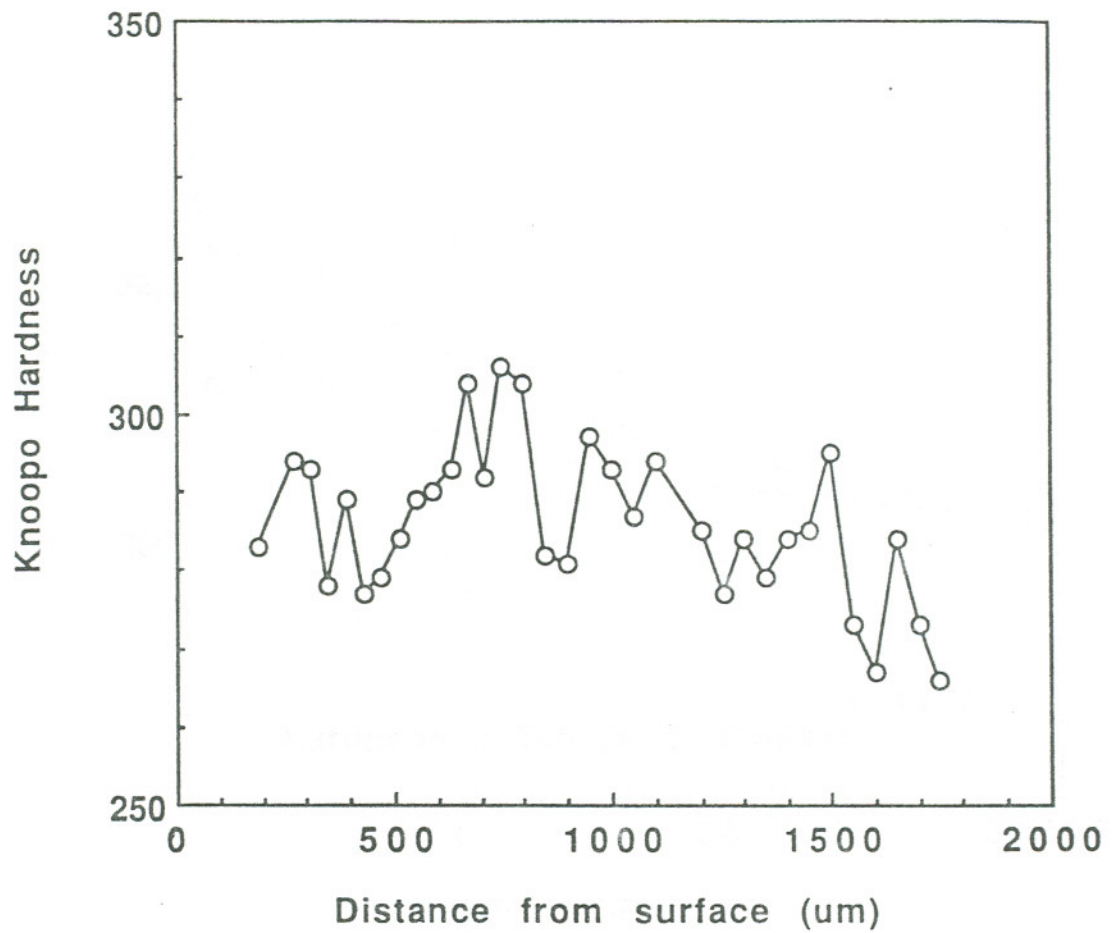


Figure 84 : Microhardness profile for 206000 cycle RCF test

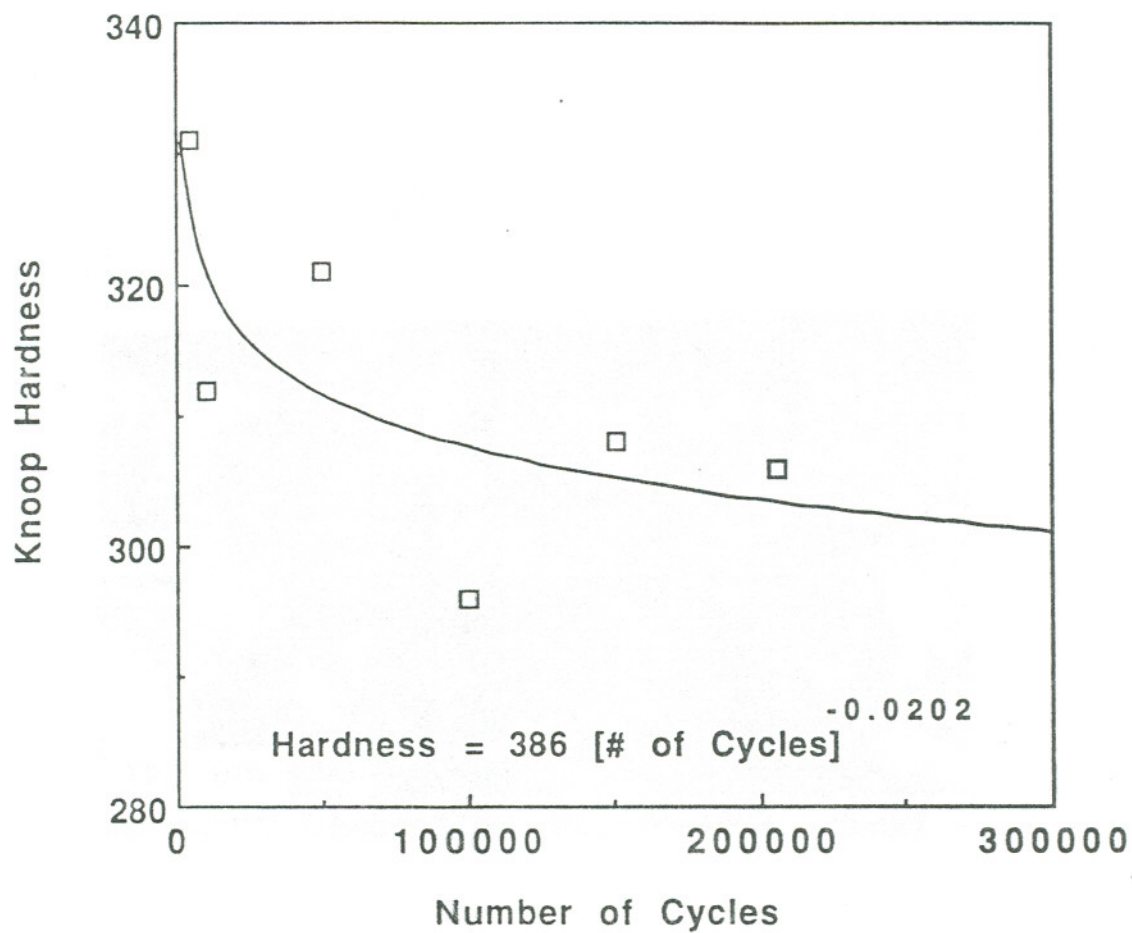


Figure 85 : Maximum hardness versus number of cycles

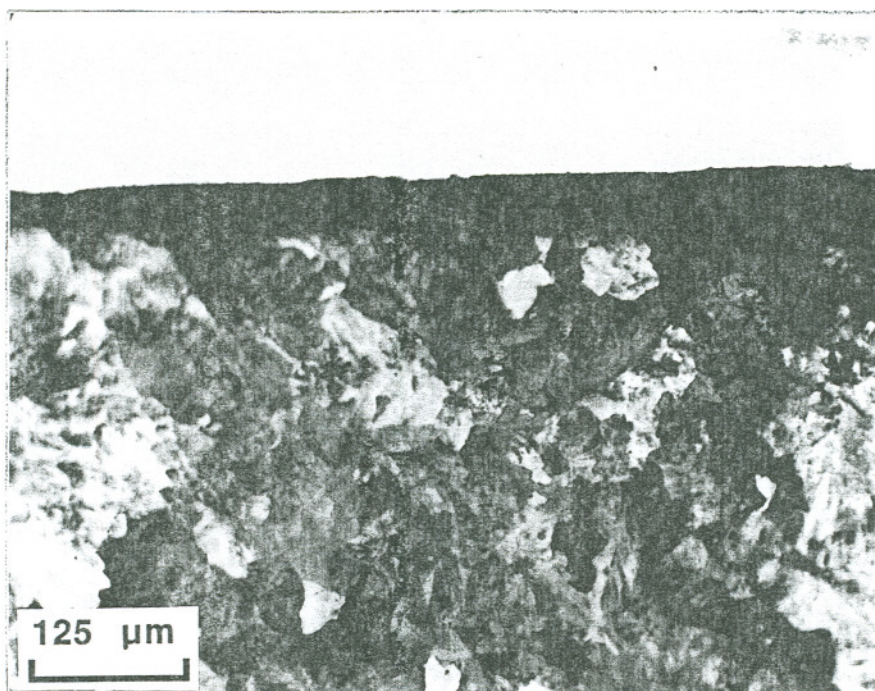


Figure 86 : Depth of deformation - 5000 cycles

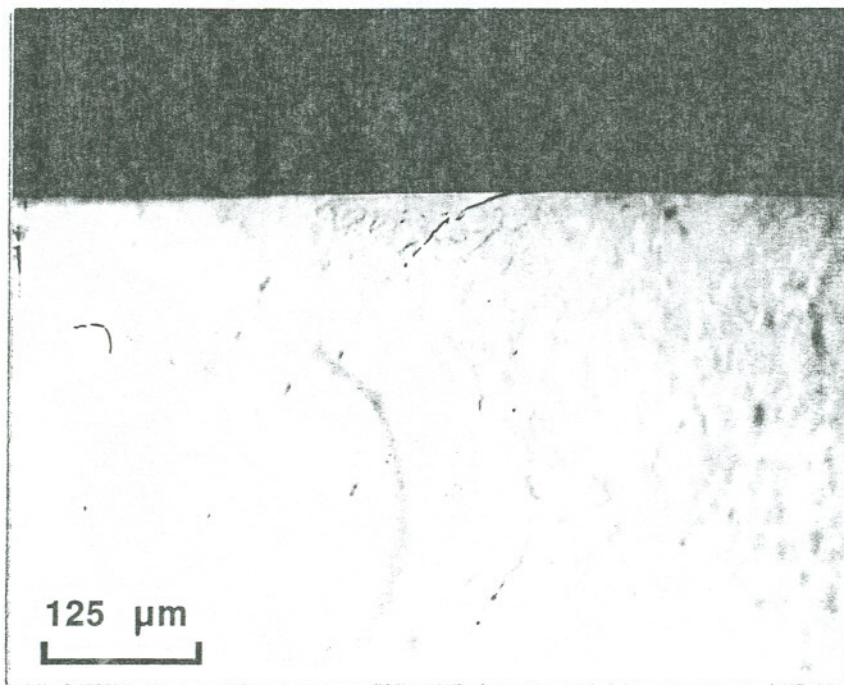


Figure 87 (A) : Maximum crack depth - 10000 cycles

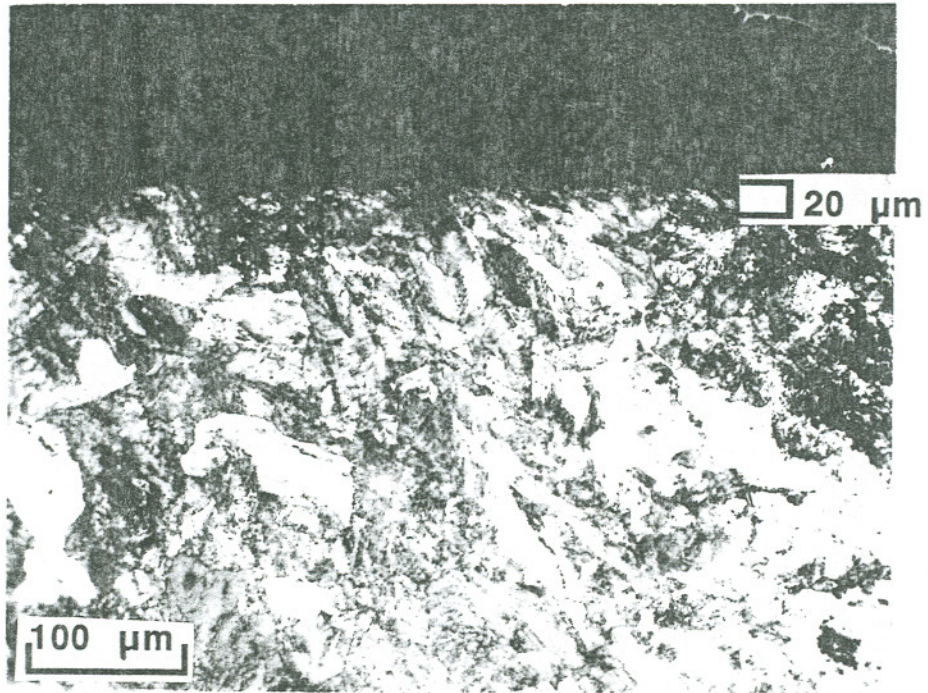


Figure 87 (B) : Depth of deformation - 10000 cycles

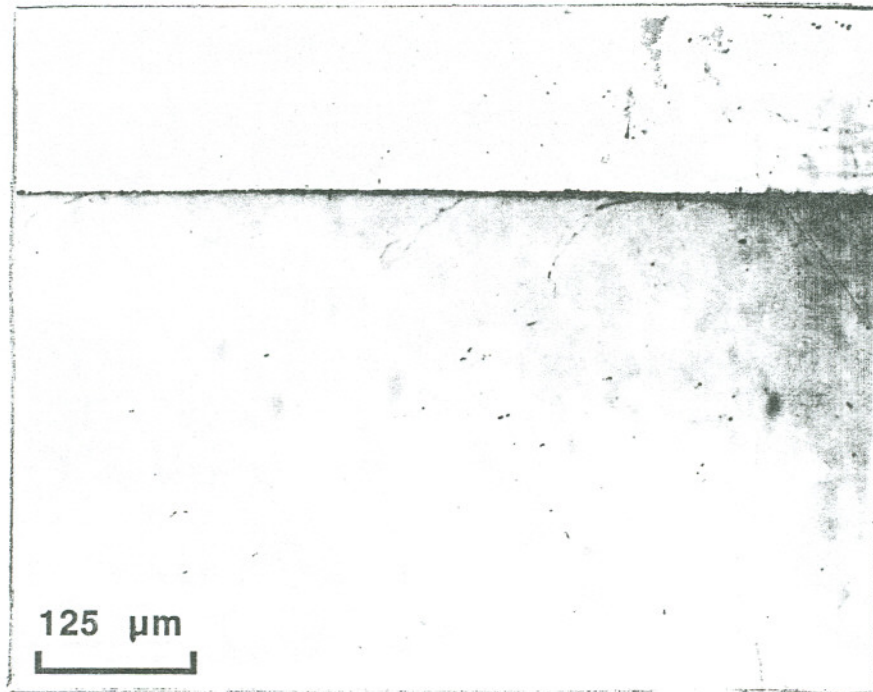


Figure 88 (A) : Maximum crack depth - 50000 cycles

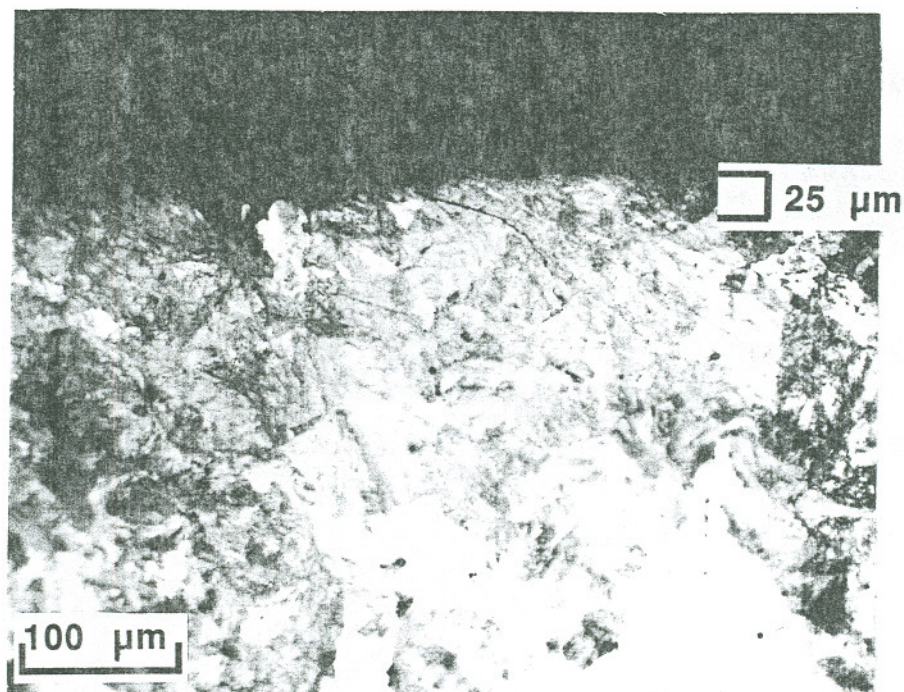


Figure 88 (B) : Depth of deformation - 50000 cycles

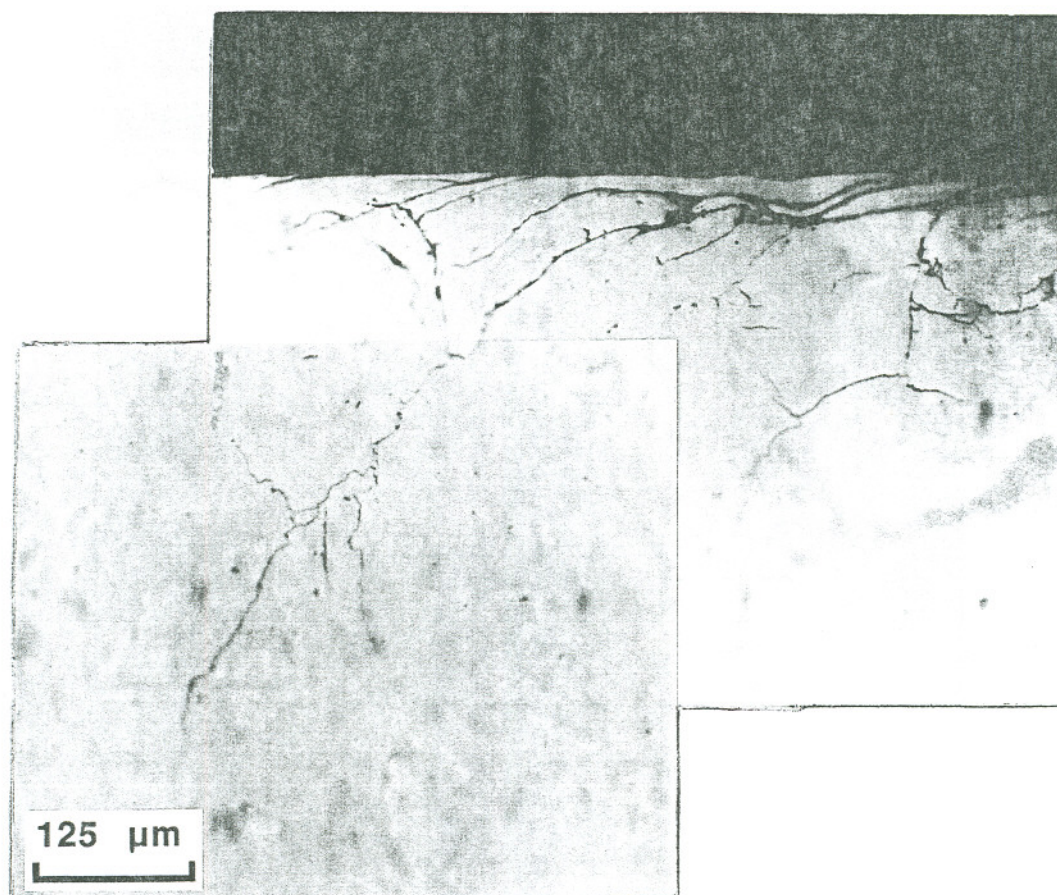


Figure 89 (A) : Maximum crack depth - 100000 cycles

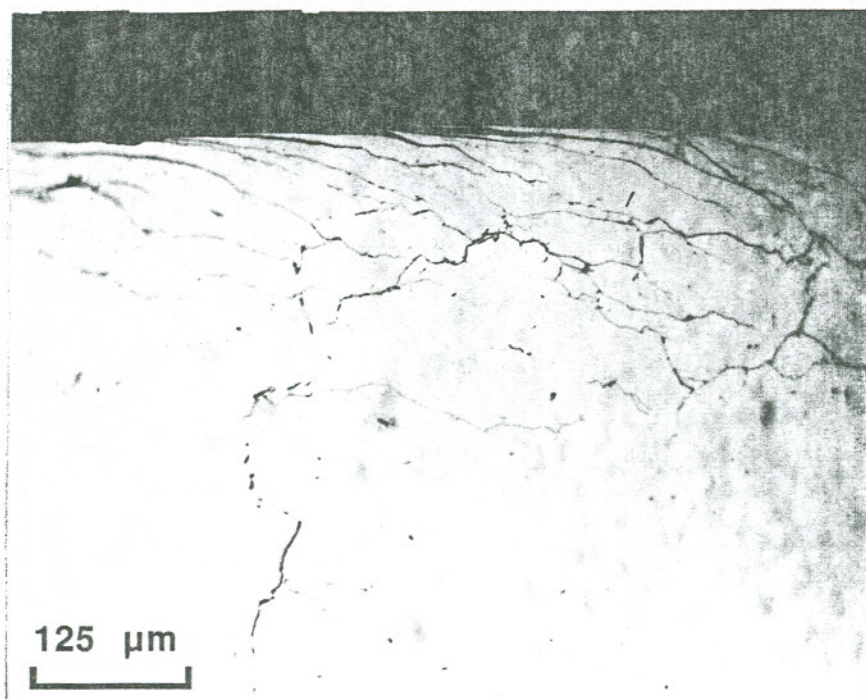


Figure 89 (B) : Crack network depth - 100000 cycles

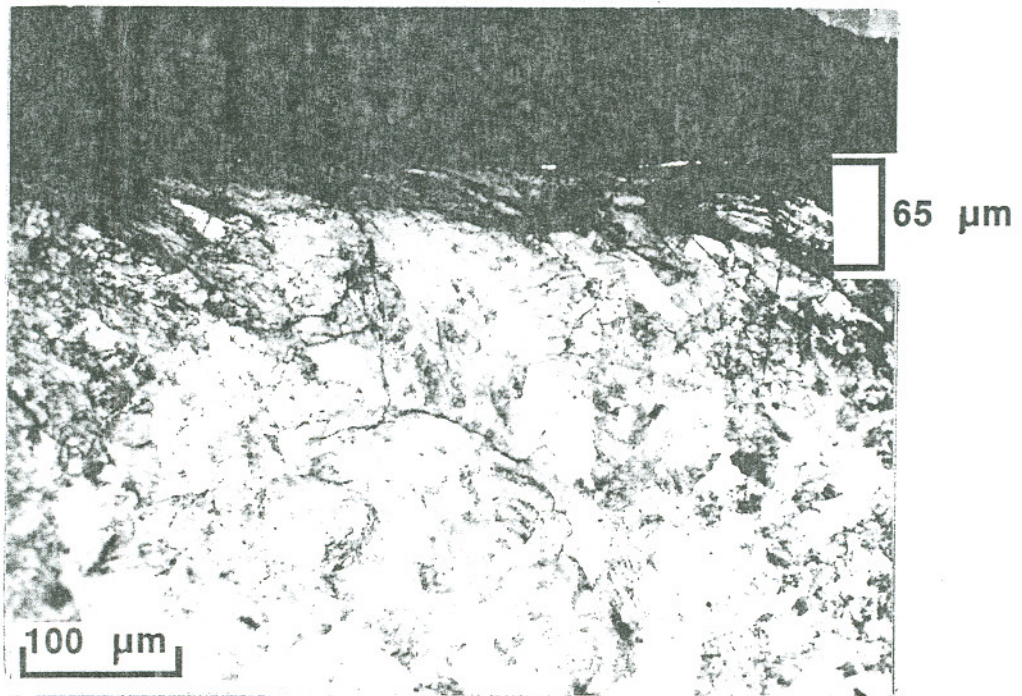


Figure 89 (C) : Depth of deformation - 100000 cycles

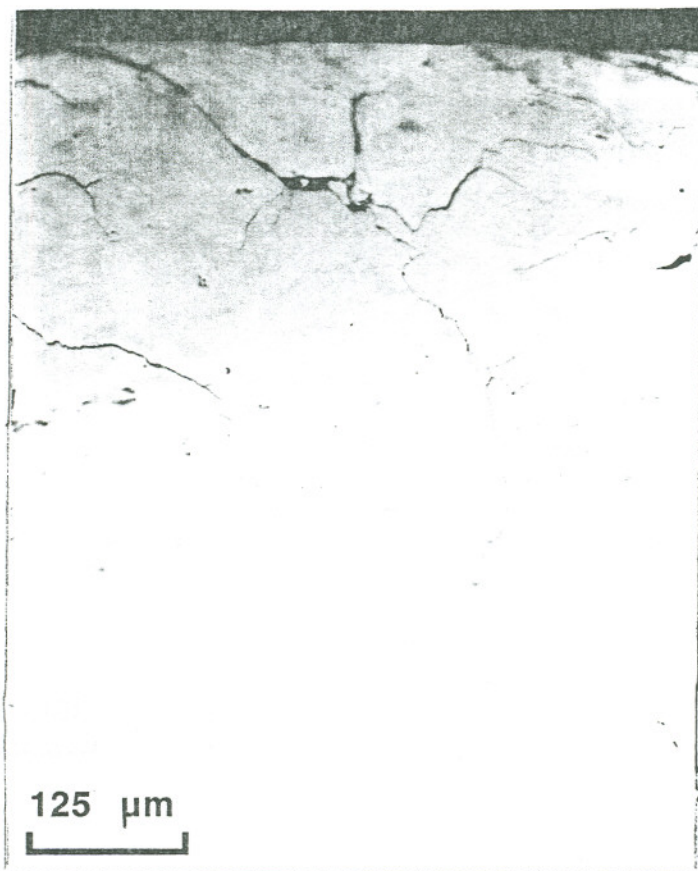


Figure 90 (A) : Maximum crack depth - 151000 cycles

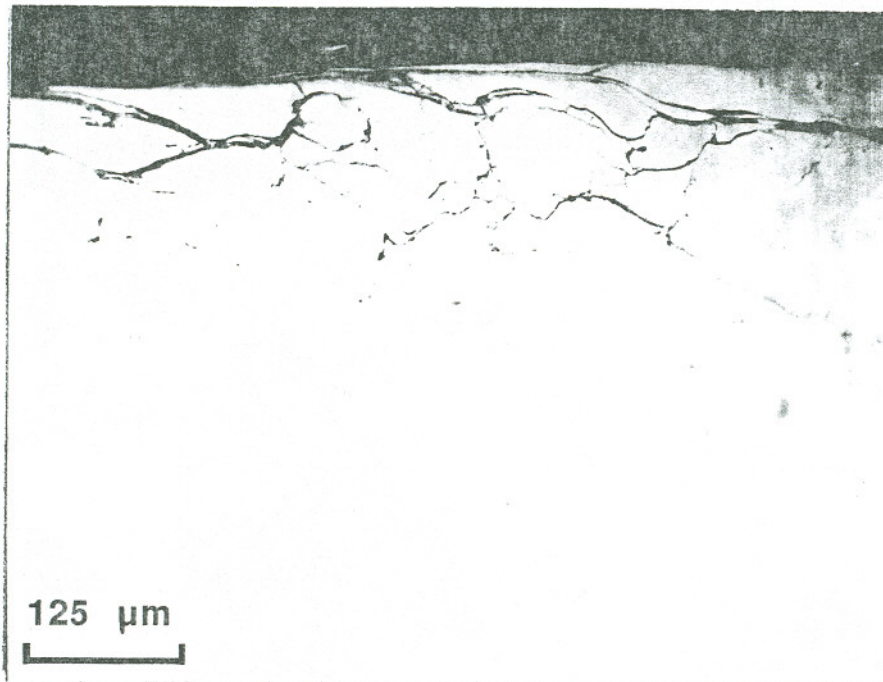


Figure 90 (B) : Crack network depth - 151000 cycles

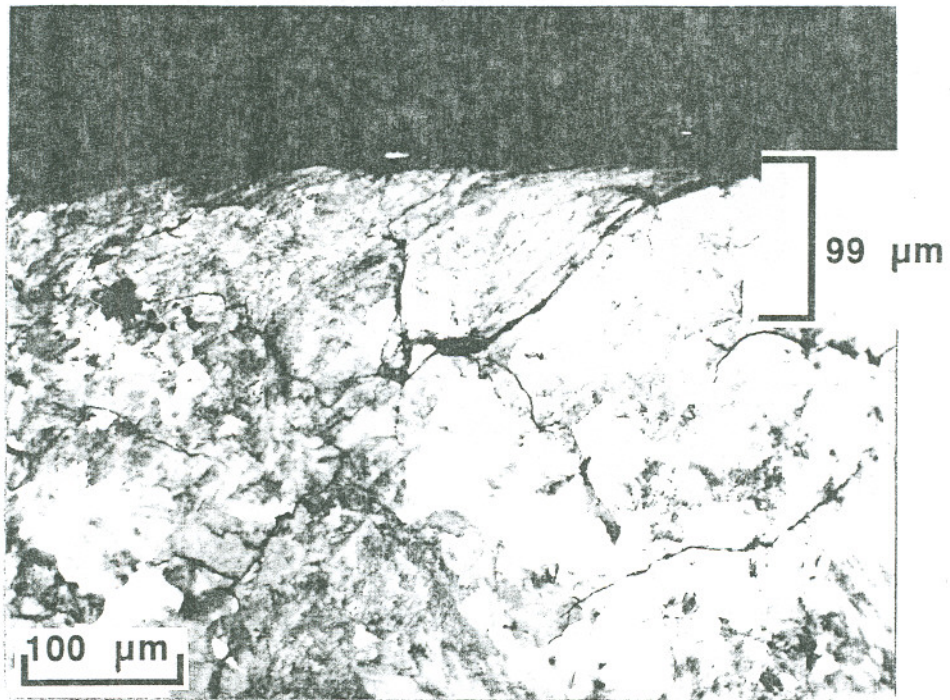


Figure 90 (C) : Depth of deformation - 151000 cycles



Figure 91 (A) : Maximum crack depth - 206000 cycles

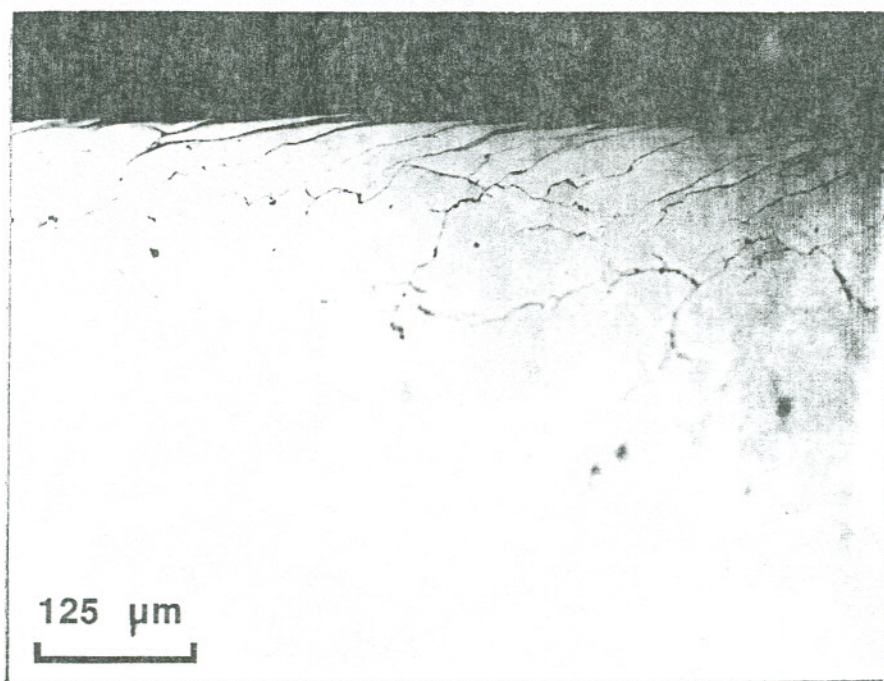


Figure 91 (B) : Crack network depth - 206000 cycles

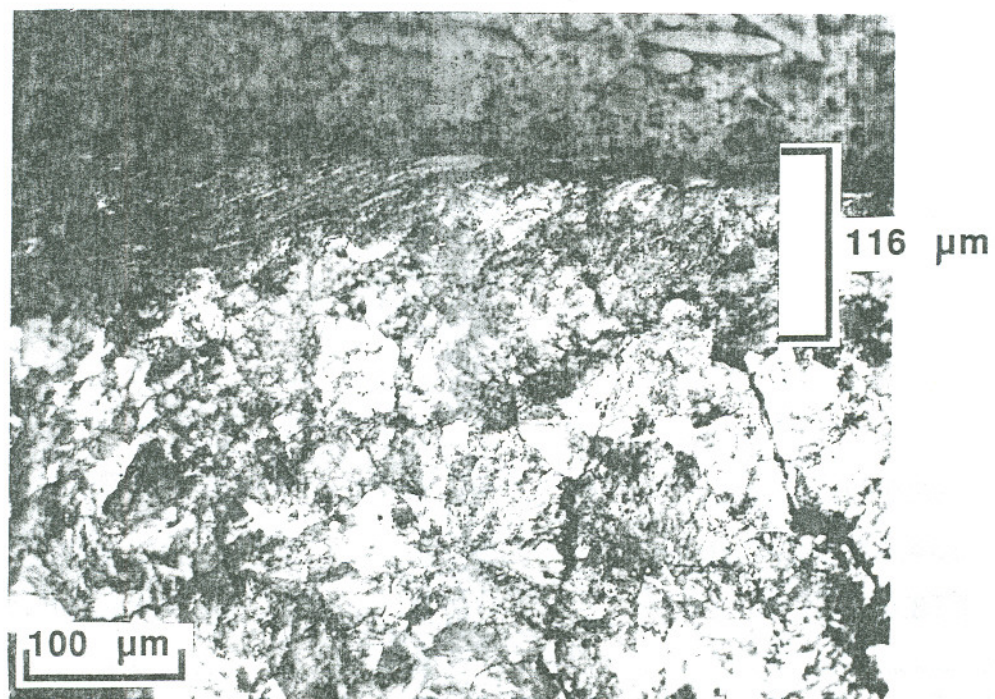


Figure 91 (C) : Depth of deformation - 206000 cycles

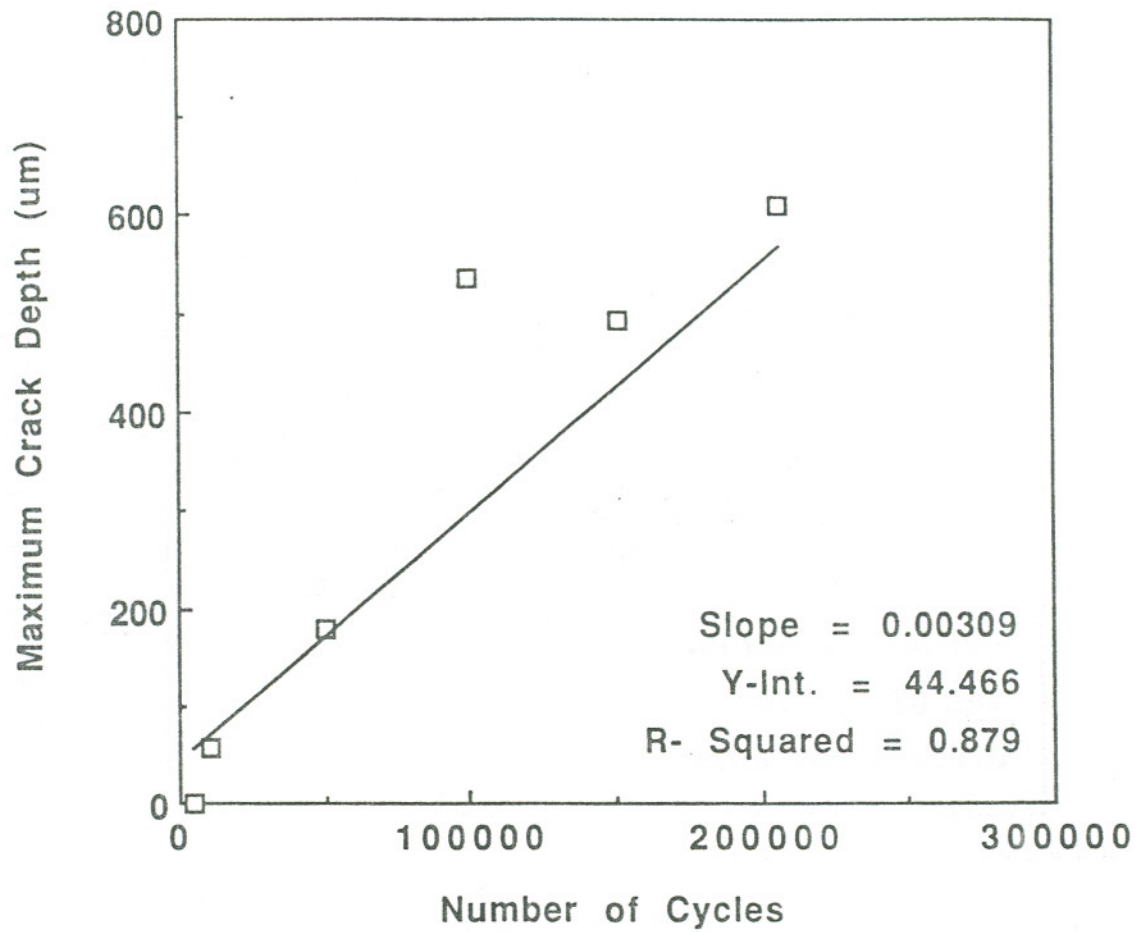


Figure 92 : Maximum crack depth vs number of cycles

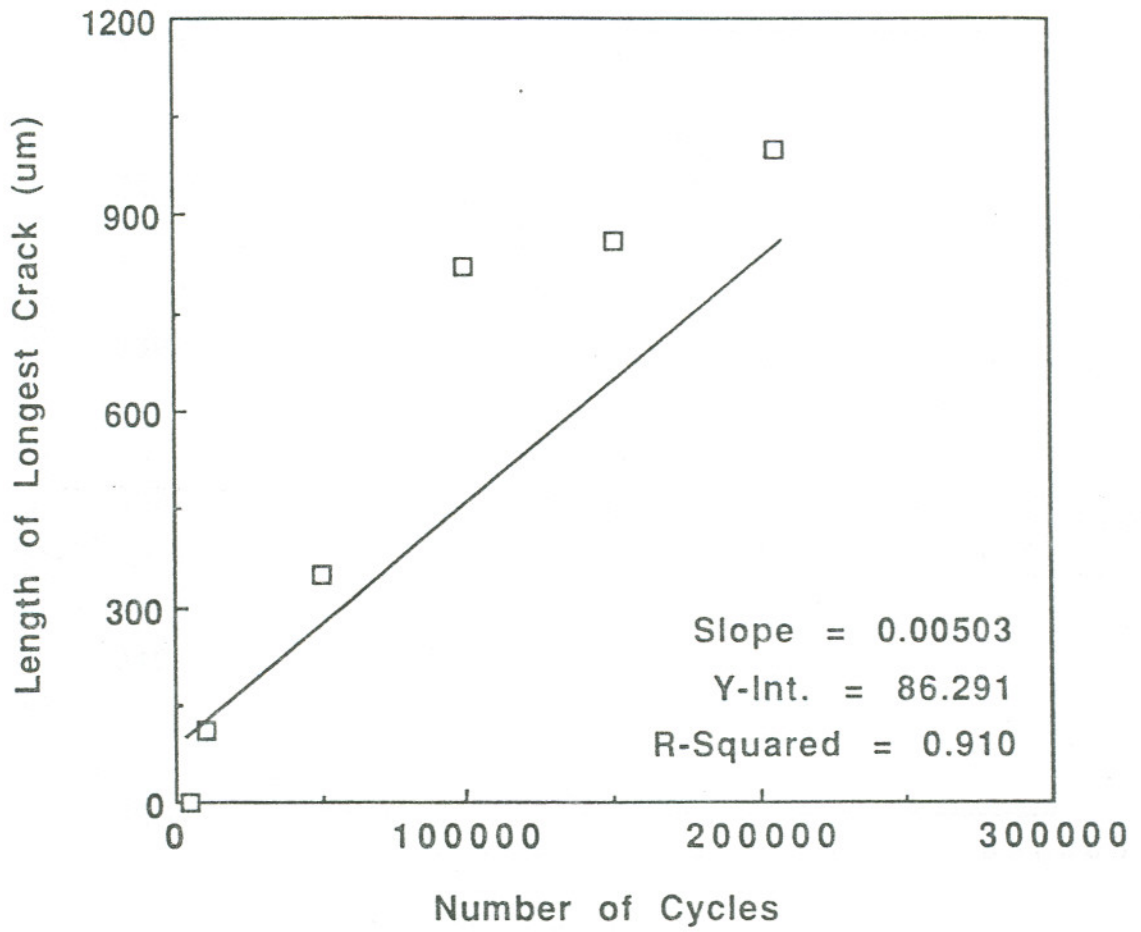


Figure 93 : Length of longest crack vs number of cycles

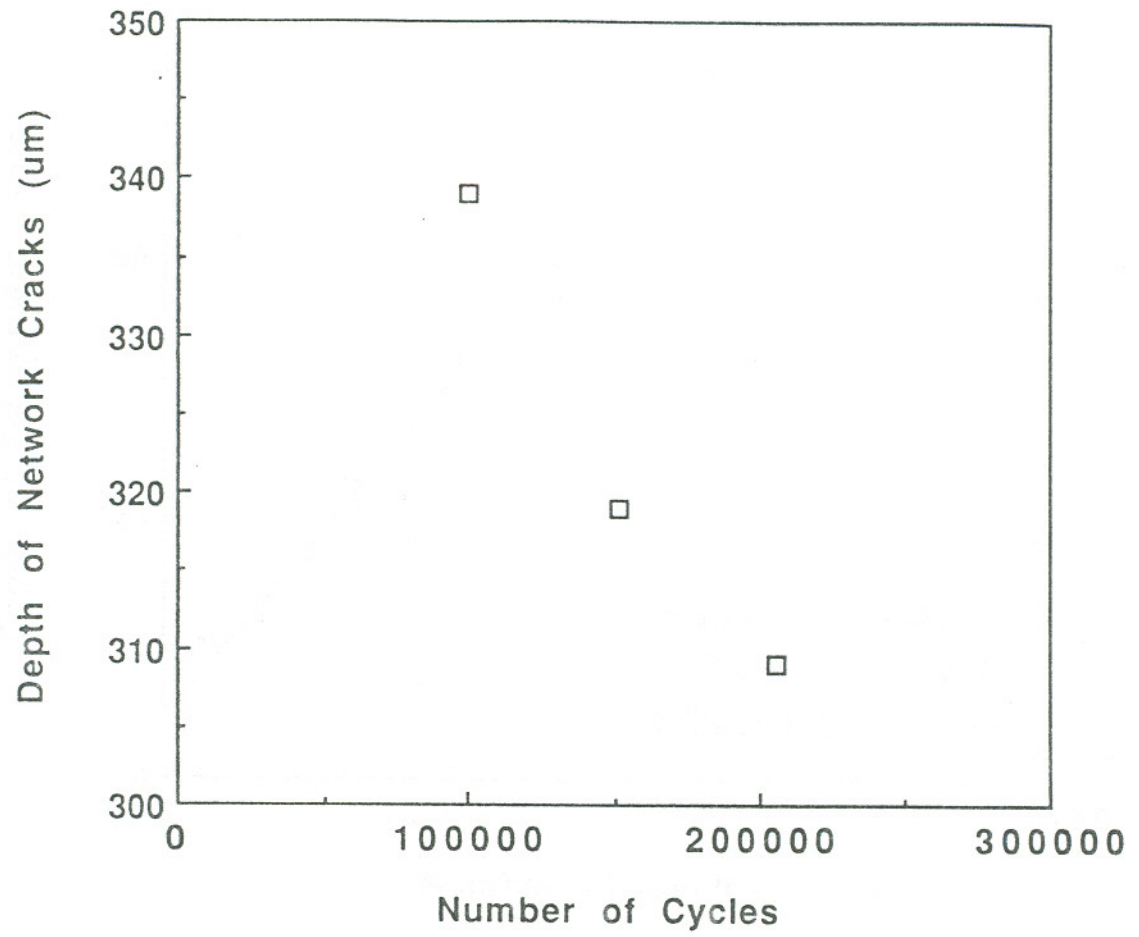


Figure 94 : Crack network depth vs number of cycles

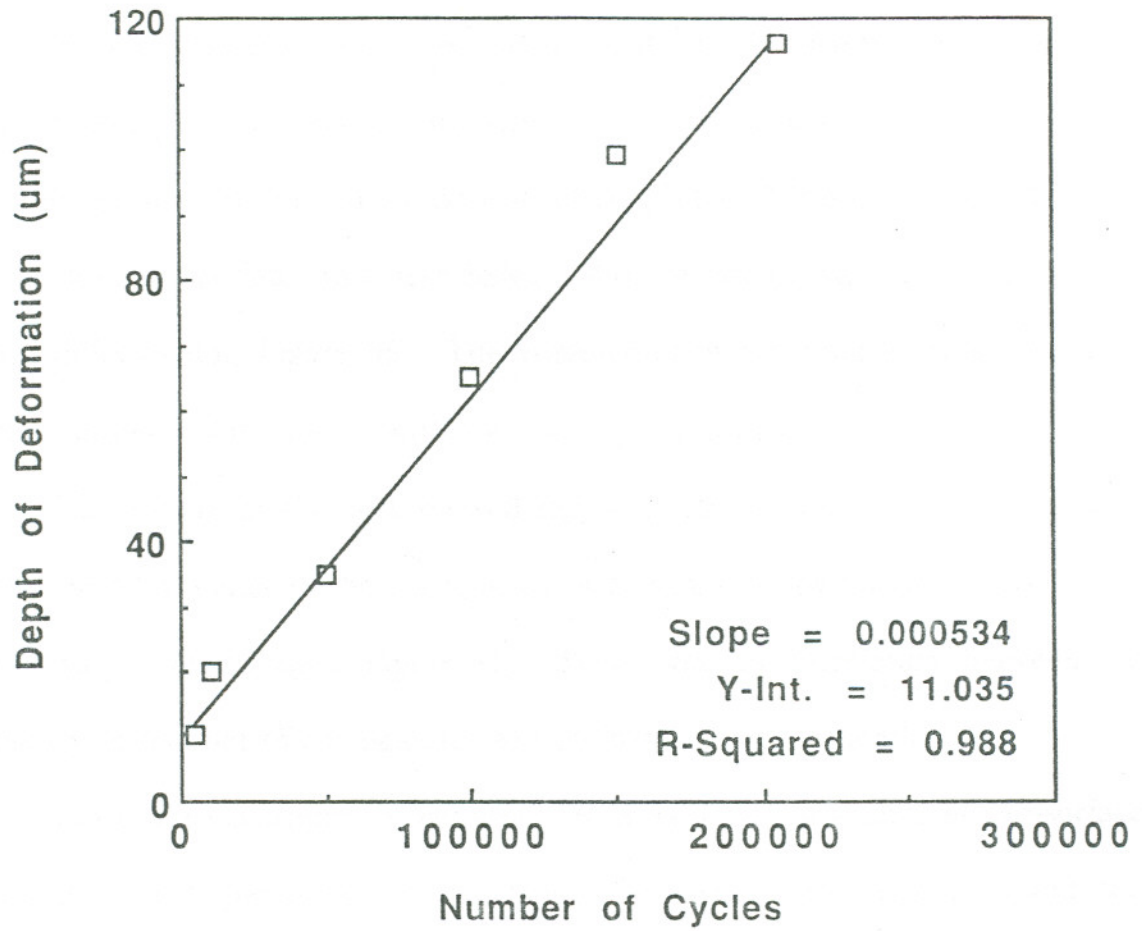


Figure 95 : Depth of deformed layers vs number of cycles

### SUB-SURFACE DEFORMATION TESTING

Rolling contact tests were carried out on the Amsler and the MTI machines using various sets of parameters to try and generate wholly sub-surface contained plastic deformation in the test rollers (Tables XII and XIII, p86-87). Of all the tests described, only test SSM04 showed wholly sub-surface contained plastic deformation, Figure 96. The corresponding microhardness profile as a function of depth from the running surface is given in Figure 97.

The rollers in this test showed the presence of corrugations. The total number and frequency of the corrugations was measured by taking a trace of the roller using carbon paper, Figure 98. There was no correlation between the frequency or number of corrugations and the number of gear teeth.

Since the occurrence of corrugations obscures the presence of sub-surface deformation, the parameters were varied for subsequent tests to avoid the formation of corrugations. According to Hamilton [64] corrugations can be avoided by either changing the diameters of the rollers or by using rollers having significantly different Young's moduli. For this the bottom rollers for some of the tests were heat treated (p77) to provide a hardness much greater than that of the test roller. While the rollers in these tests (test #s SSM05, SSM06 and SSM07) did not corrugate, they did not exhibit sub-surface deformations. The same was the case when rollers of different diameters were used (test #s SSM08-11).

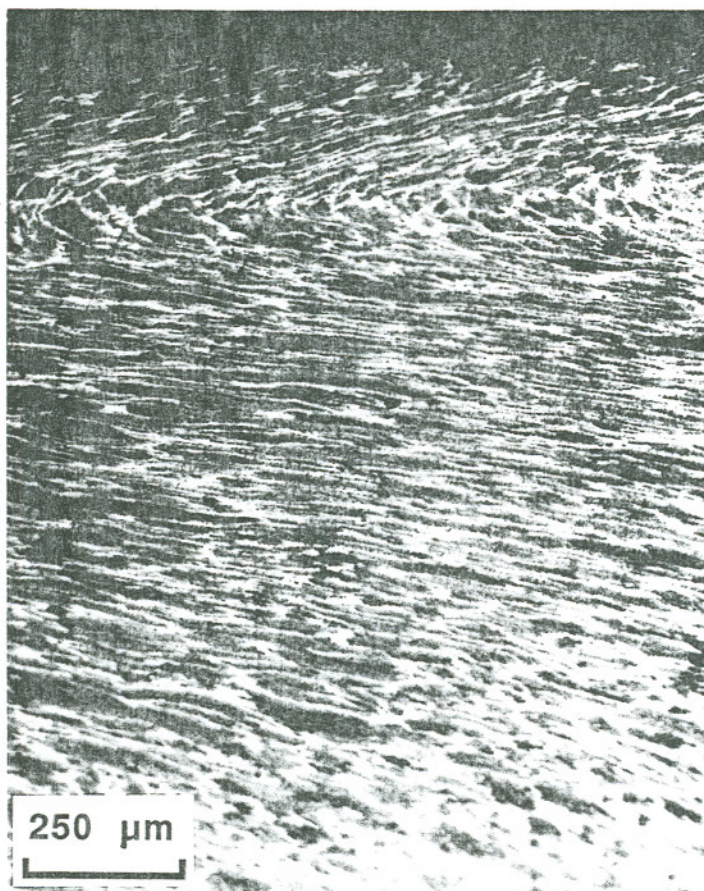


Figure 96 : Sub-surface deformation in roller SSM04

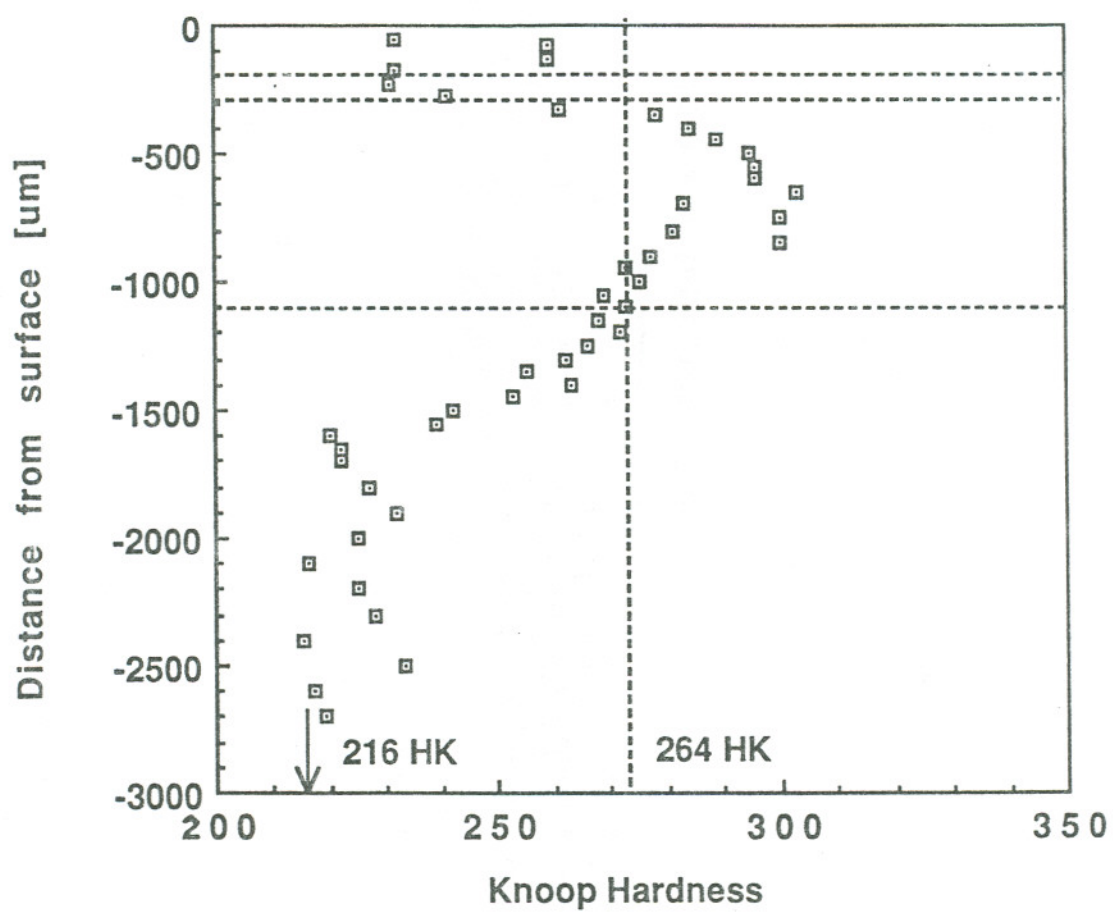


Figure 97 : Microhardness profile of sample in Figure 96

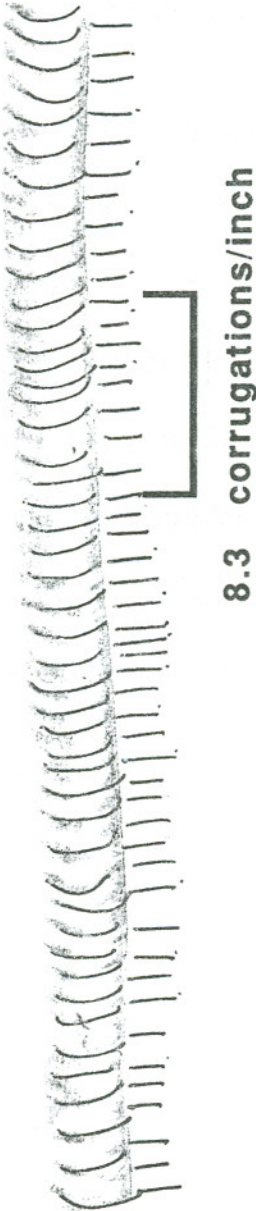


Figure 98 : Trace of corrugations in roller SSM04

### RCF TESTS TO STUDY EFFECT OF LUBRICANT

Preliminary RCF tests were run using water and oil lubrication to decide on the lubricant to be used for subsequent tests (p83 & series i-m & iii-a Table VIII, p65). These tests can be used to provide information about the effect of the lubricant in terms of the effect of the coefficient of friction,  $\mu$ .

Table XXXI gives the RCF life data for water and oil lubricated tests for the A series steel. Also included are the model predictions for the A series steel for water lubrication and the relative difference in RCF life for water lubrication (model prediction) and oil lubrication (experimental). These data are plotted in Figure 99.

**Table XXXI : RCF life for water and oil lubrication - A series**

Po (N/mm <sup>2</sup> )	Water Lubrication $\mu = 0.27$		Oil Lubrication $\mu = 0.13$	
	Predicted Life *	Experimental Life	Predicted Life *	Experimental Life
1413	0.17	0.15	0.17	3.26
1395	.039	---	0.39	13.13
1378	.059	1.64	0.59	13.70
1378	.059	1.64	0.59	13.70

\* Predicted life calculated using Eq.14, p106 - No effect of lubricant  
RCF life is in multiples of 100000 cycles

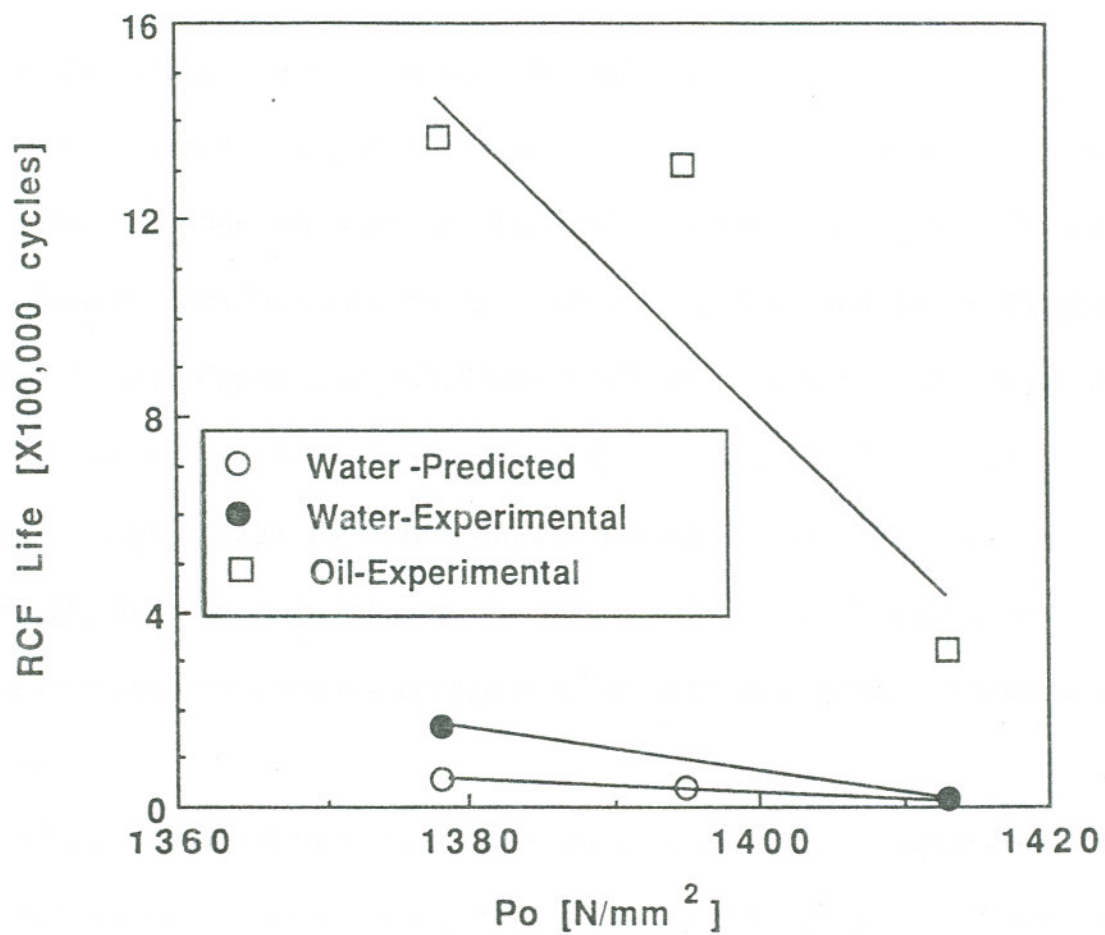


Figure 99 : RCF life plots for oil and water lubrication

## CHAPTER 4 : DISCUSSION

Under rolling contact, each time the material passes through the contact region, it is subjected to a cycle of stresses. As a result of the contact, embryonic cracks generate in both the top and bottom rollers in the early stages of the life; cracks about 0.1 mm long were found at less than 25% of RCF life by Clayton and Hill [31] and Fujitsu *et al* [91]. Dawson [70] found cracks typically 1  $\mu\text{m}$  in length and contained in the surface layers. During subsequent contact cycles, if the wear rate is high enough, these embryonic cracks are lost, or, if the wear rate is low enough, they can propagate into the substrate. When a lubricant is used, it reduces wear rates to levels low enough to allow embryonic cracks to remain and propagate.

If it is considered that a certain amount of deformation is required for the embryonic cracks to initiate, then the lubricant, by reducing the coefficient of friction, necessitates a higher number of cycles to reach the required level of deformation and hence a higher life. For the lubricant to facilitate propagation, as shown by Way [32], the cracks need to be oriented in a specific direction, so that the crack mouth enters the contact region before the crack tip does. Such a condition is prevalent when the direction of tangential traction is the same as that of rolling. This happens in the slower moving or driven roller; the upper roller in the tests described in this work. In these tests, the driven upper rollers failed from

surface initiated rolling contact fatigue while none of the bottom rollers exhibited any obvious external signs of surface cracking.

### Comparison of Failures

The main aim of this work was to formulate a model to predict the RCF of rail steels under water lubricated contact conditions. For this it was necessary to first confirm that the defects or failures produced by the laboratory test were similar to those found in rails in service. The rail defects that we are concerned with here are the surface initiated defects. Typical examples of these defects are shown in Figure 14 (p58) and 100 [79]. It has been found that the cracks associated with these defects start in the deformed surface layers and propagate into the substrate at a shallow angle of about  $30^\circ$  to the running surface, in a direction opposite to that of rolling [17,20,31]. These cracks follow the deformed microstructure.

Figure 101 shows examples of the defects produced in the laboratory tests carried out in this work. The surface features are very similar to those found in rails in service, Figure 14 (p58). Metallographic observation of the laboratory test rollers, Figure 91B (p185), shows cracks similar to those seen in rails in service, Figure 100. In both cases, the cracks follow the deformed microstructure for some depth. In the rails, the cracks stop at the end of the deformed region whereas in

the laboratory rollers, some of the cracks propagate beyond the deformed region into the substrate.

Similar trends have been observed by Sato [33], and Qiu [19]. Qiu [19] and Kalousek and Bethune [51] also report that the depth of cracks and deformed layers was inversely related to the hardness of the material for a given percentage of RCF life.

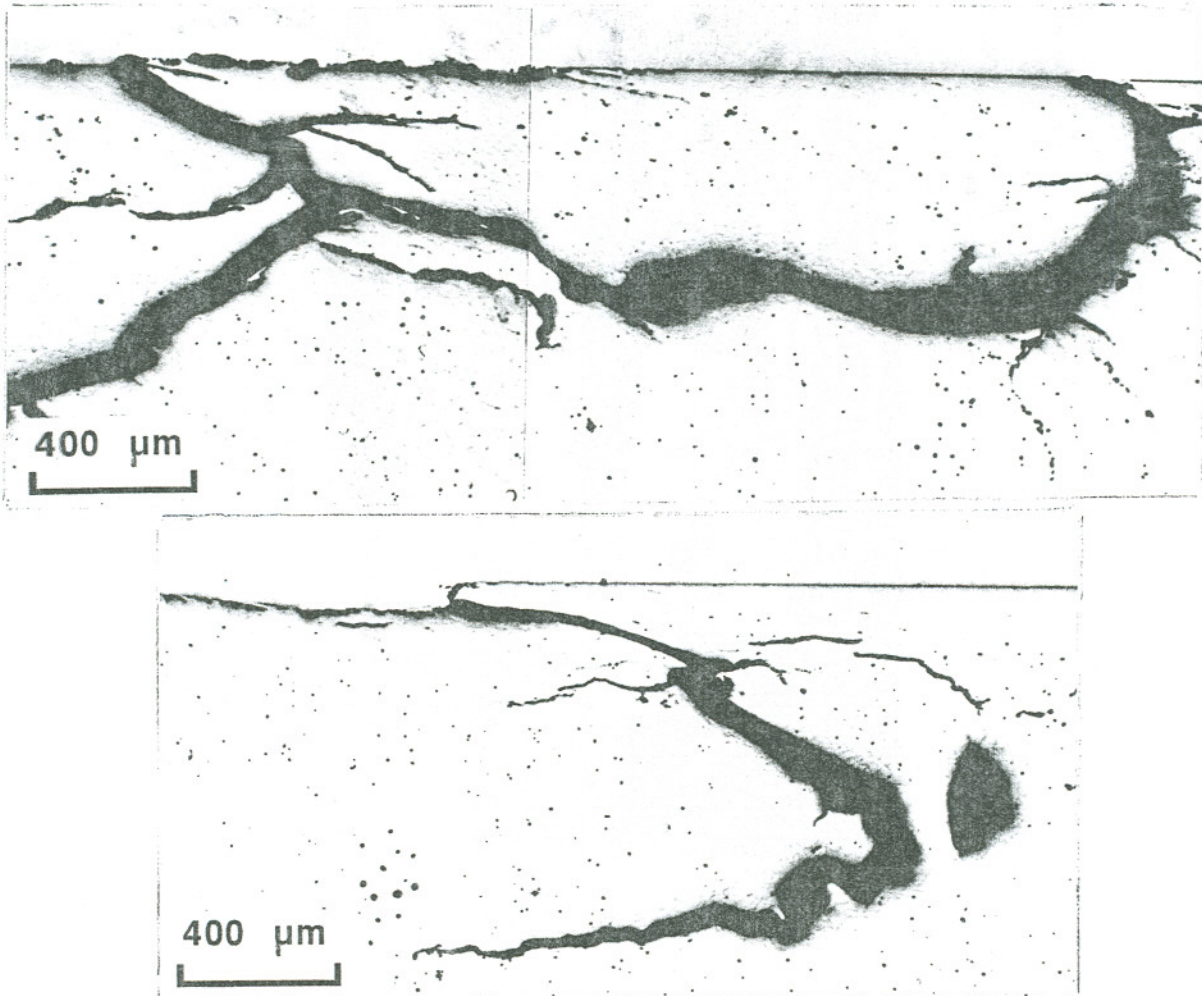


Figure 100 : Longitudinal section through head of spalled rail [79]

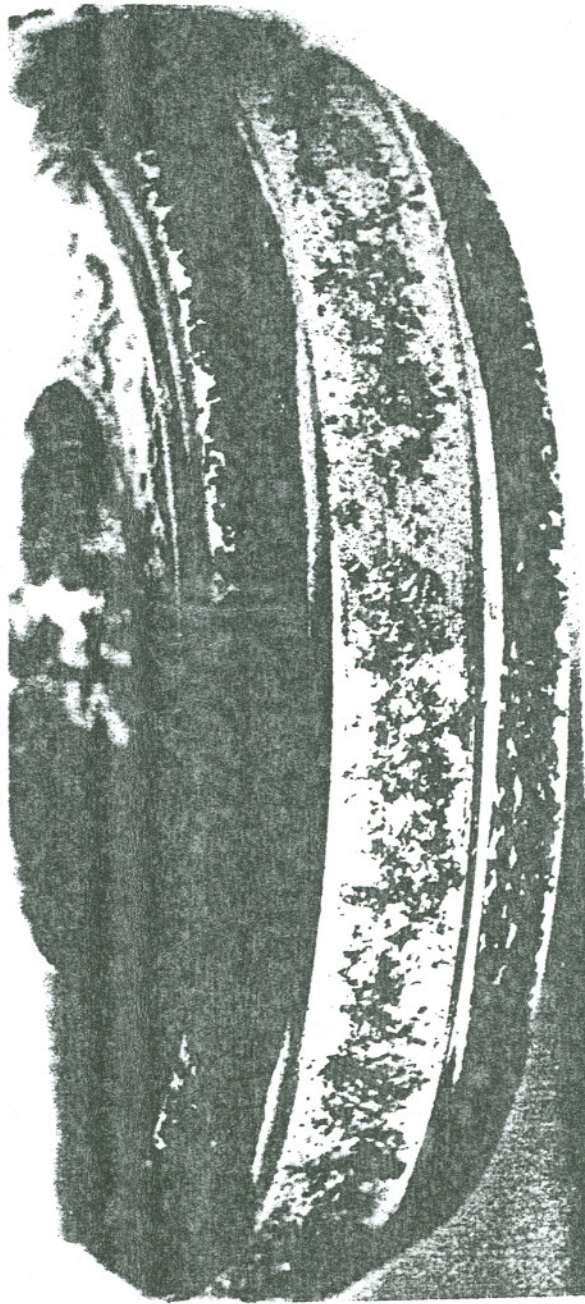


Figure 101 : Spalling in Amsler test roller

Comparing the crack networks in the rail and laboratory test rollers, Figures 100 and 102, we find that the crack networks in the laboratory rollers are much more developed (there are more linkages between cracks and the depth of the crack networks is greater) than those in the rail. This could be due to one or more of the following:

- (1) According to Johns et al [61], for an axle load of 30 tons,  $P_o = 1500$  N/mm<sup>2</sup> for new wheel/rail profiles. As loading progresses, the wheel/rail contact becomes more conformal and  $P_o$  is lowered to about 830 N/mm<sup>2</sup>. In the Amsler test, the profiles of the rollers remain substantially the same. Hence  $P_o$  stays fairly constant throughout the test. Thus the Amsler rollers are likely to experience a higher number of cycles at a higher contact stress.
- (2) On rails, water (as a lubricant) is not present at all times, thus there is likely to be an appreciable amount of wear taking place. This would help in the removal of some of the embryonic fatigue cracks and also lead to a decrease in the crack propagation rate; since lubricant is not present at all times to enter the cracks. In the Amsler test, a condition of over lubrication was present at all times during the test. This significantly reduces the wear rate of the rollers and aids fatigue crack growth.

(3) In the rails, most often, trains travel in both directions, whereas in the Amsler test, the loading direction is always the same. (In the rail samples used here for crack and WEL studies, the loaded trains travelled in one direction and empty trains in the opposite direction).

In both the Amsler test roller and in the rail, the cracks appear to be surface initiated and propagate into the substrate at an angle of approximately 30 degrees to the horizontal, in a direction opposite to that of rolling. This is typical of the surface initiated rolling contact fatigue cracks associated with shallow surface spalling and head checks in rails. Although no study was made of the mechanism of growth of the defects, the work done by Clayton and Hill [31] and Masumoto *et al* [17,22] can be cited here to state that the two defects are indeed similar to each other.

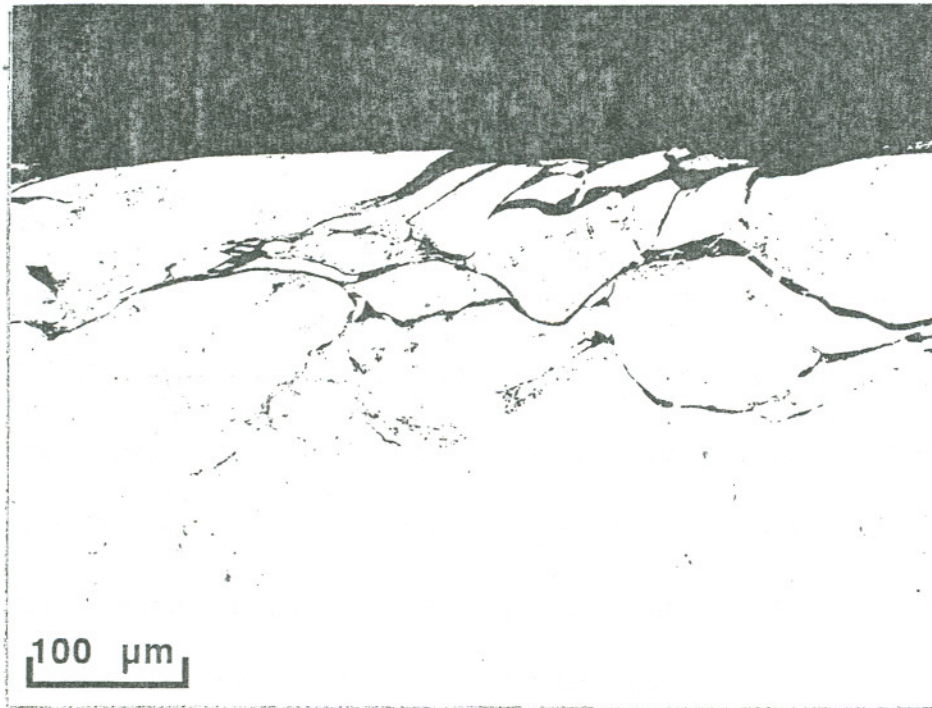


Figure 102 : Crack networks in Amsler test roller

### MODEL FOR RCF LIFE OF RAIL STEELS

The empirical model developed expresses the water lubricated rolling contact fatigue life of eutectoid pearlitic steels in terms of hardness and applied contact pressure. In keeping with previously published data, the relationship shows that RCF life decreases as the contact pressure increases and the hardness decreases.

Figure 40 (p113) shows the RCF life predicted by the model versus the experimentally determined results. The results of the repeatability tests at 1302 N/mm<sup>2</sup> are also shown on the plot. The standard deviation of 16800 cycles corresponds to about 5.7% of the average life of 292800 cycles. This is an acceptable variation and within the range anticipated from previous work [31]. The differences between predicted and experimental results can not be attributed solely to experimental scatter.

The model was formulated by regressing the experimental data to find values of N and C for the individual materials and then further regressing to establish general relationships between these terms and the hardness. The errors introduced at each stage are cumulative and account for the discrepancies in Figure 40 (p113).

During rolling contact fatigue testing the lubricant reduces wear rates to values well below those encountered for dry conditions [33,92]. However, there is

still some wear, together with a certain amount of plastic deformation, resulting in changes in the roller dimensions. The maximum diameter reduction was about 1 mm for the top roller and 0.5 mm for the lower one. This leads to a slide/roll ratio of 11.5% by the end of the test. According to the results of Clayton and Hill [31], this change in the slide/roll ratio should not affect RCF life.

The changes in roller diameters, and an increase of up to 0.87 mm in the contact width as a result of deformation, results in a decrease of about 8.5% in the value of  $P_0$  by the end of the test. The model was used to calculate the effect of these changes on RCF life. There is a difference of about 10% in the life due to a change of 8.5% in the contact pressure. Since the model takes into account only the starting contact pressure, some of the discrepancies in Figure 40 (p113) can be explained on the basis of this effect.

If the RCF life predicted by the model for the B and C heat treated steels, on the basis of their hardness, is plotted against contact pressure, Figure 103, we find that as the contact pressure increases, the plots for the different materials tend to converge. This suggests that at some higher  $P_0$  value, the RCF life would be the same irrespective of the hardness, i.e., the use of harder steels would not significantly improve the RCF life at higher contact pressures. However, a totally different picture emerges when the relative RCF life is considered. The relative

life is defined as the ratio of the RCF life of a given material to the RCF life at the same contact pressure for the B4 steel, i.e.:

$$\text{Relative RCF Life} = \frac{\text{RCF life of given material at given } P_o}{\text{RCF life of B4 steel at same } P_o} \quad (19)$$

The relative RCF life for the different steels is given in Table XXXII and plotted in Figure 104. The relative RCF life increases for all but one of the steels as the contact pressure increases. Thus there is a benefit to be gained by the use of harder steels under conditions of increased contact pressures.

The effects of hardness and contact pressure on RCF life can be understood in terms of the likely mechanism that generates failure. It would seem that there are two possibilities. A crack could be initiated by a ratchetting mechanism in which each cycle of contact promotes an increment of unidirectional strain, in the manner suggested by the work of Crook [65] and Johnson [15], leading to ductile shear. Alternatively, the material operates under conditions of plastic shakedown in which the shear stress cycles are pulsating rather than fully reversed, and the material fails by fatigue.

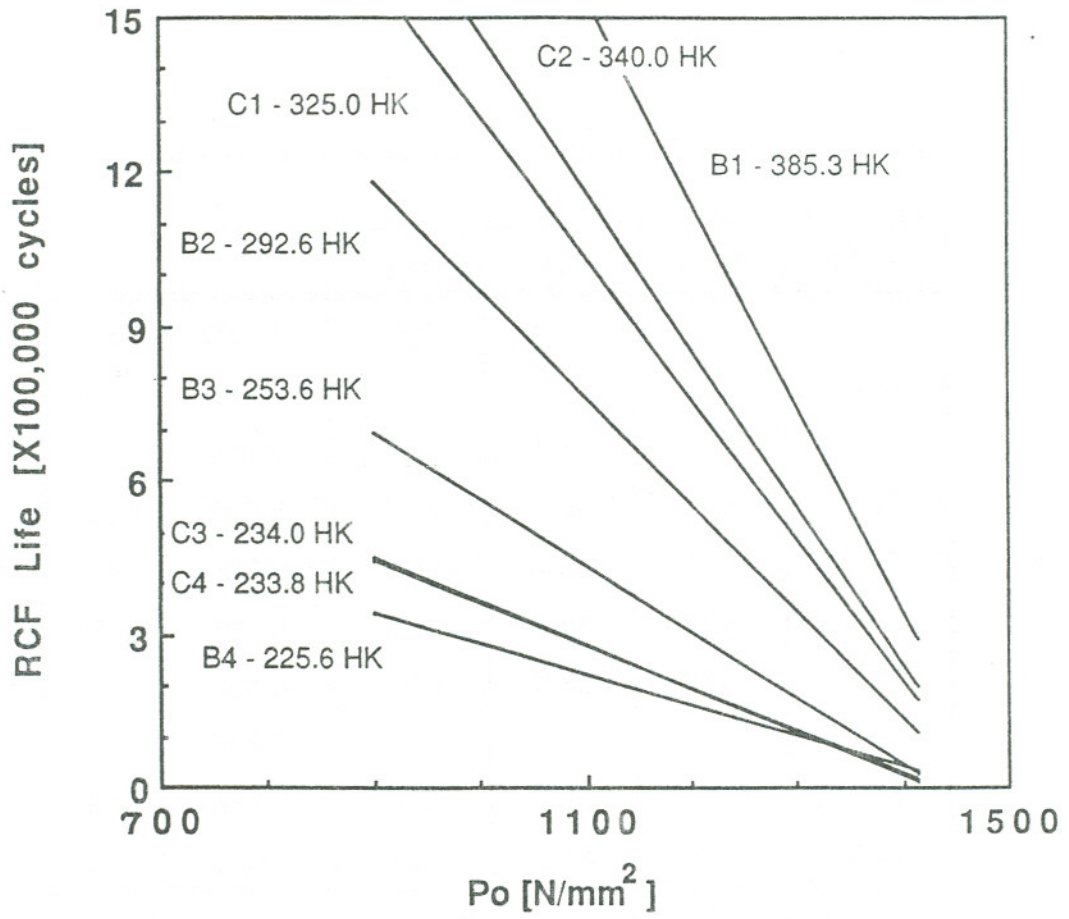


Figure 103 : Model predictions for RCF life of B & C series steels

Table XXXII : Relative RCF life

	HK	Po (N/mm <sup>2</sup> )			
		998	1223	1302	1413
C4	233.8	1.00	1.00	1.00	1.00
B4	225.6	1.11	1.24	1.37	2.38
C3	234.0	1.69	1.83	1.97	2.47
B3	253.6	2.34	1.96	1.57	1.35
B2	292.9	3.86	4.06	4.28	5.87
B0	301.0	2.22	2.59	2.98	5.88
C0	304.0	2.75	2.82	2.90	3.47
C1	325.0				
B1	385.3	6.72	7.11	9.37	10.59
C2	340.0	5.67	6.34	7.04	12.27

Relative RCF Life = RCF Life of Sample/RCF Life of B4  
(RCF Life Predicted by Regressed Lines)

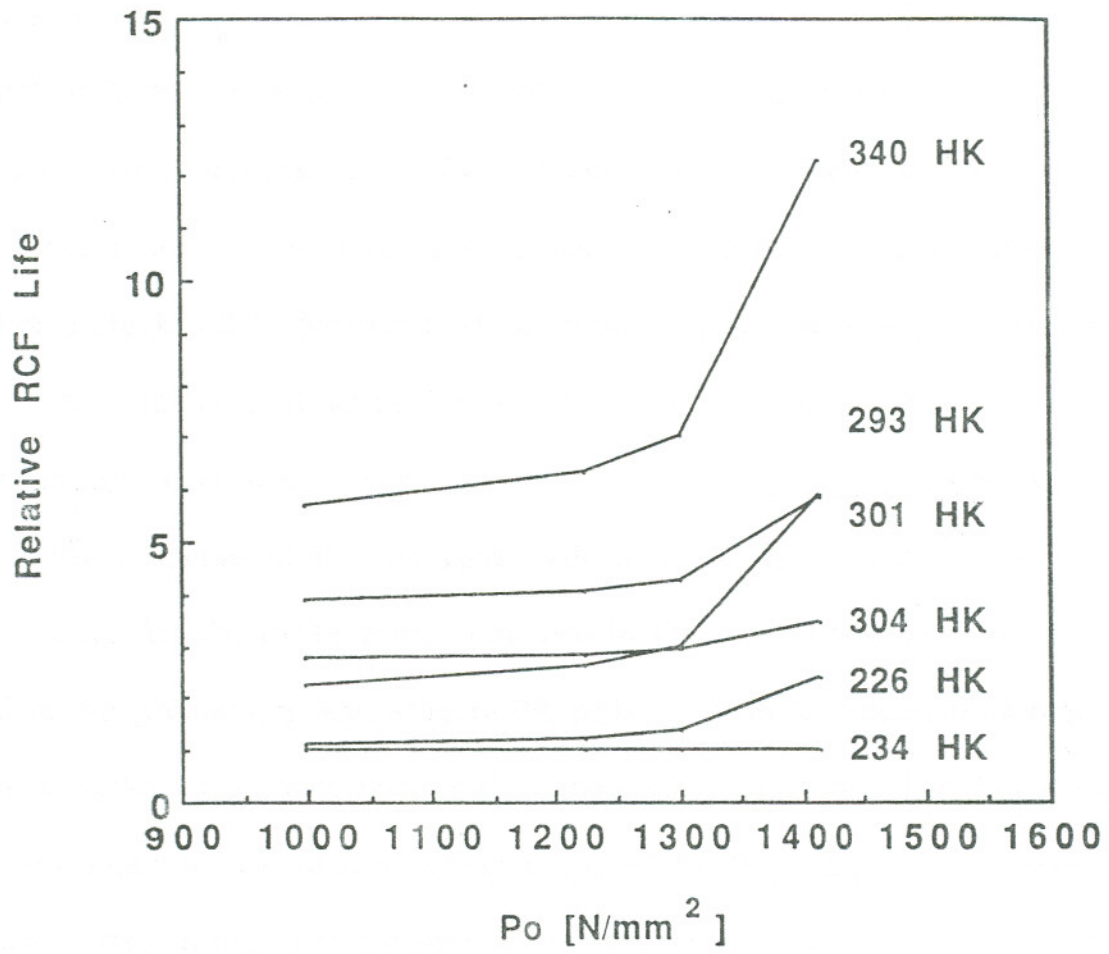


Figure 104 : Relative RCF life

In either case, the failure will be controlled by the shear forces acting on the surface of the roller,  $\mu P_o$ , and the resistance to plastic flow, which for a series of steels with the same hardening capacity (as in the case for the steels tested) will be related to hardness. Thus, if  $P_o$  is reduced or the hardness is increased, the plastic strain per cycle will be reduced and the number of cycles required to produce a crack will be increased. Since, in the case of ratchetting it is assumed that a certain total plastic strain is required to produce failure, and in fatigue, life is determined by the stress range.

The influence of the lubricant could also be explained in terms of the plastic cycles. Similar to the results obtained by Ollerton and Morey [29], it was found in the preliminary tests (Figure 99, p197) that oil lubricated tests require far more cycles to produce failures than those run with water. This has always been attributed to the viscosity effect proposed by Way [32]. For the contact conditions used in the current experiments, the coefficient of friction under water lubrication is about 0.27 compared with 0.13 for oil [ $P_o = 1413 \text{ N/mm}^2$  for A series steel]. The difference in the surface shear forces, given by  $\mu P_o$ , could have a significant influence on the plastic strain per cycle.

### Modification of Model to Include Coefficient of Friction

Table XXXI and Figure 99 (p196,197) give the RCF life for the water and oil lubricated tests. In the absence of RCF data for more than two lubricants, the relationship between life and coefficient of friction cannot be determined. However, from Table XXXI we find that oil lubrication provides a higher life than water lubrication by a consistent factor of about 26. This factor can be included in the model as follows:

$$(\text{RCF Life})_{\text{lub}} = \left[ \frac{\mu_{\text{water}}}{\mu_{\text{lub}}} \right]^K \times (\text{RCF Life})_{\text{water}} \quad (20)$$

The subscript "lub" refers to any lubricant used in the test.

The reason for selecting  $\mu_{\text{water}}/\mu_{\text{lub}}$  is to account for water lubrication (when the lubricant used is water,  $\mu_{\text{lub}} = \mu_{\text{water}}$  and the factor becomes unity, thus we get back the original life for water lubrication) and because RCF life increases as the coefficient of friction decreases (for a lubricant with a higher viscosity than water,  $\mu_{\text{lub}} < \mu_{\text{water}}$  and the factor becomes greater than one, leading to a higher life than for water lubrication).

Using the regression data for oil lubrication and the model predictions for water lubrication for the A rail steel, we find that the value of K is 4.5.

To check how well the modified model (Equation 20) fits the original data, we can substitute the hardness into the model and calculate the RCF life for different values of  $P_o$ , and compare the predictions with the original results, Table XXXIII and Figure 105. We find from Figure 105 that the modified model predictions of RCF life under oil lubrication match well with experimental results.

Since only two lubricants were used in this study, it is possible that the relationship might have to be modified further when data for other lubricants are available. Also, the model does not explain the preferred orientation for crack orientation [p30] as shown by Way [31].

**Table XXXIII : RCF life for water and oil lubrication - A series**

$P_o$ (N/mm <sup>2</sup> )	Water Lubrication $\mu = 0.27$		Oil Lubrication $\mu = 0.13$	
	Predicted Life *	Experimental Life	Predicted Life **	Experimental Life
1413	0.17	0.15	4.72	3.26
1395	.039	---	10.30	13.13
1378	.059	1.64	15.20	13.70

\* Predicted life calculated using Equation 14, p106

\*\* Predicted life calculated using Equation 20, p206

RCF life is in multiples of 100000 cycles

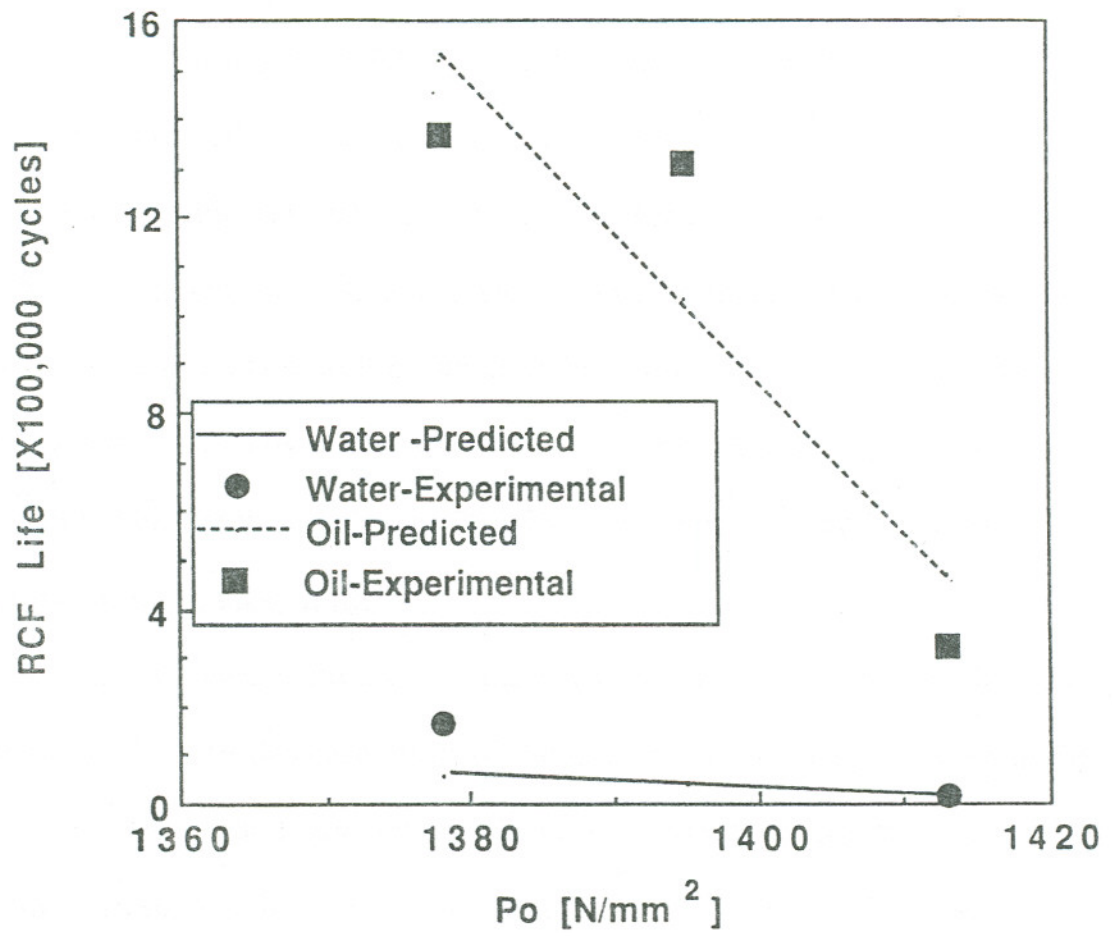


Figure 105 : RCF life plots for oil and water lubrication

### Effect of Bottom Roller Hardness on RCF Life

Instead of plotting the RCF life as a function of  $P_o$  for a given hardness, it can also be represented as a function of hardness for a given  $P_o$ . Typical examples of this are given in Figures 106 - 108. From the regression analysis data given in Table XXXIV, we find that, while a single line can be regressed through the data points, the data can equally well be described by two lines; one for the materials with hardness below 29 HRc and the other for the materials with hardness greater than 29 HRc. The hardness value of 29 HRc corresponds to the hardness of the bottom roller used in these tests.

First let us consider the case of the materials of hardness higher than that of the bottom roller. In this case, most of the deformation is likely to occur in the bottom roller. As a result, the test roller needs a greater number of cycles to accumulate the requisite level of plastic deformation for cracking. This means that its life is higher than it would be if a bottom roller of comparable or higher hardness were used.

For the second case, the situation is the exact opposite and most of the deformation is likely to be contained within the test roller. This leads to a decreased life.

In view of the foregoing discussion, let us consider the test series i-a and i-m (Table VIII, p65). Test series i-m was run using test rollers made from rail

steel A against bottom rollers made from the same material, whereas, series i-a was run using bottom rollers made from rail steel B. Thus we have the same material (rail steel A) tested against two materials with different hardnesses (rail steel A with 249 HK and rail steel B with 301 HK). Regression analysis of the data for the two test series', Table XXXV and Figure 109, shows that there is a slight difference between the regressed lines for the two test series'. The test series in which the top roller hardness was less than the bottom roller hardness (i-a) shows a lower RCF life than the test series where the top and bottom roller hardnesses were the same (i-m). However, when the results from the two series are considered together, the degree of fit is still very good and the results for the individual series are fairly well accounted for by the scatter in repeatability of the tests (5.7% variation in the life, p205).

Hence the experimental results are inconclusive with respect to the effect of the bottom roller hardness on RCF life. Also, there has been no other work to study the effect of bottom roller hardness on RCF life behavior, hence it is difficult to say if the phenomenon observed here is typical. However, there is some evidence [77,89] that the bottom roller hardness influences wear behavior of the test rollers and that wear rates can differ significantly depending upon the hardness of the bottom roller.

The way to confirm the effect of the bottom roller hardness on RCF life would be to run series' of tests using bottom rollers of differing hardnesses. If such tests were to reveal a significant effect of the bottom roller hardness on RCF life, then the model would need to be modified to include this effect.

**Table XXXIV : Regression data for RCF life vs hardness**

Po N/mm <sup>2</sup>	< 29 HRc			> 29 HRc			All HRc		
	Slope	Y-Int.	R <sup>2</sup>	Slope	Y-Int.	R <sup>2</sup>	Slope	Y-Int.	R <sup>2</sup>
999	0.27	-0.99	0.95	0.21	-6.94	-*	0.65	-7.59	0.97
1224	0.204	-2.05	-*	0.45	-6.49	0.588	0.43	-5.77	0.93
1302	0.086	-0.152	0.82	0.44	-8.85	0.483	0.345	-4.37	0.67
1358	0.07	-0.25	0.90	0.59	-15.22	-*	0.25	-3.65	0.91
1413	0.019	-0.875	0.01	0.296	-7.47	0.66	0.13	-1.99	0.51

-\*- Only 2 data points available so no R<sup>2</sup> value

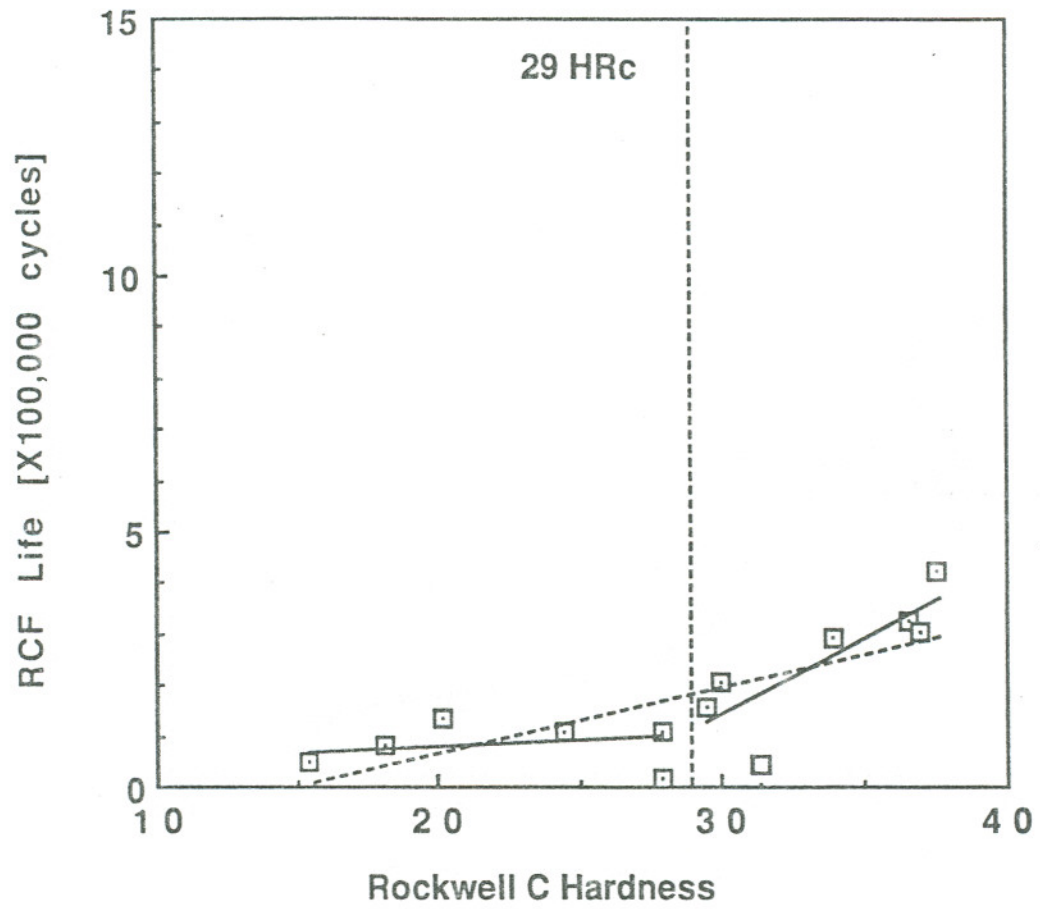


Figure 106 : RCF life vs hardness for  $P_o = 1413 \text{ N/mm}^2$

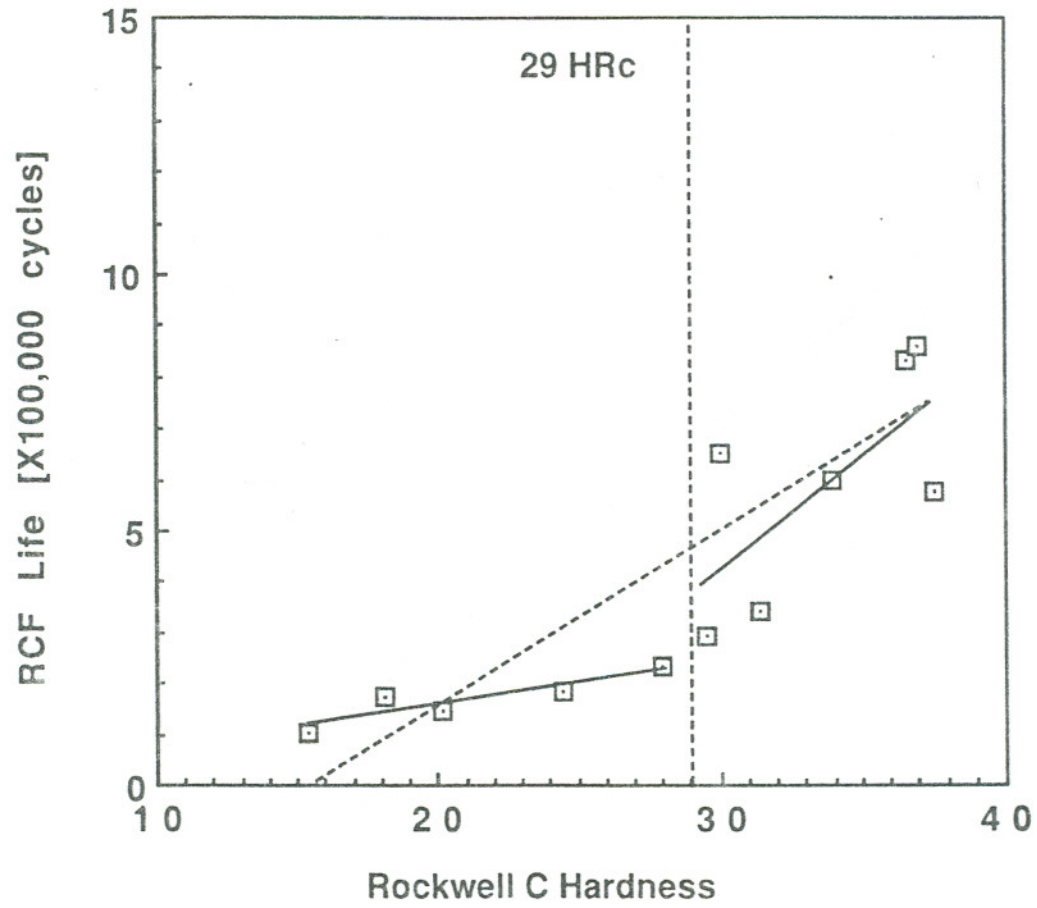


Figure 107 : RCF life vs hardness for  $P_o = 1302 \text{ N/mm}^2$

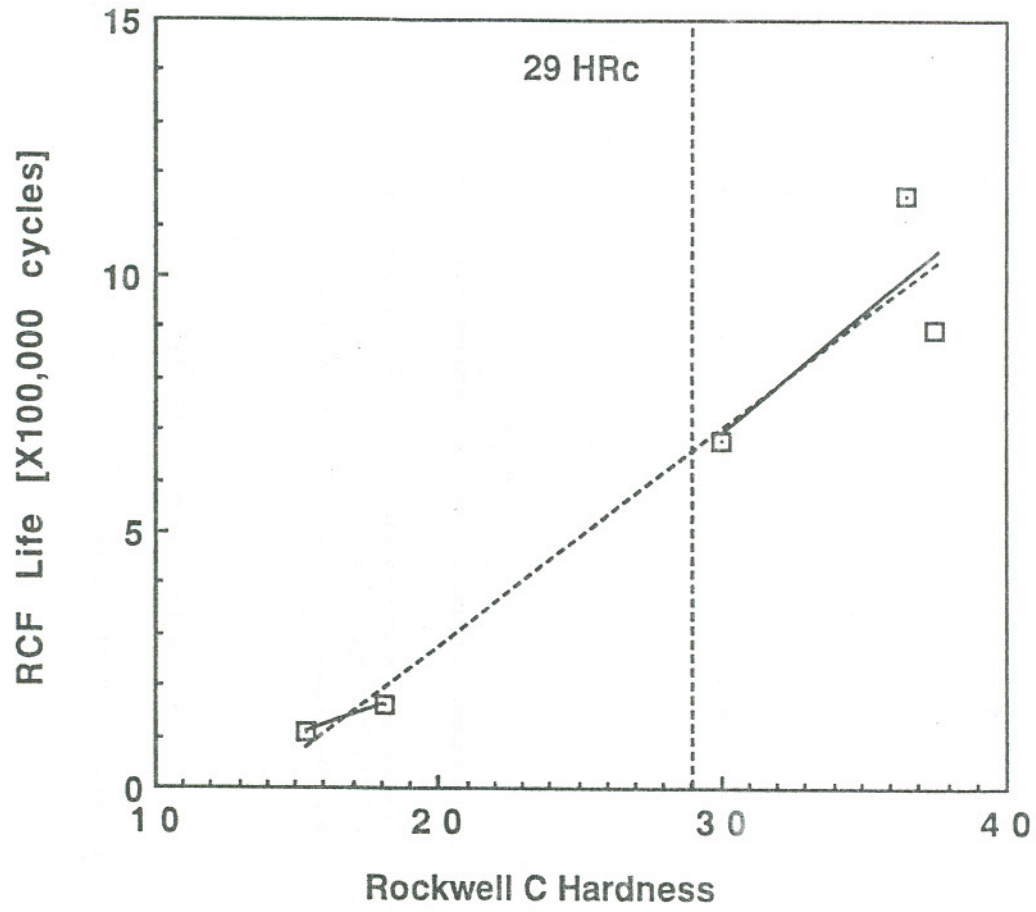


Figure 108 : RCF life vs hardness for  $P_o = 1224 \text{ N/mm}^2$

Table XXXV : Regression parameters for RCF life versus  $P_o$

for test series' i-a and i-m (Table VIII, p65)

LINEAR RELATION : RCF Life = N ( $P_o$ ) + C			
Comments	N	C	R <sup>2</sup>
Series i-a (bottom rollers from steel B)	-0.00986	14.94	-0.96
Series i-m (bottom rollers from steel A)	-0.00913	14.45	-0.75
Series i-a and i-m combined	-0.00952	14.79	-0.82

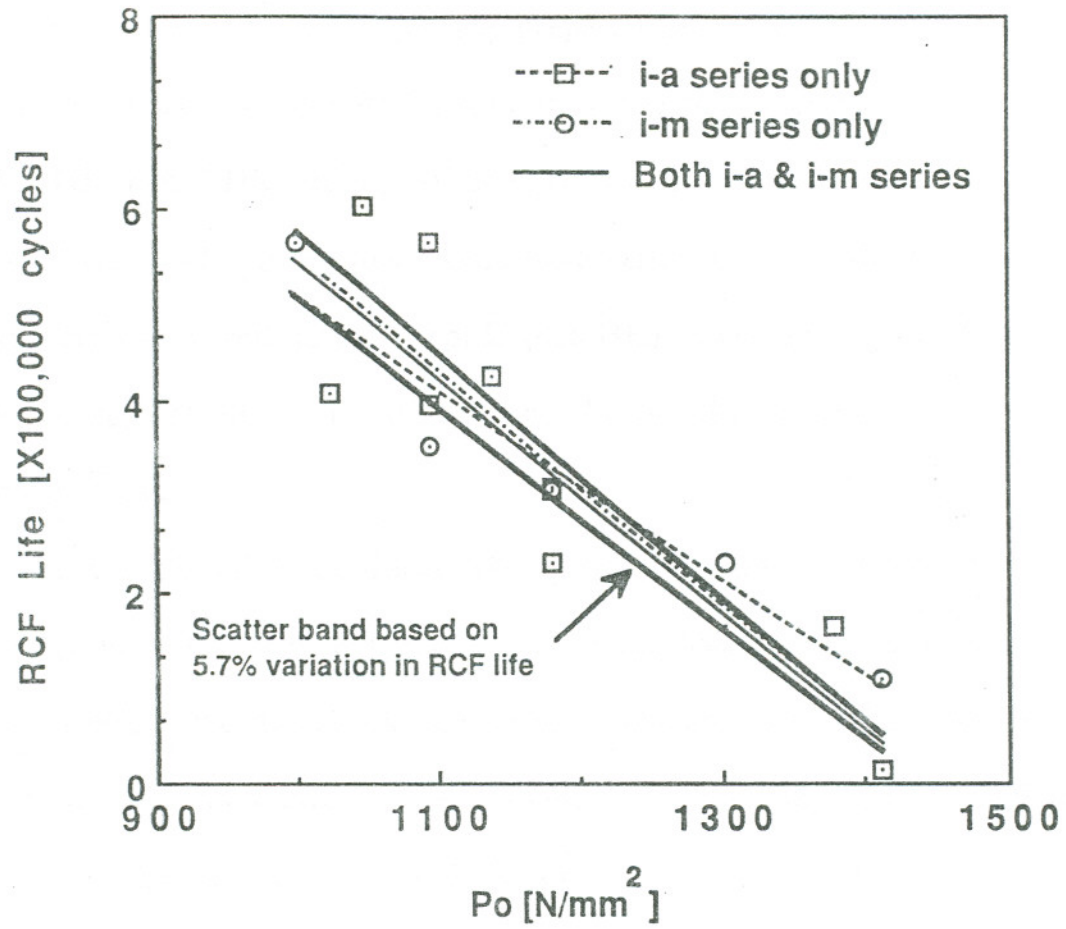


Figure 109 : RCF life vs  $P_o$  for test series i-a and i-m (Table VIII, p65)

### Validation of Model Using I Series Steels

The I series steels were specially prepared heats for a separate study [92] on the effect of inclusions on RCF behavior. These steels had hardnesses ranging from 355 HK to 420 HK and a pearlitic microstructure. Based on the hardness of the steels (Table XIX, p119), one would have expected the model to predict the RCF life reasonably well for all except I3 (420 HK). However, we find (Figures 43 and 44, p120,121) that only for I2 and I5 do the predictions match the experimental results.

From Table IV (p52), Table XIV (p101) and Table XIX (p119), we find that the hardness for I4 is at the high end of the hardness range for the steels used to formulate the model and the inclusion contents are at the lower end of the range for the steels used. I4 had a significantly lower inclusion content than three of the four rail steels used. This combination of high hardness and low inclusion content could be one reason why the experimental life for I4 was much higher than the predicted life.

Inclusions have been found to be associated with many subsurface initiated RCF defects, not only in rails [21,54,96] but also in gears [93,94], and have been thought of as being influential in helping crack propagation by providing weak links in the matrix. Blake and Cheng [93,94] have suggested that, in the absence of inclusions, cracks in gears are limited to the zone of residual

tension. However, the presence of inclusions can help the crack to propagate beyond this region. Worth *et al* [27] have found that inclusions at the WEL/pearlite interface can help the crack cross the interface and continue propagating into the matrix. In the present study of service rail, no evidence was found to support this observation.

In light of the information from the literature and the results of the model validation tests, it seems that inclusions could play an important role in determining RCF behavior, and this aspect definitely merits further attention.

### Model Predictions for Bainitic Steels

To see if the RCF life model could make useful predictions for steels other than pearlitic steels, two bainitic steels from another study [77] were considered. The model was used to make RCF life predictions based only on the hardness of these steels. These predictions were then compared to the experimental RCF lives obtained for the steels. The model predictions and experimental results are given in Table XXXVI and plotted in Figure 110. For the bainitic steel with a hardness 290 HK, the model predictions agree well with the experimental results, however for the bainitic steel with hardness 390 HK, the model does not predict RCF life very well.

This bainitic steel was found to deviate from expected behavior not only during RCF testing but also during wear testing [77]. Both, the wear resistance and the RCF life, are expected to increase with increasing hardness, however, for the bainitic steel with hardness 390 HK, the Type III wear rate and the RCF life were found to be similar to those for the bainitic steel with hardness 290 HK. The steel with the 290 HK hardness had a granular bainitic structure consisting of heavily dislocated ferrite and twinned martensite islands. The microstructure of the steel with 390 HK hardness consisted of a banded structure with discrete regions of martensite and upper bainite, with iron borocarbide precipitates along the prior austenite grain boundaries. According to Ramaswamy [77], the loss in

wear and RCF resistance can be accounted for by the twinned martensite/upper bainite interfaces and prior austenite grain boundary precipitates which form weak links.

For bainitic steels, the mechanical properties are strongly related not only to the type of bainitic microstructure present but also to the type and amount of microstructural constituents like martensite islands [77]. As a result, unlike the pearlitic steels, the hardness cannot always be directly related to a simple microstructural parameter like the pearlite interlamellar spacing. Hence, the hardness may not be such a reliable guide to RCF resistance.

Instead of using the pearlite interlamellar spacing (which can be directly related to the hardness), for the bainitic steels, a more appropriate parameter might be something more fundamental like the mean free path in ferrite; a measure that could be applied to pearlite also.

Table XXXVI : RCF data for bainitic steels

Po N/mm <sup>2</sup>	RCF Life (x100000 Cycles)			
	290 HK		390 HK	
	Experimental	Predicted	Experimental	Predicted
1413	2.4	1.0	2.6	3.1
1302	---	---	5.3	7.6
1244	---	---	5.5	9.9
1202	5.2	5.3	---	---
1094	8.8	7.5	9.0	16.1

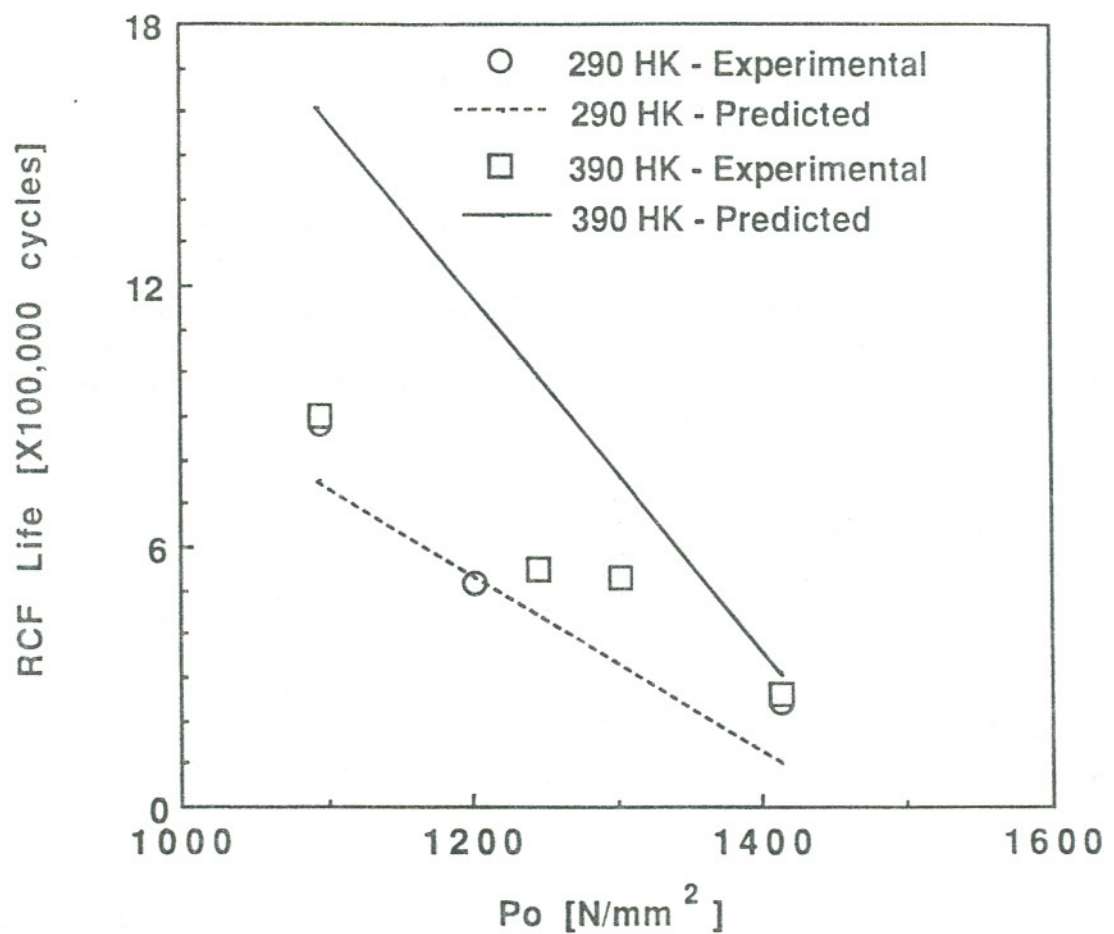


Figure 110 : RCF data for bainitic steels with model predictions

### CRACK AND WHITE ETCHING LAYER STUDIES

The nature of the data obtained in the study of WEL has to be taken into account in interpreting the results. Although a large number of metallographic samples were examined, they still represent a small part of each short rail sample. Also, any analysis of changes with MGT have to be made on the assumption that each rail sample is representative of an overall population in which there is no variation along the length of the rail.

On the basis of the information presented in Figures 46 to 55, (p129-131,137,138), and 72 to 78, (p157-162), the results of the metallographic study can be interpreted as given below.

The white etching layer formed very early on in the life of the rail, as did the RCF cracks. A lot of the cracks at this stage were associated with the WEL and most of the cracks were wholly contained within the WEL. With increasing MGT, the extent and depth of the WEL decreased, as did the number of short cracks, because some of the WEL spalled off and took away with it the cracks that were contained within it. At the same time, the number of longer cracks and the maximum crack depth increased.

Grinding removed all the cracks from the high rail, whereas it left behind numerous cracks up to 0.25 mm deep in the low rail. After grinding, no WEL was found on the high rails after about 1 MGT, while the WEL reappeared on the

low rail. The regenerated WEL was significantly more shallow than that formed initially and did not exhibit any new short cracks.

Since such a high percentage of the cracks in the initial stages of the rail life were associated with the WEL, and the trend of short crack populations paralleled that of the WEL (depth and area coverage), it seems highly likely that the WEL was instrumental in initiating the short cracks. Cracking of the WEL could result from one or more of the following:

- (1) *Residual stresses generated as a result of the formation of the WEL,*
- (2) *Tensile residual stresses at the surface of the new rail head resulting from roller straightening,*
- (3) *Repeated passage of wheels over the hard WEL.*

It seems likely that the crack growth is hindered by having to cross the WEL-pearlite interface. According to Worth *et al* [27], inclusions present at the interface aid in crack propagation across the interface. Metallographic observation of the samples from the current work failed to provide evidence to support this view.

In the rails from the west end of the curve, grinding successfully removed all the surface cracks from the high rails, whereas in the low rail some of the longer cracks were not fully removed. The situation at the east end was worse, since the cracks were longer and not fully removed from either the high or the

low rail. These cracks are the ones that obviously continue to propagate, outrunning the grinding at each cycle until, as in the few cases reported, they can eventually lead to deep spalling and premature removal of the rail from the track.

One way to overcome this problem would be to grind more deeply when surface cracks are present. This would be made much easier if the depth of the cracks could be determined prior to grinding. Some work is being carried out to use eddy current testing devices to determine crack depths. However, a more economical approach could be to remove the cracks when they are still small, in the current case, say at 10 MGT, when a grind of only 0.2 mm would probably have removed all the cracks present in both the high and the low rails. Given that no new cracks were observed immediately after grinding, this might eradicate the problem completely.

This could be the case if the cracks were initiated during the formation of the WEL. If on the other hand, the cracks were formed by fracture during subsequent passages of the wheel, the benefits might be reduced because new WEL, albeit more shallow, was observed immediately after grinding at 52.4 MGT.

To obtain some idea of the propensity of the WEL to crack as a result of concentrated contact, some laboratory RCF tests were run with samples on which WEL was formed to a depth of 35 - 50  $\mu\text{m}$ , using electrosparking. Tests were run under conditions that produced RCF failures after 280,000 cycles in the absence

of WEL on the test roller. After 450,000 cycles the roller with WEL exhibited signs of breakage and cracking as seen in the rails in service (Figure 67 - 70, p149-151).

Further, when WEL was formed by electorsparking on a piece of rail steel, it did not exhibit any cracks. Since the constraints and residual stress patterns in the piece of rail and the rail in service are likely to be completely different, this does not provide conclusive proof that the WEL seen in rails in service did not crack on formation. However, these results along with the results of the RCF tests indicate a strong possibility that the WEL cracked during the repeated contacts with the wheel.

Another possible approach to the problem would be to prevent the formation of the WEL in the first place. The WEL could be formed as a result of a thermally and/or a deformation-induced transformation. Either way, diffusion of carbon is required and the reduced interlamellar spacing found in high strength rails could be a contributory factor in the formation of the WEL. The higher strength steels could also be expected to have higher tensile residual stresses after roller straightening. These factors combined with the increased resistance of the higher strength steels to rail profile changes, might thus prolong the worn wheel-new rail profile mismatch, and could together represent a possible reason for the higher strength steels suffering from the problem encountered.

Since the high strength properties are required for a number of reasons, one possible solution would be to introduce a more conformal rail profile in the hope that this would reduce the incidence of WEL and the probability of cracks propagating beyond the WEL-pearlite interface.

### COMPARISON OF CRACKS IN AMSLER ROLLERS AND RAILS

Under rolling/sliding contact conditions wear, RCF cracks and plastic deformation of the surface layers occur simultaneously. Which of the three will be the dominant mode of failure is determined by numerous factors such as the magnitude of the contact stresses, the presence of a lubricant and the slide/roll ratio.

From Figures 46 - 53 (p129-131) we find that in the Amsler test rollers cracks initiate fairly early in the life of the sample. While it is hard to conclude from the data the exact number of cycles at which cracks initiate, the point can be narrowed down to between 5000 and 10000 cycles. For  $1302 \text{ N/mm}^2$ , the average life of the as-received B steel roller is about 293000 cycles. This means that cracks initiated in the rollers at between 2 and 3% of the total life of the sample.

The percentage of life at which cracks appear in these samples is lower than that reported by other researchers; for example Clayton and Hill [31] found that in their tests, cracks first became visible between 25 and 50% of the life of the roller. Whether the early appearance of the cracks in the current tests is due to pre-existing flaws in the rollers or due to the experimental conditions used has not been looked into.

The results of these tests are contrary to the results of Sato [33], who found that RCF cracks do not initiate and/or propagate under only lubricated

conditions. Sato found that a period of dry running followed by lubrication was the only way to produce RCF failures. However, Sato's results are for a maximum hertzian contact stress values of less than  $750 \text{ N/mm}^2$ , which is considerably lower than the range used in these tests. For a rail steel with a hardness of 330 HK (corresponding to a premium Si-Cr rail steel), the model predicts a life of about 2 million cycles at  $750 \text{ N/mm}^2$  and almost 3 million cycles at  $500 \text{ N/mm}^2$ .

After the appearance of the cracks in the very early stages of the tests, the cracks seem to follow a linear growth curve. Regression analysis of the data in Figures 92 & 93, (p187,188) give the following relationships between maximum crack depth,  $\text{MCD}_A$ , and number of cycles,  $\text{NC}_A$  and length of the longest crack,  $\text{LCL}_A$  and number of cycles,  $\text{NC}_A$  respectively:

$$\text{MCD}_A [\mu\text{m}] = 0.00309 (\text{NC}_A) + 44.5 \quad (21)$$

$$\text{MCD}_A [\mu\text{m}] = 0.00503 (\text{NC}_A) + 86.3 \quad (22)$$

For the case of 30 ton axle load cars with (33000 lb) 15 ton load per wheel, we find that about 66670 passages of the wheel adds up to 1 MGT; i.e., 66670 load cycles correspond to a cumulative million gross ton for both the high and low rails together. Thus 133340 load cycles correspond to a million gross ton for each rail.

If the maximum crack depth is expressed as a function of MGT based on the above criterion, we would get:

$$\text{MCD}_A [\mu\text{m}] = 414 (\text{MGT}) + 44.5 \quad (23)$$

This means that by 53 MGT of total track tonnage, or 26.5 MGT of tonnage per rail, the maximum crack depth would be about 11000  $\mu\text{m}$ . From Figures 46 - 53 (p129-131) we find that the maximum crack depth in the rails is about 1300  $\mu\text{m}$ ; a difference of more than 8.5 times. Several reasons could be cited that could account for at least a part of the discrepancy. Three of the reasons have already been mentioned before (p196), i.e., the conformity of the wheel/rail profiles, the intermittent presence of a lubricant and the direction of loaded train travel. Additionally, different wheels are likely to make contact at different points on the rail. This means that the number of contact cycles that any given point on the rail surface passes through is some percentage of the total number of wheel passages.

Figure 94 (p189) shows that there is a slight decrease in the depth of the network cracks with increasing number of cycles. One way to look at this is to consider that some of the surface material is lost; most probably due to wear. However, the maximum crack depth and the depth of deformation below the surface are increasing with the number of cycles, suggesting that the crack growth

rate and the rate at which the deformed layer builds up are too high for wear to have a significant effect on them.

Taking into consideration the fact that there are likely to be a lot of differences between field service and laboratory scale tests, the similarities in trends observed show that despite the differences, the laboratory test used is fairly representative of the conditions in the field.

Next let us consider the length of the longest crack as a function of the number of cycles. The slope of the linear relationship in Equation 21 gives the crack propagation rate,  $CPR_A$ , in  $\mu\text{m}/\text{cycle}$ , thus:

$$CPR_A = 0.00503 [\mu\text{m}/\text{cycle}] \quad (24)$$

or converting to inches/cycle we get :

$$CPR_A = 2 \times 10^{-7} [\text{inches}/\text{cycle}] \quad (25)$$

This value of crack propagation rates is comparable to the crack propagation rates found in conventional fatigue tests for similar steels by Feddersen and Broek [95].

### SUB-SURFACE DEFORMATION

In recent years computer programs like PHOENIX [98] have been developed that predict the formation and growth of subsurface initiated RCF defects. However, the predictions of such programs are hard to verify using field trials. The impetus for studying sub-surface deformations was the development of a laboratory scale test that would allow a means for such validation.

Wholly sub-surface contained deformation has been reported to occur under conditions of lubrication providing coefficients of friction less than about 0.05 [31]. At such low values of the coefficient of friction, the maximum shear stresses occur at some depth below the surface [56] and the plastic deformations due to shear stresses consequently occur at the corresponding depth below the surface.

In the current tests, the SAE40 oil and the solid moly-disulfide lubricants that were used gave coefficients of friction less than 0.05. The other test parameters were selected based on the work of Hamilton [64] and Crook [65]. However only one test, SSM04 showed the sought after sub-surface deformation (p185). It is interesting to note that this was one of only two tests in which the roller corrugated. This shows that the joint occurrence of corrugations and sub-surface initiated RCF defects in rails in service [ ] can be reproduced in the MTI test rollers.

As part of the continuation of the work on this aspect, the test parameters will be varied to try and generate sub-surface deformations in the MTI as well as the Amsler test rollers.

### COMPARING RCF LIFE AND WEAR RATE MODELS

In RCF tests as in wheel/rail contacts, wear of the rail head and RCF occur simultaneously [3]. In many instances wear and RCF are competing mechanisms; for example in curved sections of the track. The occurrence of one or the other depends upon various factors such as the presence of a lubricant and the slide/roll ratio. For example, when a lubricant is present, wear rates are reduced (compared to dry conditions), but the chances of forming RCF defects is increased [2]. Since, at least in certain circumstances, wear and RCF can be competing mechanisms, it should be possible to use wear rate relationships and the RCF model to predict the hardness at which the wear rate and the RCF life would be optimized.

Danks [97] has found a relationship between the pearlite interlamellar spacing and Type III wear rate (which occurs on the gauge corner of high rails in curved track) for various maximum hertzian contact pressure, Table XXXVII. These results were obtained for a series of pearlitic steels tested on an Amsler rolling/sliding machine under dry conditions using 35% slide/roll ratios. The relationships given in Table XXXVII can be combined into one equation relating the Type III wear rate (W) to pearlite interlamellar spacing (S) and the maximum hertzian contact stress ( $P_o$ )

**Table XXXVII : Parameters for relationship between wear rate and pearlite interlamellar spacing [97]**

$P_o$ [N/mm <sup>2</sup> ]	"a"	"b"	r
1220	10431	0.47	0.64
1080	2138	0.70	0.73
900	788	0.80	0.67
700	7.97	1.51	0.79
500	5.51	1.33	0.81

The parameters "a" and "b" in Table XXXVII can be related to  $P_o$  as follows:

$$a = 7.72 \times 10^{-25} (P_o)^{9.063} \quad (25)$$

$$b = -0.00139(P_o) + 2.182 \quad (26)$$

The power function was selected for "a" and the linear relation was selected for "b" since these best describe the data, Table XXXVIII.

**Table XXXVIII : Regression data for "a" & "b" (Table XXXVII)**

	"a"		"b"	
	Linear	Power	Linear	Power
R <sup>2</sup>	0.78	0.95	0.91	0.89
Slope	11.98	9.063	-0.00139	-1.199
Y-Int.	-7867	-24.12	2.182	3.45

The relationships between "a" and  $P_o$  and "b" and  $P_o$  can then be substituted into:

$$\text{Wear Rate } (\mu\text{g/m}) = a(S)^b \quad (27)$$

to yield :

$$\text{Wear Rate } (\mu\text{g/m}) = [7.62 \times 10^{-25} (P_o)^{9.063}] (S)^{[-0.00139P_o + 2.182]} \quad (28)$$

In Table XXXVIII, the very small slope of the linear regression (-0.00139) indicates that the value of "b" is essentially independent of  $P_o$ . This means that Equation 28 can be rewritten as :

$$\text{Wear Rate } (\mu\text{g/m}) = 7.62 \times 10^{-25} (P_o)^{9.063} (S)^{2.182} \quad (29)$$

The RCF life data from this work (Table XV, p105,106) can also be plotted as a function of the pearlite interlamellar spacing for varying  $P_o$ . A power function of the form :

$$\text{RCF Life} = a_o (S)^{b_o} \quad (30)$$

can be used to describe the data. Table XXXIX gives the values of  $a_o$  and  $b_o$  for the various contact pressures.

**Table XXXIX : Regression data for power relation between RCF life and pearlite interlamellar spacing**

$P_o$ [N/mm <sup>2</sup> ]	$a_o$	$b_o$	$R^2$
1413	$6.05 \times 10^5$	-1.705	0.67
1359	$1.05 \times 10^8$	-2.279	0.91
1302	$4.63 \times 10^5$	-1.541	0.88
1224	$2.42 \times 10^6$	-1.751	0.89
1161	$1.15 \times 10^9$	-2.502	0.92
1094	$3.54 \times 10^5$	-1.130	0.81
999	$1.33 \times 10^8$	-2.154	0.96

The relationships for the different  $P_o$  values can be combined into one by finding  $a_o$  and  $b_o$  as functions of  $P_o$ . Regression analysis of the data shows that a

power function and a linear function best describe the relationships for  $a_o$  and  $b_o$  respectively, Table XXXX.

The relationships between  $a_o$  and  $P_o$  and  $b_o$  and  $P_o$  can then be substituted into Equation 30 to yield :

$$\text{RCF Life (X10}^5 \text{ cycles)} = [3.17 \times 10^{32}(P_o)^{-8.288}](S)^{[-0.000072P_o - 1.954]} \quad (31)$$

However, as in the case of the wear rate, the value of the slope of  $b_o$  in Table XXXX is very small, implying that  $b_o$  is independent of  $P_o$ . Thus Equation 31 can be rewritten as:

$$\text{RCF Life (X10}^5 \text{ cycles)} = [3.17 \times 10^{32}(P_o)^{-8.288}](S)^{-1.954} \quad (32)$$

**Table XXXX : Regression data for  $a_o$  and  $b_o$  (Table XXXIX)**

	"a <sub>o</sub> "		"b <sub>o</sub> "	
	Linear	Power	Linear	Power
R <sup>2</sup>	0.23	0.31	0.02	0.03
Slope	-6.43 X 10 <sup>5</sup>	-8.288	7.2 X 10 <sup>-5</sup>	0.065
Y-Int.	9.84 X 10 <sup>8</sup>	32.501	-1.954	0.057

Equations 29 and 31 give the Type III wear rate and RCF life as functions of the pearlite interlamellar spacing ( $S$ ) and the maximum hertzian contact stress ( $P_o$ ). These functions can be plotted for any given value of  $P_o$ , Figure 111.

We find from Figure 111 that since both of the quantities involved, Type III wear rate and the RCF life, improve with decreasing pearlite interlamellar spacing, it is difficult to make a decision regarding the optimum variables to be used to increase RCF life and decrease Type III wear rates. Also, since Type III wear and RCF occur together in very few specific conditions in actual practice, it is hard to devise a set of conditions under which to study both (Type III wear and RCF) at the same time. Type I wear which often accompanies RCF might be more amenable to the formulation of a combined model for the prediction of pearlite interlamellar spacing to optimize wear rate and RCF life.

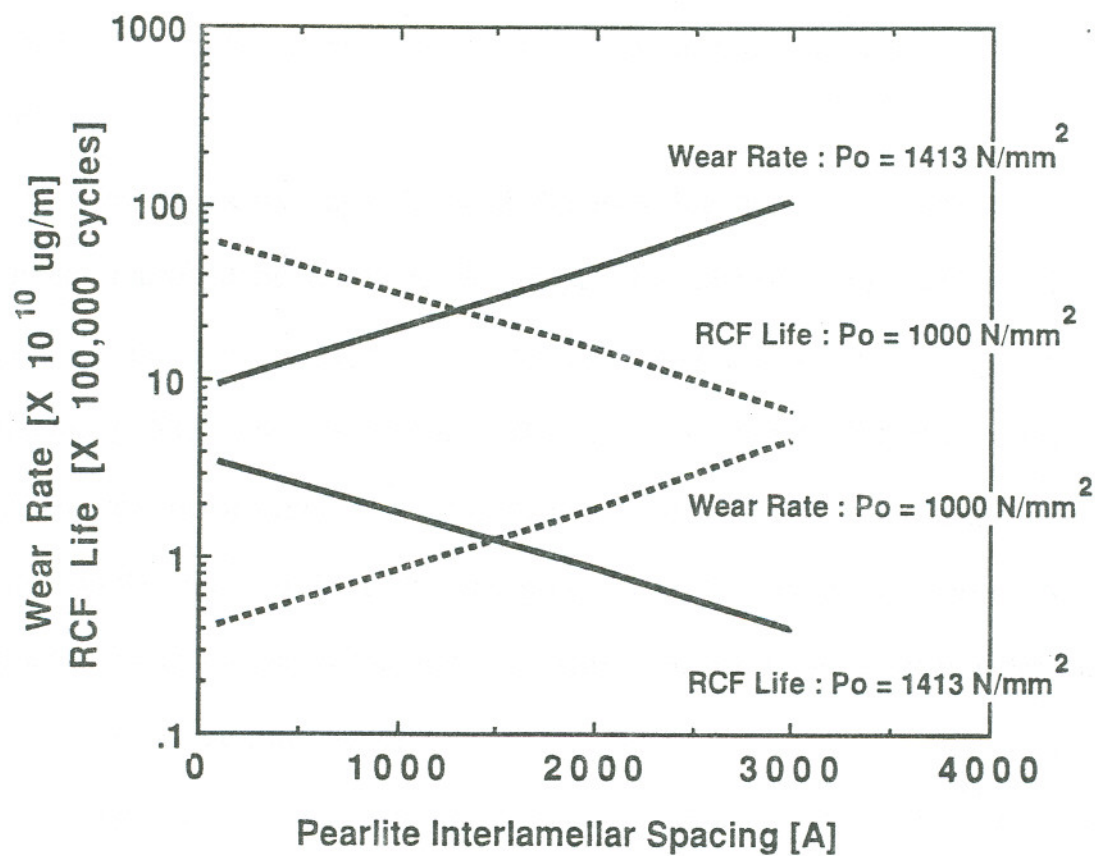


Figure 111 : Wear rate and RCF life as functions of pearlite spacing

### SUGGESTIONS FOR FUTURE WORK

The current work has raised several interesting subjects that warrant further work. The following is a brief outline of the recommendations for future work.

The predictive capabilities of the RCF life model developed in this work can be improved by widening the range of materials used. The model in its present form uses the hardness or the interlamellar spacing of the pearlitic steel in making RCF life predictions. The results of the RCF tests on steels with bainitic microstructures, however, show the inadequacies of using the pearlite interlamellar spacing in RCF life predictions. It might be better to use a parameter like the mean free path in ferrite, that can be used for a wider range of steels than just pearlitic steels.

The results of the study of crack growth rates in laboratory rollers suggests that it might be possible to get a quantitative relationship between the crack growth rates in rolling contact tests and those in conventional fatigue tests. For this further tests will need to be carried out under rolling contact and conventional fatigue. If the results of the laboratory crack growth studies do indeed provide a good correlation with conventional fatigue test crack growth rates, then, maybe even conventional fatigue test data could be used in RCF life predictions.

The model can be modified to include a generalized effect of the coefficient of friction due to different lubricants by running a series of RCF tests using different lubricants. Also if the model is to be used to make any reasonably valid predictions for field conditions, it needs to be modified to take into account the effect of sample size. Since, on the Amsler machine only rollers up to 45 mm can be tested, RCF test series will have to be run on a machine that can handle substantially larger specimens than the Amsler.

The present work demonstrates clearly that the white etching layer plays an important role in determining the RCF behavior, not only of rails but also of rollers in laboratory test. Further work needs to be done to determine the exact effect of the white etching layer in crack initiation and propagation; does the white etching layer crack on formation or due to the repeated action of load passages? On a more fundamental level this understanding might be aided if the mechanism of formation of the white etching layer on rails is better understood.

The formation of wholly subsurface contained plastic deformation has been successfully modelled and demonstrated in the past. A start has been made in this work, in trying to devise a test where the generation of such plastic deformations can be accomplished in the laboratory. Once the parameters have been established, the propensity for materials to fail due to subsurface initiated

defects can be studied. Also, such a test can provide a tool for verification of theoretical predictive models like PHOENIX.

Some of the RCF results given in this work might be interpreted as showing an effect of bottom roller hardness on RCF life. However, there is no conclusive evidence either for or against this. Further tests need to be run using materials tested against rollers of varying hardnesses. Alternatively, tests can be run using both rollers made of the same material. If there is indeed an effect on RCF life of the bottom roller hardness, then the model will have to be altered to account for it.

Since this work concentrated primarily on surface initiated RCF defects, little attention was paid to the interaction of the mechanisms of wear and RCF. Service experience has shown that these two mechanisms can occur together and in some cases can be considered as competing modes of rail failure. This work and previous work at the Oregon Graduate Institute has succeeded in defining the range of test conditions under which each of these modes occur. As was unsuccessfully attempted in this work, the next step would be to combine the models for RCF life and wear rate prediction into one relationship so as to predict the optimum operating parameters for maximizing RCF life and minimizing wear rates.

### CONCLUSIONS

- (1) A series of pearlitic eutectoid steels exhibited a linearly decreasing RCF life with increasing contact pressure, over the range of 900 - 1413 N/mm<sup>2</sup>, under water lubrication.
- (2) The slope of the RCF life - contact pressure relationship increased with increasing steel hardness such that the relative superiority of the harder steels was at least maintained throughout the contact pressure range.
- (3) The RCF life is a function of the maximum hertzian contact pressure and the hardness as given by the following relationship:

$$L = 0.039P_o - 0.000205P_oH + 0.31H - 60$$

When the maximum hertzian contact pressure,  $P_o$  is expressed in N/mm<sup>2</sup> and the Knoop Hardness (@500 gm load) is used, the relationship yields RCF life in multiples of 100,000 cycles.

- (4) For the range of pearlitic steels used, the hardness and pearlite interlamellar spacing are related by the following equation:

$$\text{Hardness} = -0.0617(S) + 431.13$$

- (5) The pearlite interlamellar spacing can be used instead of the hardness in the RCF life prediction model and the relationship becomes:

$$L = -0.049P_o + 0.000012P_oS - 0.019S + 75$$

When the maximum hertzian contact pressure,  $P_o$  is expressed in  $N/mm^2$  and the pearlite interlamellar spacing (S) is given in Angstrom units, the relationship yields RCF life in multiples of 100,000 cycles.

- (6) The effect on the coefficient of friction, by changing the lubricant from water to SAE40 motor oil can be accounted for as follows:

$$(\text{RCF Life})_{\text{SAE40}} = [\mu_{\text{water}}/\mu_{\text{SAE40}}]^{4.5} \times (\text{RCF Life})_{\text{water}}$$

- (7) The site trial and laboratory tests show a definite influence of the white etching layer on RCF behavior.
- (8) While the apparent crack growth rates calculated using laboratory tests are much higher than those found in rails, the laboratory results compare favorably with crack growth rates from conventional fatigue tests carried out by other researchers.
- (9) In laboratory test rollers the maximum hardness was found to decrease as the number of cycles increased as follows:

$$\text{Hardness} = 386 (\text{Number of Cycles})^{-0.0202}$$

## REFERENCES

1. G.G. Knupp, W.H. Chidley, J.L. Giove, H.H. Hartman, G.F. Morris and C.W. Taylor, A Review of the Manufacture, Processing, and Use of Rail Steels in North America - A Report of AISI Technical Subcommittee on Rails and Accessories, in *Rail Steels - Developments, Processing and Use*, D.H. Stone and G.G. Knupp eds., ASTM, Philadelphia, PA. STP 644, 1976, pp7-20.
2. D.H. Stone and R.K. Steel, The Effect of Mechanical Properties Upon the Performance of Railroad Rails, *Rail Steels - Developments, Processing and Use*, D.H. Stone and G.G. Knupp eds., ASTM, Philadelphia, PA. STP 644, 1976, pp21-47.
3. M.D. O'Rourke, Engineering Effects of increasing Axle Loads, *Proc. 2nd Int. Heavy Haul Conf., Colorado Springs, CO, 1982*, Association of American Railroads, Chicago, 1983, p91-98.
4. D.N. Brown and J.H. Brown, Optimizing Operational Modes on the Mt. Newman Mining Company Railroad, *Proc. 2nd Int. Heavy Haul Conf., Colorado Springs, CO, 1982*, Association of American Railroads, Chicago, 1983, p77-82.
5. W.P. Burger, Doubling the Capacity of the Heavy Haul Coal Line to Richards Bay, *Proc. 2nd Int. Heavy Haul Conf., Colorado Springs, CO, 1982*, Association of American Railroads, Chicago, 1983, pp56-67.
6. P. Clayton, The Wear Behavior of Pearlitic Steels with Reference to Rails *Ph.D. Thesis*, Brunel University, UK, March 1977.
7. H. Schmedders, Discussion on Ref. 2 in *Rail Steels - Developments, Processing and Use*, D.H. Stone and G.G. Knupp eds., ASTM, Philadelphia, PA. STP 644, 1976, pp56.
8. N.A.R. Hanks and J.F.R. Gussow, Planning for traffic Growth on Rail Lines, *Proc. 2nd Int. Heavy Haul Conf., Colorado Springs, CO, 1982* Association of American Railroads, Chicago, 1983, pp46-55.

9. F. Xianpei, Rails on Heavy Haul Sections on Chinese Railways, *Proc. 2nd Int. Heavy Haul Conf., Colorado Springs, CO, 1982*, Association of American Railroads, Chicago, 1983, pp136-141.
10. Metals Handbook 8th Edition, Vol. 10 - Failure Analysis and Prevention, ASM.
11. T.E. Tallian, Unified Rolling Contact Fatigue Model with Fatigue Limit, *Wear*, 107(1986), pp13-36.
12. *Rolling Contact Fatigue Testing of Bearing Steels*, J.J.C. Hoo, ed., ASTM, Philadelphia, PA. STP 771, 1981.
13. W.J. Davies and K.L. Day, Surface Fatigue in Ball Bearings, Roller Bearings and Gears in Aircraft Engines, *Proc. Symp. on Fatigue in Rolling Contacts*, I.M.E., London, March 1963, pp23-40.
14. *Gear Design and Performance - SP 584*, Imants Ekis and J.I. Case, eds., Published by Society of Automotive Engineers, Inc., Warrendale, PA, September 1984.
15. K.L. Johnson, The Strength of Surfaces in Rolling Contact, Third Annual BP/I Mech.E. Tribology Lecture, December 1988.
16. Rail Defect Manual, Sperry Rail Services, 1964.
17. H. Masumoto, K. Sugino, S. Nisida, R. Kurihara and S. Matsuyama, Some Features and Metallurgical Considerations of Surface Defects in Rail Due to Contact Fatigue, *Rail Steels - Developments, Processing and Use*, D.H. Stone and G.G. Knupp eds., ASTM, Philadelphia, PA. STP 644, 1976, pp233-255.
18. P. Clayton and M.B.P. Allery, Metallurgical Aspects of Surface Damage Problems in Rails, *Canadian Metallurgical Quarterly*, 21, (1), (1982), pp31-46.
19. X. Qiu, Rolling Contact Fatigue Behavior of Three Eutectoid Rail Steels, *Master Thesis*, Oregon Graduate Center, OR, USA, November 1987.
20. G.C. Martin and W.W. Hay, Influence of Wheel-Rail Contact Forces on Formation Rail Shells, ASME Paper 72 - WA/RT - 8, 1978.

21. D.H. Skinner and P.A. Judd, A Metallographic Study of Fatigue Defects in Rails, *Proc. 34th Annual Conference, Australian Inst. of Mining, Queensland Australia, 1981*, pp69-72.
22. H. Masumoto, K. Sugino, H. Hayashida, Development of Wear Resistant and Anti-Shelling High Strength Rails in Japan, *Proc. Heavy Haul Railway Conf., Perth, Western Australia, 1978* Australia Inst. of Eng., September 1978.
23. S. Marich, J.W. Cottam and P. Curcio, Laboratory Investigation of Transverse Defects in Rails, *Proc. Heavy Haul Railway Conf., Perth, Western Australia, 1978* Australia Inst. of Eng., September 1978.
24. ORE Question D 173, Review of Rolling Contact Fatigue in Rails, *ORE, Utrecht, Report D 173/RP 1*, April 1990.
25. S. Bramwell and T.F. McElroy, 25 Years of Heavy Axle Load Unit train Operation on the Quebec, North Shore and Labrador Railway, *Proc. Heavy Haul Railway Conf., Perth, Western Australia, 1978* Australian Inst. of Eng., September 1978.
26. R.P. Reiff, Introduction to the FAST/HAL Program, *Proc. Workshop on Heavy Axle Loads, Pueblo, Colorado, October 14-17, 1990*, Published by The International Heavy Haul Association, The Association of American Railroads and U.S. Department of Transportation - Federal Railroad Administration, 1990.
27. A.W. Worth, J.R. Hornaday and P.R. Richards, Prolonging Rail Life Through Rail Grinding, *Proc. 3rd Int. Heavy Haul Conf., Vancouver BC, Canada, 1986* Association of American Railroads, Chicago, 1987, IB-9-1.
28. H. Ichinose, J. Takehara, N. Iwasaki and M. Ueda, An Investigation on Rolling Contact Fatigue and Wear resistance Behavior in Rail Steels, *Proc. Heavy Haul Railway Conf., Perth, Western Australia, 1978* Australian Inst. of Eng., September 1978.
29. E. Ollerton and J.W.W. Morey, Fatigue Strength of a Rail Steel in Rolling Contact, *Proc. of Symp. on Fatigue in Rolling Contacts, London, UK, March 1963*, Inst. of Mech. Eng., 1963.

30. J. Akaoka and K. Hirasawa, Fatigue Phenomena Under Rolling Contact Accompanied with Sliding, *Bulletin of J.S.M.E., Vol. 2 (5)(1959)*, pp43-50.
31. P. Clayton and D.N. Hill, Rolling Contact Fatigue of a Rail Steel, *Wear, 117 (1987)* pp319-334.
32. S. Way, Pitting Due to Rolling Contact, *Trans. ASME, J. Appl. Mech., 57A, (1935)*, ppA49-A52.
33. M. Sato, Wear and Rolling Contact Fatigue of Rail Steels, *Masters Thesis, Ohio State University, OH, USA, 1991.*
34. K.L. Johnson and J.A. Jeffries, Plastic Flow and Residual Stress in Rolling and Sliding Contact, *Proc. of Symp. on Fatigue in Rolling Contacts, London, UK, March 1963, Inst. Mech. Eng., 1963.*
35. J.E. Merwin and K.L. Johnson, An Analysis of Plastic Deformation in Rolling Contacts, *Proc. of Symp. on Fatigue in Rolling Contacts, London, UK, March 1963, Inst. Mech. Eng., 1963.*
36. V. Bhargava, G.T. Hahn and C.A. Rubin, An Elastic-Plastic Finite Element Model of Rolling Contact, Part II: Analysis of Repeated Contacts, *J.Appl.Mech..*
37. A.F. Bower, The Influence of Crack Face Friction and Trapped Fluid on Surface Initiated Rolling Contact Fatigue Cracks, *J. of Tribology, 110 (1988)*, pp704-711.
38. A.F. Bower, The Influence of Strain Hardening on the Cumulative Plastic Deformation Caused by repeated Rolling and Sliding Contact, *Cambridge University Report - CUED/C-Mech/TR.39 (1987).*
39. The Making, Shaping and Treating of Steel - 9th Edition, United States Steel Pub., H. McGannon Ed., 1970, pp-754-762.
40. V. Bhargava, G.T. Hahn, G. Ham, S. Kulkarni, and C.A. Rubin, Influence of Kinematic Hardening on Rolling Contact Deformation, *Proc. of 2nd Int. Symp. on Contact Mechanics and Wear of Wheel/Rail Systems, URI, 1986, University of Waterloo Press, 1986.*

41. J.D. Young, United Kingdom Development of Rails from Continuously Cast Blooms, *Rail Steel - Development, Processing and Use*, D.H. Stone and G.G. Knupp eds., ASTM, Philadelphia, PA. STP 644, 1976, pp256-286.
42. ASTM A-1-84
43. J.H.S. Oliviera, Special Rails on Heavy Haul Railways, *Proc. Heavy Haul Railway Conf., Perth, Western Australia, 1978* Australia Inst. of Eng., September 1978.
44. G.M. Bouse, I.M. Bernstein and D.H. Stone, Role of Alloying and Microstructure on the Strength and Toughness of Experimental Rail Steels, *Rail Steels - Developments, Processing and Use*, D.H. Stone and G.G. Knupp eds., ASTM Philadelphia, PA. STP 644, 1976, pp145-161.
45. S. Marich and P. Curcio, Development of High-Strength, Alloyed Rail Steels Suitable for Heavy Duty Application, *Rail Steels - Developments, Processing and Use*, D.H. Stone and G.G. Knupp eds., ASTM, Philadelphia, PA. STP 644, 1976, pp167-197.
46. Y.E. Smith and F.B. Fletcher, Alloy Steels for High-Strength, As-Rolled Rails, *Rail Steels - Development, Processing and Use*, D.H. Stone and G.G. Knupp eds., ASTM, Philadelphia, PA. STP 644, 1976, pp212-232.
47. H. Ghonem and J. Kalousek, A Quantitative Model to Estimate Rail Surface Failure, *Materials Sci. & Eng.*, 97(1984), pp65-81.
48. P. Clayton, D. Danks and R.K. Steele, Assessment of Eutectoid Rail Steel Wear Performance Using Laboratory Tests, *Proc. of Conf. Antiwear-88*, The Royal Society, London, UK, 1988.
49. R.K. Steele and T.J. Devine, Wear of Rail/Wheel Systems, *Proc. of Int. Symp. on Contact Mechanics and Wear of Rail/Wheel Systems, University of British Columbia, Vancouver, BC, Canada, 1982* University of Waterloo Press, July 1982.
50. S. Kumar, B. Aronov, B. Rajakumar and R. Margasahayam, Plastic Flow in Rails for a Laboratory Wheel/Rail Simulation, *Canadian Metallurgical Quarterly*, 21 (1) (1982), pp59-66.

51. J. Kalousek and A.E. Bethune, Rail Wear Under Heavy Traffic Conditions, *Rail Steels - Developments, Processing and Use*, D.H.Stone and G.G. Knupp eds., ASTM, Philadelphia, PA. STP 644, 1976, pp63-79.
52. H. Ghonem and J. Kalousek, Experimental Study of Surface Crack Initiation, *Proc. of 2nd Int. Symp. on Contact Mechanics and Wear of Wheel/Rail Systems*, URI, 1986, University of Waterloo Press, 1986.
53. D.M. Fegredo and J. Kalousek, The Effects of Mixed Microstructure on Wear, *Proc. of 2nd Int. Symp. on Contact Mechanics and Wear of Wheel/Rail Systems*, URI, 1986, University of Waterloo Press, 1986.
54. P. Vicens, Discussion on reference 2 in *Rail Steels - Developments, Processing and Use*, D.H. Stone and G.G. Knupp eds., ASTM, Philadelphia, PA. STP 644, 1976, pp50-51.
55. K. Sugino, H. Kageyama and H. Masumoto, Development of Weldable High Strength Steel, *Proc. 2nd Int. Heavy Haul Conf., Colorado Springs, CO, 1982*, Association of American Railroads, Chicago, 1983, pp187-198.
56. J.O. Smith and C.K. Liu, Stresses Due to Tangential and Normal Loads on Elastic Solids with Application to some Contact Stress Problems, *J. Appl. Mech.*, (June 1953), pp157-166.
57. R.E. McKelvey and C.A. Moyer, The Relationship Between Critical Maximum Compressive Stress and Fatigue Life Under Rolling Contact, *Proc. Symp. on Fatigue in Rolling Contacts*, I.M.E., London, March 1963, pp1-10.
58. K.L. Johnson, Hertz Theory of Normal Contacts in, *Contact Mechanics* Ch. 4, pp84-106, 1985.
59. S.P. Timoshenko and J.N. Goodier, Hertz Theory of Elastic Contacts in *Theory of Elasticity*, Ch. 12, pp402-425, 19??.
60. B. Paul, A Review of Rail-Wheel Contact Stress Problems, *Proc. of Symp. on Railroad Track Mechanics*, 1975, Pergamon Press, 1975, pp323-351.
61. H.I. Andrews, Contact Between a Locomotive Driving Wheel and the Rail, *Wear*, 2(1958/59) pp468-485.

62. T.G. Johns, S.G. Sampath, J.C. Bell and K.B. Davies, Engineering Analysis of Stresses in Railroad Rails, *Batelle Columbus Labs - Report FRA/ORD-81/51*, October 1981.
63. R.D. Midlin, Compliance of Elastic Bodies in Contact, *Trans. ASME - J. Appl. Mech.* 71 (1949), pp259-268.
64. G.M. Hamilton, Plastic Flow in Rollers Loaded Above the Yield Point, *Proc. Symp. on Fatigue in Rolling Contacts*, I.M.E., London, March 1963, pp136-144.
65. A.W. Crook, Simulated Gear-Tooth Contacts : Some Experiments Upon Their Lubrication and Subsurface Deformations, *Proc. of IME Conf. May 1956*, pp187-213.
66. P.H. Dawson, Effect of Sliding on Rolling Contact Pitting, *J. of Mech. Eng. Sci.*, 23(6), (1981) pp289-294.
67. J.E. Garnham and J.H. Beynon, The Early Detection of Rolling-Sliding Contact Fatigue Cracks, *Communication to D.F. Cannon and ORE D173 WP3 Committee*, April 1991.
68. S.D. Regan, G.T. Hahn and C.A. Rubin, The Driving Force for Mode II Crack Growth Under Rolling Contact, *Wear*, 101 (1985), pp333-346.
69. P.H. Dawson, The Pitting of Lubricated Gear Teeth and Rollers, *J. of Power Transmission*, 30 (1961), pp209-217.
70. P.H. Dawson, Rolling Contact Fatigue Crack Initiation in 0.3% C Steel, *J. of the Institution of Mechanical Engineers*, 183 (1) (1968/69).
72. M.C. Smith, Some Aspects of Mode II Crack Growth, *Ph.D. Thesis*, Cambridge University, UK, 1985.
73. M.B.P. Allery, Laboratory Rolling Contact Fatigue Tests on Normal Grade A and Head Hardened Rail Steels Under Lubricated Conditions, *British Rail Research Report*, 1990.
74. R. Nakamura, S. Owaku and N. Enomoto, The Rail Shelly Crack in Japan, *Quarterly Report of the RTRI* 6 (3) (1965), Tokyo, pp34-44.

75. J.M. Hyzak and I.M. Bernstein, The Role of Microstructure on the Strength and Toughness of Fully Pearlitic Steels, *Met. Trans. A* 7 (1976), pp1217.
76. K. Sugino, H. Kageyama and H. Masumoto, Development of Weldable High Strength Rail Steel, *Proc. 2nd Int. Heavy Haul Conf., Colorado Springs, CO, 1982*, Association of American Railroads, Chicago, 1983, pp187-198.
77. D. Ramaswamy, Wear Behavior of Pearlitic Steels, *Ph.D. Thesis*, Oregon Graduate Institute, OR, USA, October 1991.
78. H. Sunwoo, M.E. Fine, M.Meshii and D.H. Stone, Cyclic Deformation of Pearlitic Eutectoid Rail Steel, *Met. Trans. A* 13 (November 1982), pp2035-2047.
79. *Burlington Northern Rail Integrity Study - Phase I Report*, Oregon Graduate Center Report, September 1987.
80. M.D. Roney, T.S. Lamson and M.D. Baggott, Determining the Economical Timing for Grinding and Renewal of Rail, *Proc. 2nd Int. Heavy Haul Conf., Colorado Springs, CO, 1982*, Association of American Railroads, Chicago, 1983, pp358-371.
81. B.J. Griffiths and D.C. Furze, Tribological Advantages of White Etching Layers Produced by Machining, *J. of Tribology* 109 (April 1987), pp338-342.
82. B.J. Griffiths, Mechanisms of White Layer Generation with Reference to Machining and Deformation Processes, *J. of Tribology* 109 (July 1987), pp525-530.
83. S.B. Newcomb and W.M. Stobbs, A Transmission Electron Microscopy Study of the White-Etching Layer on a Rail Head, *Materials Sci. & Eng.* 66 (1984), pp195-204.
84. D.H. Stone, The Increasing Demands on Serviceability of Rails, *Canadian Metallurgical Quarterly* 21 (1) (1982), pp17-24.
85. Isothermal Transformation Diagrams, United States Steel Publication - 3rd Edition, 1966, pp22.
86. G.V. Vandervoort and A. Roosz, Measurement of the Interlamellar Spacing of Pearlite, *Metallography* 17 (1984), pp1-7.

87. ASTM E-112-85
88. ASTM E-542-83
89. D. Danks, Wear and Microstructure of Eutectoid Steels, *Ph.D. Thesis* Oregon Graduate Center, OR, USA, March 1989.
90. G.E. Deiter, *Mechanical Metallurgy* 2nd Edition (ISE), McGraw Hill International Book Co., 1981.
91. K. Fujita and A. Yoshida, Effect of Changing the Rolling Direction on the Rolling Contact Fatigue Lives of Annealed and Case-Hardened Steel Rollers, *Wear* 43 (1977), pp315-327.
92. *Unpublished Work*, Oregon Graduate Institute, Beaverton, Oregon, U.S.A., 1990.
93. J.W. Blake and H.S. Cheng, A Surface Pitting Model for Spur Gears - Part I : Life Prediction, *From manuscript that is to be published.*
94. J.W. Blake and H.S. Cheng, A Surface Pitting Model for Spur Gears - Part II : Failure Probability Prediction, *From a manuscript that is to be published.*
95. C.E. Federsen and D. Broek, Fatigue Crack Propagation in Rail Steels, *Rail Steels - Developments, Processing and Use*, D.H. Stone and G.G. Knupp eds., ASTM, Philadelphia, PA. STP 644, 1976, pp99-117.
96. D.E. Sonon, J.V. Pellegrino and J.M. Wandrisco, A Metallurgical Examination of Control-Cooled Carbon-Steel Rails with Service-Developed Defects, *Rail Steels - Developments, Processing and Use*, D.H. Stone and G.G. Knupp eds., ASTM, Philadelphia, PA. STP 644, 1976, pp99-117.
97. P. Clayton and D. Danks, Effect of Interlamellar Spacing on the Wear Resistance of Eutectoid Steels Under Rolling-Sliding Conditions, *Wear* 135 (119), pp369-389.

### BIOGRAPHICAL NOTE

Vivek was born in Bombay, India on the 31st of January 1964. He received his Bachelor of Technology degree in Metallurgical Engineering from the Indian Institute of Technology, Bombay, India, in May 1985. After his undergraduate studies he worked for a year, from August 1985 to August 1986 at Special Steels Limited, Bombay, India.

In September 1986 he joined the Oregon Graduate Institute, (then Oregon Graduate Center) to pursue graduate studies.